

UC San Diego

UC San Diego Electronic Theses and Dissertations

Title

Synthetic and Biocatalytic Strategies for Natural Product Synthesis via ortho-Quinone Methide Intermediates

Permalink

<https://escholarship.org/uc/item/2gm3f25j>

Author

Purdy, Trevor Nelson

Publication Date

2021

Supplemental Material

<https://escholarship.org/uc/item/2gm3f25j#supplemental>

Peer reviewed|Thesis/dissertation

UNIVERSITY OF CALIFORNIA SAN DIEGO

Synthetic and Biocatalytic Strategies for Natural Product Synthesis via *ortho*-Quinone
Methide Intermediates

A dissertation submitted in partial satisfaction of the
requirements for the degree of Doctor of Philosophy

in

Marine Biology

by

Trevor Nelson Purdy

Committee in charge:

Professor Bradley Moore, Chair
Professor William Fenical
Professor William Gerwick
Professor Alexis Komor
Professor Emmanuel Theodorakis

2021

©

Trevor Nelson Purdy, 2021

All rights reserved

The Dissertation of Trevor Nelson Purdy is approved, and it is acceptable in quality and form for publication on microfilm and electronically.

University of California San Diego

2021

DEDICATION

For my parents, Martin and Jana, who have unconditionally supported me as I pursued my dreams

For my wife, Kailey, whose undeserved selflessness made this dream a reality.

TABLE OF CONTENTS

Dissertation Approval Page	iii
Dedication	iv
Table of Contents	v
List of Abbreviations	vii
List of Figures	ix
List of Schemes	xi
List of Supplemental Files	xiii
Acknowledgements	xiv
Vita	xvii
Abstract of the Dissertation	xix
Chapter 1. Enzymatic Generation of <i>o</i> -QMs	1
1.1. Introduction	2
1.2. Berberine Bridge Enzyme-like Oxidases	5
1.3. Tropolonic hetero-Diels-Alderases	16
1.4. SAM-Dependent <i>O</i> -Methyltransferase-like Pericyclase	21
1.5. α -Ketoglutarate Dependent Non-heme Iron Oxidases	23
1.6. Biocatalytic Utility of Enzymatic <i>ortho</i> -Quinone Methides	24
1.7. Concluding Remarks	28
Chapter 2. Progress Towards the Biomimetic Total Synthesis of (\pm)-Chlorizidine A... ..	38
Chapter 3. Discovery and Biosynthesis of Tetrachlorizine Reveals Enzymatic Benzylic Dehydrogenation via an <i>ortho</i> -Quinone Methide	104
Chapter 4. Exploring the Structure-Function Relationship of Clz9 and Tcz9 for Benzylic(sp ³) C–H Functionalization Applications	182
4.1. Introduction	183
4.2. Results	
4.2.1. Site-Directed Mutagenesis of Clz9 and Tcz9	188
4.2.2. Benzylic Hydroxylation Reactions with Non-Native Substrates ...	189
4.2.3. Temperature and Solvent Effects on Tcz9 Stability	191
4.2.4. Time Course Analysis Monitoring the Reaction Progress of Tcz9 and 9	192
4.2.5. <i>In vitro</i> and <i>in vivo</i> cannabinoid production with Clz9 and Tcz9 .	193

4.2.6. <i>In vivo</i> cannabinoid production with Tcz9 T405Y	198
4.3. Discussion and Conclusions	199

LIST OF ABBREVIATIONS

AAE – Acyl activating enzyme
ACP – Acyl carrier protein
ArPT – Aromatic prenyltransferase
AT – Adenyltransferase
ATP – Adenosinetriphosphate
BBE-like – Berberine bridge enzyme-like
BGC – Biosynthetic Gene Cluster
Boc – *tert*-Butyloxycarbonyl
bp – Base pair
CBC – Cannabichromene
CBCA – Cannabichromenic acid
CBCVA – Cannabichromevarinic acid
CBD – Cannabidiol
CBDA – Cannabidiolic acid
CBGA – Cannabigerolic acid
CBGOA – Cannabigerorcinic acid
CBGVA – Cannabigerovarinic acid
Cbz – Benzyl chloroformate
CCD – Charged coupled device
CMOS – Complementary metal-oxide semiconductor
CoA – Coenzyme A
COSY – Correlation spectroscopy
DCA – Daurichromenic acid
DCM – Dichloromethane
DMF – Dimethylformamide
DMSO – Dimethylsulfoxide
EtOAc – Ethyl acetate
FAD – Flavin adenine dinucleotide
FADH₂ – Reduced flavin adenine dinucleotide (hydroquinone form)
FAS – Fatty acid synthase
Fmoc – Fluorenylmethoxycarbonyl
GABA_A – γ -Aminobutyrate A
hDA – hetero-Diels-Alder(ase)
HMBC – Heteronuclear multiple-bond correlation spectroscopy
HPLC – High-performance liquid chromatography
HR-ESI-TOFMS – High resolution electrospray ionization mass spectrometry
HR-LC-MS – High resolution liquid chromatography mass spectrometry
HSQC – Heteronuclear single-quantum correlation spectroscopy

IPTG – Isopropylthio- β -galactoside
KS – Ketosynthase
 α -KG – α -Ketoglutarate
LB – Lysogeny broth
Mal-CoA – Malonyl-coenzyme A
MBP – Maltose binding protein
MeCN – Acetonitrile
MeOH – Methanol
MOM – Methoxymethyl
MS – Mass spectrometry
MWCO – Molecular weight cut-off
NMR – Nuclear magnetic resonance
NOE(SY) – Nuclear Overhauser effect (spectroscopy)
OAC – olivetolic acid cyclase
o-QM – *ortho*-Quinone methide
PCR – Polymerase chain reaction
PKS – Polyketide synthase
PPTase – Phosphopantetheinyl transferase
Q-TOF – Quadrupole time of flight
R – Thioester reductase
ROESY – Rotating-frame nuclear Overhauser effect correlation spectroscopy
SAM – S-Adenosyl methionine
SDS-PAGE – Sodium dodecyl sulfate polyacrylamide gel electrophoresis
SSN – Sequence similarity network
TB – Terrific broth
TFA – Trifluoroacetic acid
THC – Δ^9 -Tetrahydrocannabinolic acid
THCA – Δ^9 -Tetrahydrocannabinolic acid
THF – Tetrahydrofuran
TKS – Tetraketide synthase
UV/Vis – Ultraviolet-visible spectroscopy

LIST OF FIGURES

Figure 1.1. (a) Examples of natural products proposed to require a biosynthetic *o*-QM intermediate. *o*-QM portion of the molecules are highlighted in teal. (b) Representative structures of commonly observed quinone methides. (c) Canonical representations of *ortho*-quinone methide zwitterionic, geometric, and biradical isomers. [...] 3

Figure 1.2. Crystal structure of EcBBE (PDB 3D2H) illustrating bicovalent attachment of His104 and Cys166 to the 8 α - and 6-positions of the isoalloxazine ring of FAD. 5

Figure 1.3. Protein homology models comparing key active site residues of BBE-like cannabinoid synthases. (a) Overlay of THCA synthase (PDB 3VTE, green), CBDA synthase model (blue), and CBCA synthase model (orange). (b) Overlay of CBCA synthase model (orange) with DCA synthase model (pink). [...] 9

Figure 1.4. *In vitro* reactions with DCA synthase. (a) Confirmation of the role of DCA synthase in daurichromenic acid (**15**) biosynthesis. (b) Substrate screening with DCA synthase exhibits activity with various prenyl attachments but no activity with grifolin (**20**) or cannabigerolic acid (**7**). [...] 13

Figure 1.5. Representative examples of tropolonic sesquiterpenoids likely derived from hetero-Diels-Alder cyclization reactions. The *o*-QM portion is highlighted in teal. 17

Figure 1.6. (a) Clavatul (**77**)-derived natural products from *Penicillium* sp. (b) Regioselective benzylic hydroxylation by α -KG dependent non-heme iron oxygenase ClaD, which undergoes “indirect” (spontaneous) dehydration to produce a reactive *o*-QM. 23

Figure 1.7. Biocatalytic developments for *in vivo* *o*-QM formation and benzylic functionalization with non-natural substrates, resulting in the rapid generation of diverse “pseudo-natural product” libraries. (a) Chaetophenol A (**80**) undergoes reductive cyclization by an endogenous enzyme [...] 26

Figure 2.1. Structures of (–)-chlorizidine A (**1**) and a purported degradation analog chlorizidine B (**2**). 39

Figure 3.1. Molecular basis for tetrachlorizine biosynthesis. (a) Alignment of the tetrachlorizine (*tcz*) and chlorizidine A (*clz*) BGCs. Genes are color-coded by associated function. (b) Structures of novel dichloropyrrole-containing natural products, tetrachlorizine (**1**) and dihydrotetrachlorizine [...] 107

Figure 3.2. (a) HPLC analysis of the *in vitro* conversion with **2** and either Tcz9 or Clz9 after 12 hours: UV absorption monitored at 360 nm; (i) purified **2** standard; (ii) purified **1** standard. (iii) **2** + Tcz9, confirming Tcz9’s role in **1** biosynthesis; (iv) **2** + Clz9, yielding the cyclized derivative **8** in addition to **1**. [...] 109

Figure 4.1. Investigation of active site residues that may be involved in the deprotonation event that differentiates the catalytic function of Tcz9 from Clz9. (a) Model overlay of Clz9 (green) and Tcz9 (blue) with THCA synthase (pink; 3VTE). The bicovalently attached FAD cofactor is yellow. [...] 189

Figure 4.2. Biocatalytic properties of Tcz9. (a) Initial HPLC analysis of benzylic hydroxylation reaction *in vitro* with 2 mol% Clz9 or Tcz9 and **8** or **9** after 12 hours at 37 °C. Combined extracted ion chromatogram (EIC) for $m/z = 216.1, 232.1 [M-H]^-$ (left); $m/z = 284.0, 300.0 [M-H]^-$ (right). [...] 191

Figure 4.3. HPLC analysis of the *in vitro* reactions of CBGA (**12a**) with Clz9 or Tcz9 variants after incubation for 12 hours at pH 7.5 and 37 °C. No production of THCA (**13**) or CBDA (**14**) was detected at this pH. The major product observed was CBCA (**15a**). **16-18a** have yet to be structurally characterized. [...] 194

Figure 4.4. HPLC analysis of the *in vitro* reactions of **12b** (left) or **12c** (right) with Clz9 and Tcz9 variants after incubation for 12 hours at pH 7.5 and 37 °C. **16-18b-c** have yet to be structurally characterized. UV absorption monitored at 300 nm. 196

Figure 4.5. HPLC analysis of the *in vitro* reactions of **19** with Clz9 and Tcz9 variants after incubation for 12 hours at pH 7.5 and 37 °C. [...] 198

LIST OF SCHEMES

- Scheme 1.1.** Abbreviated biosynthesis of cannabinoids. Structural diversification is generated by BBE-like enzymes CBDA synthase, THCA synthase, and CBDA synthase. Abbreviations: AAE, acyl activating enzyme; TKS, tetraketide synthase; OAC, olivetolic acid cyclase; ArPT, aromatic prenyltransferase. 6
- Scheme 1.2.** Proposed mechanisms for (a) THCA synthase, (b) CBDA synthase, and (c) CBCA synthase cyclization via *o*-QM intermediates. 7
- Scheme 1.3.** (a) Proposed mechanisms for cyclization vs. dehydrogenation with microbial BBE-like oxidases Clz9 and Tcz9. (b) Comparing and contrasting catalytic functions of Clz9 and Tcz9 with non-native biosynthetic precursors. 14
- Scheme 1.4.** Proposed biosynthesis of xenovulene A (**46**) via a tropolonic *o*-QM intermediate. The function of AsR5 was not verified *in vitro*, however, the presence of shunt products **47-50** is evidence supporting an *o*-QM intermediate. 18
- Scheme 1.5.** Proposed biosynthesis of eupenifeldin (**36**) via two *o*-QM intermediates. Genes responsible for production of neosetophomone B (**35**), EupfA-F and EupF, a homolog of EupfF were characterized by heterologous expression or *in vitro* experiments. 20
- Scheme 1.6.** Leporin C (**65**) biosynthetic pathway. In the absence of LepI, **60** undergoes spontaneous dehydration and forms a mixture of non-enzymatic intramolecular Diels-Alder (IMDA) and hetero-Diels-Alder (hDA) products. Structures in gray are generated non-enzymatically. [...] 22
- Scheme 1.7** Chemoenzymatic benzylic functionalization reactions *via* an *o*-QM with a-KG dependent non-heme iron oxygenases ClaD and CitB. (a) Various aryl-substituted substrates could be accepted. Additional nucleophiles could be added to the reaction mixture after benzyl alcohol protection. [...] 27
- Scheme 2.1.** (a) Proposed biosynthetic mechanism for stereoselective intramolecular cyclization of prechlorizidine (**3**) to (–)-chlorizidine A (**1**). (b) Retrobiosynthetic strategy to access **3** and 13-hydroxyprechlorizidine (**4**) for biomimetic cyclization. 41
- Scheme 2.2.** Synthesis of pyrroloisoindolone core by an intramolecular Heck reaction. 42
- Scheme 2.3.** Synthesis of Fmoc-protected dichloropyrrole acyl chloride **7**. 43
- Scheme 2.4.** Convergence of **6** and **7** followed by a regioselective Friedel-Crafts Acylation and global deprotection using BBr₃. Two chemoselective reduction strategies to access 13-hydroxyprechlorizidine (**4**) (Path A) or prechlorizidine (**3**) (Path B). The final cyclization step to reach (±)-chlorizidine has yet to be achieved. 45

Scheme 3.1. Abbreviated reaction scheme depicting the enzymatic process for oxidation of **4** to (*E*)-**9** and (*Z*)-**9** catalyzed by Tcz9, which non-enzymatically coalesce to **10** in the presence of water. Key HMBC correlations for assigning the structure of **10** are included. 110

Scheme 4.1. Representative examples of characterized FAD-dependent BBE-like enzymes catalyzing C–C bond forming reactions (1-3) and dehydrogenation reactions (4-6) in natural product biosynthesis. 184

Scheme 4.2. Benzylic functionalization reactions with microbial BBE-like enzymes Clz9 and Tcz9 *via* an *o*-QM intermediate. (a) Clz9 catalyzes intramolecular cyclization, while Tcz9 catalyzes a dehydrogenation. (b) Clz9 exhibits selectivity as a cyclase not observed with Tcz9 and **3**, while Tcz9 has preferential dehydrogenation activity [...] 187

LIST OF SUPPLEMENTAL FILES

Clz9_vs_Tcz9_Timelapse.mp4

ACKNOWLEDGEMENTS

This dissertation would not have been possible without the encouragement, guidance, and mentorship of so many people in the Scripps community, the broader natural products community, and greater San Diego community to whom I am indebtedly grateful. Thank you to the entire 2015 cohort, and a special thank you to Benni Birner and Chase James, two lifelong friends I can always rely on. Thank you to my teammates from college, club, and professional ultimate – especially to Coach Kevin Stuart, who taught me discipline and perseverance, two qualities I needed to complete this PhD.

Thank you, Paige Stout, for encouraging me to pursue a PhD in marine natural products chemistry. And Bailey Miller, my fantastic mentor – I'll cherish your longboard as long as I can. Thank you, Chambers Hughes, for believing in me and investing so much time to help me grow. I certainly would not have survived the first few years if I didn't have Daniella Reimer, Gabriel Castro, and Grant Seiler to commiserate with. Thank you to the Shore Rider crew – Grant, Gabriel, Nick Tuttle, Doug Sweeney, Charlie Larson, and Nathan Moss – for providing a weekly outlet to decompress.

Thank you to the many former post-docs and visiting scholars for their patience and wisdom – Peter Jordan, Leesa Klau, Jehad Almaliti, Eduardo Caro, Jon Chekan, Percival Y.T. Chen, Dave Yi, and Shaun McKinnie. Thank you to my fantastic collaborators, Amanda Alker, Min Kim, and Reiko Cullum, who shared their exciting research projects with me. I'd also like to thank my committee members, Professors Emmanuel Theodorakis and Alexis Komor, for providing their research expertise. The CMBB professors Paul Jensen, Bill Gerwick, and Bill Fenical deserve an enormous thank

you for their ideas, contributions, and (personal and professional) advice over the past six years.

I am grateful for the financial support from the Dickinson family, the McCrink family, the Green Family, the Taubmann Foundation, the NIH Marine Biotechnology Training Grant, and the American Society of Pharmacognosy, who made all this research possible. I am also grateful for the analytical and technical support of Anthony Mrse, Brendan Duggan, and Yongxuan Su, all of whom provide excellent care for the NMR and mass spectrometry instrumentation.

Finally, I am thankful for all the Moore lab group members who have helped me reach this goal: Rebecca Schäfer, Sanjoy Adak, Monica Thukral, Steffaney Wood, Immo Burkhardt, April Lukowski, Tim Fallon, Vikram Shende, Kate Bauman, Tristan de Rond, Kayla Wilson, Leah Bushin, Patrick Brunson, and Taylor Steele. The group's enthusiasm is exhilarating and your willingness to help others is truly admirable. You taught me a real sense of community that I'll never forget. This incredible lab culture – this sense of *ohana* -- is fostered by Professor Bradley Moore, one of the greatest human beings I will ever know. You have shown me what it takes to become a great scientist, role model, and father, and I hope to become a fraction of the man you are.

Chapter 1 has been submitted for publication in the *Journal of Natural Products*, 2022, Purdy, Trevor N.; Moore, Bradley S.; Lukowski, April L. The dissertation author was primary author of this material.

Chapter 2 is coauthored with Purdy, Trevor N.; Seiler, Grant S.; Kim, Daria E.; Hughes, Chambers C. The dissertation author was the primary investigator and author of this material.

Chapter 3 is a reprint in full of the material as it appears in the *Journal of the American Chemical Society* **2021**, *143*, 3682-3686. Purdy, Trevor N.; Kim, Min C.; Cullum, Reiko; Fenical, William; Moore, Bradley S. The dissertation author was a co-primary investigator and author of this paper.

Chapter 4 is coauthored by Purdy, Trevor N. and Moore, Bradley S. The dissertation author was the primary investigator and author of this paper.

VITA

- 2014 – 2015 Research Associate
Sirenas Marine Discovery, La Jolla, CA
- 2015 Bachelor of Science, Molecular Synthesis
Department of Chemistry and Biochemistry, University of California
San Diego
- 2017 Master of Science, Marine Biology
Scripps Institution of Oceanography, University of California San
Diego, CA
- 2021 Doctor of Philosophy, Marine Biology
Scripps Institution of Oceanography, University of California San
Diego, CA

Fellowships and Grants

NIH Marine Biotechnology & Biomedicine Training Grant (2020)
Herman P. and Sophia Taubman Foundation Endowed Graduate Fellowship (2018)
Lloyd Green Family Endowed Fellowship (2017)
Donald C. and Elizabeth M. Dickinson Foundation Fellowship (2015)
McCrink Family Graduate Fellowship for the Center for Marine Biotechnology and
Biomedicine (2015)

Awards

American Society of Pharmacognosy Student Research Award (2020)

SELECTED PUBLICATIONS

Purdy, T. N.; Kim, M. C.; Cullum R.; Fenical, W.; Moore, B. S. “Discovery and Biosynthesis of Tetrachlorizine Reveals Enzymatic Benzylic Dehydrogenation via an *ortho*-Quinone Methide.” *J. Am. Chem. Soc.* **2021**, *143*, 3682-3686.

Alker, A. T.; Delherbe, N.; **Purdy, T. N.**; Moore, B. S.; Shikuma, N. J. “Genetic examination of the marine bacterium *Pseudoalteromonas luteoviolacea* and effects of its metamorphosis-inducing factors.” *Environmental Microbiology* **2020**, *22*, 4689-4701.

Chekan, J. R.; Lee, G. Y.; Gamal, A. E.; **Purdy, T. N.**; Houk, K. N.; Moore, B. S. "Bacterial Tetrabromopyrrole Debrominase Shares a Reductive Dehalogenation Strategy with Human Thyroid Deiodinase." *Biochemistry* **2019**, 58, 5329-5338.

Petras, P.; Nothias, L.-F.; Quinn, R. A.; Alexandrov, T.; Bandeira, N.; Bouslimani, A.; Castro-Falcón, G.; Chen, L.; Dang, T.; Floros, D. J.; Hook, V.; Garg, N.; Hoffner, N.; Jiang, Y.; Kapon, C.A.; Koester, I.; Knight, R.; Leber, C. A.; Ling, T.-J.; Luzzatto-Knaan, T.; McCall, L.-I.; McGrath, A. P.; Meehan, M. J.; Merritt, J. K.; Mills, R. H.; Morton, J.; Podvin, S.; Protsyuk, I.; **Purdy, T. N.**; Satterfield, K.; Searles, S.; Shah, S.; Shires, S.; Steffen, D.; White, M.; Todoric, J.; Tuttle, R.; Wojnicz, A.; Sapp, V.; Vargas, F.; Yang, J.; Zhang, C.; Dorrestein, P. C. "Mass Spectrometry-Based Visualization of Molecules Associated with Human Habitats" *Anal. Chem.* **2016**, 88, 10775-10784.

ABSTRACT OF THE DISSERTATION

Synthetic and Biocatalytic Strategies for Natural Product Synthesis via *ortho*-Quinone Methide Intermediates

by

Trevor Nelson Purdy

Doctor of Philosophy in Marine Biology

University of California San Diego, 2021

Professor Bradley S. Moore, Chair

Organisms across all domains of life have developed elegant strategies to produce specialized metabolites, also referred to as natural products, for defense, structure, and communication. Natural products provide novel inspiration for pharmaceutical development given their potent biological activities and structural diversity. Recent advancements in DNA sequencing technology and the development of predictive

bioinformatics tools have unveiled a vast collection of biosynthetic machinery responsible for generating this structural diversity that may be harnessed by synthetic chemists. Many of the enzymes encoded by biosynthetic genes catalyze chemical reactions that are difficult to replicate with the same selectivity by traditional synthetic methods. An example of this discrepancy is illustrated by the current enzymatic and chemical methods known to generate a highly reactive *ortho*-quinone methide (*o*-QM) intermediate. The utility of *o*-QMs in total synthesis has been hampered by complications that surround the preparation of their precursors, the harsh generation methods, and poor chemo-, regio-, and stereoselective control. In contrast, multiple enzymes have been reported to catalyze *o*-QM formation under mild conditions with remarkable selectivity. Chapter 1 of this dissertation examines several different enzymatic strategies developed to generate *o*-QMs. Chapter 2 describes progress towards the biomimetic total synthesis of (–)-chlorizidine A that aims to synthetically replicate the final biosynthetic intramolecular cyclization via an *o*-QM intermediate. Chapter 3 reports the discovery of tetrachlorizine, a novel tetrachlorinated marine natural product, and the identification of its associated biosynthetic gene cluster. Biochemical characterization of a pivotal flavin-dependent oxidase revealed a dehydrogenation reaction that proceeds via an unprecedented *o*-QM mechanism. This oxidase was then repurposed to generate an isolable *o*-QM, an extremely rare chemical motif. Chapter 4 investigates the structure-function relationships of two homologous flavin-dependent oxidases with divergent reaction selectivities and highlights their favorable biocatalytic properties. This chapter also discloses the first reported bacterial enzymes capable of performing oxidative cyclization reactions to produce cannabinoids.

Chapter 1

Harnessing *ortho*-Quinone Methides in Natural Product Biosynthesis and Biocatalysis

Trevor N. Purdy, Bradley S. Moore, April. L. Lukowski

Abstract: The implementation of *ortho*-quinone methide (*o*-QM) intermediates in complex molecule assembly represents a remarkably efficient strategy designed by Nature and utilized by synthetic chemists. *o*-QMs have been taken advantage of in biomimetic syntheses for decades, yet relatively few examples of *o*-QM-generating enzymes in natural product biosynthetic pathways have been reported. The biosynthetic enzymes that have been discovered thus far exhibit tremendous potential for biocatalytic applications, enabling the selective production of desirable compounds that are otherwise intractable or inherently difficult to achieve by traditional synthetic methods. Characterization of this biosynthetic machinery has the potential to shine a light on new enzymes capable of similar chemistry on diverse substrates, thus expanding our knowledge of Nature's catalytic repertoire. The presently known *o*-QM-generating enzymes include flavin-dependent oxidases, hetero-Diels-Alderases, S-adenosyl-L-methionine (SAM)-dependent pericyclases, and α -ketoglutarate-dependent non-heme iron enzymes. In this review, we discuss their diverse enzymatic mechanisms and potential as biocatalysts in constructing natural product molecules.

1. Introduction

Natural product molecules are a profound source of inspiration for synthetic chemists and biochemists alike. The elaborate structures expertly assembled by Nature serve as blueprints for designing synthetic and biocatalytic routes to pharmaceuticals¹, feedstock chemicals², and other important materials.³ Understanding the fundamental mechanisms refined by Nature for the biosynthesis of natural products enables the development of improved methods for accessing complex molecules. Modern nucleic acid sequencing technologies have rapidly accelerated the discovery of the biosynthetic machinery responsible for the assembly of numerous natural products.^{4,5} Such technological advancements have facilitated the study of natural product biosynthetic pathways from unculturable organisms⁶, entire microbial communities⁷, and higher order organisms such as macroalgae⁸, plants⁹, and animals.¹⁰ This influx of information has also resulted in the discovery of new enzyme classes and enzymes with unprecedented chemistry, accelerating the development of biocatalysts for chemical synthesis.

A prime example of a chemical motif designed by Nature and utilized by synthetic chemists is the *ortho*-quinone methide (*o*-QM), a reactive intermediate that has been extensively reviewed and often used in complex biomimetic syntheses and chemical manufacturing.^{11–18} *o*-QMs are suspected to be involved in the formation of several bioactive natural products, for example parvinaphthol C (**1**)¹⁹ and busseihydroquinone C (**2**)²⁰ isolated from plants and peniphenone D (**3**)²¹, (–)-xyloketal D (**4**)²², and epolone B (**5**)²³ derived from fungi (Figure 1.1a). In its simplest representation, an *o*-QM is composed of a 2,4-cyclohexadienone core with an exocyclic methylene *ortho* to the carbonyl group (Figure 1.1b). These innately reactive intermediates can also be depicted as zwitterionic

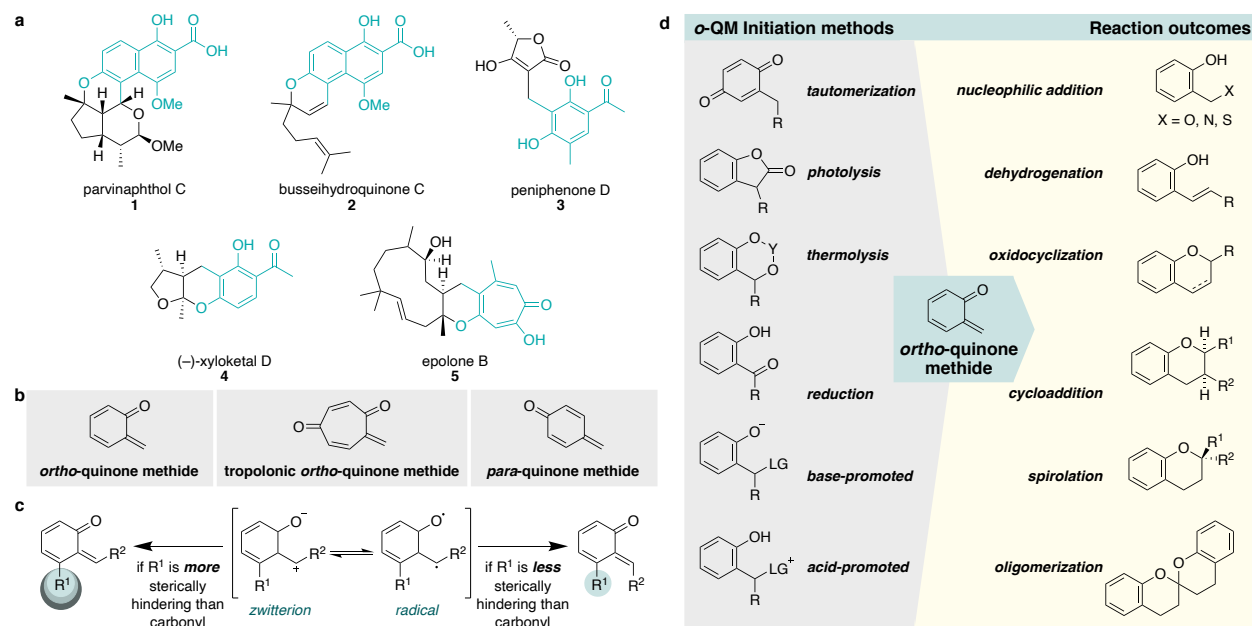


Figure 1.1. (a) Examples of natural products proposed to require a biosynthetic *o*-QM intermediate. *o*-QM portion of the molecules are highlighted in teal. (b) Representative structures of commonly observed quinone methides. (c) Canonical representations of *ortho*-quinone methide zwitterionic, geometric, and biradical isomers. (d) Common synthetic and biosynthetic approaches to *o*-QM formation and reaction outcomes.

or biradical species and may exist as *E/Z* geometric isomers depending on steric hindrance from adjacent functional groups (Figure 1.1c). The reestablishment of aromaticity drives *o*-QM reactivity, and this logic also extends to non-benzenoid aromatics, such as tropolones (Figure 1.1b), which favor aromaticity rather than *o*-QM dearomatization. In contrast to the well-documented *para*-quinone methide regioisomer (Figure 1.1b), *o*-QMs exhibit a greater charge dipole and are therefore less stable and more reactive such that nearly all *o*-QMs are unable to be isolated and will undergo rapid oligomerization in the absence of a suitable nucleophile.¹³ Further, the zwitterionic nature of *o*-QMs makes them both electrophilic and nucleophilic, rendering their utility as nucleophiles and electron-poor dienes particularly attractive for synthetic purposes.

The utility of *o*-QMs extends to a variety of complexity-building reactions, including cycloaddition, spirocyclization, and oligomerization reactions (Figure 1.1d). *o*-QMs are

highly versatile yet challenging to employ due to rapid degradation and the formation of unwanted byproducts, impeding their selectivity and overall utility. In traditional synthetic approaches, careful consideration must be taken as to the reaction conditions used to generate the *o*-QM, especially when invoked at later stages in the route. Figure 1.1d summarizes some of the strategies for *o*-QM initiation, including examples of the most commonly used *o*-QM precursors. Many of these strategies require phenolic protection and activation of the benzylic carbon prior to thermal, photolytic, or chemical generation of the *o*-QM, and exorbitant amounts of a nucleophile or diene to mitigate oligomerization (Figure 1.1d). Despite the versatility of the *o*-QM intermediate, such reaction requirements undermine its accessibility in synthetic endeavors. As a complementary approach, biosynthetic pathways involving enzymatic *o*-QM intermediates have the potential to expedite the development of biocatalytic methods that are more efficient, selective, and sustainable relative to traditional synthetic techniques.

Although *o*-QMs were first described over a century ago and have gained traction in organic synthesis over the past 50 years,²⁴ evidence for their involvement in natural product biosynthetic pathways has only recently been reported due to the highly reactive nature of the intermediate.²⁵ Recent investigations into the enzymatic generation of *o*-QMs have uncovered a diverse collection of enzymes from bacterial, fungal, and plant sources. These enzymes have demonstrated remarkable regio-, stereo-, and chemoselectivity that is difficult to replicate with comparable atom economy using traditional chemical methods. Perhaps even more remarkable is the fact that these enzymatic reactions take place under aqueous conditions traditionally avoided due to the nucleophilicity of water promoting rapid quenching of *o*-QMs. Given these unique

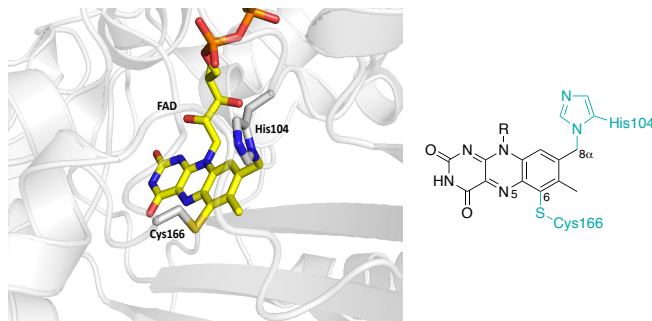


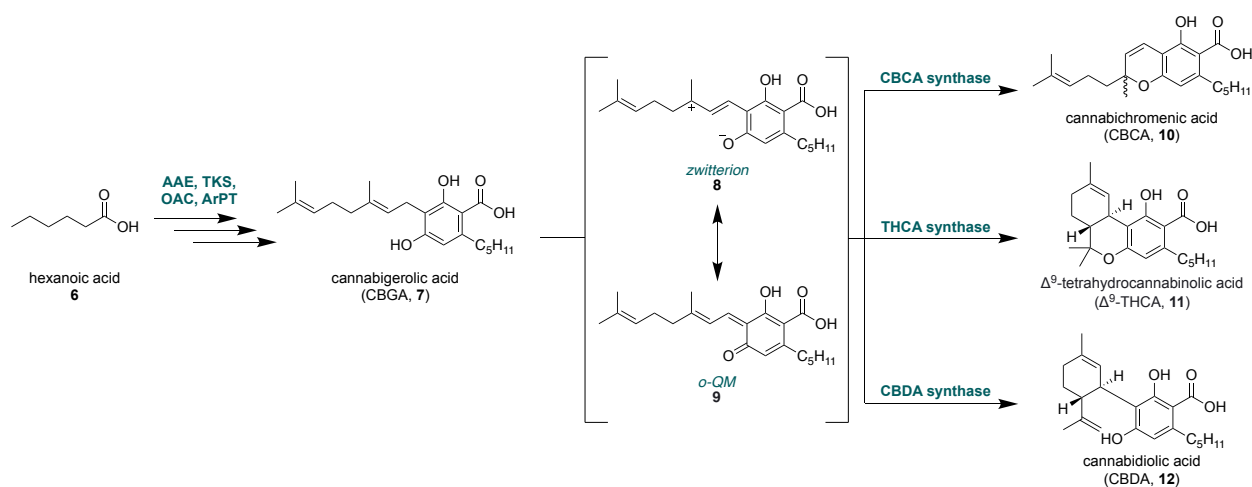
Figure 1.2. Crystal structure of EcBBE (PDB 3D2H) illustrating bicovalent attachment of His104 and Cys166 to the 8a- and 6-positions of the isoalloxazine ring of FAD.

attributes, enzymes capable of generating *o*-QMs are well positioned to supplement synthetic endeavors that require these highly reactive intermediates. Herein, we review the known enzymes associated with *o*-QM generation in natural product biosynthetic pathways, including examples of berberine bridge enzyme-like (BBE-like) oxidases, tropolonic hetero-Diels-Alderase, S-adenosyl-L-methionine (SAM)-dependent pericyclases, and α -ketoglutarate-dependent non-heme iron oxygenases. In addition to mechanistic details, the biocatalytic potentials of these enzymes are also discussed including substrate scope, scalability, and use in chemoenzymatic syntheses. Finally, an outlook on the discovery of new *o*-QM-generating enzymes with biocatalytic potential is presented.

2. Berberine Bridge Enzyme-Like (BBE-Like) Oxidases

Flavin-dependent enzymes are versatile redox catalysts in primary and secondary metabolic pathways and account for more than half of the characterized enzymes involved in generating *o*-QMs.^{26,27} This versatility is exemplified not only by the diversity of substrates accepted, but also in the impressive chemo-, regio-, and stereoselectivity displayed by the enzymes. Coincidentally, all of the characterized flavin-dependent

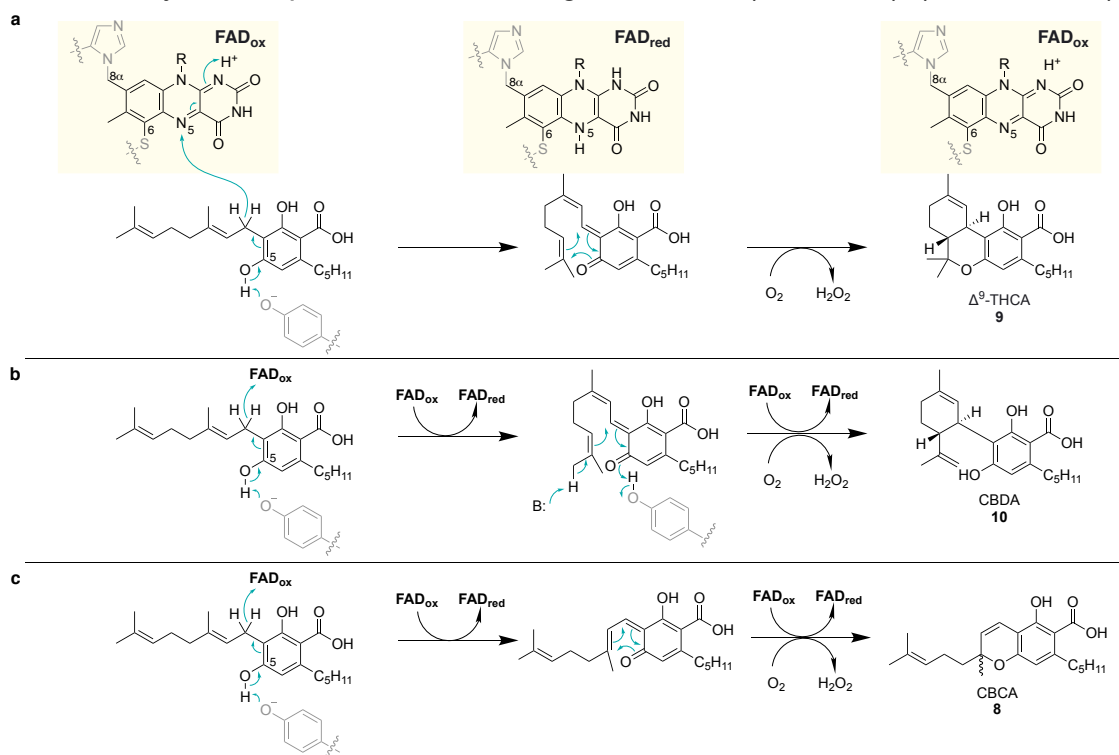
enzymes associated with *o*-QM formation belong to the berberine bridge enzyme-like (BBE-like) oxidases family.²⁸ The BBE-like oxidase name is derived from the first enzyme characterized example, (*S*)-reticuline oxidase (EcBBE) from the California poppy (*Eschscholzia californica*), which catalyzes formation of the intramolecular C–C bond known as the “berberine bridge” observed in many benzyloquinoline alkaloids.^{29–31} BBE-like oxidases can facilitate many types of oxidation reactions, including intermolecular C–C bond formation, cyclizations, nucleophilic additions, and dehydrogenation reactions.²⁸ Structurally, BBE-like oxidases share a fold comparable to that observed in vanillyl-alcohol oxidases.^{32–34} These enzymes are distinguished by the bicovalent attachment of flavin adenine dinucleotide (FAD) to the protein by histidine and cysteine residues at the 8 α - and 6-positions of FAD, respectively (Figure 1.2).^{35,36} This bicovalent attachment increases the redox potential of FAD, provides additional structural stability to the active site, and prevents cofactor dissociation.^{37–40} Several BBE-like oxidases are hypothesized to invoke formation of an *o*-QM intermediate.^{25,41,42} In these particular examples, the oxidized FAD cofactor facilitates hydride abstraction from the



Scheme 1.1. Abbreviated biosynthesis of cannabinoids. Structural diversification is generated by BBE-like enzymes CBDA synthase, THCA synthase, and CBGA synthase. Abbreviations: AAE, acyl activating enzyme; TKS, tetraketide synthase; OAC, olivetolic acid cyclase; ArPT, aromatic prenyltransferase.

benzylic carbon and molecular oxygen acts as the terminal electron acceptor to recycle the reduced FAD, generating hydrogen peroxide as the sole byproduct in the catalytic cycle.

BBE-like oxidases are most well-recognized for their roles in the biosynthesis of phytocannabinoids (more commonly known as cannabinoids), natural products consisting of an isoprenylated resorcinol core with a *para*-positioned alkyl side chain. Cannabinoids are predominantly found in *Cannabis sativa* L. (Cannabaceae), a plant well known for its recreational and medicinal applications, and have also been isolated from certain species of liverworts and fungi.^{43–46} To date, over 100 different cannabinoids have been isolated and characterized.⁴⁷ Three primary constituents, cannabichromenic acid (CBCA, **10**), tetrahydrocannabinolic acid (THCA, **11**), cannabidiolic acid (CBDA, **12**), are derived from the same biosynthetic precursor, cannabigerolic acid (CBGA, **7**) (Scheme 1.1). The



Scheme 1.2. Proposed mechanisms for (a) THCA synthase, (b) CBDA synthase, and (c) CBCA synthase cyclization *via* *o*-QM intermediates.

decarboxylated forms of CBCA (**10**), THCA (**11**), and CBDA (**12**), cannabichromene (CBC), tetrahydrocannabinol (THC), and cannabidiol (CBD), respectively, are among the most commonly recognized cannabinoids. Hexanoic acid (**6**) is converted to CBGA (**7**) through a series of enzymatic reactions requiring an acyl activating enzyme (AAE), tetraketide synthase (TKS), olivetolic acid cyclase (OAC), and an aromatic prenyltransferase (ArPT). Rigorous biochemical investigations have elucidated the function and relationship of three BBE-like oxidases responsible for catalyzing the oxidative cyclizations of CBGA (**7**) into their respective acid products: THCA synthase, CBDA synthase, and CBCA synthase (Scheme 1.2).^{48–50} All three enzymes facilitate hydride abstraction from the benzylic position of CBGA (**7**) by the N-5 position of FAD and are differentiated by their ability to uniquely position CBGA (**7**) in the active site, resulting in different cyclized products.

There are two competing mechanisms for the subsequent cyclization reaction resulting in a carbocation shift or *o*-QM formation. Although a carbocation intermediate (**8**) is the more commonly depicted in the literature for THCA and CBDA cyclization, this zwitterionic species is simply a resonance structure of the *o*-QM (**9**) that is generated upon phenol deprotonation. Elucidation of the formal mechanism for CBCA (**10**), THCA (**11**), and CBDA (**12**) cyclization by each respective BBE-like oxidase has yet to be resolved, but proposed mechanisms are shown in Scheme 1.2. In general, an active site tyrosine residue is proposed to deprotonate the C-5 hydroxyl group of CBGA (**7**), initiating dearomatization of the benzene ring and hydride abstraction by the oxidized FAD cofactor (FAD_{ox}) to generate an *o*-QM intermediate and reduced FAD (FAD_{red}). Intramolecular

cyclization takes place along with activation of oxygen and elimination of hydrogen peroxide to regenerate FAD_{ox} and the cyclized product (Scheme 1.2).

THCA synthase has received the most attention of all reported cannabinoid BBE-like oxidases. The first reports identified a 74 kDa monomeric protein from *C. sativa* leaf extracts capable of converting CBGA (**7**) to THCA (**11**).⁴⁸ Subsequent sequencing efforts identified a 1635 base pair (bp) open reading frame encoding THCA synthase, which was heterologously expressed in insect cells using a baculovirus expression system.⁵¹ The tertiary structure of THCA synthase was determined to 2.75 Å resolution by X-ray crystallography, revealing key amino acid residues important for substrate orientation and stabilization.²⁵ In accordance with previously characterized BBE-like oxidases, Cys176 and His114 were covalently tethered to the 6- and 8 α -positions of FAD, respectively (Figure 1.3a, green). Ten additional hydrogen-bonding interactions and a disulfide bridge across Cys37 and Cys99 stabilize FAD within THCA synthase and provide structural integrity to the active site.

Mutagenesis experiments have revealed several key active site residues essential for enzyme activity.²⁵ In particular, H114A and T484F completely abolished activity,

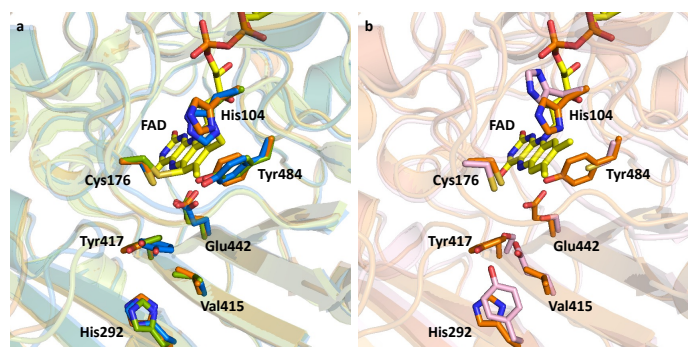


Figure 1.3. Protein homology models comparing key active site residues of BBE-like cannabinoid synthases. (a) Overlay of THCA synthase (PDB 3VTE, green), CBDA synthase model (blue), and CBCA synthase model (orange). (b) Overlay of CBCA synthase model (orange) with DCA synthase model (pink). Residue numbering is relative to THCA synthase numbering.

whereas H292A decreased activity by 95%. The loss of activity in the H114A variant can be rationalized by the loss of covalent attachment to FAD, affecting the positioning and redox potential of the cofactor. Tyr484 is hypothesized to facilitate deprotonation of the C-5 phenol, a necessary step for generating the *o*-QM and promoting regioselective cyclization (see Scheme 1.2). For reasons not fully understood, the carboxylic acid moiety in the substrate is essential for enzymatic activity.

In vitro experiments with fiber-type *C. sativa* (hemp) led to the discovery of a second BBE-like oxidase, CBDA synthase.⁴⁹ Using a similar homology-based cloning strategy to that previously implemented for THCA synthase, a 1632 bp open reading frame for CBDA synthase was identified, sharing ~84% sequence identity with THCA synthase.⁵² Sequence analysis confirmed the presence of the RSGGH and CxxI/V/LG motifs consistent with bicovalent attachment to FAD. Biochemical characterization revealed that CBDA synthase catalyzed a mechanistically similar oxidative cyclization reaction to THCA synthase but generated a different cyclized product. A second basic residue in CBDA synthase is hypothesized to abstract a proton from the terminal allylic carbon in the geranyl side chain of CBGA (**7**, Scheme 1.2b). This deprotonation step is anticipated to drive the divergent oxidative cyclization reactions between THCA synthase and CBDA synthase. Protein homology models comparing the published crystal structure of THCA synthase with CBDA synthase revealed only a small number of differences, with high conservation of the key active site residues responsible for THCA synthase activity (Figure 1.3a, blue). Recent investigations into the structure-function relationships of THCA synthase and CBDA synthase revealed that most single point THCA synthase substitutions generated to reflect the corresponding residue in CBDA synthase had little

effect on activity or product specificity.⁵³ However, a CBDA synthase A414V variant created to reflect the homologous THCA synthase residue exhibited a 3.3-fold increase in CBDA (**12**) production and a 19-fold increase in THCA (**11**) production.⁵³ Until a crystal structure of CBDA synthase is elucidated, further mutagenesis studies exploring the structure-function relationship between these two enzymes will provide further insight into the mechanisms of product differentiation.

A third BBE-like oxidase, CBCA synthase, has been characterized from *C. sativa* and was the first plant chromene-forming oxidase identified. Chromene is a common structural motif observed in natural products, including several compounds with significant antimicrobial and anticancer properties.^{50,54–56} A similar mechanistic initiation as observed with THCA and CBDA synthases can be envisioned for CBCA synthase by formation of the *o*-QM intermediate. CBCA synthase then facilitates nucleophilic attack by the phenolic oxygen, similar to THCA synthase, but differs by generating a mixture of enantiomeric chromenes (Scheme 1.2c). The reaction is known to generate a mixture of spirocyclic enantiomers, but the absolute stereochemical assignment as to which is the favored remains unknown.⁵⁷ Similar to CBCA synthase, protein homology models do not indicate any significant variations within the active site (Figure 1.3a, orange). The difference is the stereoselectivity observed between THCA synthase and CBDA synthase, which produce one enantiomeric product exclusively, while the mixture of enantiomers generated by CBCA synthase suggests that cyclization may not take place within the enzyme active site.

A CBCA synthase homolog was the only reported FAD-dependent oxidase capable of generating chromenes until the recent discovery of daurichromenic acid

synthase, which shares 49% sequence identity with THCA synthase.^{58,59} Daurichromenic acid (DCA, **15**), isolated from *Rhododendron dauricum* (Ericaceae), is a meroterpenoid natural product structurally related to cannabinoids with potent anti-HIV properties.⁶⁰ DCA (**15**) and its biosynthetic precursor, grifolic acid (**13**), differ from the previously described cannabinoids by the longer, farnesyl group and shorter alkyl chain (Figure 1.4a). DCA synthase generates the chromene moiety via a similar *o*-QM intermediate as CBCA synthase (**14**) but differs in that a single enantiomer is produced (DCA, **15**), suggesting that cyclization may occur within the active site (Figure 1.3b). Further experiments demonstrated that DCA synthase can accept grifolic acid derivatives (**16**, **18**) with prenyl groups of various lengths but exhibited no activity with CBGA (**7**). This is presumably due to substrate binding interference by the pentyl chain, as DCA synthase was able to react with cannabigerorcinic acid (**18**), which only differs from CBGA (**7**) by alkyl chain length, to produce cannabichromeorcinic acid (**19**, Figure 1.4b). DCA synthase also showed no activity with the derivative lacking the carboxylic acid, grifolin (**20**), which is consistent with the carboxylic acid moiety requirement observed with THCA, CBDA, and CBCA synthases.

Beyond *Cannabis* and *Rhododendron* species, cannabinoids have been isolated from several species of lower plants and fungi. Two CBCA-like natural products, cannabiorcichromenic acid (**19**) and its halogenated analog 8-chlorocannabiorcichromenic acid (**22**), have been isolated from the fungus *Cylindrocarpon olidum* (Nectriaceae).⁶¹ *Albatrellus* spp. are known to produce confluentin (**23**), the decarboxylated analog of DCA (**15**).⁶² Several bibenzylc cannabinoids with THCA-like cyclizations have been isolated from the liverworts *Radula*

perrottetii, *R. marginata*, and *R. laxiramea*, including (–)-*cis*-perrottetinene (**24**) and perrottetinenic acid (**25**) (Figure 1.4c).^{44–46} Given the structural similarities to previously studied cannabinoids, it is likely that the enzymes responsible for oxidative cyclization in these bibenzylic natural products also belong to the FAD-dependent subfamily of BBE-like oxidases. Identification and characterization of these enzymes will create opportunities to engineer unprecedented cannabinoid derivatives with unique prenyl moieties, alkyl chains, and cyclized patterns. Additionally, the presently characterized cannabinoid synthases could be used as genetic hooks in attempting to identify homologs

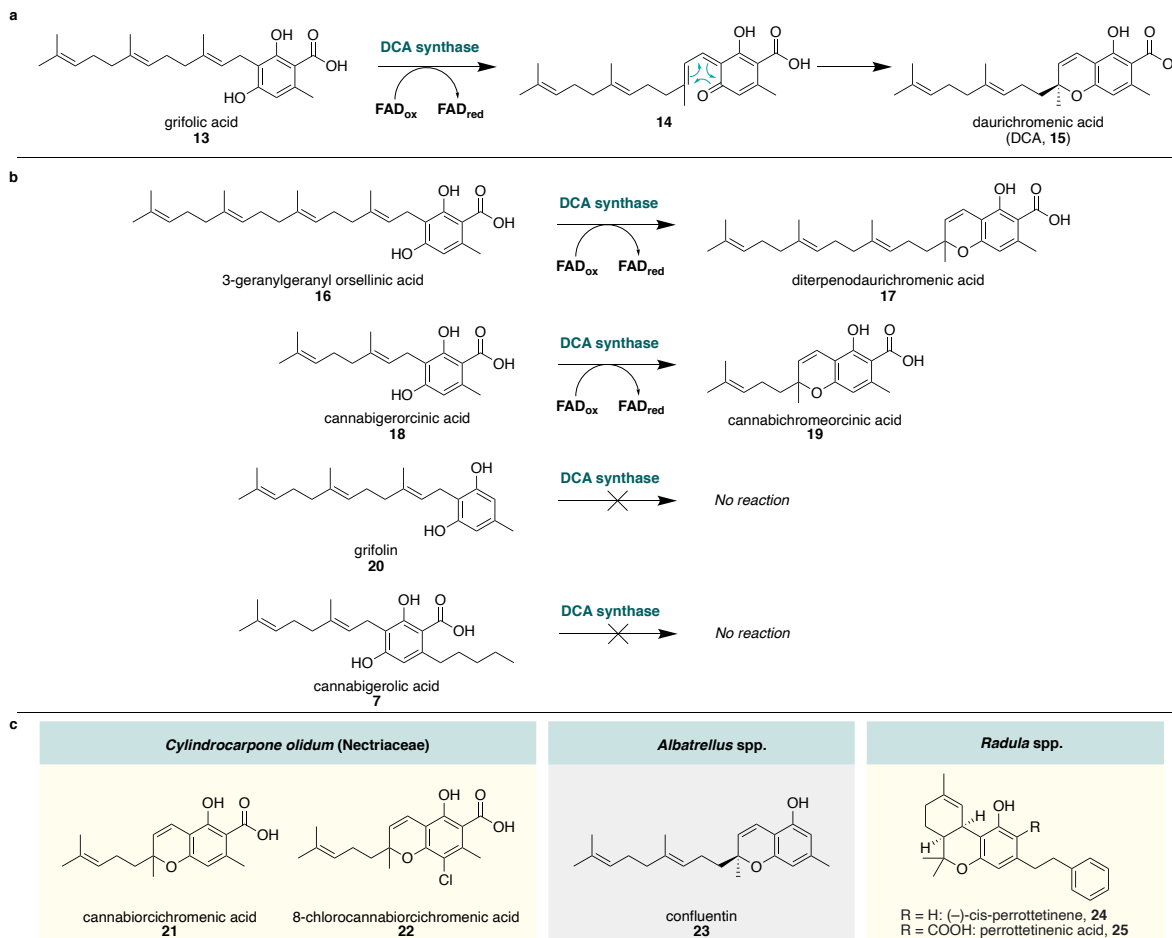
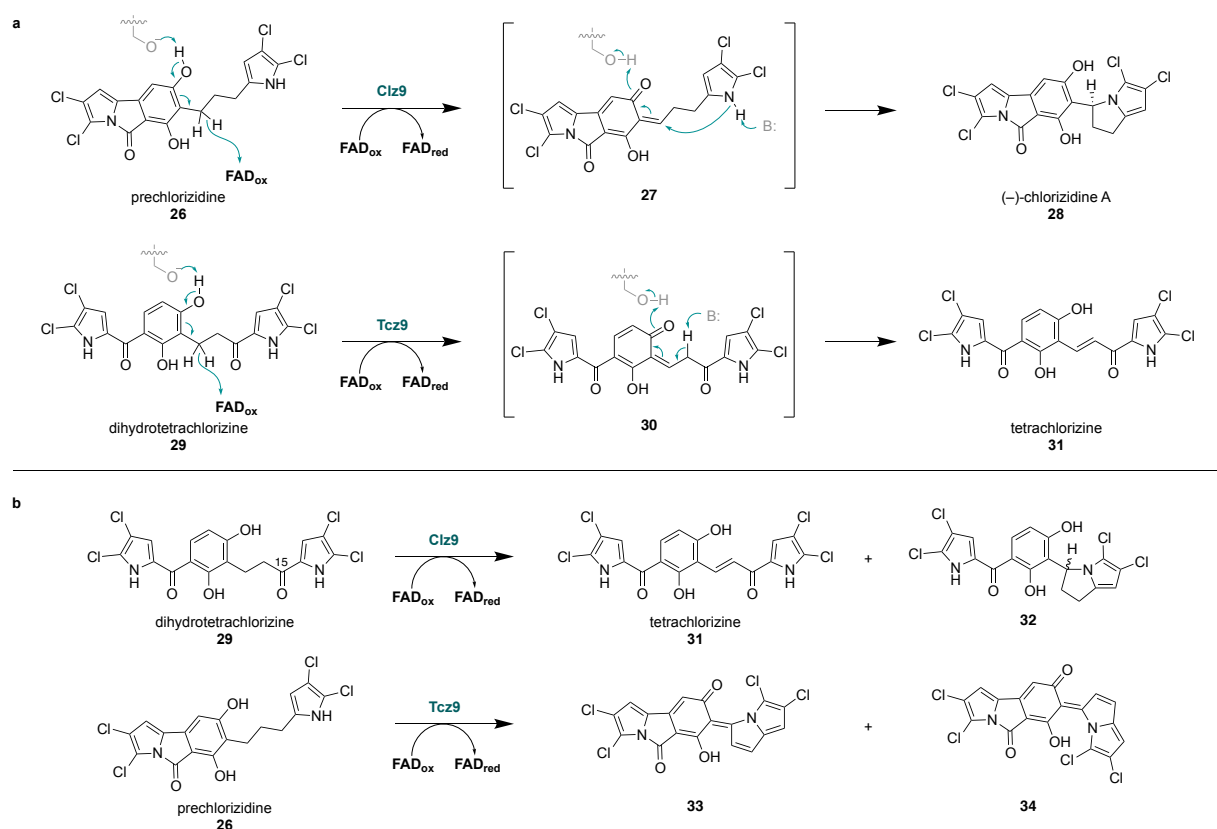


Figure 1.4. *In vitro* reactions with DCA synthase. (a) Confirmation of the role of DCA synthase in daurichromenic acid (**15**) biosynthesis. (b) Substrate screening with DCA synthase exhibits activity with various prenyl attachments but no activity with grifolin (**20**) or cannabigerolic acid (**7**). (c) Structurally related cannabinoids isolated from liverworts and fungi.

from publicly available genomic datasets that may accept similar substrates and perform the desired chemistry on complimentary substrate scopes.

Bacterial flavoenzymes are well-documented to catalyze a broad range of redox reactions in natural product biosynthesis.^{26,27} Coincidentally, the only two reported bacterial enzymes capable of generating *o*-QMs also belong to the BBE-like oxidase family of flavoenzymes. Next generation sequencing of the marine bacterium *Streptomyces* sp. CNH-287 revealed a biosynthetic gene cluster (BGC) putatively capable of producing the tetrachlorinated alkaloid, (-)-chlorizidine A (**28**, *clz*).⁴¹ Genetic knockout experiments and *in vitro* biochemical characterization of the putative BBE-like oxidase Clz9 confirmed its role in chlorizidine A (**28**) biosynthesis. This reaction is thought



Scheme 1.3. (a) Proposed mechanisms for cyclization vs. dehydrogenation with microbial BBE-like oxidases Clz9 and Tcz9. (b) Comparing and contrasting catalytic functions of Clz9 and Tcz9 with non-native biosynthetic precursors.

to be mechanistically similar to cannabinoid synthases, initiated by benzylic hydride abstraction of prechlorizidine (**26**) via a bicovalently tethered FAD cofactor and phenolic deprotonation by a basic residue within the active site to generate the reactive *o*-QM intermediate **27**. Clz9 catalyzes a stereoselective, intramolecular cyclization by nucleophilic addition of the pyrrole nitrogen, ultimately generating the unusual dihydropyrrolizine ring of chlorizidine A (Scheme 1.3a).

Support for the proposed benzylic functionalization via an *o*-QM in Clz9 was provided with the recent discovery of a second bacterial BBE-like oxidase, Tcz9. Next generation sequencing of a taxonomically distinct marine *Actinomyces* strain AJS-327 revealed a BGC with striking similarities to the BGC associated with (–)-chlorizidine A biosynthesis and was proposed to be linked to the production of two novel tetrachlorinated alkaloids produced by the strain, dihydrotetrachlorizine (**29**) and tetrachlorizine (**31**).⁴² Genes in the associated cluster, abbreviated *tcz*, were heterologously expressed. *In vitro* biochemical characterization of the BBE-like oxidase from the BGC, Tcz9, confirmed its catalytic function acting as a dehydrogenase in tetrachlorizine (**31**) biosynthesis (Scheme 1.3a). Similar to Clz9, an *o*-QM intermediate (**30**) is proposed from hydride abstraction on dihydrotetrachlorizine (**29**). Rather than undergoing intramolecular cyclization with the pyrrole, the *o*-QM intermediate is deprotonated to yield the dehydrogenated tetrachlorizine (**31**) product. The C-15 carbonyl of dihydrotetrachlorizine (**29**) is thought to influence the reaction outcome by lowering the pKa of the α -proton, but further substrate screening is required to provide evidence for this hypothesis. This is the first reported example of a dehydrogenated product generated via an *o*-QM intermediate, further expanding the utility of *o*-QMs and the unique chemoselectivity facilitated by enzymes.

Clz9 and Tcz9 have also been shown to catalyze intriguing oxidative reactions with non-native substrates (Scheme 1.3b).⁴² Incubation of Clz9 with dihydrotetrachlorizine (**29**), the biosynthetic precursor to tetrachlorizine, yielded a mixture of dehydrogenated (**31**) and cyclized (**32**) products. This indicates Clz9 preferentially acts as a cyclase but must also compete with dehydrogenation in the presence of the C-15 carbonyl moiety. More intriguing are the products generated upon incubation of Tcz9 with prechlorizidine (**26**), the biosynthetic precursor to (–)-chlorizidine A (**28**). Not only is Tcz9 capable of acting as a cyclase, but it also performs two subsequent dehydrogenation reactions on prechlorizidine (**26**), generating two isolable *o*-QM configurational isomers that are stable at room temperature (**33-34**). These products provide key mechanistic insight into how these BBE-like oxidases function and demonstrate their exceptional utility in generating a variety of oxidized products. Further structure-activity relationship studies will reveal key mutations that are responsible for the functional differences between these two enzymes.

3. Tropolonic Hetero-Diels-Alderases

The Diels-Alder reaction is one of the most powerful concerted pericyclic transformations for efficiently constructing complex natural product scaffolds. Although Diels-Alder reactions have been utilized in organic synthesis for nearly a century and have long been postulated as key steps in biosynthetic reactions, Diels-Alderases belong to a relatively new enzyme family.^{18,63–66} Several multifunctional enzymes have demonstrated the ability to catalyze concerted [4+2] cycloaddition reactions, but the discovery of SpnF in spinosyn A biosynthesis ushered in a wave of standalone intramolecular Diels-Alder

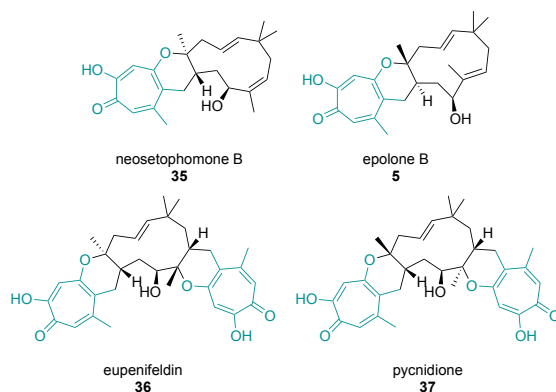


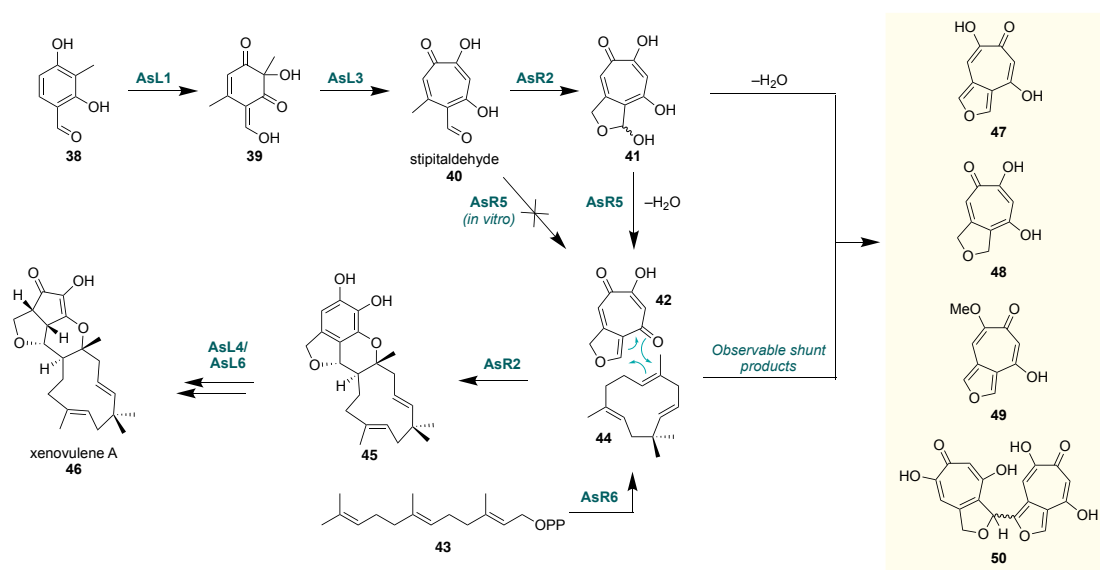
Figure 1.5. Representative examples of tropolonic sesquiterpenoids likely derived from hetero-Diels-Alder cyclization reactions. The *o*-QM portion is highlighted in teal.

cyclases.⁶⁷ Recently, the first standalone [4+2] intermolecular carbocyclase, MaDA, was characterized from *Moraceae alba* and exhibits promising biocatalytic utility.⁶⁸

Hetero-Diels-Alderase have also received considerable interest for their suspected role in meroterpenoid biosyntheses.^{69,70} Many of these proposed biosyntheses suggest an *o*-QM acts as an electron-deficient diene that reacts with a dienophile, such as an alkene, forming a dihydropyran ring. This motif is common in hundreds of plant meroterpenoids, especially those found in *Eucalyptus* spp. and *Psidium guajava* L. (guava).⁷¹⁻⁷⁷ Synthetic approaches have demonstrated some of these hetero-Diels-Alder (hDA) reactions can occur non-enzymatically, but one class of meroterpenoid natural products, tropolonic sesquiterpenoids, have proven difficult to synthesize biomimetically.^{78,79} Furthermore, the isolation of enantiopure metabolites suggests enzymatic influence, as a non-enzymatic reaction would theoretically generate a racemic mixture. Given the therapeutic interests and structural complexities of example compounds shown in Figure 1.5 (**5**, **35-37**), identifying enzymes that can catalyze stereospecific hDA reactions using a reactive species like a tropolone *o*-QM will likely have tremendous biocatalytic value.

Genes associated with the biosynthesis of humulene (**44**) and the tropolone core have been previously characterized and are highly conserved across fungal species known to produce tropolonic sesquiterpenoids.^{80,81} However, the key linkage between the aromatic core and terpene remained elusive. The first tropolonic hetero-Diels-Alderase was reported in 2018 with the identification of a gene cluster in *Sarocladium schorii* (previously *Acremonium strictum* IMI 501407) that resembled previously characterized gene clusters associated with the production of tropolones, but also included several genes with unknown functions.⁶⁹ Heterologous expression of the captured gene cluster in *Aspergillus oryzae* led to the production of xenovulene A (**46**), a meroterpenoid natural product and potent antagonist for the human γ -aminobutyrate A (GABAA) benzodiazepine receptor with promising anti-depressant properties (Scheme 1.4).

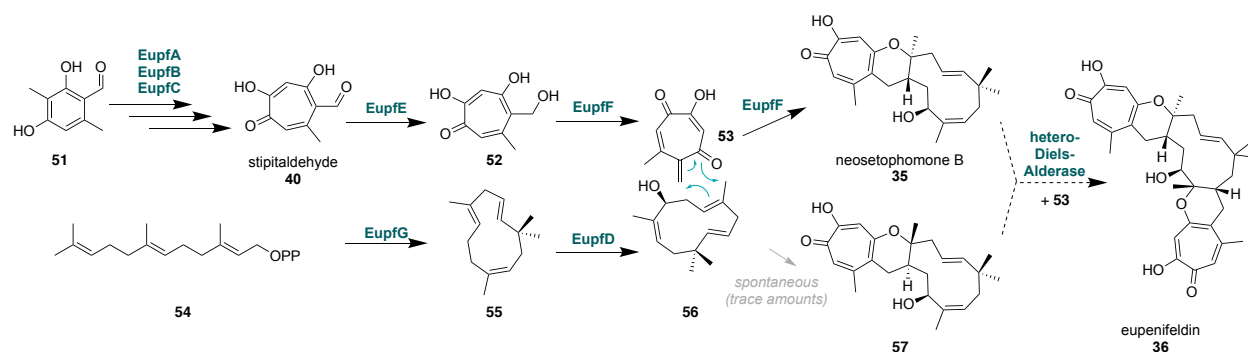
In xenovulene A (**46**) biosynthesis, the humulene (**44**) constituent is produced by AsR6 from farnesyl pyrophosphate (**43**), while stipitaldehyde (**40**) is generated in a two-



Scheme 1.4. Proposed biosynthesis of xenovulene A (**46**) via a tropolonic *o*-QM intermediate. The function of AsR5 was not verified *in vitro*, however, the presence of shunt products **47-50** is evidence supporting an *o*-QM intermediate.

enzyme cascade starting with aldehyde **38** to form *o*-QM **39** that undergoes ring expansion via AsL3. The two pieces, stipitaldehyde (**40**) and humulene (**44**), were thought to be coupled by AsR5, a gene encoding a 401 amino acid protein with no significant sequence homology to any reported Diels-Alderaes, as indicated by knockout experiments. Unfortunately, *in vitro* experiments investigating the function of AsR5 were inconclusive, as AsR5 exhibited no activity when attempting to couple stipitaldehyde (**40**) with humulene (**44**). It is proposed that **40** requires further oxidation by a cytochrome P450 embedded in the BGC (AsR2), forming hemiacetal **41** prior to hDA cyclization. This intermediate could not be isolated, but non-enzymatic dehydration and formation of a tropolonic *o*-QM could explain the isolable shunt products **47-50**. Further evidence for enzymatic *o*-QM formation and hDA cyclization is supported by the isolation of a single stereoenriched product **42**, and biomimetic syntheses that have demonstrated hDA reactions between a tropolonic *o*-QM and humulene (**44**) require harsh reaction conditions,^{78,79} suggesting the reaction is unlikely to occur spontaneously.

Shortly after the characterization of the xenovulene A (**46**) biosynthetic gene cluster, a second gene cluster associated with the production of the potent anti-glioma meroterpenoid eupenifeldin (**36**) was identified by genomic analysis and genetic disruption of *Phoma* sp. CGMCC 10481.⁷⁰ Sequence analysis confirmed genes with high sequence identity to those previously reported in tropolone and humulene (**44**) biosynthesis, including a gene encoding a putative hetero-Diels-Alderase (*eupF*). *In vitro* experiments confirming the function of the putative hetero-Diels-Alderase were inconclusive yet again due to protein solubility issues and the instability of the tropolone *o*-QM precursor (Scheme 1.5). Later the same year, whole genome sequencing



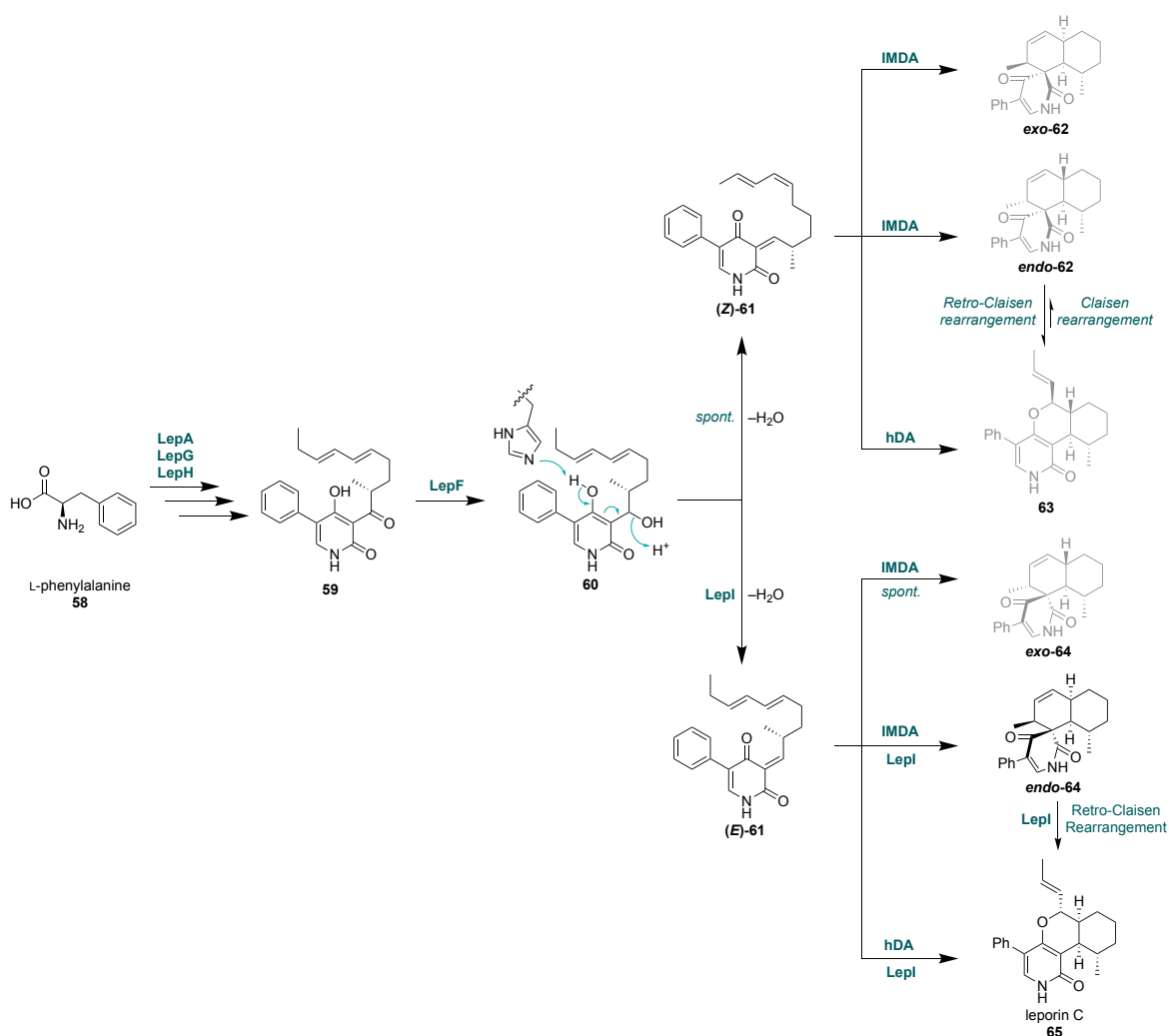
Scheme 1.5. Proposed biosynthesis of eupenifeldin (**36**) via two *o*-QM intermediates. Genes responsible for production of neosetophomone B (**35**), EupfA-F and EupF, a homolog of EupfF were characterized by heterologous expression or *in vitro* experiments.

of *Penicillium janthinellum* led to the discovery of a third biosynthetic gene cluster (*eupfA-J*) containing all the necessary genes from tropolonic sesquiterpenoid production, including another putative hetero-Diels-Alderase (EupfF) with 67% identity to EupF.⁸² A key finding in this work was the *in vitro* characterization of EupfE, a short-chain dehydrogenase that reduces stipitaldehyde (**40**), this time generated in a three-enzyme cascade from aldehyde **51**, to the alcohol **52**, priming this intermediate for dehydration and subsequent *o*-QM formation. EupfF exhibited similar solubility issues to previous accounts, but follow-up attempts to obtain the previously reported homolog EupF as a soluble protein eventually proved to be successful. Alcohol **52** can undergo spontaneous dehydration, *o*-QM formation (**53**), and non-enzymatic cyclization with **55** to generate **57**, but the addition of EupfF significantly accelerates the reaction and generates a single diastereomer product, neosetophomone B (**35**). However, EupfF did not exhibit any activity to catalyze a second hDA reaction, leaving the possibility open for a second hetero-Diels-Alderase enzyme to complete the biosynthesis of bistropolonic meroterpenoid eupenifeldin (**36**). The efficient construction of stereospecific products via *o*-QMs using prochiral substrates has tremendous biocatalytic utility. Although this family

of intermolecular hetero-Diels-Alderase is relatively new, genome mining efforts and biochemical validation will unveil new enzymes with similar capabilities.

4. SAM-Dependent O-Methyltransferase-Like Pericyclase

S-Adenosyl-L-methionine (SAM)-dependent methyltransferases are a ubiquitous family of enzymes in primary and secondary metabolism. Canonical SAM-dependent methyltransferases catalyze the transfer of a methyl group to C, N, O, or S atoms from SAM, but this family of enzymes has expanded over time to include several non-methylation reactions.⁸³⁻⁸⁶ LepI is one such example of a non-canonical SAM-dependent O-methyltransferase, acting as a dehydratase and pericyclase in leporin C (**65**) biosynthesis.⁸⁷ Pathway reconstruction of key genes associated with leporin C (**65**) biosynthesis unveiled LepI is not essential for production; however, *in vitro* experiments confirmed that LepI is required for the accelerated and exclusive production of leporin C (**65**). The pathway begins in a three-enzyme cascade from L-phenylalanine (**58**) to yield **59**. Reduction of **59** and production of the alcohol intermediate **60** by LepF leads to non-enzymatic dehydration and formation of both (*E/Z*) geometric isomers of the *o*-QM intermediate (**61**), yielding multiple intramolecular and inverse electron demand hetero-Diels-Alder reaction outcomes (**62-64**) (Scheme 1.6). In comparison, incubation of **60** with LepI leads to the stereospecific production of leporin C (**65**) via an *o*-QM. Small amounts of *endo*-**64** were detectable at early timepoints when **60** was incubated with LepI; however, LepI can recycle this byproduct via a retro-Claisen rearrangement to produce leporin C (**65**) exclusively. Crystallographic analysis of LepI has revealed key active site residues that form a hydrogen bonding network for proper substrate stabilization and



Scheme 1.6. Leporin C (**65**) biosynthetic pathway. In the absence of LepI, **60** undergoes spontaneous dehydration and forms a mixture of non-enzymatic intramolecular Diels-Alder (IMDA) and hetero-Diels-Alder (hDA) products. Structures in gray are generated non-enzymatically. LepI can recycle endo-IMDA product **64** to stereoselectively produce leporin C (**65**).

orientation. Although the precise catalytic role of the SAM cofactor is not fully understood, the positively charged sulfonium ion is suggested to electrostatically stabilize *o*-QM intermediate (*E*)-**61**.⁸⁸ Understanding the role of the SAM cofactor will be critical in genome mining and protein engineering efforts to broaden the utility of the SAM-dependent methyltransferase enzyme family capable of manipulating *o*-QMs for additional oxidative reactions.

5. α -KG Dependent Non-Heme Iron Oxygenases

α -Ketoglutarate (α -KG) dependent non-heme iron oxygenases are a versatile family of enzymes known to catalyze remarkably diverse reactions, including hydroxylation, halogenation, epoxidation, desaturation, epimerization, endoperoxidation, ring contraction, and ring expansion.^{89–91} As their name suggests, these enzymes require α -KG for activation of a Fe(II) cofactor. ClaD is an α -KG dependent non-heme iron oxygenase associated with the biosynthesis of penilactone and peniphenone natural products produced by *Penicillium* spp., as confirmed by genetic knockout experiments.⁹² Penilactones and pheniphenones are aromatic polyketide fungal metabolites derived from clavatul (**77**) coupled with a range of adducts giving rise to diverse biological activities (**3**, **66-76**, Figure 1.6a).^{21,93–95} ClaD shares high sequence identity (54%) with CitB, an α -KG dependent non-heme iron oxygenase known to catalyze a benzylic

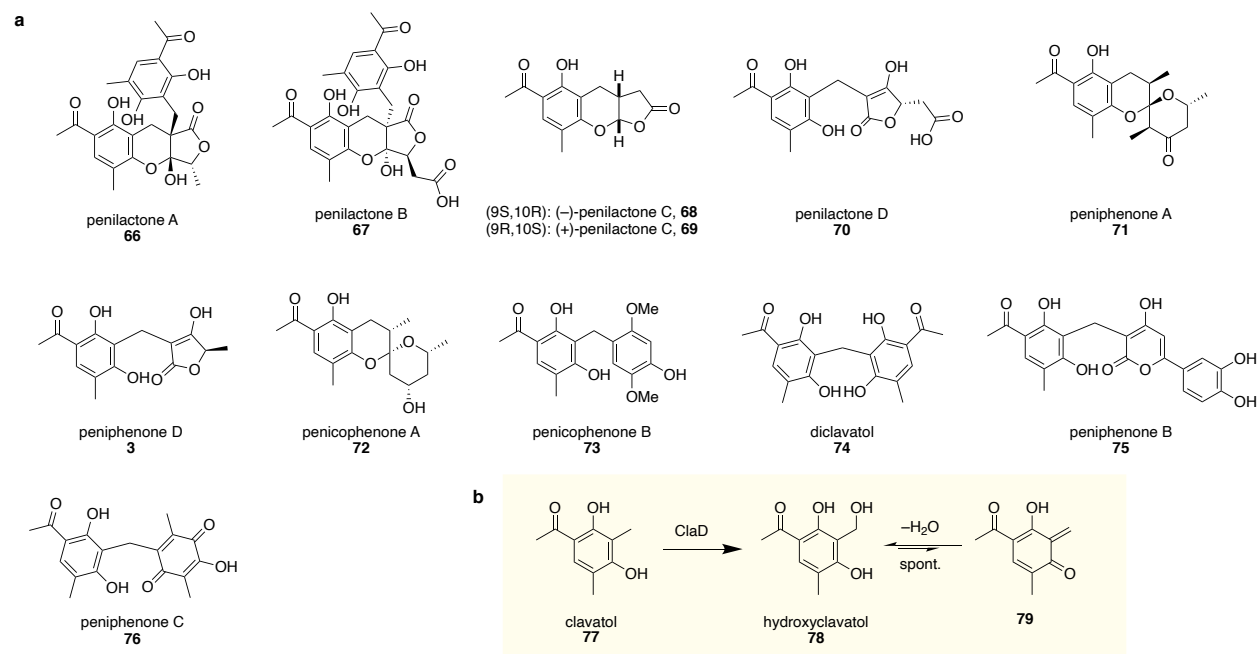


Figure 1.6. (a) Clavatul (**77**)-derived natural products from *Penicillium* sp. (b) Regioselective benzylic hydroxylation by α -KG dependent non-heme iron oxygenase ClaD, which undergoes “indirect” (spontaneous) dehydration to produce a reactive *o*-QM.

hydroxylation in citrinin biosynthesis. *In vitro* experiments demonstrated ClaD also hydroxylates clavatul (**77**) regioselectively, activating this biosynthetic intermediate for *o*-QM formation through hydroxyclavatul (**78**) to yield **79** (Figure 1.6b).⁹² This distinguishes ClaD from the previously described BBE-like oxidases, tropolonic hetero-Diels-Alderases, and SAM-dependent *O*-methyltransferase LepI, which catalyze “direct” *o*-QM formation, stabilizing and orienting the *o*-QM within the active site for further manipulation. Instead, ClaD facilitates “indirect” *o*-QM formation, activating clavatul (**77**) for subsequent non-enzymatic dehydration. This process can be observed by isotope labeling experiments with H₂¹⁸O which can add be incorporated by reversible dehydration of hydroxyclavatul (**78**) and nucleophilic addition by isotope labeled water.⁹² The reversibility of the dehydration and nucleophilic addition reactions via the *o*-QM allows other nucleophiles present in solution to react, as observed by the coupling of various electron-rich functional groups with clavatul (**77**). This benzylic functionalization strategy developed by Nature has been validated by biomimetic syntheses of several clavatul-derived natural products via *o*-QMs.⁹⁶

6. Biocatalytic Utility of Enzymatic *o*-QMs

Synthetic approaches to *o*-QM formation have been reported in numerous biomimetic natural product syntheses, but these approaches typically suffer from poor atom economy and require toxic chemical reagents, only to achieve the same reaction outcome that nature has already optimized. Some complex molecules derived from *o*-QMs, such as the tropolonic sesquiterpenes previously described in this review, are still synthetically intractable. Thus, leveraging enzymes for biocatalytic generation of *o*-QMs

and engineering these proteins to perform chemo-, regio-, and stereoselective reactions efficiently will supplement traditional synthetic approaches.

Heterologous expression is an attractive solution to access rare or unnatural cannabinoids that cannot be efficiently produced by current cultivation and synthetic methods.^{97–99} THCA synthase, CBDA synthase, and CBCA synthase have received considerable attention for their ability to catalyze cyclization reactions and have been successfully integrated into numerous eukaryotic expression systems.^{98,100–103} Mutagenesis experiments have identified several key active site residues, but additional mutagenic and crystallographic experiments are required to fully understand how these enzymes catalyze different cyclization reactions from the same *o*-QM intermediate. The recent characterization of DCA synthase is a promising start for generating analogs with various prenyl attachments. Further genome mining and engineering efforts of BBE-like enzymes across all domains of life may provide access to additional cannabinoid-like scaffolds.

Synthetic approaches coupling clavatul-like precursors with non-biogenic coupling partners have been reported; however, these typically require high temperatures, organic solvents, and protection of the clavatul (**77**) intermediate prior to *o*-QM generation. Alternatively, biological systems have been developed to achieve this same purpose using milder conditions and aqueous buffers. Cloning the fungal non-reducing polyketide synthase (PKS) gene *pksCH-2* into an *Aspergillus oryzae* heterologous host produced chaetophenol A (**80**) and derivatives **81–82**. These intermediates are reductively cyclized by an endogenous enzyme *in vivo*, yielding the isochromenes **83–85** that tautomerize to *o*-QMs (**86–88**), leading to production of chaetophenol E (**93**) and new oligomeric

analogs.¹⁰⁴ Acid- or base-promoted tautomerization or chemical oxidation also invoked to *o*-QM formation. In total, 40 novel polyketide oligomers (e.g. **92-93**), azaphilone-type molecules (e.g. **89-91**), and indole-polyketide hybrid molecules (e.g. **94-96**) were prepared using this diversity-oriented semi-synthetic process and screened for antiviral activity (Figure 1.7a). A similar combinatorial approach was developed by incubating nucleophiles with the hydroxyclavatul (**78**)-producing strain *Penicillium crustosum* PRB-2, which led to the isolation of 15 novel clavatul-alkaloid derivatives screened for antiviral activity (e.g. **97-100**, Figure 1.7b).¹⁰⁵ These semi-synthetic approaches achieve both

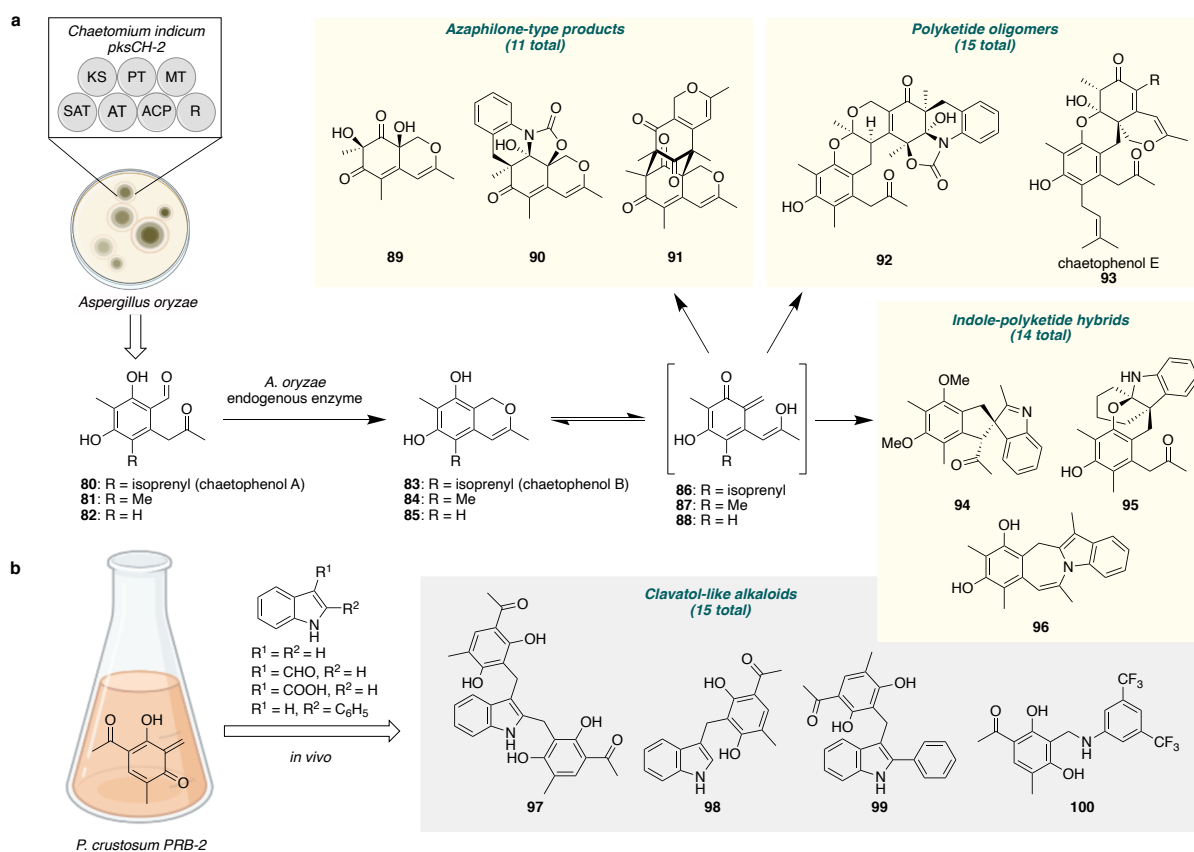
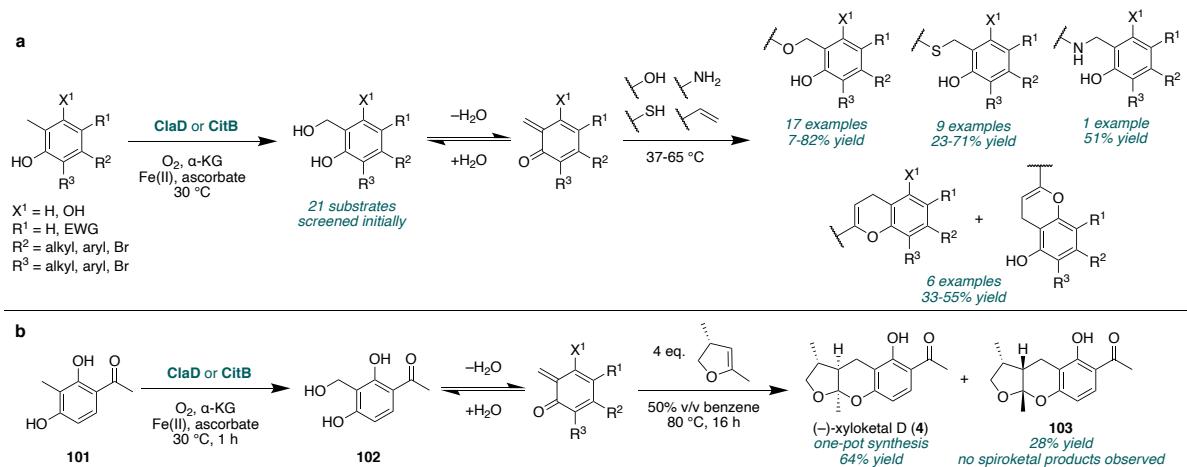


Figure 1.7. Biocatalytic developments for *in vivo* *o*-QM formation and benzylic functionalization with non-natural substrates, resulting in the rapid generation of diverse “pseudo-natural product” libraries. (a) Chaetophenol A (**80**) undergoes reductive cyclization by an endogenous enzyme in the heterologous host, which readily tautomerizes to produce a highly reactive *o*-QM intermediate. (b) Production of clavatul-like alkaloids by reacting hydroxyclavatul (**78**) with indoles and aniline-type nucleophiles *in vivo*.



Scheme 1.7. Chemoenzymatic benzylic functionalization reactions *via* an *o*-QM with α -KG dependent non-heme iron oxygenases ClaD and CitB. (a) Various aryl-substituted substrates could be accepted. Additional nucleophiles could be added to the reaction mixture after benzylic alcohol protection. (b) One-pot chemoenzymatic synthesis of (-)-xyloketal D (**4**).

efficient construction of *o*-QMs and structural diversification for rapid combinatorial library generation.

ClaD and CitB have also demonstrated remarkable substrate promiscuity to generate benzylic alcohols that can undergo facile *o*-QM formation.¹⁰⁶ In total, 21 of the 22 aromatic substrates screened *in vitro* were accepted by either ClaD or CitB (Scheme 1.7a). The only substrate that showed no activity with both ClaD and CitB was lacking any substituents at R1, indicating that an electron withdrawing group is essential at this position. These benzylic alcohols could be further functionalized by gentle heating and addition of various alcohols, amines, thiols, and alkenes to the reaction mixture. This process is compatible with chemoselectively labeling cysteine-containing peptides *in situ*, which could be applicable for biorthogonal chemistry applications. These reactions could be scaled up to >500 mg with no enzyme purification required. This mild one-pot process was also applied to chemoenzymatically synthesize (-)-xyloketal D (**4**) and its diastereomer (**103**) from **101** in a 2:1 ratio with overall improved yields compared to any previously reported total synthesis (Scheme 1.7b). This strategy is amenable to

chemoenzymatically synthesize chromane-containing natural products and derivatives alike.

7. Conclusions and Future Directions

ortho-Quinone methides are notoriously reactive chemical intermediates that require careful manipulation to achieve desired chemo-, regio-, and stereoselective outcomes. Numerous chemical approaches have been designed to harness *o*-QMs in natural product total syntheses but face many obstacles to be effectively utilized. Nature has refined its own strategies to generate *o*-QMs with greater chemo-, regio-, and stereoselectivity. Recent advancements in sequencing technology and synthetic biology have revealed eleven enzymes across four distinct families thus far that can generate *o*-QMs and perform oxidative cyclizations, intra- and intermolecular nucleophilic addition reactions, dehydrogenations, and hetero-Diels-Alder reactions. The remarkable enzyme and substrate diversity reported so far is a promising starting point for engineering enzymes for biocatalytic *o*-QM generation and utilization. Furthermore, the presently known enzymes can be used as probes in genome mining efforts to identify similar enzymes with complementary reactivity, improved catalytic activity, and to aid in the discovery of new biosynthetic gene clusters.

Chapter 1 has been submitted for publication in the Journal of Natural Products, 2022, Purdy, Trevor N.; Moore, Bradley S.; Lukowski, April L. The dissertation author was primary author of this material.

References

1. Atanasov, A. G.; Zotchev, S. B.; Dirsch, V. M.; Supuran, C. T. Natural Products in Drug Discovery: Advances and Opportunities. *Nat. Rev. Drug Discov.* **2021**, *20*, 200–216.
2. Bergquist, P. L.; Siddiqui, S.; Sunna, A. Cell-Free Biocatalysis for the Production of Platform Chemicals. *Front. Energy Res.* **2020**, *8*, 1–22.
3. Tibrewal, N.; Tang, Y. Biocatalysts for Natural Product Biosynthesis. *Annu. Rev. Chem. Biomol. Eng.* **2014**, *5*, 347–66.
4. Medema, M. H.; de Rond, T.; Moore, B. S. Mining Genomes to Illuminate the Specialized Chemistry of Life. *Nat. Rev. Genet.* **2021**, *22*, 553–571.
5. Scherlach, K.; Hertweck, C. Mining and Unearthing Hidden Biosynthetic Potential. *Nat. Commun.* **2021**, *12*, 1–12.
6. Liu, Z.; Zhao, Y.; Huang, C.; Luo, Y. Recent Advances in Silent Gene Cluster Activation in *Streptomyces*. *Front. Bioeng. Biotechnol.* **2021**, *9*, 1–10.
7. Milshteyn, A.; Schneider, J. S.; Brady, S. F. Mining the Metabiome: Identifying Novel Natural Products from Microbial Communities. *Chem. Biol.* **2014**, *21*, 1211–1223.
8. Chekan, J. R.; McKinnie, Shaun M. K.; Moore, Malia L.; Poplawski, Shane G.; Michael, Todd P, Moore, Bradley S. Scalable Biosynthesis of the Seaweed Neurochemical, Kainic Acid. *Angew. Chemie Int. Ed.* **2019**, *58*, 8454–8457.
9. Han, R.; Rai, A.; Nakamura, M.; Suzuki H.; Takahashi H.; Yamazaki M.; Saito K. *De Novo* Deep Transcriptome Analysis of Medicinal Plants for Gene Discovery in Biosynthesis of Plant Natural Products. In *Methods in Enzymology*, Vol. 576; Academic Press, 2016.
10. Suryamohan, K.; Krishnankutty, S. P.; Guillory, J.; Jevit, M.; Schröder, M. S.; Wu, M.; Kuriakose, B.; Mathew, O. K.; Perumal, R. C.; Koludarov, I.; Goldstein, L. D.; Senger, K.; Dixon, M. D.; Velayutham, D.; Vargas, D.; Chaudhuri, S.; Muraleedharan, M.; Goel, R.; Chen, Y.-J. J.; Ratan, A.; Liu, P.; Faherty, B.; de la Rosa, G.; Shibata, H.; Baca, M.; Sagolla, M.; Ziai, J.; Wright, G. A.; Vucic, D.; Mohan, S.; Antony, A.; Stinson, J.; Kirkpatrick, D. S.; Hannoush, R. N.; Durinck, S.; Modrusan, Z.; Stawiski, E. W.; Wiley, K.; Raudsepp, T.; Kini, R. M.; Zachariah, A.; Seshagiri, S. The Indian Cobra Reference Genome and Transcriptome Enables Comprehensive Identification of Venom Toxins. *Nat. Genet.* **2020**, *52*, 106–117.
11. Vieira de Castro, T.; Yahiaoui, O.; Peralta, R. A.; Fallon, T.; Lee, V.; George, J. H. Biomimetic Synthesis Enables the Structure Revision of Littordials E and F and Drychampone B. *Org. Lett.* **2020**, *22*, 8161–8166.

12. Van de Water, R. W.; Pettus, T. R. R. *o*-Quinone Methides: Intermediates Underdeveloped and Underutilized in Organic Synthesis. *Tetrahedron* **2002**, *58*, 5367–5405.
13. Amouri, H.; Le Bras, J. Taming Reactive Phenol Tautomers and *o*-Quinone Methides with Transition Metals: A Structure-Reactivity Relationship. *Acc. Chem. Res.* **2002**, *35*, 501–510.
14. Ferreira, S. B.; Da Silva, F. D. C.; Pinto, A. C.; Gonzaga, D. T. G.; Ferreira, V. F. Syntheses of Chromenes and Chromanes via *o*-Quinone Methide Intermediates. *J. Heterocycl. Chem.* **2009**, *46*, 1080–1097.
15. Willis, N. J.; Bray, C. D. *ortho*-Quinone Methides in Natural Product Synthesis. *Chem. - A Eur. J.* **2012**, *18*, 9160–9173.
16. Singh, M. S.; Nagaraju, A.; Anand, N.; Chowdhury, S. *ortho*-Quinone Methide (*o*-QM): A Highly Reactive, Ephemeral and Versatile Intermediate in Organic Synthesis. *RSC Adv.* **2014**, *4*, 55924–55959.
17. Bai, W. J.; David, J. G.; Feng, Z. G.; Weaver, M. G.; Wu, K. L.; Pettus, T. R. R. The Domestication of *ortho*-Quinone Methides. *Acc. Chem. Res.* **2014**, *47*, 3655–3664.
18. Yang, B.; Gao, S. Recent Advances in the Application of Diels-Alder Reactions Involving *o*-Quinodimethanes, Aza-*o*-Quinone Methides and *o*-Quinone Methides in Natural Product Total Synthesis. *Chem. Soc. Rev.* **2018**, *47*, 7926–7953.
19. Abdissa, N.; Pan, F.; Gruhonjic, A.; Gräfenstein, J.; Fitzpatrick, P. A.; Landberg, G.; Rissanen, K.; Yenesew, A.; Erdélyi, M. Naphthalene Derivatives from the Roots of *Pentas parvifolia* and *Pentas bussei*. *J. Nat. Prod.* **2016**, *79*, 2181–2187.
20. Endale, M.; Ekberg, A.; Akala, H. M.; Alao, J. P.; Sunnerhagen, P.; Yenesew, A.; Máteérdeiyi, M. Bussei hydroquinones A–D from the Roots of *Pentas bussei*. *J. Nat. Prod.* **2012**, *75*, 1299–1304.
21. Li, H.; Jiang, J.; Liu, Z.; Lin, S.; Xia, G.; Xia, X.; Ding, B.; He, L.; Lu, Y.; She, Z. Peniphenones A–D from the Mangrove Fungus *Penicillium dipodomyicola* HN4-3A as Inhibitors of *Mycobacterium tuberculosis* Phosphatase MptpB. *J. Nat. Prod.* **2014**, *77*, 800–806.
22. Lin, Y.; Wu, X.; Feng, S.; Jiang, G.; Luo, J.; Zhou, S.; Vrijmoed, L. L. P.; Jones, E. B. G.; Krohn, K.; Steingröver, K.; Zsila, F. Five Unique Compounds: Xyloketal from Mangrove Fungus *Xylaria* sp. from the South China Sea Coast. *J. Org. Chem.* **2001**, *66*, 6252–6256.
23. Cai, P.; Smith, D.; Cunningham, B.; Brown-Shimer, S.; Katz, B.; Pearce, C.; Venables, D.; Houck, D. Epolones: Novel Sesquiterpene-Tropolones from Fungus OS-F69284 That Induce Erythropoietin in Human Cells. **1998**, *61*, 791–795.

24. Fries, K.; Kann, K. Ueber die Einwirkung von Brom und von Chlor auf Phenole: Substitutionsproducte, Pseudobromide und Pseudochloride. Ueber *o*-Pseudohalogenide und *o*-Methylenchinone aus *o*-Oxymesitylalkohol. *Justus Liebigs Ann. Chem.* **1907**, 353, 335–356.
25. Shoyama, Y.; Tamada, T.; Kurihara, K.; Takeuchi, A.; Taura, F.; Arai, S.; Blaber, M.; Shoyama, Y.; Morimoto, S.; Kuroki, R. Structure and function of Δ^1 -tetrahydrocannabinolic acid (THCA) synthase, the enzyme controlling the psychoactivity of *Cannabis sativa*. *J. Mol. Biol.* **2012**, 423, 96–105.
26. Walsh, C. T.; Wencewicz, T. A. Flavoenzymes: Versatile Catalysts in Biosynthetic Pathways. *Nat. Prod. Rep.* **2013**, 30, 175–200.
27. Teufel, R.; Agarwal, V.; Moore, B. S. Unusual Flavoenzyme Catalysis in Marine Bacteria. *Curr. Opin. Chem. Biol.* **2016**, 31, 31–39.
28. Daniel, B.; Konrad, B.; Toplak, M.; Lahham, M.; Messenlehner, J.; Winkler, A.; Macheroux, P. The Family of Berberine Bridge Enzyme-Like Enzymes: A Treasure-Trove of Oxidative Reactions. *Arch. Biochem. Biophys.* **2017**, 632, 88–103.
29. Rink, E.; Böhm, H. Conversion of Reticuline Into Scoulerine by a Cell Free Preparation from *Macleaya microcarpa* Cell Suspension Cultures. *FEBS Lett.* **1975**, 49, 396–399.
30. Steffens, P.; Nagakura, N.; Zenk, M. H. Purification and Characterization of the Berberine Bridge Enzyme from *Berberis beaniana* Cell Cultures. *Phytochemistry* **1985**, 24, 2577–2583.
31. Winkler, A.; Hartner, F.; Kutchan, T. M.; Glieder, A.; Macheroux, P. Biochemical Evidence that Berberine Bridge Enzyme Belongs to a Novel Family of Flavoproteins Containing a Bi-covalently Attached FAD Cofactor. *J. Biol. Chem.* **2006**, 281, 21276–21285.
32. Mattevi, A.; Fraaije, M. W.; Mozzarelli, A.; Olivi, L.; Coda, A.; Berkel, W. J. van. Crystal Structures and Inhibitor Binding in the Octameric Flavoenzyme Vanillyl-Alcohol Oxidase: The Shape of the Active-Site Cavity Controls Substrate Specificity. *Structure* **1997**, 5, 907–920.
33. Fraaije, M. W.; Van Berkel, W. J. H.; Benen, J. A. E.; Visser, J.; Mattevi, A. A Novel Oxidoreductase Family Sharing a Conserved FAD-Binding Domain. *Trends Biochem. Sci.* **1998**, 23, 206–207.
34. Ewing, T. A.; Fraaije, M. W.; Mattevi, A.; van Berkel, W. J. H. The VAO/PCMH Flavoprotein Family. *Arch. Biochem. Biophys.* **2017**, 632, 104–117.
35. Huang, C. H.; Lai, W. L.; Lee, M. H.; Chen, C. J.; Vasella, A.; Tsai, Y. C.; Liaw, S. H. Crystal Structure of Glucosyltransferase from *Acremonium strictum*:

- A Novel Flavinylation of 6-S-Cysteinylyl, 8 α -N1-Histidyl FAD. *J. Biol. Chem.* **2005**, *280*, 38831–38838.
36. Heuts, D. P. H. M.; Scrutton, N. S.; McIntire, W. S.; Fraaije, M. W. What's in a Covalent Bond? *FEBS J.* **2009**, *276*, 3405–3427.
 37. Massey, V. Activation of Molecular Oxygen by Flavins and Flavoproteins. *J. Biol. Chem.* **1994**, *269*, 22459–22462.
 38. Winkler, A.; Kutchan, T. M.; Macheroux, P. 6-S-Cysteinylation of Bi-Covalently Attached FAD in Berberine Bridge Enzyme Tunes the Redox Potential for Optimal Activity. *J. Biol. Chem.* **2007**, *282*, 24437–24443.
 39. Heuts, D. P. H. M.; Winter, R. T.; Damsma, G. E.; Janssen, D. B.; Fraaije, M. W. The Role of Double Covalent Flavin Binding in Chito-Oligosaccharide Oxidase from *Fusarium graminearum*. *Biochem. J.* **2008**, *413*, 175–183.
 40. Winkler, A.; Motz, K.; Riedl, S.; Puhl, M.; Macheroux, P.; Gruber, K. Structural and Mechanistic Studies Reveal the Functional Role of Bicovalent Flavinylation in Berberine Bridge Enzyme. *J. Biol. Chem.* **2009**, *284*, 19993–20001.
 41. Mantovani, S. M.; Moore, B. S. Flavin-Linked Oxidase Catalyzes Pyrrolizine Formation of Dichloropyrrole-Containing Polyketide Extender Unit in Chlorizidine A. *J. Am. Chem. Soc.* **2013**, *135*, 18032–18035.
 42. Purdy, T. N.; Kim, M. C.; Cullum, R.; Fenical, W.; Moore, B. S. Discovery and Biosynthesis of Tetrachlorizine Reveals Enzymatic Benzylic Dehydrogenation via an *ortho*-Quinone Methide. *J. Am. Chem. Soc.* **2021**, *143*, 3682–3686.
 43. Gülck, T.; Møller, B. L. Phytocannabinoids: Origins and Biosynthesis. *Trends Plant Sci.* **2020**, *25*, 985–1004.
 44. Toyota, M.; Kinugawa, T.; Asakawa, Y. Bibenzyl Cannabinoid and Bisbibenzyl Derivative from the Liverwort *Radula perrottetii*. *Phytochemistry* **1994**, *37*, 859–862.
 45. Toyota, M.; Kinugawa, T.; Asakawa, Y. New Bibenzyl Cannabinoid from the New Zealand Liverwort *Radula marginata*. *Chem. Pharm. Bull.* **2002**, *50*, 1390–1392.
 46. Chicca, A.; Schafroth, M. A.; Reynoso-Moreno, I.; Erni, R.; Petrucci, V.; Carreira, E. M.; Gertsch, J. Uncovering the Psychoactivity of a Cannabinoid from Liverworts Associated with a Legal High. *Sci. Adv.* **2018**, *4*, 1–10.
 47. Hanuš, L. O.; Meyer, S. M.; Muñoz, E.; Tagliabatella-Scafati, O.; Appendino, G. Phytocannabinoids: A Unified Critical Inventory. *Nat. Prod. Rep.* **2016**, *33*, 1357–1392.
 48. Taura, F.; Morimoto, S.; Shoyama, Y.; Mechoulam, R. First Direct Evidence for the Mechanism of Δ^1 -Tetrahydrocannabinolic Acid Biosynthesis. *J. Am. Chem. Soc.* **1995**, *117*, 9766–9767.

49. Taura, F.; Morimoto, S.; Shoyama, Y. Purification and Characterization of Cannabidiolic-acid Synthase from *Cannabis sativa* L. *J. Biol. Chem.* **1996**, *271*, 16411–17416.
50. Morimoto, S.; Komatsu, K.; Taura, F.; Shoyama, Y. Purification and Characterization of Cannabichromenic Acid Synthase from *Cannabis sativa*. *Phytochemistry* **1998**, *49*, 1525–1529.
51. Sirikantaramas, S.; Morimoto, S.; Shoyama, Y.; Ishikawa, Y.; Wada, Y.; Shoyama, Y.; Taura, F. The Gene Controlling Marijuana Psychoactivity: Molecular Cloning and Heterologous Expression of Δ^1 -Tetrahydrocannabinolic acid synthase from *Cannabis sativa* L. *J. Biol. Chem.* **2004**, *279*, 39767–39774.
52. Taura, F.; Sirikantaramas, S.; Shoyama, Y.; Yoshikai, K.; Shoyama, Y.; Morimoto, S. Cannabidiolic-acid Synthase, the Chemotype-Determining Enzyme in the Fiber-Type *Cannabis sativa*. *FEBS Lett.* **2007**, *581*, 2929–2934.
53. Zirpel, B.; Kayser, O.; Stehle, F. Elucidation of Structure-Function Relationship of THCA and CBDA Synthase from *Cannabis sativa* L. *J. Biotechnol.* **2018**, *284*, 17–26.
54. Pratap, R.; Ram, V. J. Natural and Synthetic Chromenes, Fused Chromenes, and Versatility of Dihydrobenzo[*h*]chromenes in Organic Synthesis. *Chem. Rev.* **2014**, *114*, 10476–10526.
55. Costa, M.; Dias, T. A.; Brito, A.; Proença, F. Biological Importance of Structurally Diversified Chromenes. *Eur. J. Med. Chem.* **2016**, *123*, 487–507.
56. Raj, V.; Lee, J. 2H/4H-Chromenes—A Versatile Biologically Attractive Scaffold. *Front. Chem.* **2020**, *8*, 1–23.
57. Morimoto, S.; Komatsu, K.; Taura, F.; Shoyama, Y. Enzymological Evidence for Cannabichromenic Acid Biosynthesis. *J. Nat. Prod.* **1997**, *60*, 854–867.
58. Taura, F.; Iijima, M.; Lee, J.-B.; Hashimoto, T.; Asakawa, Y.; Kurosaki, F. Daurichromenic Acid-producing Oxidocyclase in the Young Leaves of *Rhododendron dauricum*. *Nat. Prod. Commun.* **2014**, *9*, 1329–1332.
59. Iijima, M.; Munakata, R.; Takahashi, H.; Kenmoku, H.; Nakagawa, R.; Kodama, T.; Asakawa, Y.; Abe, I.; Yazaki, K.; Kurosaki, F.; Taura, F. Identification and Characterization of Daurichromenic Acid Synthase Active in Anti-HIV Biosynthesis. *Plant Physiol.* **2017**, *174*, 2213–2230.
60. Taura, F.; Iijima, M.; Kurosaki, F. Daurichromenic Acid and Grifolic Acid: Phytotoxic Meroterpenoids that Induce Cell Death in Cell Culture of their Producer *Rhododendron dauricum*. *Plant Signal. Behav.* **2018**, *13*, 1–4.
61. Quaghebeur, K.; Coosemans, J.; Toppet, S.; Compennolle, F. Cannabiorci- and 8-Chlorocannabiorcichromenic Acid as Fungal Antagonists from *Cylindrocarpon olidum*. *Phytochemistry* **1994**, *37*, 159–161.

62. Hellwig, V.; Nopper, R.; Mauler, F.; Freitag, J.; Ji-Kai, L.; Zhi-Hui, D.; Stadler, M. Activities of Prenylphenol Derivatives from Fruitbodies of *Albatrellus* spp. on the Human and Rat Vanilloid Receptor 1 (VR1) and Characterisation of the Novel Natural Product, Confluentin. *Arch. der Pharm. Med. Chem.* **2003**, *336*, 119–126.
63. Nicolaou, K. C.; Snyder, S. A.; Montagnon, T.; Vassilikogiannakis, G. E. The Diels–Alder Reaction in Total Synthesis. *Angew. Chemie Int. Ed.* **2002**, *41*, 1668–1698.
64. Stocking, E. M.; Williams, R. M. Chemistry and Biology of Biosynthetic Diels–Alder Reactions. *Angew. Chemie Int. Ed.* **2003**, *42*, 3078–3115.
65. Klas, K.; Tsukamoto, S.; Sherman, D. H.; Williams, R. M. Natural Diels–Alderases: Elusive and Irresistible. *J. Org. Chem.* **2015**, *80*, 11672–11685.
66. Jeon, B.; Wang, S.-A.; Ruzsyczky, M. W.; Liu, H. Natural [4+2]-Cyclases. *Chem. Rev.* **2016**, *117*, 5367–5388.
67. Kim, H. J.; Ruzsyczky, M. W.; Choi, S.; Liu, Y.; Liu, H. Enzyme-Catalysed [4+2] Cycloaddition is a Key Step in the Biosynthesis of Spinosyn A. *Nature* **2011**, *473*, 109–112.
68. Gao, L.; Su, C.; Du, X.; Wang, R.; Chen, S.; Zhou, Y.; Liu, C.; Liu, X.; Tian, R.; Zhang, L.; Xie, K.; Chen, S.; Guo, Q.; Guo, L.; Hano, Y.; Shimazaki, M.; Minami, A.; Oikawa, H.; Huang, N.; Houk, K. N.; Huang, L.; Dai, J.; Lei, X. FAD-Dependent Enzyme-Catalysed Intermolecular [4+2] Cycloaddition in Natural Product Biosynthesis. *Nat. Chem.* **2020**, *12*, 620–628.
69. Schor, R.; Schotte, C.; Wibberg, D.; Kalinowski, J.; Cox, R. J. Three Previously Unrecognised Classes of Biosynthetic Enzymes Revealed During the Production of Xenovulene A. *Nat. Commun.* **2018**, *9*, 1–9.
70. Zhai, Y.; Li, Y.; Zhang, J.; Zhang, Y.; Ren, F.; Zhang, X.; Liu, G.; Liu, X.; Che, Y. Identification of the Gene Cluster for Bistropolone-Humulene Meroterpenoid Biosynthesis in *Phoma* sp. *Fungal Genet. Biol.* **2019**, *129*, 7–15.
71. Singh, I. P.; Bharate, S. B. Phloroglucinol Compounds of Natural Origin. *Nat. Prod. Rep.* **2006**, *23*, 558–591.
72. Fu, H.-Z.; Luo, Y.-M.; Li, C.-J.; Yang, J.-Z.; Zhang, D.-M. Psidials A–C, Three Unusual Meroterpenoids from the Leaves of *Psidium guajava* L. *Org. Lett.* **2010**, *12*, 656–659.
73. Shao, M.; Wang, Y.; Liu, Z.; Zhang, D.-M.; Cao, H.-H.; Jiang, R.-W.; Fan, C.-L.; Zhang, X.-Q.; Chen, H.-R.; Yao, X.-S.; Ye, W.-C. Psiguadials A and B, Two Novel Meroterpenoids with Unusual Skeletons from the Leaves of *Psidium guajava*. *Org. Lett.* **2010**, *12*, 5040–5043.
74. Shao, M.; Wang, Y.; Jian, Y.-Q.; Huang, X.-J.; Zhang, D.-M.; Tang, Q.-F.; Jiang, R.-W.; Sun, X.-G.; Lv, Z.-P.; Zhang, X.-Q.; Ye, W.-C. Guadial A and Psiguadials C

- and D, Three Unusual Meroterpenoids from *Psidium guajava*. *Org. Lett.* **2012**, *14*, 5262–5265.
75. Jian, Y.-Q.; Huang, X.-J.; Zhang, D.-M.; Jiang, R.-W.; Chen, M.-F.; Zhao, B.-X.; Wang, Y. Guapsidial A and Guadials B and C: Three New Meroterpenoids with Unusual Skeletons from the Leaves of *Psidium guajava*. *Chem. - A Eur. J.* **2015**, *21*, 9022–9027.
 76. Tang, G.-H.; Dong, Z.; Guo, Y.-Q.; Cheng, Z.-B.; Zhou, C.-J.; Yin, S. Psiguajadials A-K: Unusual *Psidium* Meroterpenoids as Phosphodiesterase-4 Inhibitors from the Leaves of *Psidium guajava*. *Sci. Rep.* **2017**, *7*, 1–15.
 77. Ning, S.; Liu, Z.; Wang, Z.; Liao, M.; Xie, Z. Biomimetic Synthesis of Psiguajdianone Guided Discovery of the Meroterpenoids from *Psidium guajava*. *Org. Lett.* **2019**, *21*, 8700–8704.
 78. Baldwin, J. E.; Mayweg, A. V. W.; Neumann, K.; Pritchard, G. J. Studies toward the Biomimetic Synthesis of Tropolone Natural Products via a Hetero Diels–Alder Reaction. *Org. Lett.* **1999**, *1*, 1933–1935.
 79. Adlington, R. M.; Baldwin, J. E.; Mayweg, A. V. W.; Pritchard, G. J. Biomimetic Cycloaddition Approach to Tropolone Natural Products via a Tropolone *ortho*-Quinone Methide. *Org. Lett.* **2002**, *4*, 3009–3011.
 80. Davison, J.; al Fahad, A.; Cai, M.; Song, Z.; Yehia, S. Y.; Lazarus, C. M.; Bailey, A. M.; Simpson, T. J.; Cox, R. J. Genetic, Molecular, and Biochemical Basis of Fungal Tropolone Biosynthesis. *Proc. Natl. Acad. Sci. U. S. A.* **2012**, *109*, 7642–7647.
 81. Yu, F.; Okamoto, S.; Nakasone, K.; Adachi, K.; Matsuda, S.; Harada, H.; Misawa, N.; Utsumi, R. Molecular Cloning and Functional Characterization of α -Humulene Synthase, a Possible Key Enzyme of Zerumbone Biosynthesis in Shampoo Ginger (*Zingiber zerumbet* Smith). *Planta* **2008**, *227*, 1291–1299.
 82. Chen, Q.; Gao, J.; Jamieson, C.; Liu, J.; Ohashi, M.; Bai, J.; Yan, D.; Liu, B.; Che, Y.; Wang, Y.; Houk, K. N.; Hu, Y. Enzymatic Intermolecular Hetero-Diels–Alder Reaction in the Biosynthesis of Tropolonic Sesquiterpenes. *J. Am. Chem. Soc.* **2019**, *141*, 14052–14056.
 83. Frey, P. A.; Magnusson, O. T. S-Adenosylmethionine: A Wolf in Sheep's Clothing, or a Rich Man's Adenosylcobalamin? *Chem. Rev.* **2003**, *103*, 2129–2148.
 84. Fontecave, M.; Atta, M.; Mulliez, E. S-Adenosylmethionine: Nothing Goes to Waste. *Trends Biochem. Sci.* **2004**, *29*, 243–249.
 85. Struck, A.-W.; Thompson, M. L.; Wong, L. S.; Micklefield, J. S-Adenosyl-Methionine-Dependent Methyltransferases: Highly Versatile Enzymes in Biocatalysis, Biosynthesis and Other Biotechnological Applications. *ChemBioChem* **2012**, *13*, 2642–2655.

86. Sun, Q.; Huang, M.; Wei, Y. Diversity of the Reaction Mechanisms of SAM-Dependent Enzymes. *Acta Pharm. Sin. B* **2021**, *11*, 632–650.
87. Ohashi, M.; Liu, F.; Hai, Y.; Chen, M.; Tang, M. cheng; Yang, Z.; Sato, M.; Watanabe, K.; Houk, K. N.; Tang, Y. SAM-Dependent Enzyme-Catalysed Pericyclic Reactions in Natural Product Biosynthesis. *Nature* **2017**, *549*, 502–506.
88. Cai, Y.; Hai, Y.; Ohashi, M.; Jamieson, C. S.; Garcia-Borras, M.; Houk, K. N.; Zhou, J.; Tang, Y. Structural Basis for Stereoselective Dehydration and Hydrogen-Bonding Catalysis by the SAM-Dependent Pericyclase LepI. *Nat. Chem.* **2019**, *11*, 812–820.
89. Martinez, S.; Hausinger, R. P. Catalytic Mechanisms of Fe(II)- and 2-Oxoglutarate-dependent Oxygenases. *J. Biol. Chem.* **2015**, *290*, 20702–20711.
90. Nakamura, H.; Matsuda, Y.; Abe, I. Unique Chemistry of Non-Heme Iron Enzymes in Fungal Biosynthetic Pathways. *Nat. Prod. Rep.* **2018**, *35*, 633–645.
91. Herr, C. Q.; Hausinger, R. P. Amazing Diversity in Biochemical Roles of Fe(II)/2-Oxoglutarate Oxygenases. *Trends Biochem. Sci.* **2018**, *43*, 517–532.
92. Fan, J.; Liao, G.; Kindinger, F.; Ludwig-Radtke, L.; Yin, W. B.; Li, S. M. Peniphenone and Penilactone Formation in *Penicillium crustosum* via 1,4-Michael Additions of *ortho*-Quinone Methide from Hydroxyclovatol to γ -Butyrolactones from Crustosic Acid. *J. Am. Chem. Soc.* **2019**, *141*, 4225–4229.
93. Wu, G.; Ma, H.; Zhu, T.; Li, J.; Gu, Q.; Li, D. Penilactones A and B, Two Novel Polyketides from Antarctic Deep-Sea Derived Fungus *Penicillium crustosum* PRB-2. *Tetrahedron* **2012**, *68*, 9745–9749.
94. Fan, J.; Liao, G.; Kindinger, F.; Ludwig-Radtke, L.; Yin, W. B.; Li, S. M. Three New Polyketides Produced by *Penicillium crustosum*, a Mycoparasitic Fungus from *Ophiocordyceps sinensis*. *Phytochem. Lett.* **2020**, *36*, 150–155.
95. Sun, W.; Chen, X.; Tong, Q.; Zhu, H.; He, Y.; Lei, L.; Xue, Y.; Yao, G.; Luo, Z.; Wang, J.; Li, H.; Zhang, Y. Novel Small Molecule 11 β -HSD1 Inhibitor from the Endophytic Fungus *Penicillium commune*. *Sci. Rep.* **2016**, *6*, 1–10.
96. Spence, J. T. J.; George, J. H. Total Synthesis of Peniphenones A–D via Biomimetic Reactions of a Common *o*-Quinone Methide Intermediate. *Org. Lett.* **2015**, *17*, 5970–5973.
97. Carvalho, Â.; Hansen, E. H.; Kayser, O.; Carlsen, S.; Stehle, F. Designing Microorganisms for Heterologous Biosynthesis of Cannabinoids. *FEMS Yeast Res.* **2017**, *17*, 1–11.
98. Luo, X.; Reiter, M. A.; D’Espaux, L.; Wong, J.; Denby, C. M.; Lechner, A.; Zhang, Y.; Grzybowski, A. T.; Harth, S.; Lin, W.; Lee, H.; Yu, C.; Shin, J.; Deng, K.; Benites, V. T.; Wang, G.; Baidoo, E. E. K.; Chen, Y.; Dev, I.; Petzold, C. J.;

- Keasling, J. D. Complete Biosynthesis of Cannabinoids and their Unnatural Analogues in Yeast. *Nature* **2019**, *567*, 123–126.
99. Lim, K. J. H.; Lim, Y. P.; Hartono, Y. D.; Go, M. K.; Fan, H.; Yew, W. S. Biosynthesis of Nature-Inspired Unnatural Cannabinoids. *Molecules* **2021**, *26*, 1–30.
100. Zirpel, B.; Stehle, F.; Kayser, O. Production of Δ^9 -Tetrahydrocannabinolic Acid from Cannabigerolic Acid by Whole Cells of *Pichia (Komagataella) pastoris* Expressing Δ^9 -Tetrahydrocannabinolic Acid Synthase from *Cannabis sativa* L. *Biotechnol. Lett.* **2015**, *37*, 1869–1875.
101. Poulos, J. L.; Farnia, A. N. Production of Cannabinoids in Yeast. WO 2016/010827A1, **2016**.
102. Thomas, F.; Schmidt, C.; Kayser, O. Bioengineering Studies and Pathway Modeling of the Heterologous Biosynthesis of Tetrahydrocannabinolic Acid in Yeast. *Appl. Microbiol. Biotechnol.* **2020**, *104*, 9551–9563.
103. Page, J. E.; Stout, J. M. Cannabichromenic Acid Synthase from *Cannabis sativa*. US 10,724,009 B2, **2020**.
104. Asai, T.; Tsukada, K.; Ise, S.; Shirata, N.; Hashimoto, M.; Fujii, I.; Gomi, K.; Nakagawara, K.; Kodama, E. N.; Oshima, Y. Use of a Biosynthetic Intermediate to Explore the Chemical Diversity of Pseudo-natural Fungal Polyketides. *Nat. Chem.* **2015**, *7*, 737–743.
105. Wu, G.; Yu, G.; Yu, Y.; Yang, S.; Duan, Z.; Wang, W.; Liu, Y.; Yu, R.; Li, J.; Zhu, T.; Gu, Q.; Li, D. Chemoreactive-Inspired Discovery of Influenza A Virus Dual Inhibitor to Block Hemagglutinin-Mediated Adsorption and Membrane Fusion. *J. Med. Chem.* **2020**, *63*, 6924–6940.
106. D Doyon, T. J.; Perkins, J. C.; Baker Dockrey, S. A.; Romero, E. O.; Skinner, K. C.; Zimmerman, P. M.; H Narayan, A. R. Chemoenzymatic *o*-Quinone Methide Formation. *J. Am. Chem. Soc.* **2019**, *141*, 20269–20277.

Chapter 2

Progress Towards the Biomimetic Total Synthesis of (±)-Chlorizidine A

Trevor N. Purdy, Grant S. Seiler, Daria E. Kim, Chambers C. Hughes

Abstract: A chemoenzymatic formal synthesis of the marine microbial natural product (–)-chlorizidine A is herein described by synthesizing the biosynthetic precursor, prechlorizidine. An intramolecular Heck reaction was first used to construct the unusual pyrrolo[2,1-*a*]indolone ring system, and the pyrrolizine ring was then attached using an intermolecular Friedel-Crafts acylation. Subsequent reduction and deprotection steps generated a late-stage hydroxylated derivative of prechlorizidine. The final target reaction required generation of a highly reactive *ortho*-quinone intermediate to facilitate a biomimetic, intramolecular cyclization reaction. Unfortunately, these attempts led to rapid degradation of the late-stage intermediate before any product could be observed. An alternative reduction strategy by ketone deoxygenation using Luche conditions and subsequent hydrogenation shows promising results to access the biosynthetic intermediate prechlorizidine. In total, the convergent total synthesis of 13-hydroxyprechlorizidine was reached in 16 total steps with a longest linear sequence of 11 steps and 3.6% yield.

(-)-Chlorizidine A (**1**) is a tetrachlorinated alkaloid first reported in 2013 from culture broths of marine *Streptomyces* species CNH-287, which was collected from marine sediment off the coast of San Clemente, California, USA.¹ As a naturally-occurring molecule, the structure of chlorizidine is unprecedented; the pyrrolo[2,1-a]isoindolone ring system has not appeared in any natural product to date (Figure 2.1). Importantly, chlorizidine A exhibits low micromolar cytotoxicity toward an HCT-116 colon cancer cell line. Early structure-activity relationship studies demonstrated that the intact pyrroloisoindolone moiety is essential for cytotoxicity; chlorizidine B (**2**), assumed to be a degradation product of **1**, exhibits no significant cytotoxicity.

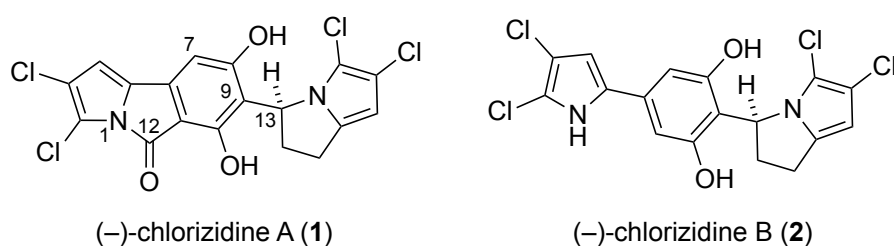


Figure 2.1. Structures of (-)-chlorizidine A (**1**) and a purported degradation analog chlorizidine B (**2**).

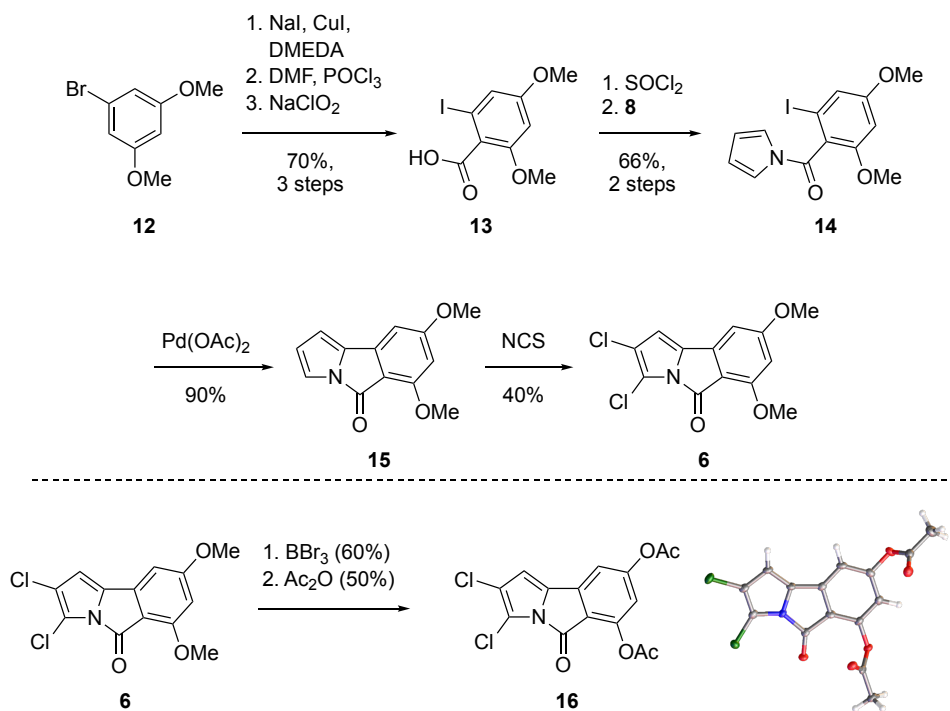
In addition to its unique structure and cytotoxic characteristics, chlorizidine has a novel mechanism of action. The compound appears to bind to and inhibit the glycolytic enzyme enolase as demonstrated by co-immunoprecipitation of a fluorescent chlorizidine-derived probe with target proteins in a whole-cell lysate.² Interestingly, cancer cells rely heavily on glycolysis for energy production compared to normal cells, a phenomenon called the “Warburg effect,” and glycolytic inhibitors have been shown to have anticancer properties.³⁻⁵ Given that there are very few cell permeable small molecules that target

and inhibit enolase, chlorizidine could serve as a lead compound and stimulate the development of anti-enolase cancer chemotherapies.⁶⁻⁸

Further biological studies have been hindered by an inadequate supply of **1**. Isolation from bacterial culture is low-yielding and unreliable owing, at least in part, to the high pH reached during cultivation, the presence of various nucleophiles in the culture medium, and the apparent electrophilicity of the metabolite's C-12 amide functionality.¹ In addition, there is currently no reported synthesis of chlorizidine; the only published approach toward the total synthesis of (\pm)-chlorizidine A culminated in the 10-step synthesis of an inactive methylated derivative that could not be demethylated.⁹

Our retrosynthetic analysis was inspired by the reported biosynthesis of the molecule. Two dichloropyrrole units derived from L-proline are prepared in parallel by PKS and fatty acid synthase (FAS) extension and then coupled together by a decarboxylative Claisen condensation reaction to yield prechlorizidine (**3**). We wanted to replicate this convergent approach developed by Nature by preparing two independent dichloropyrrole units separately that could be coupled together at a late stage. In the final biosynthetic step, the flavin-dependent oxidase Clz9 catalyzes benzylic oxidation of **3** via an *ortho*-quinone methide (*o*-QM), which is attacked by the pendant pyrrole nucleophile to form the pyrrolizine ring in an enantioselective fashion (Scheme 2.1a).¹⁰ Given the utility of *o*-QMs in numerous biomimetic syntheses, we imagined we could effect this same transformation using chemical oxidants, though perhaps without the exquisite stereocontrol characteristic of biosynthetic enzymes (Scheme 2.1b).¹¹⁻¹⁴ Prechlorizidine or 13-hydroxyprechlorizidine (**4**) were retrosynthetically disconnected by Friedel-Crafts acylation via the oxidized intermediate **5**, into pyrroloisoindolone **6** and protected acyl

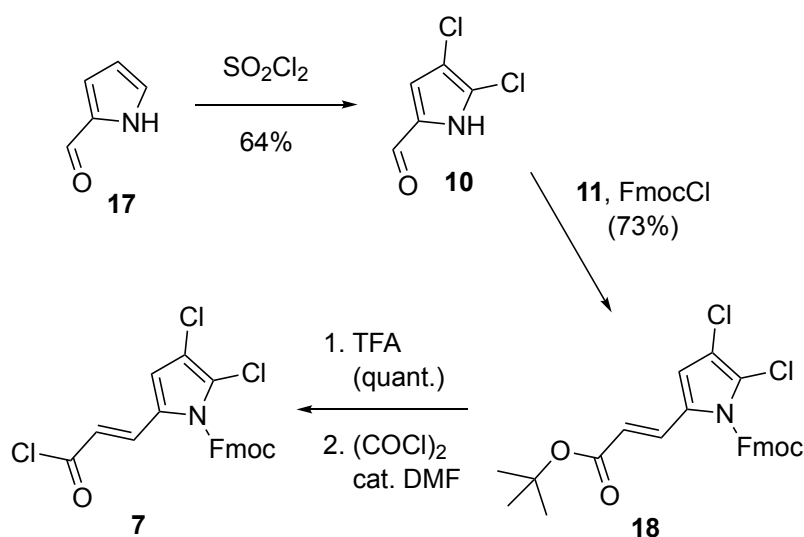
We first directed our efforts toward the synthesis of methyl-protected pyrroloisindolone **6**. 1-Bromo-3,5-dimethoxybenzene (**12**) was successfully converted to 1-iodo-3,5-dimethoxybenzene (**13**) by a copper-catalyzed aromatic Finkelstein reaction.¹⁵ We chose this protocol instead of the more common lithium-halogen exchange protocols because it was much easier to perform on a multigram scale and did not require purification before the following steps. The iodobenzene intermediate could then be subjected to Vilsmeier-Haack formylation and subsequent Pinnick oxidation conditions, yielding carboxylic acid **13** in 57% overall yield over 3 steps (Scheme 2.2).¹⁶ Acyl chloride formation with thionyl chloride provided **9** that was used to *N*-acylate the sodium salt of pyrrole (**8**) to yield **14** in 66% over two steps. A palladium-catalyzed intramolecular Heck reaction was then used to generate **15** in 90% yield, which was chlorinated with *N*-chlorosuccinimide to give dichlorinated pyrroloisindolone **6** in 40% yield after column chromatography. This chlorination reaction suffered from a low yield due to the



Scheme 2.2. Synthesis of pyrroloisindolone core by an intramolecular Heck reaction.

unavoidable mono-, di-, and trichlorinated byproducts; however, these byproducts could be used to generate various halogenated analogs of chlorizidine A and screened for biological activity. To verify the structure of **6**, the compound was demethylated with BBr_3 in 60% yield and acetylated with Ac_2O in 50% yield to give **16**. The product was then crystallized and analyzed by X-ray crystallographic methods, confirming the desired regiochemistry the dichloropyrrole moiety (Figure S49).

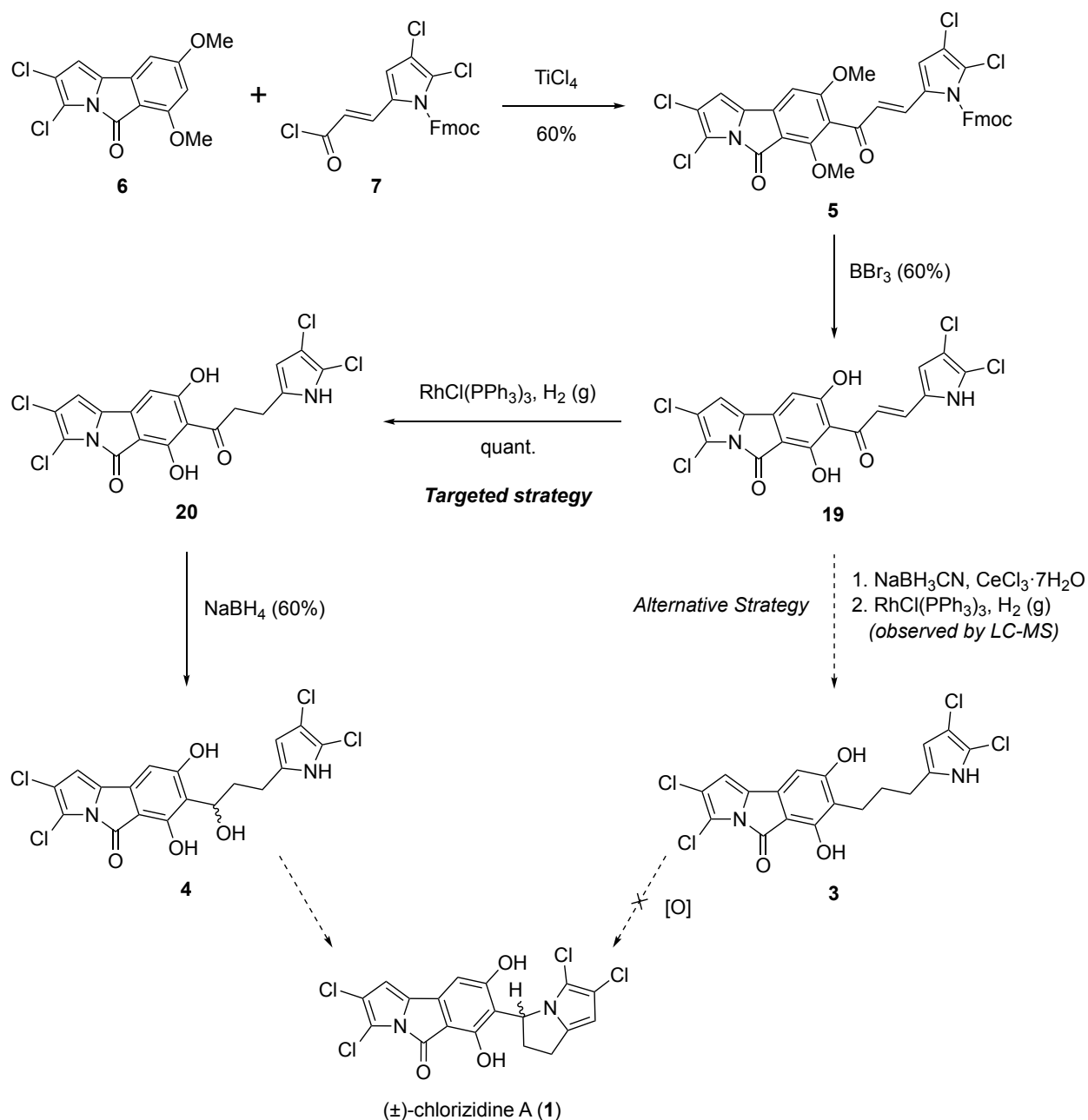
The next goal was to develop a high-yielding synthetic route to dichloropyrrole **7**. Although dichlorination of pyrrole-2-carboxylate could be performed according to the literature,¹⁷ subsequent oxidation-reduction reactions to form **10** were problematic. So, we tried to dichlorinate pyrrole-2-carboxyaldehyde (**17**) directly, despite there being no precedence for this transformation (Scheme 2.3); only regioselective dibromination has been reported.¹⁸ Treatment of **17** with cold sulfuryl chloride gave a mixture of mono-, di-, and trichlorinated products, similar to the chlorination of **15**, which were carefully separated by column chromatography yielding **10** in 64% yield. A one-pot reaction by *in situ* preparation of the Wittig from the commercially available phosphonium bromide **11**



Scheme 2.3. Synthesis of Fmoc-protected dichloropyrrole acyl chloride **7**.

with **10** coupled with Fmoc protection of the pyrrole nitrogen gave the protected *tert*-butyl ester **18** in 73% yield. Protecting the pyrrole nitrogen proved to be necessary for subsequent Friedel-Crafts acylation. Several other protecting groups were explored, including Boc, Cbz, and MOM; however, these alternatives were ultimately too labile or too difficult to selectively remove in later steps. Intermediate **18** was quantitatively hydrolyzed with TFA and the resulting carboxylic acid was converted to acid chloride **7** using oxalyl chloride.

In the second carbon-carbon bond forming event, **6** and **7** were coupled to give **5** using titanium(IV) chloride in 60% yield (Scheme 2.4). The structure of **5**, including the regioselectivity of the acylation at C-9, was confirmed using 2D NMR experiments (COSY, HSQC, HMBC; see Figure S27-29). Since previous attempts at the total synthesis of chlorizidine A reported degradation upon demethylation of late-stage intermediates,⁹ the compound was globally deprotected prior to any further manipulation with excess BBr₃ in 60% yield to give **19**. Deprotection significantly decreased the solubility of subsequent intermediates in organic solvents. Our initial attempts to reduce the α,β -ketone to the benzyl alcohol **4** at this stage resulted in dechlorination, reduction of the pyrroloisoindolone carbonyl, or degradation of the starting material. Reduction attempts with NaBH₄ did show some promise but generated a mixture of products. Thus, we first reduced the olefin using Wilkinson's catalyst to generate the saturated ketone intermediate **20**. We also attempted a procedure employing a Hantzsch ester reagent as the reductant, but we could not push the reaction to completion.¹⁹ **20** could then be



Scheme 2.4. Convergence of **6** and **7** followed by a regioselective Friedel-Crafts Acylation and global deprotection using BBr_3 . Two chemoselective reduction strategies to access 13-hydroxyprchlorizidine (**4**) (Path A) or prechlorizidine (**3**) (Path B). The final cyclization step to reach (±)-chlorizidine has yet to be achieved.

chemoselectively reduced to yield the racemic saturated alcohol **4** using NaBH_4 . Next, we subjected **4** to several commonly employed techniques known to induce formation of an o-QM intermediate in hopes that we could induce intramolecular cyclization.^{11–13}

Unfortunately, gentle heating to 50 °C in THF or MeOH resulted in a mixture of undesired products, and our attempts promote acid-catalyzed o-QM formation immediately degraded the starting material. Base-catalyzed cyclization strategies were not tested due to the reported reactivity of the C-12 amide. Given the instability of **20**, we tried to complete the synthesis by either a Mitsunobu reaction or Appel reaction, but both attempts led to degradation of starting material. It is worth noting that a Mitsunobu reaction was used in the synthesis methyl-protected chlorizidine, suggesting that protection of the phenols may be necessary for this reaction to succeed.⁹ Another alternative strategy could be to synthesize prechlorizidine (**3**). Regioselective reductive deoxygenation using Luche conditions with NaBH₃CN and CeCl₃ showed conversion of **19** to a product with mass $m/z = 440.9381$ ([M-H]⁻; C₁₈H₁₀Cl₄N₂O₃) and UV/vis profile matching the previously characterized pyrroloisindolone intermediates, suggesting chemoselective reduction and deoxygenation of the benzylic ketone. Subsequent hydrogenation with Wilkinson's catalyst yielded product that matches the exact mass, UV/vis spectral characteristics, and retention time of **3** by HR-LC-MS analysis (Figures S43, 47-48). However, these products have yet to be purified and confirmed by NMR. This reduction sequence to **3** would access a biosynthetic that could then be enantioselectively cyclized to (-)-**1** using the flavin-dependent oxidase Clz9.¹⁰

Many of the challenges arise following the demethylation of **5**, including issues with solubility and stability. We decided to demethylate **5** at this point because the reported synthesis of methyl-protected (±)-chlorizidine A could not remove the methyl groups at the final step.⁹ Therefore, any routes following this procedure will have greater chances to succeed by replacing the two methyl groups with a different protecting group at an

earlier stage. However, this approach has several drawbacks. First, our preliminary attempts to chemoselectively protect the phenolic hydroxyls with MOM or Ac₂O showed a mixture of di- and tri-protected products, suggesting the pendant dichloropyrrole nitrogen was also protected under these conditions. Second, protecting group options are severely limited: base-sensitive protecting groups are not recommended, due to likely hydrolysis of the pyrroloisindolone amide; metal-catalyzed deprotection strategies (e.g. Pd-based strategies for benzyl ether deprotections) are also discouraged due to possible metal-halide insertion into either dichloropyrrole unit. Acid-labile protecting groups are possible but cannot be introduced until a late stage given the acidic conditions during acyl chloride formation to generate **8** and the production of HCl during Friedel-Crafts acylation to generate **5**. Using acid-labile protecting groups, such as silyl-ethers or MOM are proven strategies to mask *o*-QMs until ready for activation.^{20,21} Exchanging methyl groups for something that can be removed at a step concurrent with *o*-QM formation would be the recommended way to mitigate undesired reactions prior to biomimetic cyclization. Given all these obstacles, protecting groups must be carefully chosen at different stages of the synthesis in future attempts.

In summary, we have achieved the synthesis of racemic 13-hydroxyprechlorizidine towards the biomimetic total synthesis of (±)-chlorizidine A. While the total synthesis of chlorizidine A, in its racemic or enantiopure form, has yet to be achieved, the route outlined in this chapter lays the groundwork for future attempts to reach the target molecule. Through this synthetic endeavor, we developed a novel route to pyrroloisindolones by an intramolecular Heck reaction and devised a convergent route that is amenable to the production of various halogenated or even heteroaryl derivatives.

We also describe the first report to generate chlorinated pyrrole-2-carboxaldehyde. The convergent nature of this approach is amenable to producing a library of multihalogenated synthetic derivatives that can be screened for biological activity. The challenges faced in the final steps of this work highlight the delicate nature of complex natural products and the inspiration synthetic chemists can draw upon to replicate processes already optimized by Nature.

Chapter 2 is coauthored with Purdy, Trevor N.; Seiler, Grant S.; Kim, Daria E.; Hughes, Chambers C. The dissertation author was the primary investigator and author of this material.

References

1. Alvarez-Mico, X.; Jensen, P. R.; Fenical, W.; Hughes, C. C. Chlorizidine, a cytotoxic 5H-pyrrolo[2,1-a]isoindol-5-one-containing alkaloid from a marine *Streptomyces* sp. *Org. Lett.* **2013**, *15*, 988–991.
2. Álvarez-Micó, X.; Rocha, D. D.; Guimarães, L. A.; Ambrose, A.; Chapman, E.; Costa-Lotufo, L. V.; La Clair, J. J.; Fenical, W. The Hybrid Pyrroloisoindolone-Dehydropyrrolizine Alkaloid (–)-Chlorizidine A Targets Proteins within the Glycolytic Pathway. *ChemBioChem* **2015**, *16*, 2002–2006.
3. Gatenby, R. A.; Gillies, R. J. Why do cancers have high aerobic glycolysis? *Nat. Rev. Cancer* **2004**, *4*, 891–899.
4. Granchi, C.; Minutolo, F. Anticancer Agents That Counteract Tumor Glycolysis. *ChemMedChem* **2012**, *7*, 1318–1350.
5. Gill, K. S.; Fernandes, P.; O'Donovan, T. R.; McKenna, S. L.; Doddakula, K. K.; Power, D. G.; Soden, D. M.; Forde, P. F. Glycolysis inhibition as a cancer treatment and its role in an anti-tumour immune response. *Biochim. Biophys. Acta - Rev. Cancer* **2016**, 1866, 87–105.
6. Diaz-Ramos, A.; Roig-Borrellas, A.; Garcia-Melero, A.; Lopez-Aleman, R. α -Enolase, a Multifunctional Protein: Its Role on Pathophysiological Situations. *J.*

Biomed. Biotechnol. **2012**, 2012, 1–12.

7. Leonard, P. G.; Satani, N.; Maxwell, D.; Lin, Y.; Hammoudi, N.; Peng, Z.; Pisaneschi, F.; Link, T. M.; Lee IV, G. R.; Sun, D.; Prasad, B. A. B.; Di Francesco, M. E.; Czako, B.; Asara, J. M.; Wang, Y. A.; Bornmann, W.; Depinho, R. A.; Muller, F. L. SF2312 is a natural phosphonate inhibitor of enolase. *Nat. Chem. Biol.* 2016, 12, 1053–1058.
8. Schofield, L.; Lincz, L. F.; Skelding, K. A. Unlikely role of glycolytic enzyme α -enolase in cancer metastasis and its potential as a prognostic biomarker. *J. Cancer Metastasis Treat.* **2020**, 6, 1-12.
9. Mahajan, J. P.; Mhaske, S. B. Synthesis of Methyl-Protected (\pm)-Chlorizidine A. *Org. Lett.* **2017**, 19, 2774–2776.
10. Mantovani, S. M.; Moore, B. S. Flavin-linked oxidase catalyzes pyrrolizine formation of dichloropyrrole-containing polyketide extender unit in Chlorizidine A. *J. Am. Chem. Soc.* **2013**, 135, 18032–18035.
11. Van de Water, R. W.; Pettus, T. R. R. *o*-Quinone methides: Intermediates underdeveloped and underutilized in organic synthesis. *Tetrahedron* **2002**, 58, 5367–5405.
12. Willis, N. J.; Bray, C. D. *ortho*-Quinone methides in natural product synthesis. *Chem. - A Eur. J.* **2012**, 18, 9160–9173.
13. Bai, W. J.; David, J. G.; Feng, Z. G.; Weaver, M. G.; Wu, K. L.; Pettus, T. R. R. The domestication of *ortho*-quinone methides. *Acc. Chem. Res.* **2014**, 47, 3655–3664.
14. Singh, M. S.; Nagaraju, A.; Anand, N.; Chowdhury, S. *ortho*-Quinone methide (*o*-QM): A highly reactive, ephemeral and versatile intermediate in organic synthesis. *RSC Adv.* **2014**, 4, 55924–55959.
15. Chen, J.; McNeil, A. J. Analyte-Triggered Gelation: Initiating Self-Assembly via Oxidation-Induced Planarization. *J. Am. Chem. Soc.* **2008**, 130, 16496–16497.
16. Petriguet, J.; Inack Ngi, S.; Abarbri, M.; Thibonnet, J. Short and convenient synthesis of two natural phthalides by a copper(I) catalysed Sonogashira/oxacyclisation copper(I) process. *Tetrahedron Lett.* **2014**, 55, 982–984.
17. Smith, J. A.; Ng, S.; White, J. The regioselective synthesis of aryl pyrroles. *Org. Biomol. Chem.* **2006**, 4, 2477–2482.
18. Rane, R. A.; Sahu, N. U.; Gutte, S. D.; Mahajan, A. A.; Shah, C. P.; Bangalore, P. Synthesis and evaluation of novel marine bromopyrrole alkaloid-based hybrids as

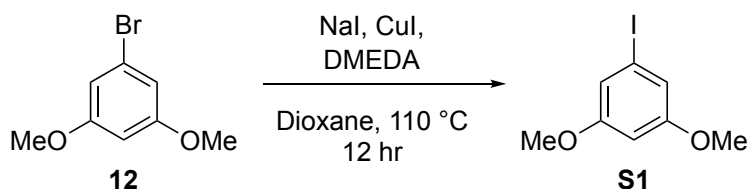
anticancer agents. *Eur. J. Med. Chem.* **2013**, 63, 793–799.

19. Che, J.; Lam, Y. Rapid and regioselective hydrogenation of α,β -unsaturated ketones and alkylidene malonic diesters using Hantzsch ester catalyzed by titanium tetrachloride. *Synlett* **2010**, 2010.
20. Mao, Y.-L.; Boekelheide, V. Benzocyclobutene—*o*-xylylene valence tautomerization: Oxygen and sulfur analogs. *Proc. Natl. Acad. Sci.* **1980**, 77, 1732–1735.
21. Seiichi, I.; Masatoshi, A.; Kiyoshi, H.; Hidekazu, M. A Facile Synthesis of Angularly-Fused 3,4,4a,10b-Tetrahydro-2H,5H-pyrano[3,2-c][1]benzopyrans by the One-pot Condensation between Salicylaldehydes and Unsaturated Alcohols. *Chem. Lett.* **2006**, 25, 889–890.

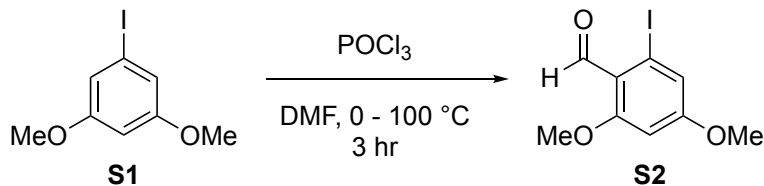
Materials

All reactions requiring inert conditions were carried out under an atmosphere of nitrogen with magnetic stirring. THF, DMF, MeCN, DCM, and MeOH were dried under nitrogen prior to use. Air sensitive reagents and solutions were transferred via syringe or cannula and were introduced to the apparatus via rubber septa. All reagents, starting materials and solvents were obtained from commercial suppliers and used as such without further purification. Reactions were monitored by thin layer chromatography over silica gel 60 F₂₅₄ (Merck) and visualized by irradiation with ultraviolet light (254 nm). Preparative column chromatography was carried out on a Teledyne ISCO CombiFlash® Rf+ Lumen™ flash chromatography system using diatomaceous earth for sample loading and silica gel 60 (EMD, 40-63µm) for the stationary phase. Infrared spectra were recorded on a Nicolet IR 100 FT-IR (Thermo) spectrometer. The ¹H NMR spectra were recorded on 500 MHz Jeol NMR spectrometer using solvent residue signal as an internal standard [¹H NMR: CDCl₃ (7.27), (CD₃)₂CO (2.05), CD₃CN (1.94), DMSO-d₆ (2.50); ¹³C NMR: CDCl₃ (77.0), (CD₃)₂CO (29.8, 206.3), CD₃CN (1.3, 118.3), DMSO-d₆ (39.5)]. LC-MS/MS analyses were conducted with an Agilent 6530 Accurate-Mass Q-TOF MS (MassHunter software, Agilent) equipped with a Dual electrospray ionization source and an Agilent 1260 LC system (ChemStation software, Agilent) with diode array detector.

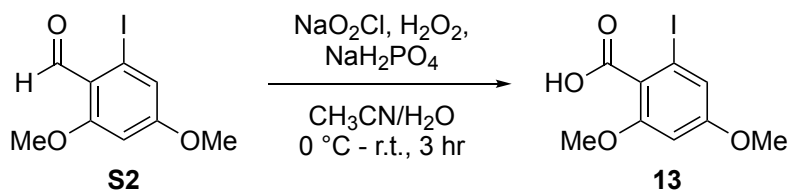
Experimental Procedures



A 500 mL round bottom flask equipped with a stir bar was oven-dried, charged with N_2 , and filled with 250 mL dioxane. Sequentially, 1-bromo-3,5-dimethoxybenzene (**12**) (50.0 g, 230 mmol), sodium iodide (69.0 g, 461 mmol), copper iodide (2.19 g, 11.5 mmol), and trans-N,N'-dimethylcyclohexane-1,2-diamine (3.63 mL, 23.0 mmol) were added to the flask. The solution was heated to 110 °C overnight. After cooling to room temperature, the reaction was quenched with 250 mL of water, filtered, and rinsed with EtOAc. The mixture was then extracted with EtOAc (3 x 300 mL). The organic layer was then washed with brine, dried with anhydrous Na_2SO_4 , filtered, and concentrated to dryness under reduced pressure to yield a crude gray solid. The crude material was pushed forward without further purification. UV/Vis: $\lambda_{max} = 252, 277, 284$ nm; 1H NMR (500 MHz, $CDCl_3$) δ 6.85 (d, 2H, $J = 2.3$ Hz), 6.40 (t, 1H, $J = 2.3$ Hz), 3.76 (s, 6H). HR-ESI-TOFMS: m/z (M+H)⁺ calculated for $C_8H_9IO_2$ 264.9620, found 264.9674. Data for 1-iodo-3,5-dimethoxybenzene matched that previously reported in the literature.¹

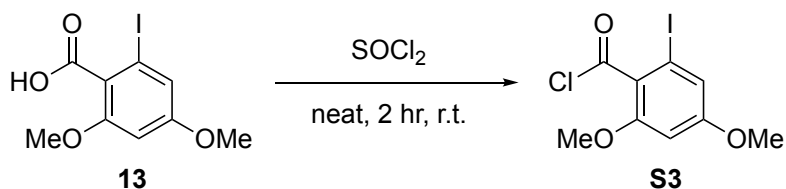


A 250 mL round bottom flask equipped with a stir bar was oven-dried, charged with N_2 , filled with 75 mL DMF, and cooled to 0 °C. 1-iodo-3,5-dimethoxybenzene (**S1**) (62.0 g, 235 mmol) was added to the flask, followed by dropwise addition of phosphoryl chloride (24.1 mL, 258 mmol). The solution was stirred for 10 minutes, then warmed to 100 °C in an oil bath and stirred for 3 hours. The reaction was quenched with a 1 M solution of sodium acetate (175 mL), poured into 1.5 L of water and extracted with EtOAc (3 x 300 mL). The organic layer was then washed with brine, dried with anhydrous Na_2SO_4 , filtered, and concentrated under reduced pressure. The crude material was pushed forward without further purification. UV/Vis: $\lambda_{\text{max}} = 232, 289, 316 \text{ nm}$; $^1\text{H NMR}$ (500 MHz, CDCl_3) $\delta = 10.1$ (s, 1H), 7.13 (d, 1H, $J = 2.2 \text{ Hz}$), 6.48 (d, 1H, $J = 2.1 \text{ Hz}$), 3.89 (s, 3H), 3.86 (s, 3H). HR-ESI-TOFMS: m/z ($\text{M}+\text{H}$) $^+$ calculated for $\text{C}_9\text{H}_9\text{IO}_3$ 292.9663, found 292.9647. Data for 2-iodo-4,6-dimethoxybenzaldehyde matched that previously reported in the literature.²

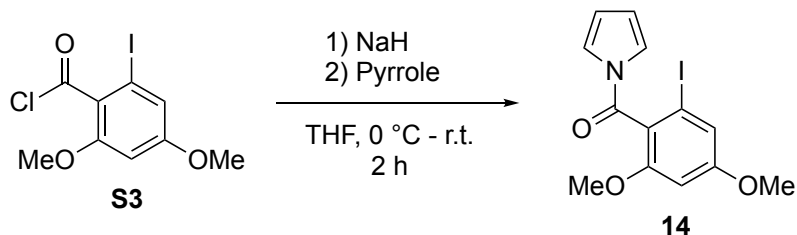


A 2 L round bottom flask was filled with 1 L acetonitrile and 100 mL water, then cooled to 0 °C. Sequentially, 2-iodo-4,6-dimethoxybenzaldehyde (**S2**) (30.0 g, 103 mmol),

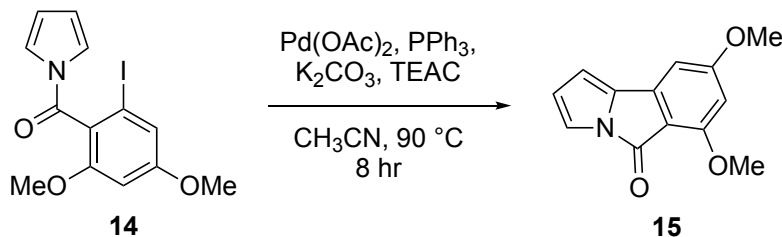
sodium phosphate monobasic (6.16 g, 51.4 mmol), 30% H₂O₂ in water (25 mL) and sodium chlorite (37.2 g, 411 mmol) were added to the flask. The solution was warmed to room temperature over 3 hours, and then concentrated under reduced pressure to remove acetonitrile. An additional 150 mL of water was added, and the mixture was extracted with EtOAc (3 x 200 mL). The organic layer was then washed with brine, dried with anhydrous Na₂SO₄, filtered, and concentrated under reduced pressure. The crude mixture was purified by flash chromatography using silica gel and a gradient from 0% to 100% hexanes/EtOAc as eluent over 25 minutes to yield a white solid (28.8 g, 57% over three steps). UV/Vis: λ_{max} = 234, 280, 286 nm; ¹H NMR (500 MHz, CDCl₃) δ 7.00 (d, 1H, *J* = 2.2 Hz), 6.47 (d, 1H, *J* = 2.1 Hz), 6.48 (d, 1H, *J* = 2.1 Hz), 3.85 (s, 3H), 3.81 (s, 3H). HR-ESI-TOFMS: *m/z* (M-H)⁻ calculated for C₉H₉IO₄ 306.9473, found 306.9467. Data for **13** matched that previously reported in the literature.²



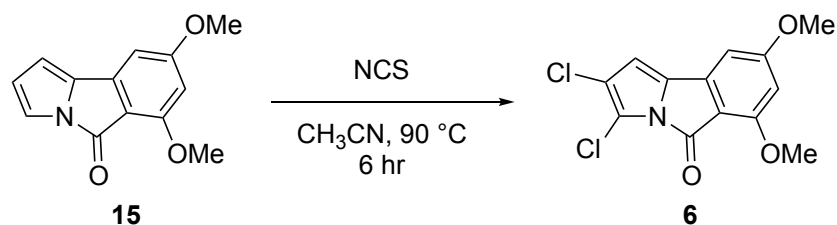
A 100 mL round bottom flask equipped with a stir bar was oven-dried and charged with N₂. 2-iodo-4,6-dimethoxybenzoic acid (**13**) (28.8 g, 93.5 mmol) was added to the flask, followed by addition of thionyl chloride (30 mL). The solution was stirred at room temperature for 2 hours. The reaction was concentrated to complete dryness under reduced pressure and the crude material was pushed forward without purification.



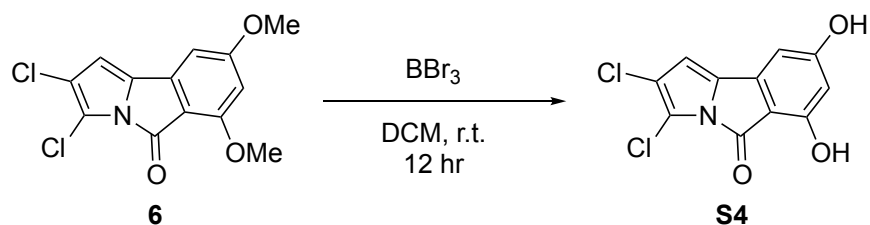
A 500 mL round bottom flask equipped with a stir bar was oven-dried, charged with N₂, filled with 200 mL THF, and cooled to 0 °C. Sodium hydride (60% dispersion in mineral oil; 9.35 g, 234 mmol) was added to the flask, followed by dropwise addition of pyrrole (13.0 mL, 187 mmol). The mixture was stirred for 30 minutes, until the evolution of H₂ gas ceased. The reaction was then cooled to 0 °C and treated dropwise with 2-iodo-4,6-dimethoxybenzoyl chloride (**S3**) (30 g, 93 mmol) dissolved in a minimal amount of THF. The resulting mixture was warmed to room temperature over 2 hours, then quenched with a saturated solution of ammonium chloride (200 mL) and extracted with EtOAc (3 x 300 mL). The organic layer was washed with brine, dried with anhydrous Na₂SO₄, filtered, and concentrated under reduced pressure. The crude mixture was purified by flash chromatography using silica gel and a gradient from 0% to 40% hexanes/EtOAc as eluent over 25 minutes to yield a white solid (22.0 g, 66%). UV/Vis: λ_{max} = 239, 280 nm; ¹H NMR (500 MHz, CDCl₃) δ 7.59 (br. s, 2H), 6.96 (d, 1H, *J* = 2.1 Hz), 6.50 (d, 1H, *J* = 2.1 Hz), 6.29 (br. s, 2H), 3.82 (s, 3H), 3.72 (s, 3H); ¹³C{¹H} NMR (125 MHz, CDCl₃) δ 165.9, 162.1, 158.2, 122.9, 115.4, 113.7, 98.9, 93.6, 56.1, 55.9. HR-ESI-TOFMS: *m/z* (M+H)⁺ calculated for C₁₃H₁₂I₂O₃ 357.9935, found 357.9948.



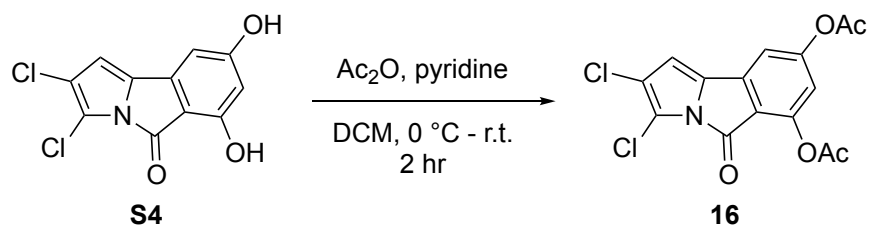
A 1 L round bottom flask equipped with a reflux condenser and stir bar was oven-dried, charged with N₂, and filled with 300 mL acetonitrile. Sequentially, (2-iodo-4,6-dimethoxyphenyl)(1*H*-pyrrol-1-yl)methanone (**14**) (11.0 g, 30.8 mmol), triphenylphosphine (4.84 g, 18.5 mmol), potassium carbonate (8.51 g, 6.16 mmol), tetraethylammonium chloride (5.10 g, 30.8 mmol), and palladium (II) acetate (2.07 g, 9.24 mmol) were added to the flask, and the reaction was heated to reflux for 8 hours. Upon completion, the reaction was filtered through celite and concentrated under reduced pressure to remove the acetonitrile. The reaction was then washed with 150 mL of water and extracted with EtOAc (3 x 150 mL). The organic layer was washed with brine, dried with anhydrous Na₂SO₄, filtered, and concentrated under reduced pressure. The crude mixture was purified by flash chromatography using silica gel and a gradient from 0% to 70% hexanes/EtOAc over 25 minutes as eluent to yield a yellow solid (6.35 g, 90%). UV/Vis: λ_{max} = 260, 340, 354, 408 nm; ¹H NMR (500 MHz, CDCl₃) δ 7.00 (dd, 1H, *J* = 3.06, 0.84 Hz), 6.44 (d, 1H, *J* = 1.88 Hz), 6.18 (dd, 1H, *J* = 3.11, 0.83 Hz), 6.16 (d, 1H, *J* = 1.87 Hz), 6.13 (t, 1H, *J* = 3.09 Hz), 3.92 (s, 3H), 3.87 (s, 3H); ¹³C{¹H} NMR (125 MHz, CDCl₃) δ 167.4, 161.6, 160.5, 140.3, 134.2, 116.7, 116.0, 110.3, 107.2, 98.6, 96.7, 56.0, 56.0. HR-ESI-TOFMS: *m/z* (M+H)⁺ calculated for C₁₃H₁₁NO₃ 230.0812, found 230.0827.



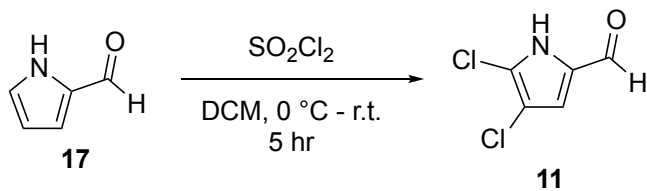
A 1 L round bottom flask equipped with a reflux condenser and stir bar was oven-dried and filled with 275 mL acetonitrile. 6,8-dimethoxy-5H-pyrrolo[2,1-a]isoindol-5-one (**15**) (6.35 g, 27.7 mmol) and N-chlorosuccinimide (7.77 g, 58.2 mmol) were added to the flask, and the solution was heated to reflux for 6 hours. Upon completion, the reaction was washed with 150 mL of water and extracted with DCM (2 x 150 mL). The organic layer was washed with brine, dried with anhydrous Na₂SO₄, filtered, and concentrated under reduced pressure. The crude mixture was purified by flash column chromatography using silica gel and a gradient from 0% to 20% hexanes/DCM over 30 minutes as eluent to yield a yellow solid (3.03 g, 40%). UV/Vis: λ_{max} = 269, 327, 343, 416 nm; ¹H NMR (500 MHz, CDCl₃) δ 6.62 (s, 1H), 6.17 (d, 1H, *J* = 3.4 Hz), 6.02 (d, 1H, *J* = 3.4 Hz), 4.10 (s, 3H), 3.98 (s, 3H); ¹³C{¹H} NMR (125 MHz, CDCl₃) δ 162.0, 159.4, 157.3, 136.2, 133.4, 117.5, 115.3, 115.1, 114.3, 107.4, 98.8, 62.7, 57.0; HR-ESI-TOFMS: *m/z* (M+Na)⁺ calculated for C₁₃H₉Cl₂NO₃ 319.9851, found 319.9860.



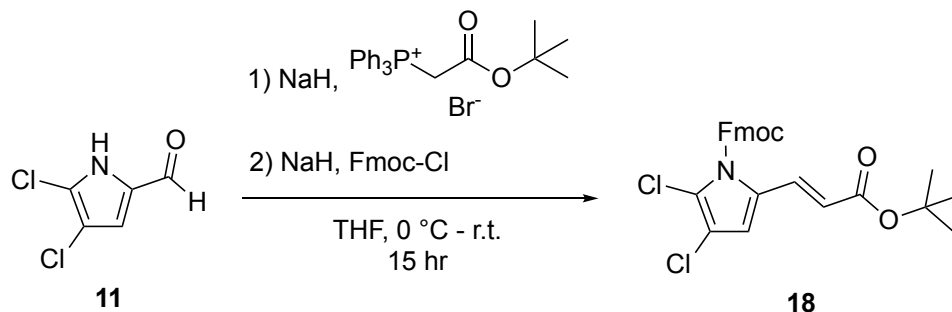
A 50 mL round bottom flask equipped with a reflux condenser and stir bar was oven-dried, charged with N₂, and filled with 10 mL DCM. 2,3-dichloro-6,8-dimethoxy-5*H*-pyrrolo[2,1-*a*]isoindol-5-one (**6**) (500 mg, 1.68 mmol) and 5 mL of a 1.0 M solution of BBr₃ in DCM (5 mmol) were added to the flask, and the solution at room temperature for 12 hours. Upon completion, the reaction was slowly poured over ice water and extracted with EtOAc (3 x 20 mL). The organic layer was washed with brine, dried with anhydrous Na₂SO₄, filtered, and concentrated under reduced pressure. The crude mixture was purified by flash column chromatography using silica gel and a gradient from 0% to 20% DCM/MeOH over 20 minutes as eluent to yield an orange solid (270 mg, 60%). UV/Vis: λ_{max} = 267, 352, 398 nm; ¹H NMR (500 MHz, CD₃CN) δ 6.37 (d, 1H, *J* = 1.7 Hz), 6.54 (d, 1H, *J* = 1.7 Hz), 6.42 (s, 1H); ¹³C{¹H} (125 MHz, CD₃CN) δ 159.0, 133.3, 113.9, 111.8, 111.1, 108.2, 107.6^a; HR-ESI-TOFMS: *m/z* (M-H)⁻ calculated for C₁₁H₅Cl₂NO₃ 267.9573, found 267.9585. ^a4 carbons not observed from HSQC and HMBC data.



A 10 mL round bottom flask equipped with a stir bar was oven-dried and filled with 5 mL DCM. 2,3-dichloro-6,8-dihydroxy-5*H*-pyrrolo[2,1-*a*]isoindol-5-one (**S4**) (125, 0.462 mmol) and pyridine were added to the flask. The reaction was then cooled to 0 °C and treated dropwise with acetic anhydride. The resulting mixture was warmed to room temperature over 2 hours, then quenched with H₂O and extracted with DCM (3 x 5 mL). The organic layer was washed with brine, dried with anhydrous Na₂SO₄, filtered, and concentrated under reduced pressure. The crude mixture was purified by flash chromatography using silica gel and a gradient from 0% to 20% hexanes/EtOAc as eluent over 20 minutes to yield a yellow solid (80.7 mg, 50%). UV/Vis: λ_{max} = 266, 317, 420 nm; ¹H NMR (500 MHz, CDCl₃) δ 6.98 (d, 1H, *J* = 1.6 Hz), 6.71 (d, 1H, *J* = 1.6 Hz), 6.26 (s, 1H), 2.39 (s, 3H), 2.32 (s, 3H), 3.72; HR-ESI-TOFMS: *m/z* (M+Na)⁺ calculated for C₁₅H₉Cl₂NO₅ 375.9751, found 375.9791.

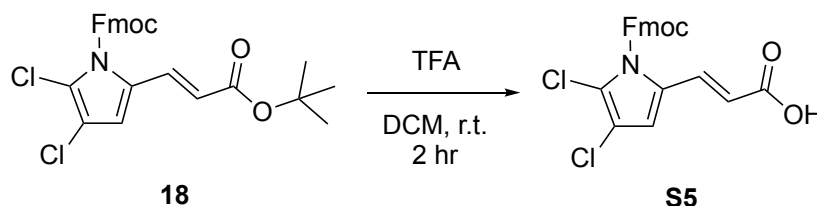


A 1 L round bottom flask equipped with a stir bar was oven-dried, charged with N₂, filled with 500 mL DCM, and cooled to 0 °C. 1*H*-pyrrole-2-carboxaldehyde (**17**) (8.33 g, 87.6 mmol) was added to the flask, followed by slow addition of sulfuryl chloride (21.2 mL, 263 mmol). The solution was slowly warmed to room temperature over 5 hours, then diluted with a saturated solution of K₂CO₃ (400 mL) and extracted with DCM (3 x 300 mL). The organic layer was washed with brine, dried with anhydrous Na₂SO₄, filtered, and concentrated under reduced pressure. The crude mixture was purified by flash chromatography using silica gel and a gradient from 0% to 8% hexanes/EtOAc over 45 minutes as eluent to yield a white solid (9.24 g, 64%). UV/Vis: λ_{max} = 251, 280, 313 nm; ¹H NMR (500 MHz, CDCl₃) δ 10.42 (br. s, 1H), 9.36 (s, 1H), 6.92 (s, 1H); ¹³C{¹H} NMR (125 MHz, CDCl₃) δ 178.2, 129.6, 123.6, 120.5, 112.9; HR-ESI-TOFMS: *m/z* (M-H)⁻ calculated for C₅H₃Cl₂NO 161.9519, found 161.9515.

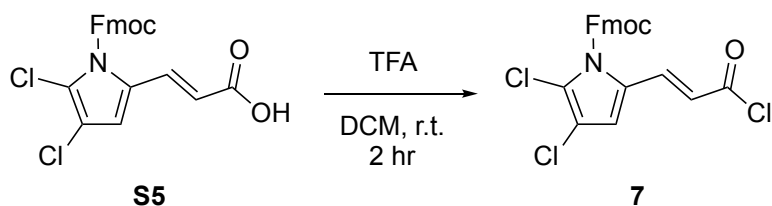


A 1 L round bottom flask equipped with a stir bar was oven-dried, charged with N_2 , filled with 400 mL THF, and cooled to 0 °C. Sodium hydride (60% dispersion in mineral oil, 1.64 g, 40.9 mmol) and (*tert*-butoxycarbonylmethyl)-triphenylphosphonium bromide (18.8 g, 40.9 mmol) were added to the flask. The mixture was stirred for 30 minutes before 4,5-dichloro-1*H*-pyrrole-2-carbaldehyde (**11**) (5.37g, 32.7 mmol) was added to the solution, and stirred for another 12 hours. A second portion of sodium hydride (60% dispersion in mineral oil, 1.64 g, 40.9 mmol) was added to the reaction mixture and stirred for an additional 30 minutes, followed by the addition of 9-fluorenylmethyl chloroformate (10.6 g, 40.9 mmol). The reaction was stirred at room temperature for 2 hours, then quenched with a saturated solution of ammonium chloride (300 mL) and extracted with EtOAc (3 x 500 mL). The organic layer was quenched with brine, dried with anhydrous Na_2SO_4 , filtered, and concentrated under reduced pressure. The crude mixture was purified by flash column chromatography using silica gel and a gradient from 0% to 30% hexanes/EtOAc as eluent over 20 minutes to yield a white solid (11.6 g, 73%). UV/Vis: $\lambda_{\text{max}} = 264, 305, 324$; $^1\text{H NMR}$ (500 MHz, CDCl_3) δ 7.87 (d, 1H, $J = 15.8$ Hz), 7.78 (d, 2H, $J = 7.5$ Hz), 7.61 (d, 2H, $J = 7.5$ Hz), 7.43 (t, 2H, $J = 7.5$ Hz), 7.33 (t, 2H, $J = 7.5$ Hz), 6.13 (d, 1H, $J = 15.8$), 4.81 (d, 2H, $J = 6.2$ Hz), 4.38 (t, 1H, $J = 6.2$ Hz), 1.47 (s, 9H); $^{13}\text{C}\{^1\text{H}\}$ NMR (125 MHz, CDCl_3) δ 165.8, 149.2, 143.0, 141.6, 132.1, 131.1, 128.2, 127.4,

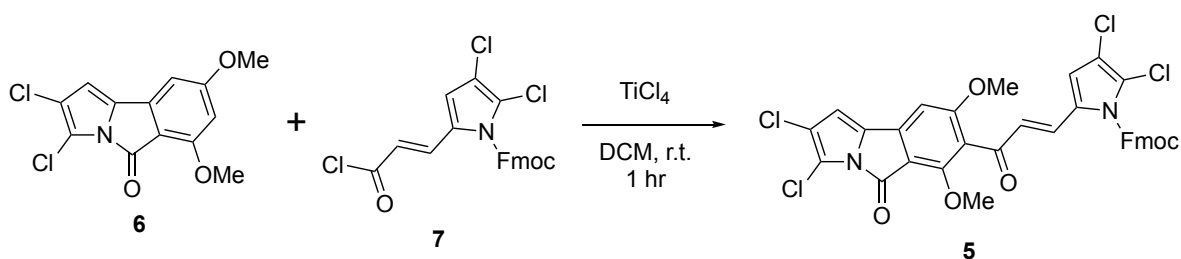
125.0, 20.7, 120.3, 117.6, 116.5, 112.8, 80.9, 70.4, 46.6, 28.2; HR-ESI-TOFMS: m/z ($M-C_{15}H_{11}O_2$) $^-$ $C_{26}H_{23}Cl_2NO_4$ calculated for 260.0245, detected 260.0250. Loss of $C_{15}H_{11}O_2$ $^-$ indicative of in-source fragmentation of the Fmoc protecting group.



A 500 mL round bottom flask equipped with a stir bar was oven-dried, charged with N_2 , and filled with 190 mL THF. (9H-fluoren-9-yl)methyl (*E*)-5-(3-(*tert*-butoxy)-3-oxoprop-1-en-1-yl)-2,3-dichloro-1H-pyrrole-1-carboxylate (**18**) (18.5 g, 38.2 mmol) was added to the flask, followed by trifluoroacetic acid (36.9 mL, 382 mmol). The resulting solution was stirred at room temperature for 2 hours. The reaction was then concentrated to complete dryness under reduced pressure to yield a tan solid (14.7 g, 34.4 mmol) without further purification. UV/Vis: λ_{max} = 264, 301, 322 nm; 1H NMR (500 MHz, $(CD_3)_2CO$) δ 10.8 (br. s, 1H) 7.99 (d, 1H, J = 15.9 Hz), 7.88 (d, 2H, J = 7.5 Hz), 7.76 (d, 2H, J = 7.5 Hz), 7.43 (t, 2H, J = 7.5 Hz), 7.35 (t, 2H, J = 7.5 Hz), 7.01 (s, 1H) 6.34 (d, 1H, 15.9 Hz), 5.05 (d, 2H, J = 5.3 Hz), 4.52 (t, 1H, J = 5.3 Hz); $^{13}C\{^1H\}$ NMR (125 MHz, $(CD_3)_2CO$) δ 167.4, 149.7, 144.3, 142.4, 134.1, 132.0, 128.8, 128.1, 125.9, 120.9, 119.3, 117.9, 116.5, 113.6, 70.9, 47.4; HR-ESI-TOFMS: m/z ($M-C_{15}H_{11}O_2$) $^-$ $C_{26}H_{23}Cl_2NO_4$ calculated for 203.9624, detected 203.9663 and m/z ($2M-H$) $^-$ $C_{26}H_{23}Cl_2NO_4$ calculated for 853.0683, detected 853.1684. Loss of $C_{15}H_{11}O_2$ $^-$ indicative of in-source fragmentation of the Fmoc protecting group.

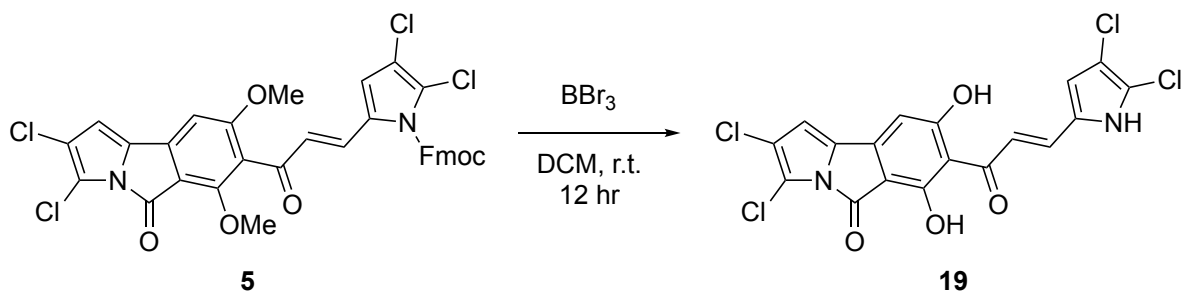


A 125 mL round bottom flask equipped with a stir bar was oven-dried and charged with N₂, then filled with 60 mL DCM and a catalytic amount DMF. (*E*)-3-(1-((9*H*-fluoren-9-yl)methoxy)carbonyl)-4,5-dichloro-1*H*-pyrrol-2-yl)acrylic acid (**S5**) (2.62 g, 6.12 mmol) was added to the flask, followed by dropwise addition of oxalyl chloride (1.56 mL, 61.2 mmol). The reaction mixture was stirred at room temperature for 2 hours. The reaction was then concentrated to complete dryness under reduced pressure and the crude material was pushed forward without purification.



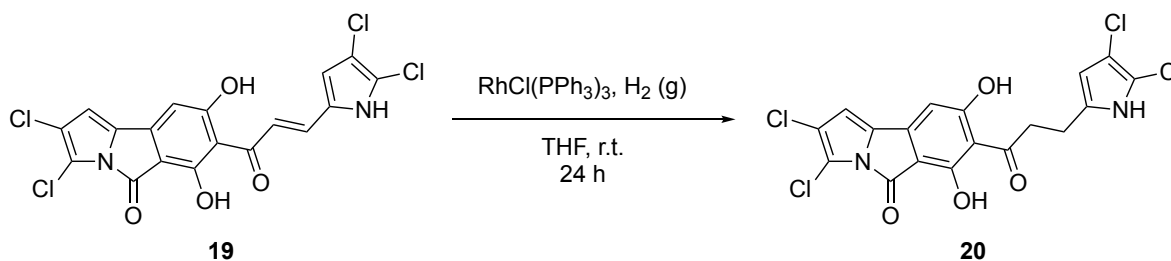
A 100 mL round bottom flask equipped with a stir bar was oven-dried and charged with N₂, then filled with 20 mL DCM. 2,3-dichloro-6,8-dimethoxy-5*H*-pyrrolo[2,1-*a*]isoindol-5-one (**6**) (1.46 g, 4.89 mmol) was added to the flask, followed by 12.2 mL of a 1.0 M solution of TiCl₄ in DCM (12.2 mmol). The reaction was stirred for 5 minutes before a solution of (9*H*-fluoren-9-yl)methyl (*E*)-2,3-dichloro-5-(3-chloro-3-oxoprop-1-en-1-yl)-1*H*-pyrrole-1-carboxylate (2.73 g, 6.12 mmol) dissolved in 20 mL DCM was slowly added to the reaction. The reaction was stirred at room temperature for 2 hours, then quenched with a saturated solution of ammonium chloride (50 mL) and extracted with EtOAc (3 x

50 mL). The organic layer was quenched with brine, dried with anhydrous Na₂SO₄, filtered, and concentrated under reduced pressure. The crude mixture was purified by flash column chromatography using silica gel and a gradient from 0% to 30% hexanes/EtOAc as eluent over 20 minutes to yield a yellow solid (2.07 g, 60%). UV/Vis: λ_{max} = 264, 383; ¹H NMR (500 MHz, CDCl₃) δ 8.04 (d, 1H, *J* = 15.5 Hz), 7.76 (d, 2H, *J* = 7.5 Hz), 7.60 (d, 2H, *J* = 7.5 Hz), 7.42 (t, 2H, *J* = 7.5 Hz), 7.32 (t, 2H, *J* = 7.5 Hz), 7.24 (d, 1H, *J* = 15.5), 6.77 (s, 1H), 6.76 (s, 1H), 6.69 (s, 1H), 4.85 (d, 2H, *J* = 6.1 Hz), 4.38 (t, 1H, *J* = 6.1 Hz), 4.13 (s, 3H), 4.00 (s, 3H); ¹³C{¹H} NMR (125 MHz, CDCl₃) δ 182.9, 162.3, 157.3, 142.7, 141.6, 135.1, 132.3, 132.2, 130.8, 128.4, 127.7, 127.6, 124.9, 123.3, 120.2, 118.3, 116.2, 113.7, 113.3, 107.4, 99.2, 70.2, 62.5, 56.8, 46.2; HR-ESI-TOFMS: *m/z* (M-H)⁻ C₃₅H₂₂Cl₄N₂O₆ calculated for 705.0159, detected 705.0176. ^a4 carbons not observed in HSQC or HMBC data.



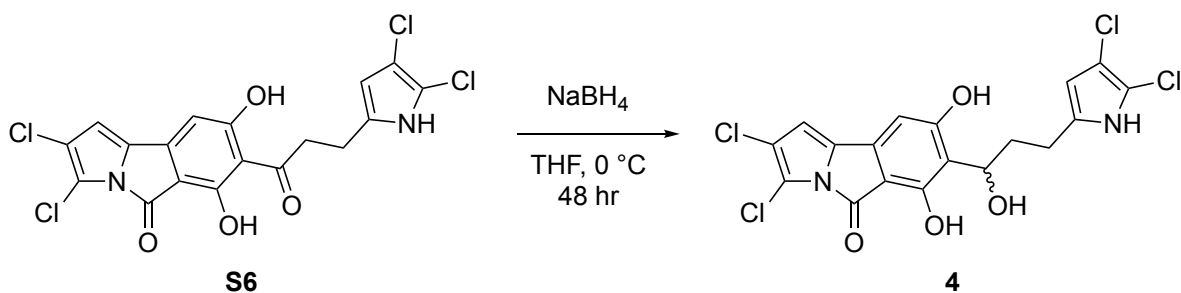
A 50 mL round bottom flask equipped with a stir bar was oven-dried, charged with N₂, and filled with 10 mL DCM. (9*H*-fluoren-9-yl)methyl (*E*)-2,3-dichloro-5-(3-(2,3-dichloro-6,8-dimethoxy-5-oxo-5*H*-pyrrolo[2,1-*a*]isoindol-7-yl)-3-oxoprop-1-en-1-yl)-1*H*-pyrrole-1-carboxylate (**5**) (1.00 g, 1.41 mmol) and 5 mL of a 1.0 M solution of BBr₃ in DCM (5 mmol) were added to the flask, and the reaction was stirred for 12 hours at room

temperature. Upon completion, the reaction was slowly poured over ice water and extracted with EtOAc (3 x 20 mL). The organic layer was washed with brine, dried with anhydrous Na_2SO_4 , filtered, and concentrated under reduced pressure. The crude mixture was purified by flash column chromatography using silica gel and a gradient from 0% to 25% DCM/MeOH over 25 minutes as eluent to yield a yellow-brown solid (646 mg, 60%). UV/Vis: $\lambda_{\text{max}} = 262, 381 \text{ nm}$; $^1\text{H NMR}$ (500 MHz, DMSO-d_6) δ 12.72 (br. s, 1H), 11.72 (br. s, 1H), 7.34 (s, 1H), 7.33 (s), 7.02 (s, 1H), 6.88 (s, 1H), 6.68 (s, 1H); $^{13}\text{C}\{^1\text{H}\}$ NMR (125 MHz, CD_3CN) δ 182.8, 131.9, 130.9, 127.8, 127.0, 118.8, 116.3, 113.8, 108.3, 107.1, 106.5, 100.2; HR-ESI-TOFMS: m/z (M-H) $^-$ calculated for $\text{C}_{18}\text{H}_8\text{Cl}_4\text{N}_2\text{O}_4$ 454.9165, found 454.9225. ^a6 carbons not observed in HSQC or HMBC data.



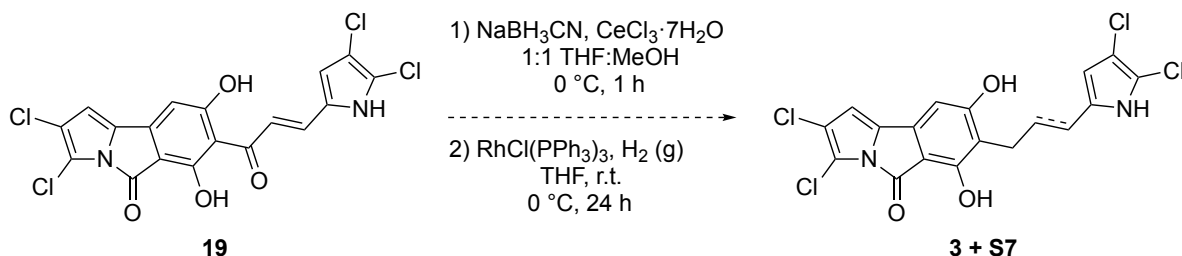
A 25 mL round bottom flask equipped with a stir bar was oven-dried, charged with N_2 , and filled with 15 mL THF. (*E*)-2,3-dichloro-7-(3-(4,5-dichloro-1*H*-pyrrol-2-yl)acryloyl)-6,8-dihydroxy-5*H*-pyrrolo[2,1-*a*]isoindol-5-one (**19**) (400 mg, 0.873 mmol) and $\text{RhCl(PPh}_3)_3$ (40 mg, 0.043 mmol) were added to the flask. A balloon filled with H_2 gas was then used to backfill the flask several times. The reaction was stirred for 24 hours at room temperature. Upon completion, the reaction was diluted with water and extracted with EtOAc (3 x 20 mL). The organic layer was washed with brine, dried with anhydrous Na_2SO_4 , filtered, and concentrated under reduced pressure. The crude mixture was

purified by flash column chromatography using silica gel and a gradient from 0% to 10% DCM/MeOH over 25 minutes as eluent to yield a yellow solid (390 mg, quant.). UV/Vis: λ_{\max} = 268, 308, 355, 396 nm; $^1\text{H NMR}$ (500 MHz, $(\text{CD}_3)_2\text{CO}$) δ 6.92 (s, 1H), 6.84 (s, 1H), 5.95 (s, 1H), 3.20 (t, 2H, J = 7.5 Hz), 2.90 (t, 2H, J = 7.5 Hz); HR-ESI-TOFMS: m/z (M-H^-) calculated for $\text{C}_{18}\text{H}_{10}\text{Cl}_4\text{N}_2\text{O}_4$ 456.9322, found 456.9369.



A 10 mL round bottom flask equipped with a stir bar was oven-dried, charged with N_2 , filled with 5 mL THF, and cooled to 0 °C. 2,3-dichloro-7-(3-(4,5-dichloro-1H-pyrrol-2-yl)propanoyl)-6,8-dihydroxy-5H-pyrrolo[2,1-a]isoindol-5-one (**20**) (200 mg, 0.453 mmol) and NaBH_4 (41 mg, 1.09 mmol) were added to the flask. The reaction was stirred for 48 hours at room temperature. Upon completion, the reaction was slowly poured over cold ammonium chloride and extracted with EtOAc (3 x 5 mL). The organic layer was washed with brine, dried with anhydrous Na_2SO_4 , filtered, and concentrated under reduced pressure. The crude mixture was purified by flash column chromatography using silica gel and a gradient from 0% to 10% DCM/MeOH over 25 minutes as eluent to yield a yellow solid (120 mg, 60%). UV/Vis: λ_{\max} = 267, 339, 354, 405 nm; $^1\text{H NMR}$ (500 MHz, CD_3OD) δ 6.52 (s, 1H), 6.39 (s, 1H), 5.79 (s, 1H), 4.57 (t, 1H, J = 6.8 Hz), 2.55 (m, 2H), 1.97 (m, 2H); $^{13}\text{C}\{^1\text{H}\}$ NMR (125 MHz, CD_3OD) δ 161.7, 134.2, 131.7, 131.3, 131.2, 113.5, 109.4, 108.1, 106.5, 106.4, 105.8, 101.3, 65.1, 37.1, 24.5; HR-ESI-TOFMS: m/z (M-H^-)

calculated for $C_{18}H_{12}Cl_4N_2O_4$ 458.9478, found 458.9507. a3 carbons not observed in HSQC or HMBC data.



An 8 mL vial equipped with a stir bar was oven-dried, charged with N_2 , filled with 2 mL 1:1 THF:MeOH, and cooled to 0 °C. (*E*)-2,3-dichloro-7-(3-(4,5-dichloro-1*H*-pyrrol-2-yl)acryloyl)-6,8-dihydroxy-5*H*-pyrrolo[2,1-*a*]isoindol-5-one (**19**) (10 mg, 0.022 mmol) was added to the vial, followed by cerium(III) chloride heptahydrate (41 mg, 0.109 mmol) and stirred for 10 minutes before adding $NaBH_3CN$ (13.7 mg, 0.109 mmol). The reaction was stirred at 0 °C for 1 hour before slowly quenching with a cold saturated solution of ammonium chloride and extracted with EtOAc (3 x 3 mL). The organic layer was washed with brine, dried with anhydrous Na_2SO_4 , filtered, and concentrated under a stream of nitrogen gas. The crude mixture was reconstituted in 2 mL dry THF and $RhCl(PPh_3)_3$ (2 mg, 2.16 μ mol) was added to the flask. A balloon filled with H_2 gas was then used to backfill the vial. The reaction was stirred for 24 hours at room temperature. Upon completion, the reaction was diluted with water and extracted with EtOAc (3 x 20 mL). The organic layer was concentrated under a stream of nitrogen gas and reconstituted in acetonitrile for LC-MS analysis.

S7: UV/Vis: λ_{max} = 278, 345, 361, 409 nm; HR-ESI-TOFMS: m/z (M-H) $^-$ calculated for $C_{18}H_{10}Cl_4N_2O_3$ 440.9368, found 440.9381.

3: UV/Vis: λ_{\max} = 265, 346, 358, 408 nm; HR-ESI-TOFMS: m/z (M-H)⁻ calculated for C₁₈H₁₂Cl₄N₂O₃ 442.9524, found 442.9550.

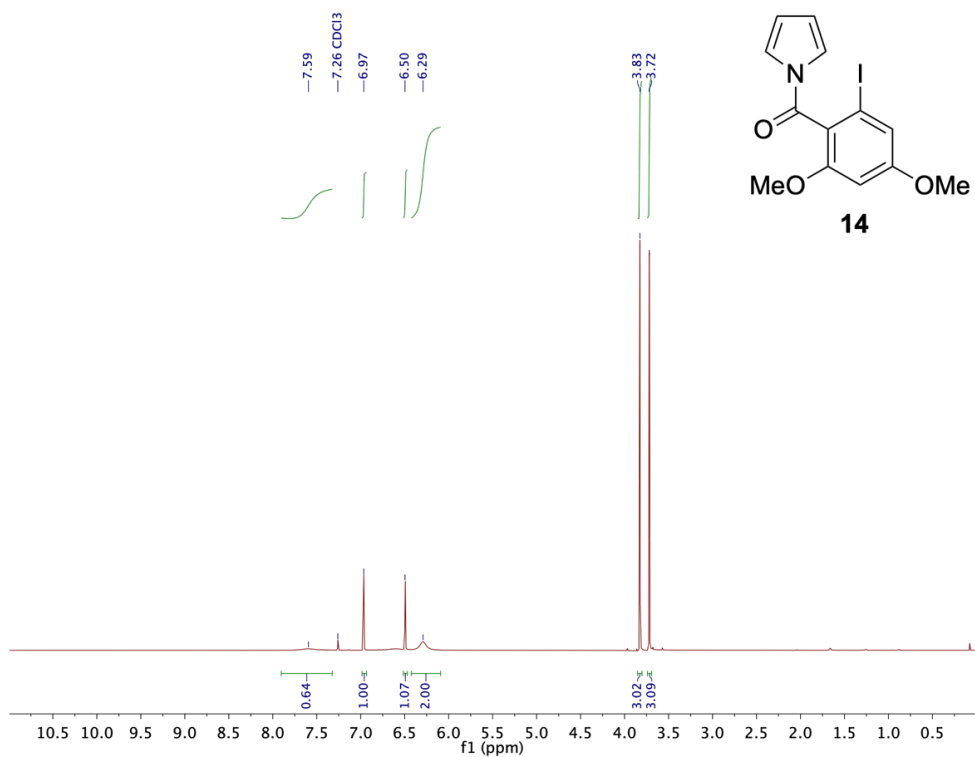


Figure S1: ¹H NMR spectrum of **14** (500 MHz, CDCl₃).

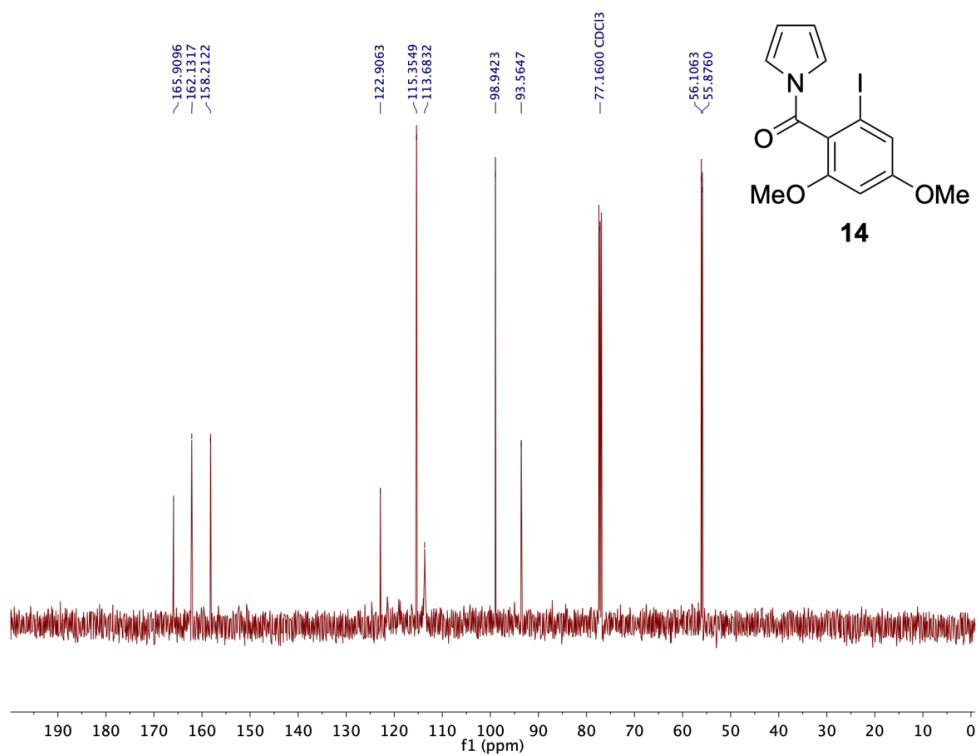


Figure S2: ¹³C NMR spectrum of **14** (125 MHz, CDCl₃).

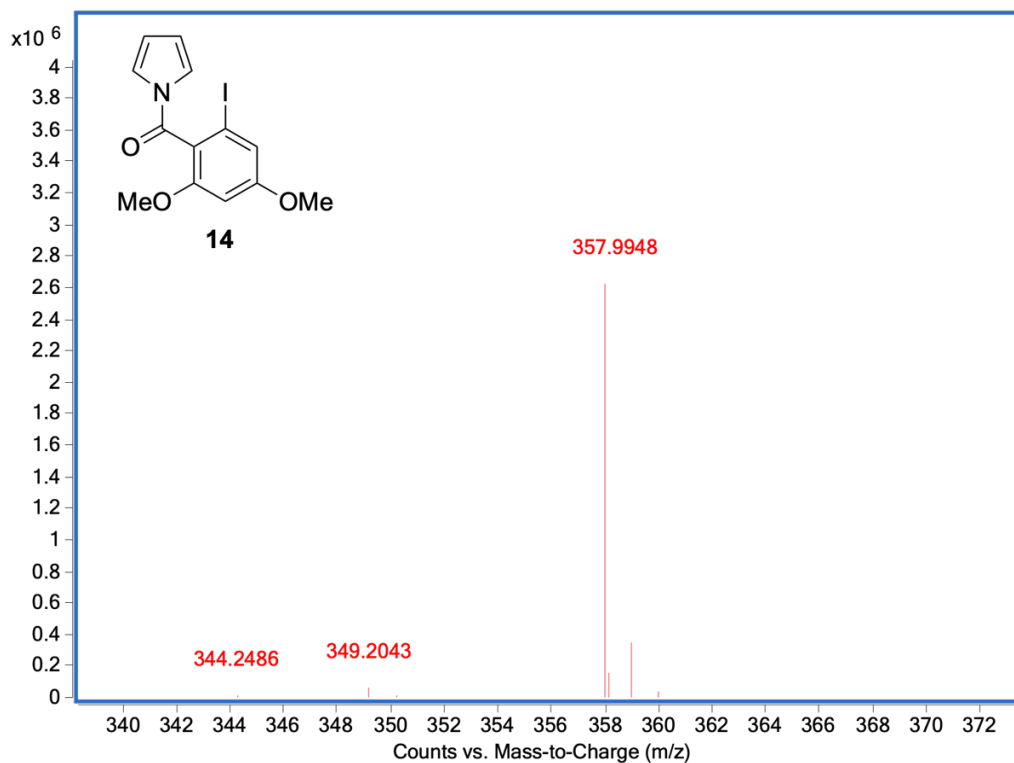


Figure S3: HR-ESI-TOFMS of **14**.

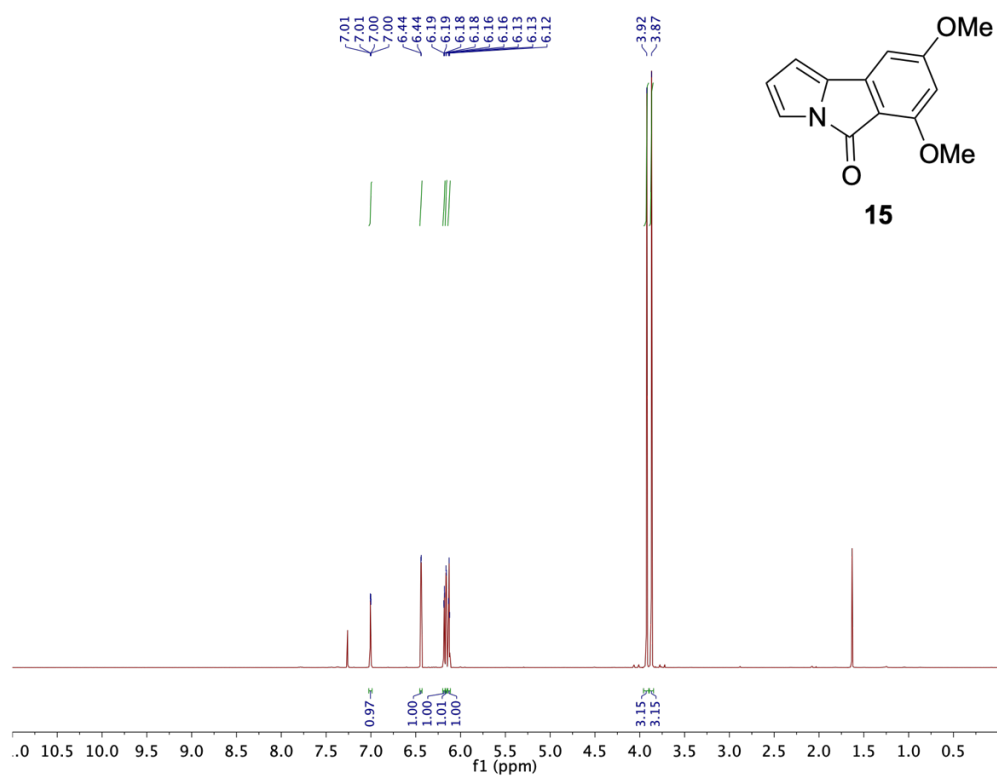


Figure S4: ^1H NMR spectrum of **15** (500 MHz, CDCl_3).

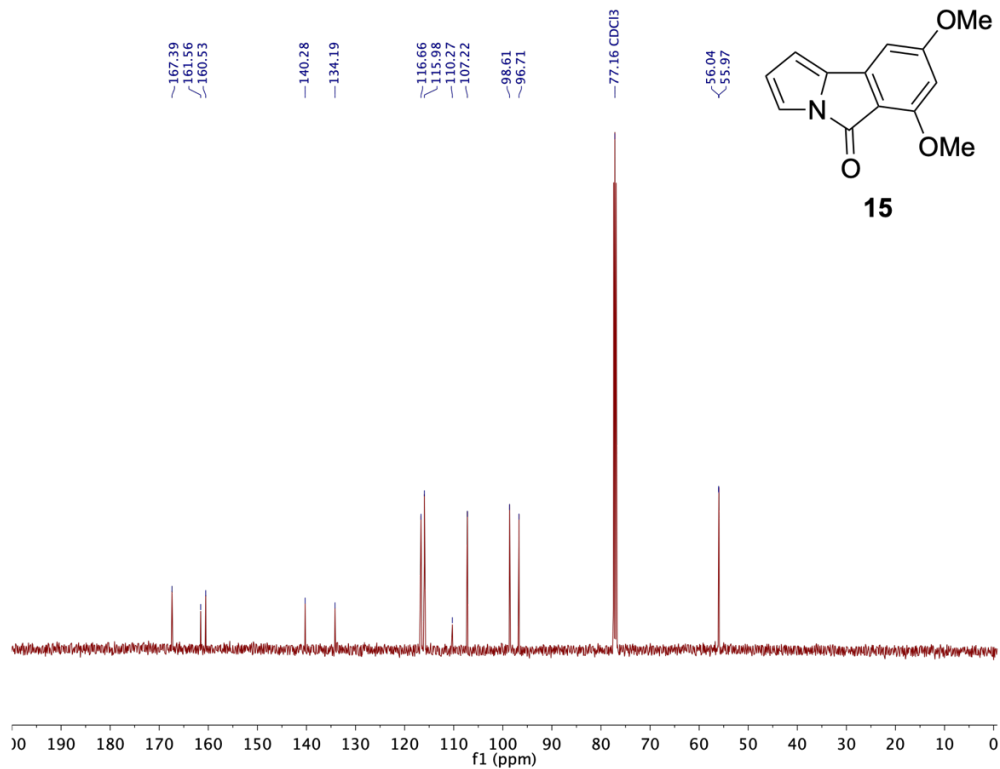


Figure S5: ¹³C NMR spectrum of **15** (125 MHz, CDCl₃).

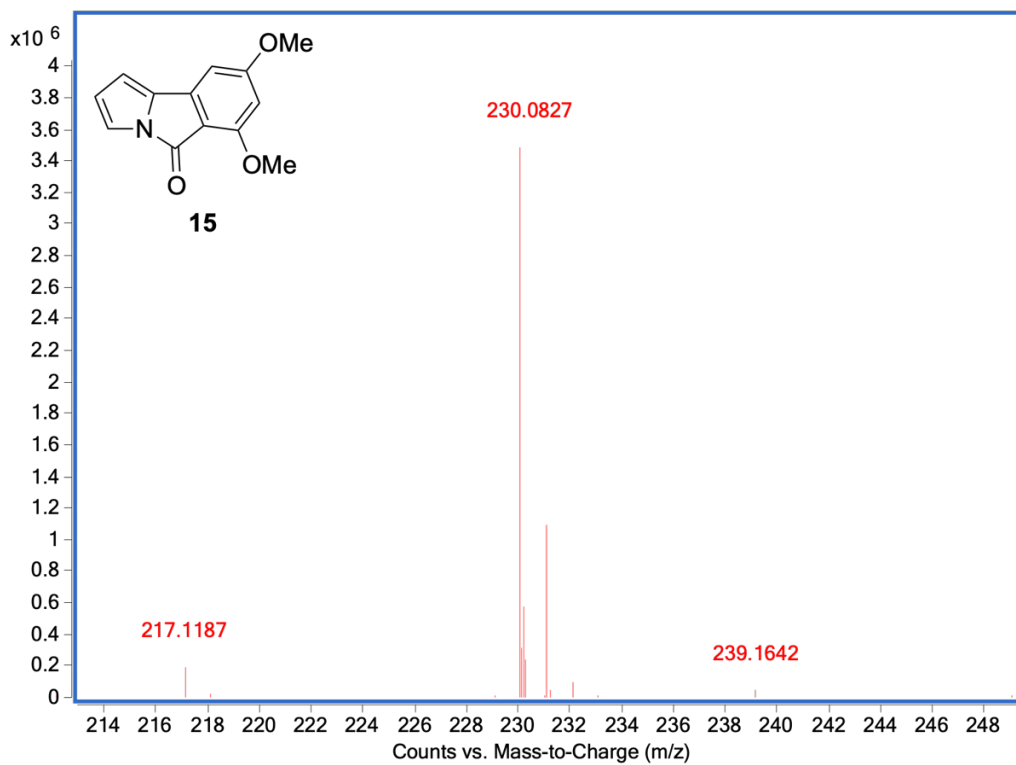


Figure S6: HR-ESI-TOFMS of **15**.

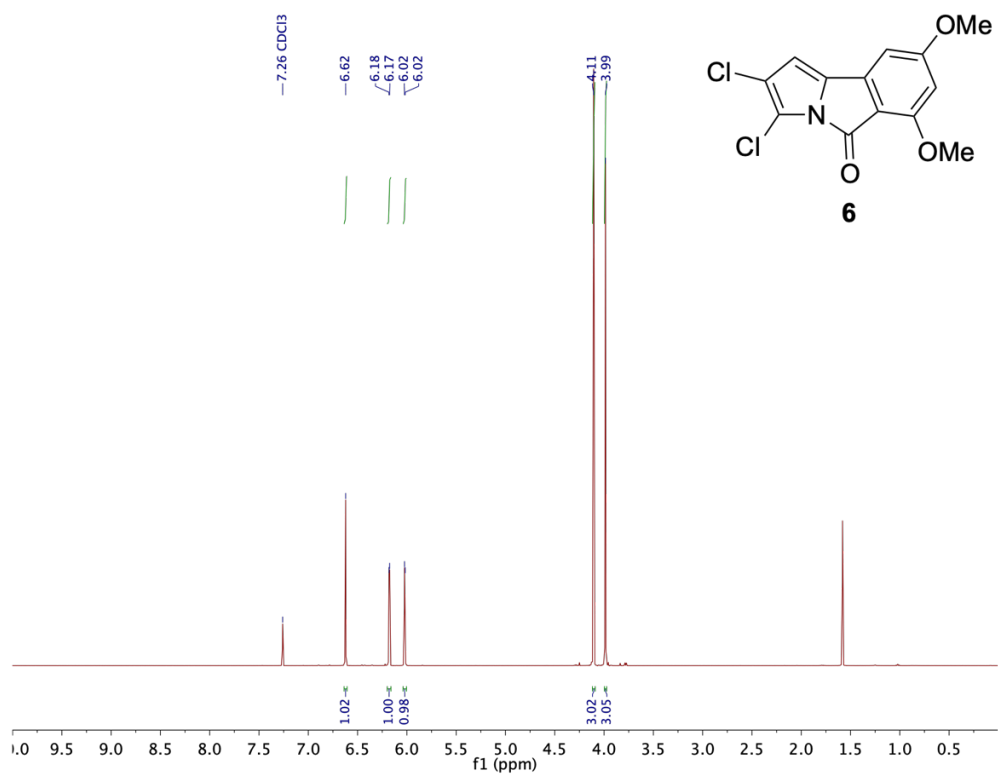


Figure S7: ¹H NMR spectrum of **6** (500 MHz, CDCl₃).

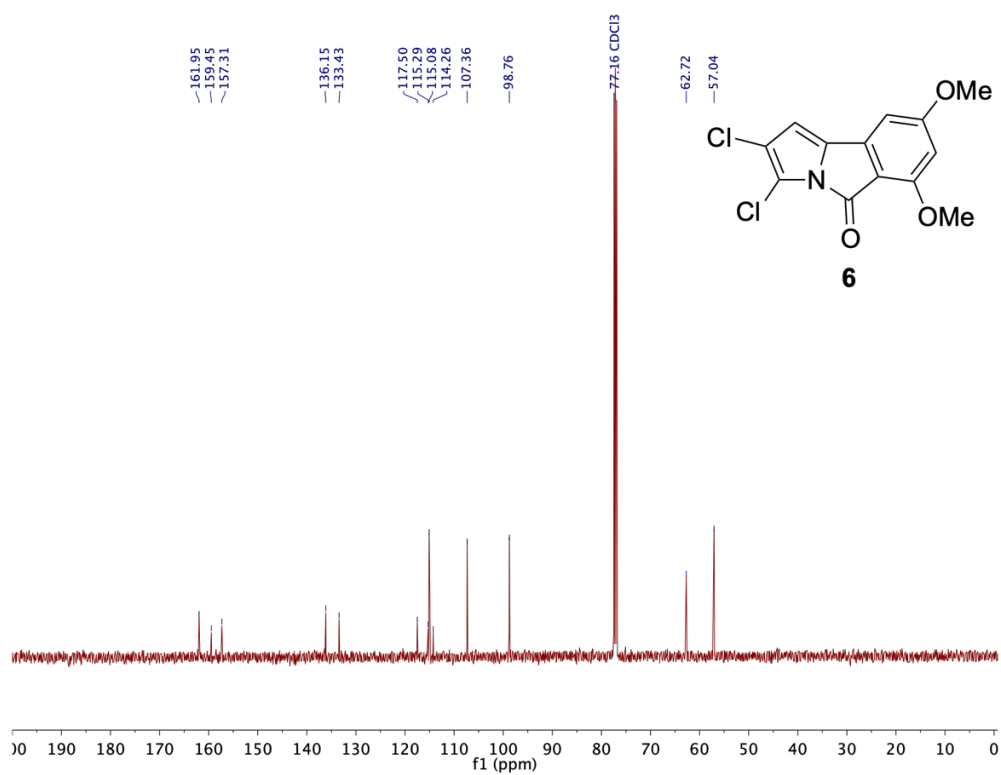


Figure S8: ¹³C NMR spectrum of **6** (125 MHz, CDCl₃).

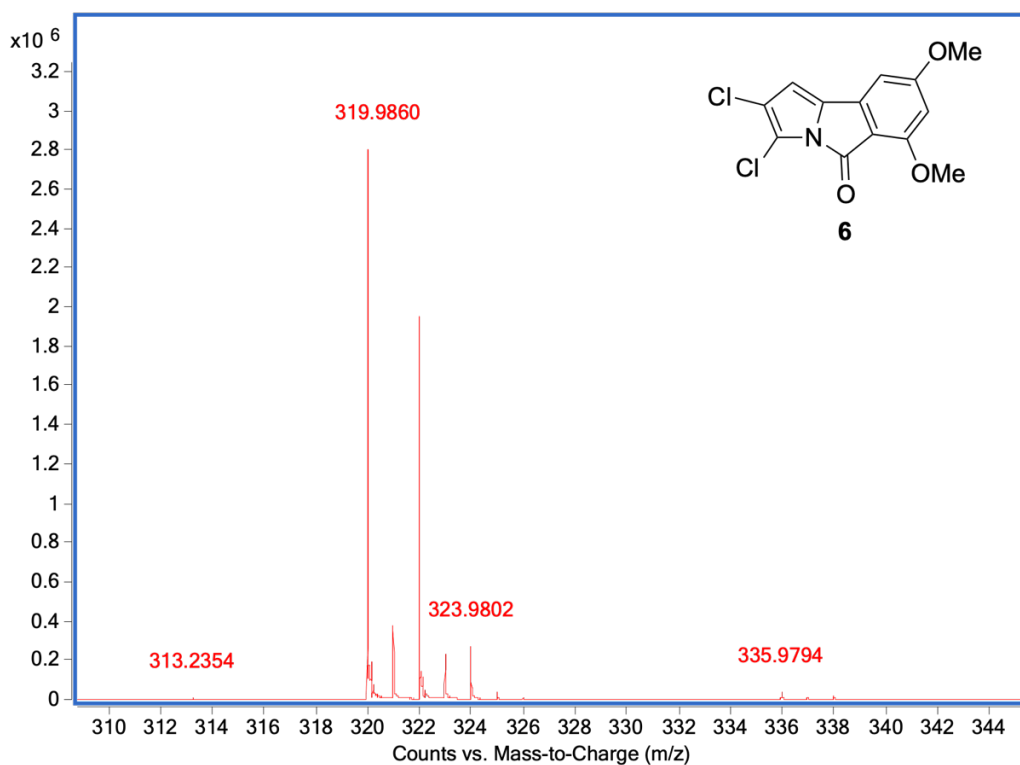


Figure S9: HR-ESI-TOFMS of **6**.

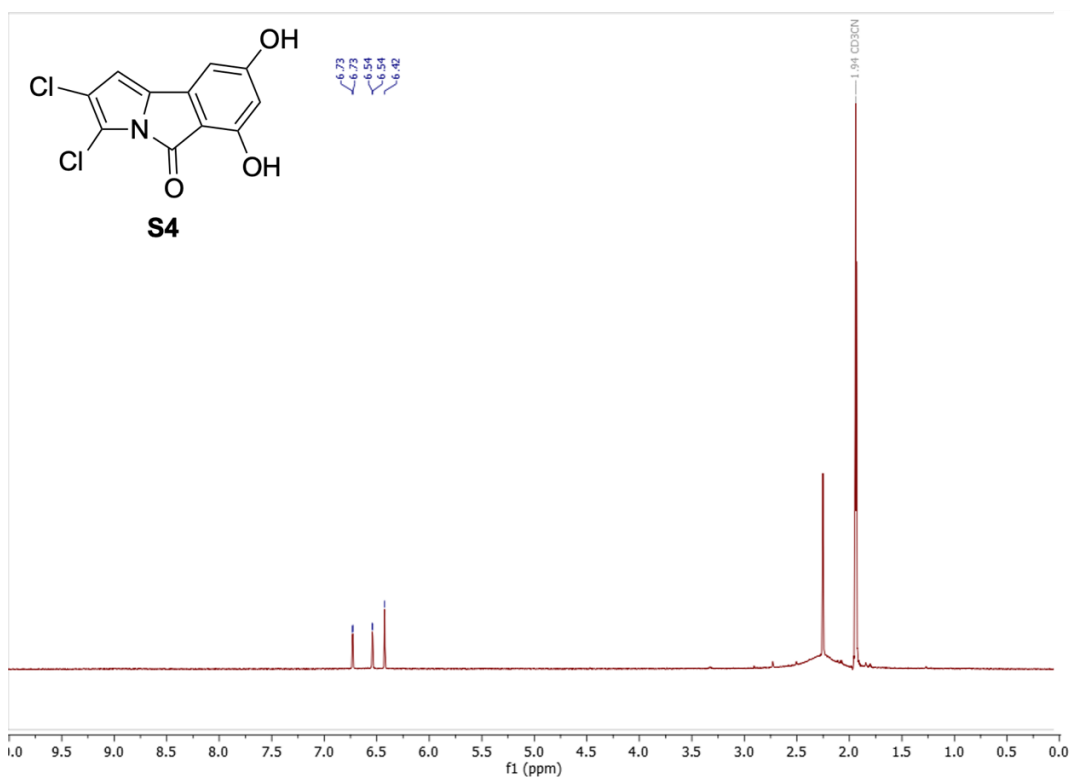


Figure S10: ^1H NMR spectrum of **S4** (500 MHz, CD_3CN).

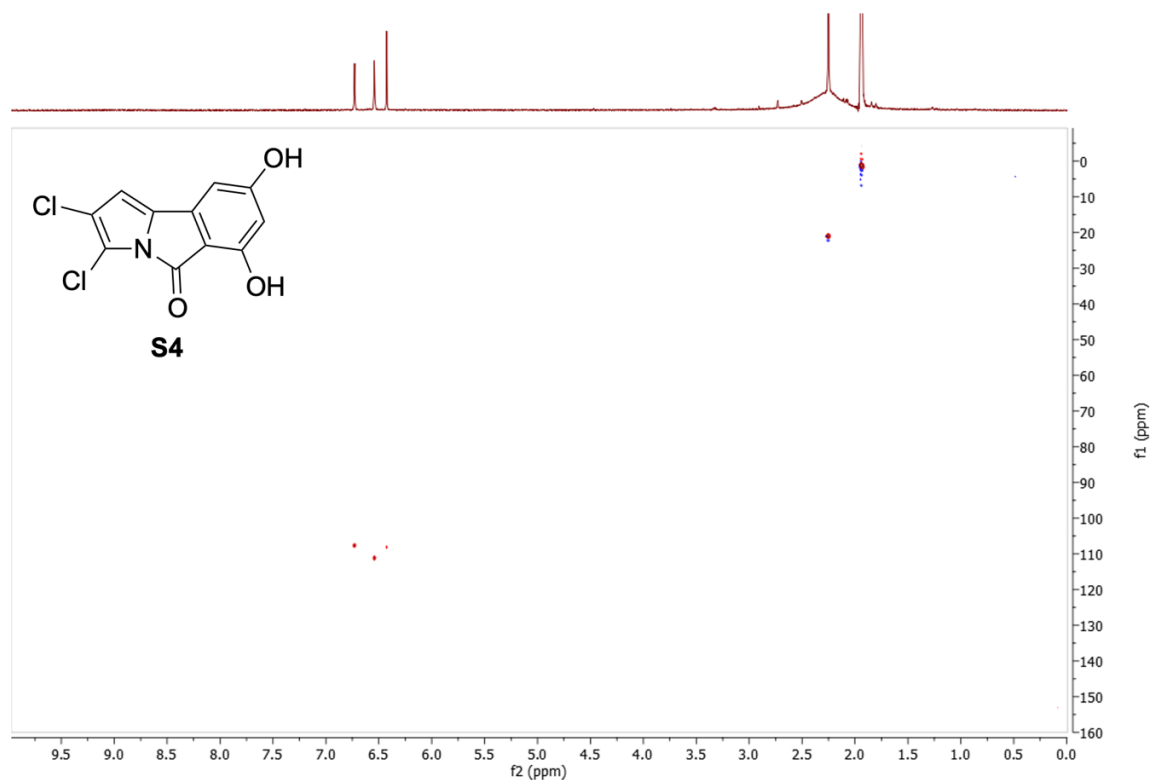


Figure S11: HSQC NMR spectrum of **S4** (125 MHz, CD₃CN).

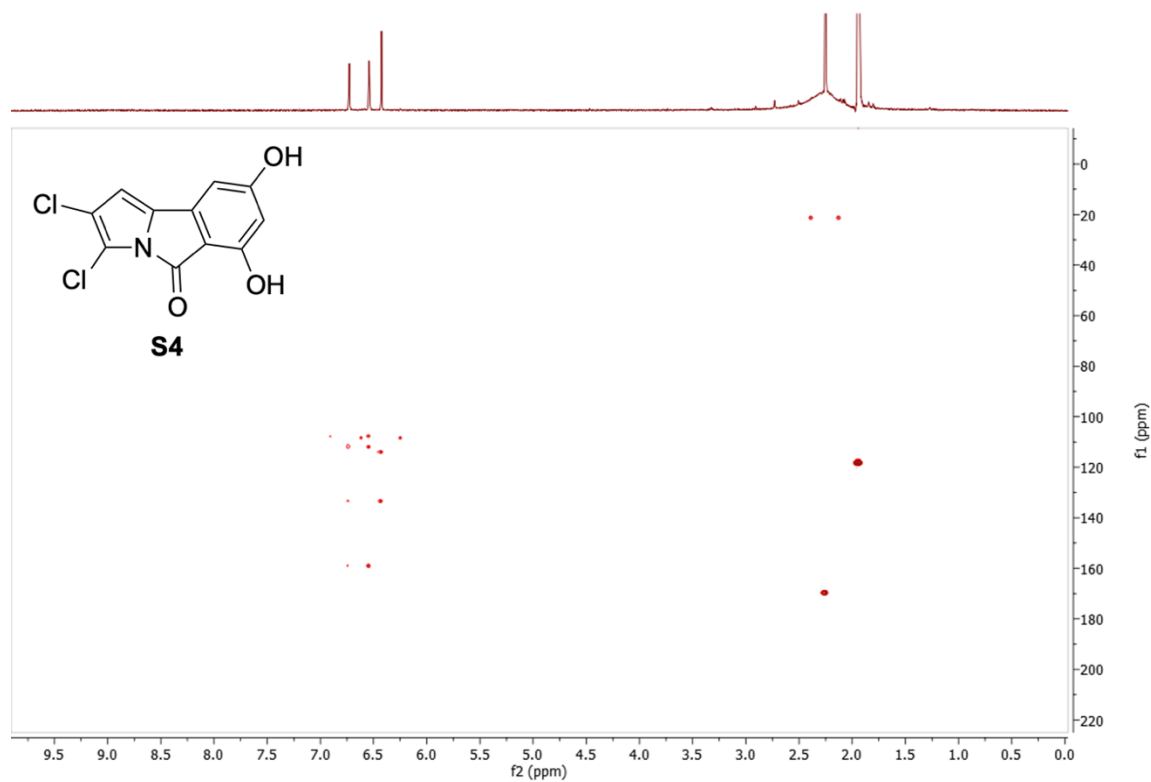


Figure S12: HMBC NMR spectrum of **S4** (125 MHz, CD₃CN).

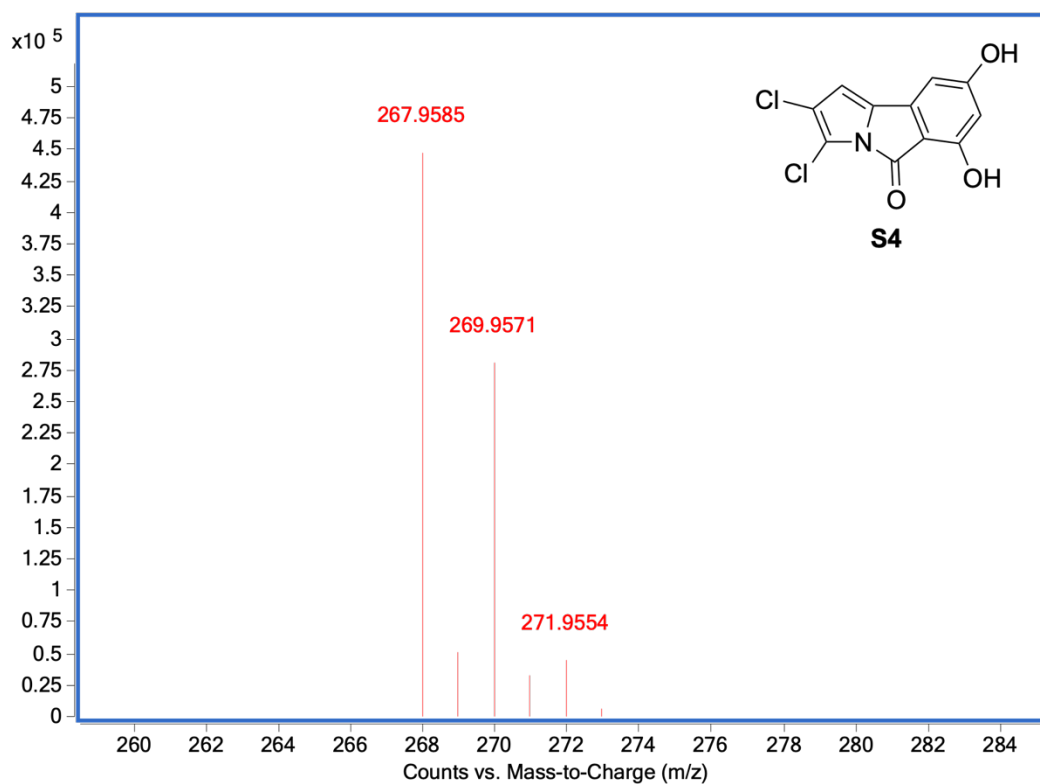


Figure S13: HR-ESI-TOFMS of **S4**.

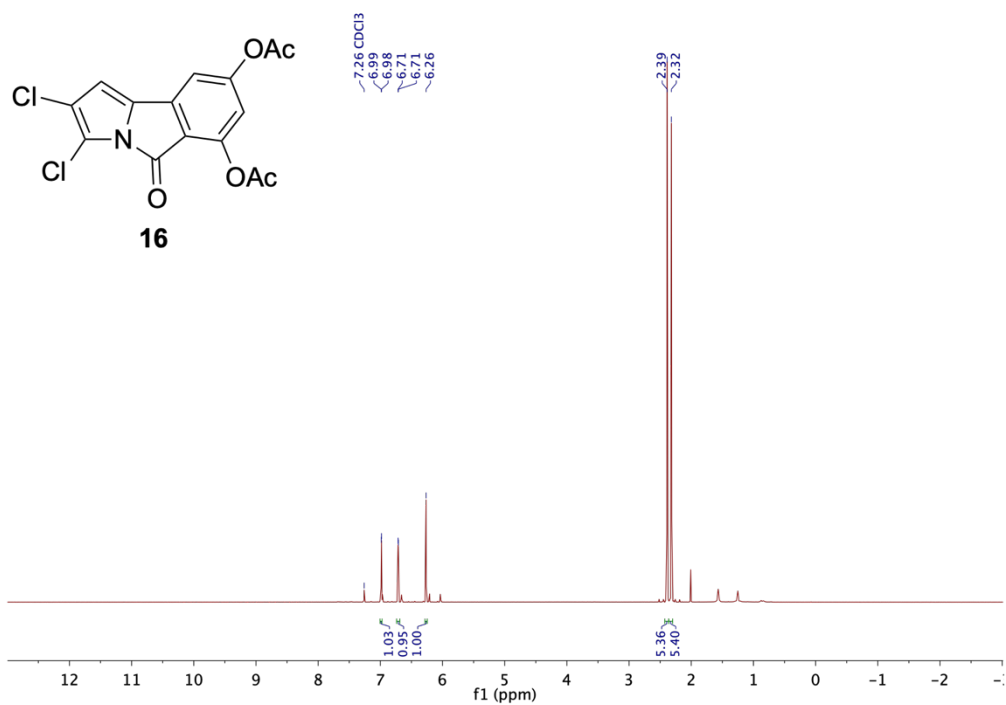


Figure S14: ^1H NMR spectrum of **16** (500 MHz, CDCl_3).

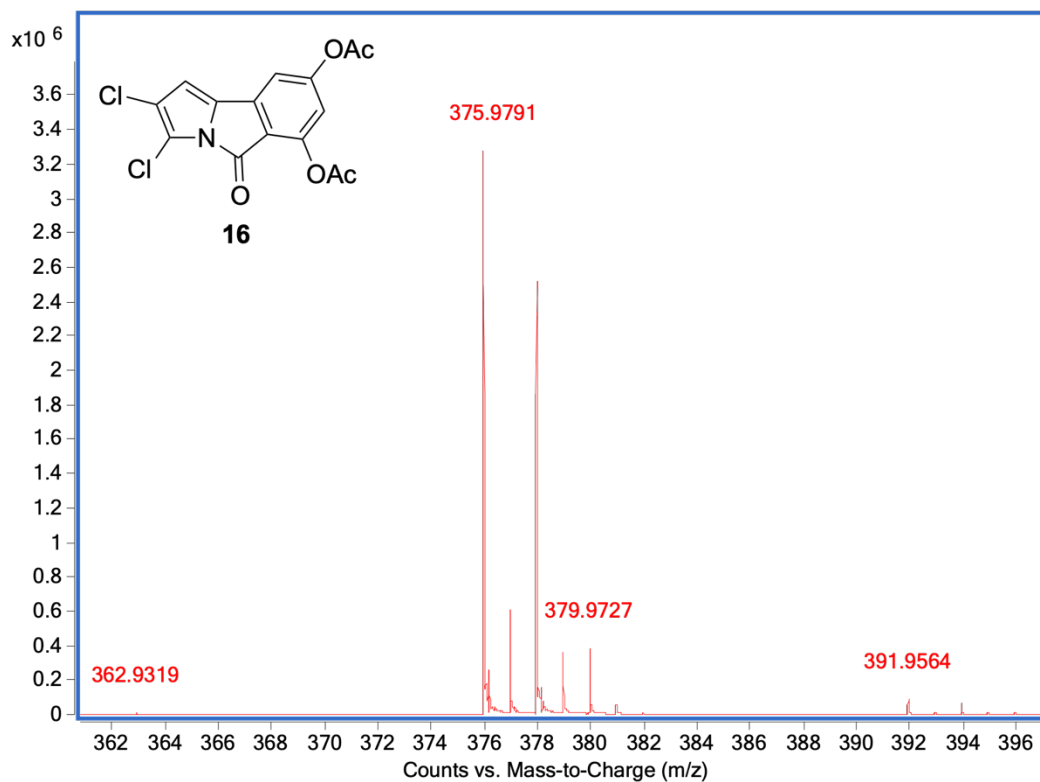


Figure S15: HR-ESI-TOFMS of **16**.

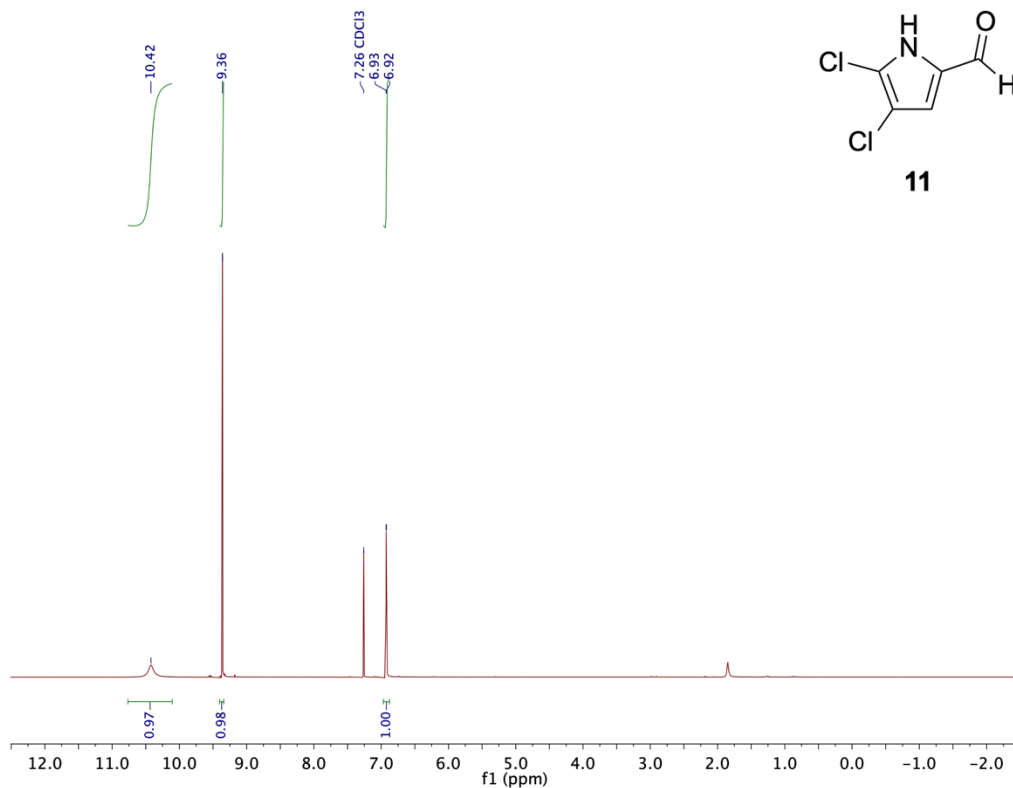


Figure S16: ¹H NMR spectrum of **11** (500 MHz, CDCl₃).

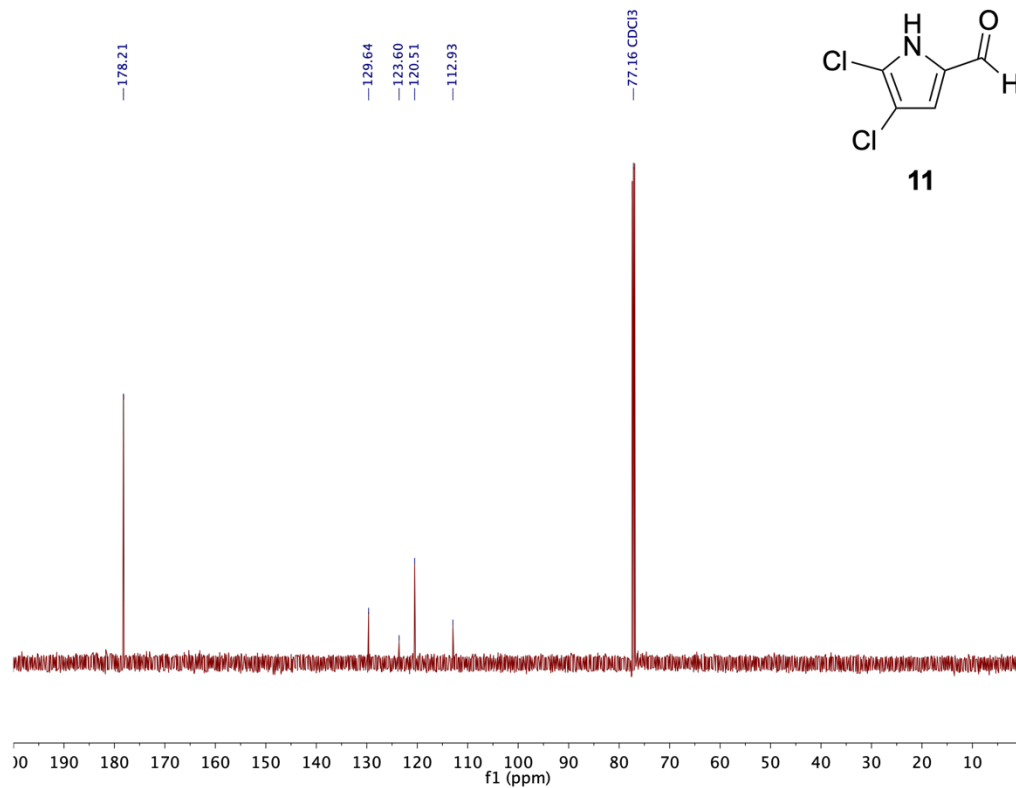


Figure S17: ¹³C NMR spectrum of **11** (125 MHz, CDCl₃).

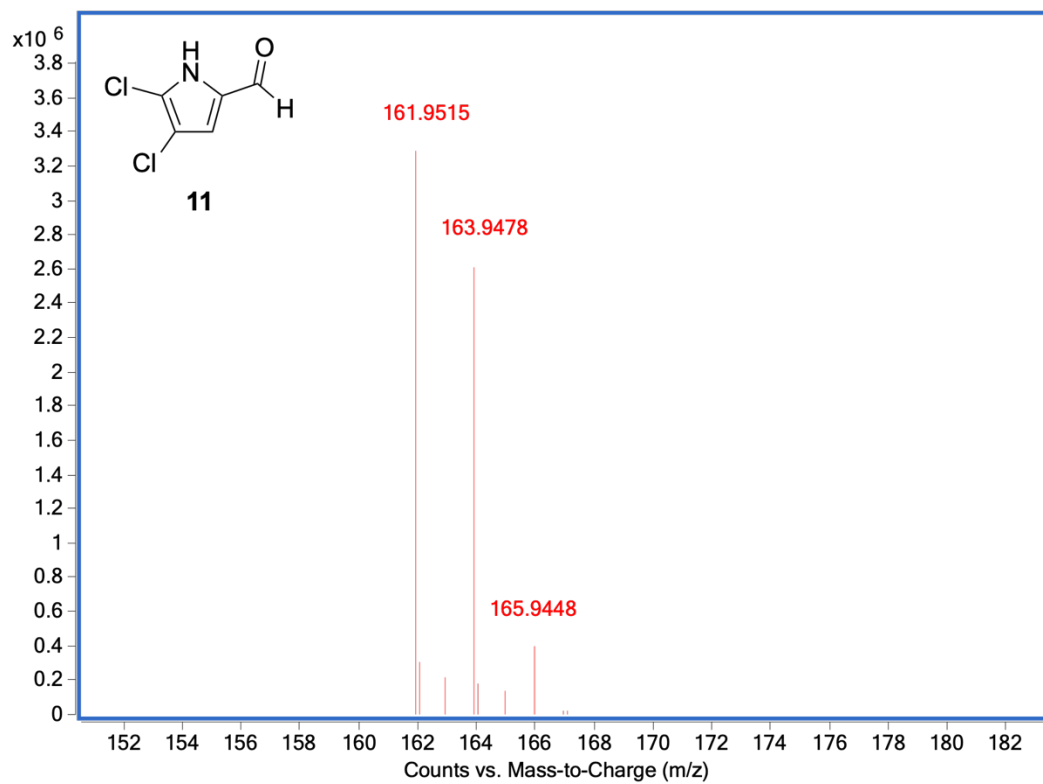


Figure S18: HR-ESI-TOFMS of **11**.

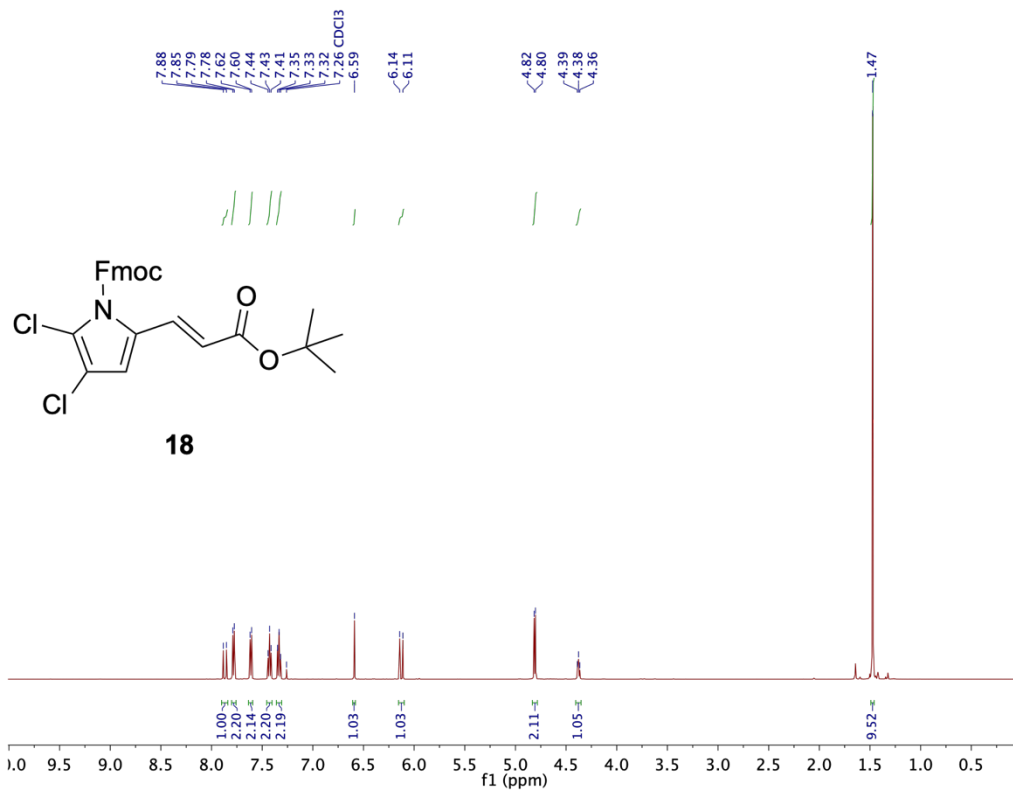


Figure S19: ¹H NMR spectrum of **18** (500 MHz, CDCl₃).

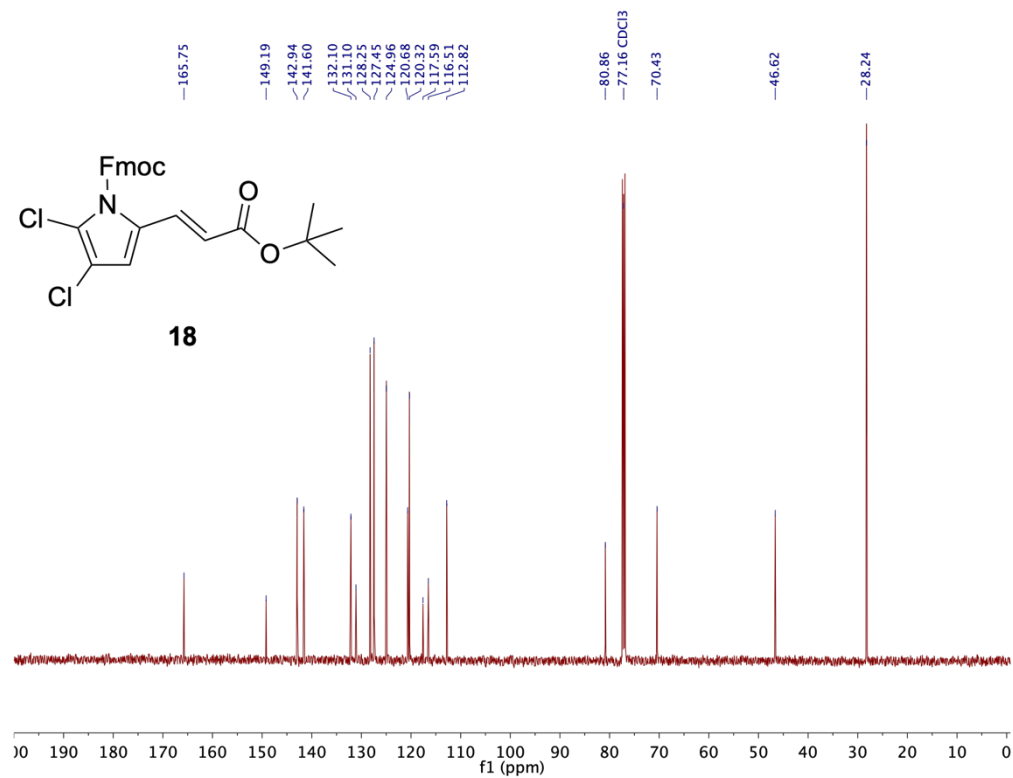


Figure S20: ¹³C NMR spectrum of **18** (125 MHz, CDCl₃).

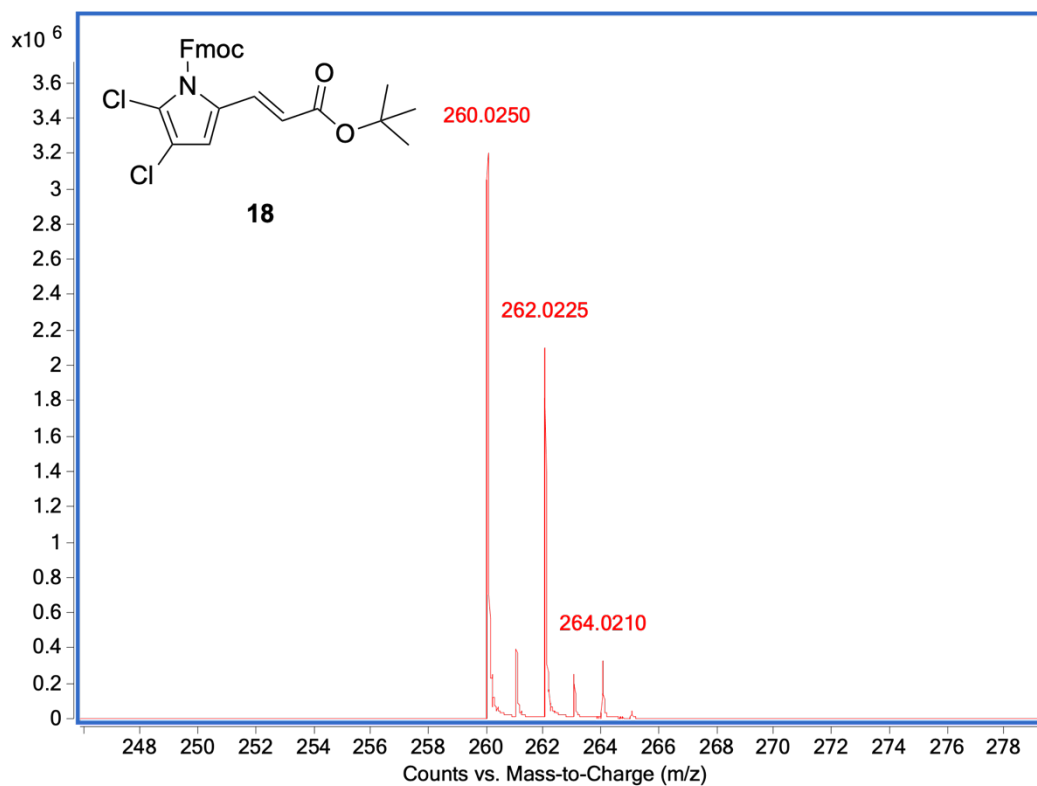


Figure S21: HR-ESI-TOFMS of **18**.

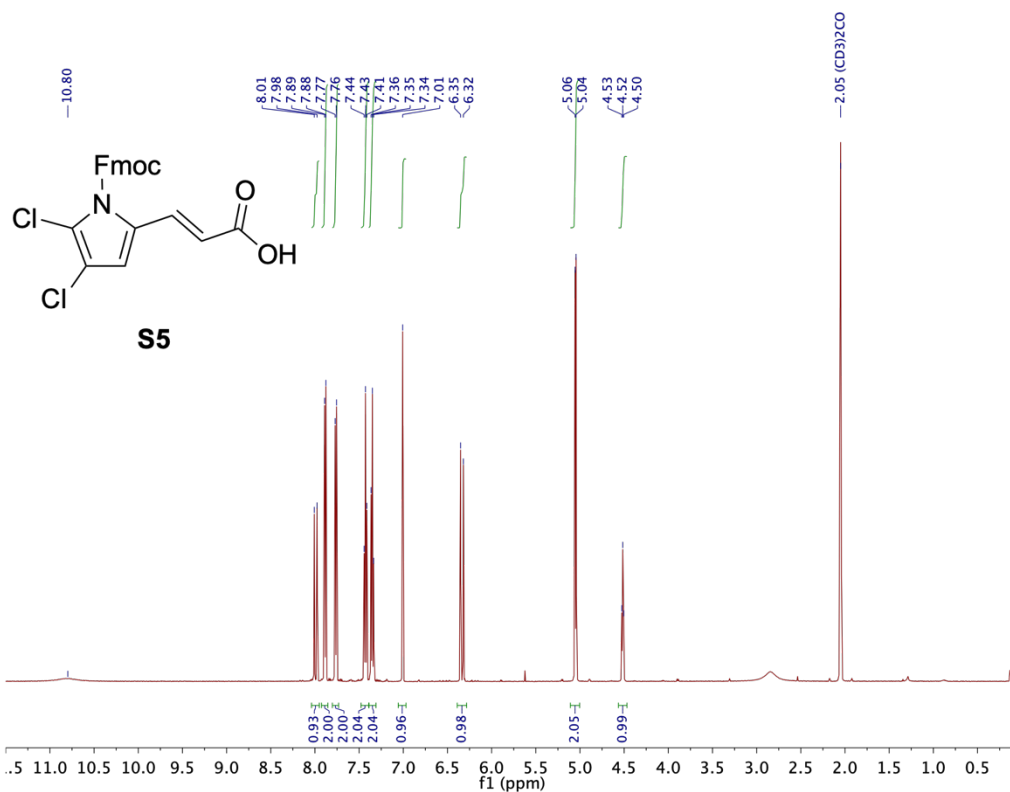


Figure S22: ^1H NMR spectrum of **S5** (500 MHz, $(\text{CD}_3)_2\text{CO}$).

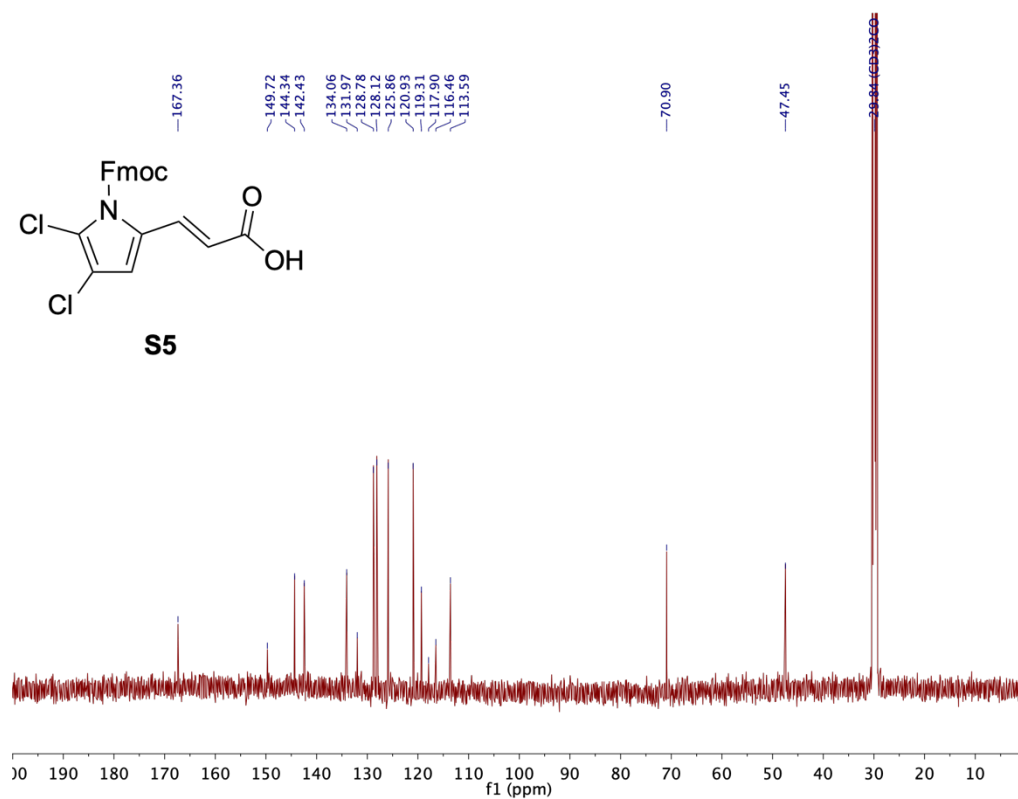


Figure S23: ¹³C NMR spectrum of **S5** (125 MHz, (CD₃)₂CO).

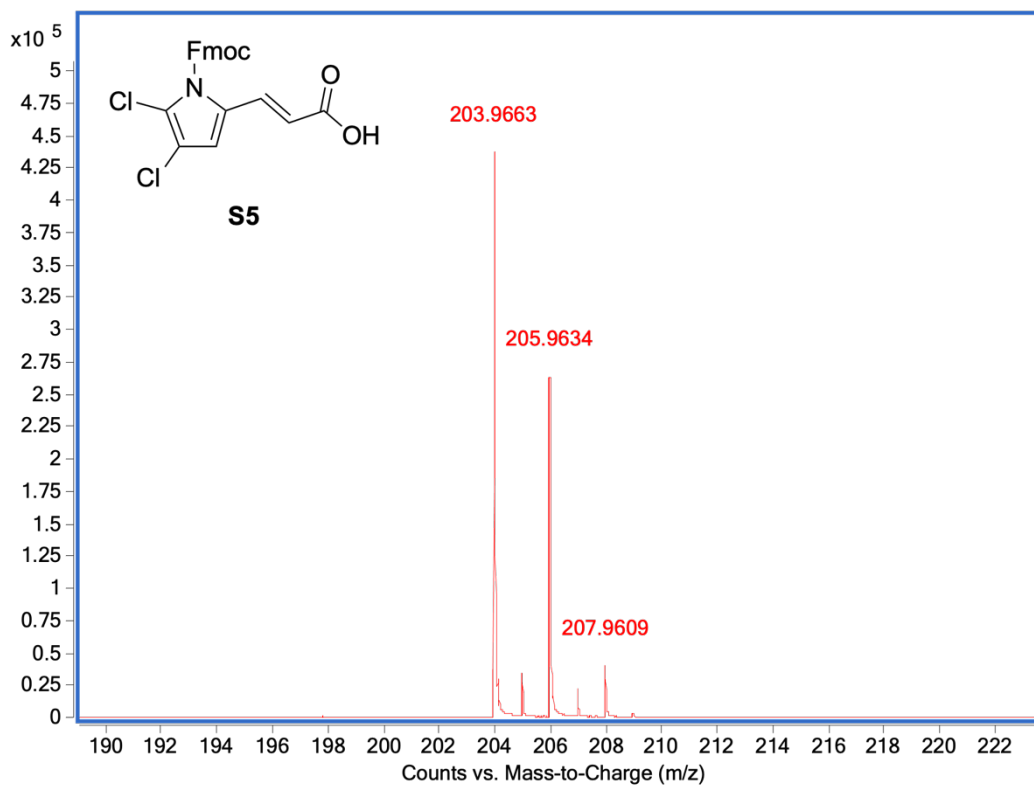


Figure S24: HR-ESI-TOFMS of **S5**.

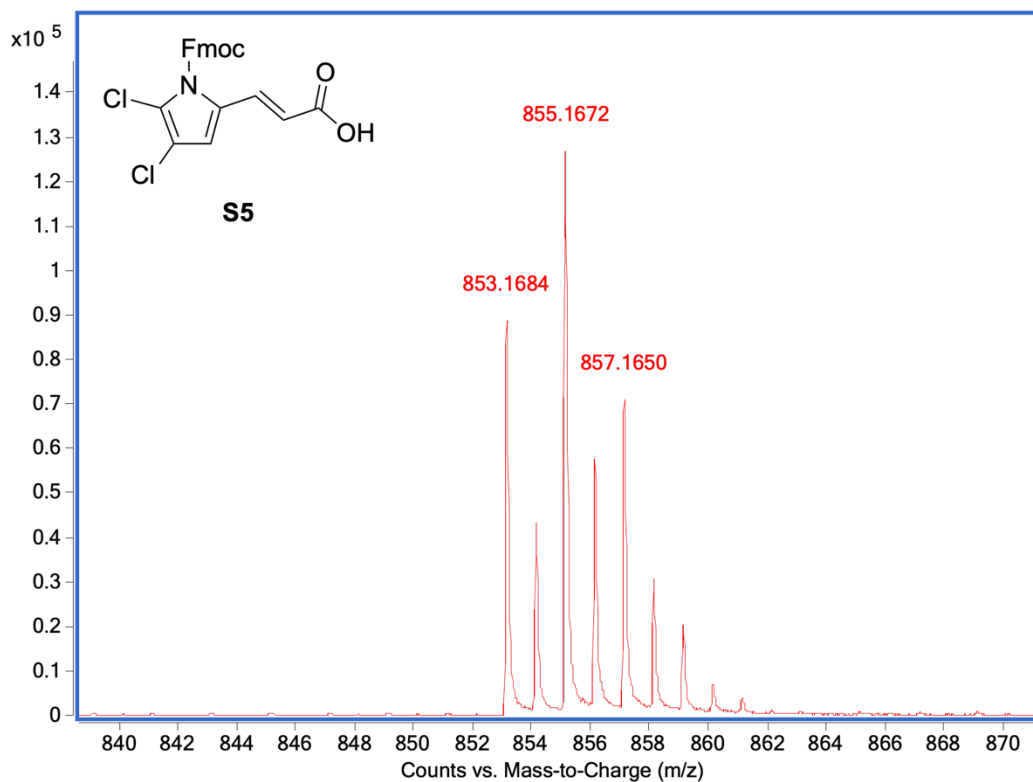


Figure S25: HR-ESI-TOFMS of **S5**.

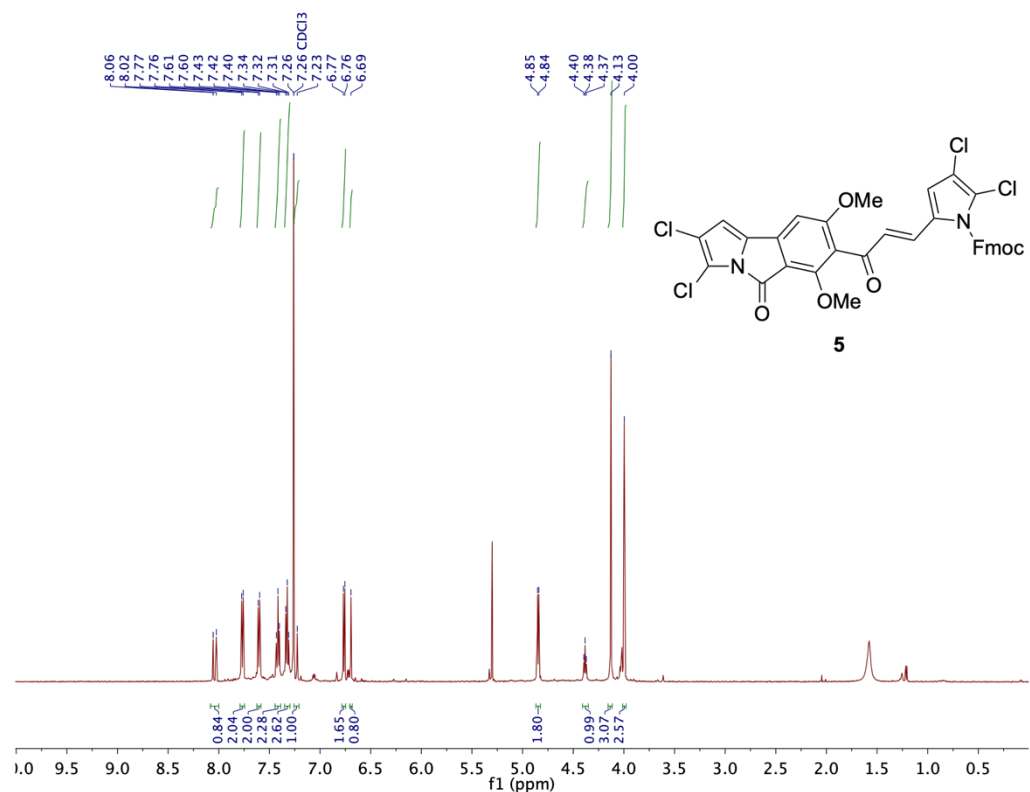


Figure S26: ¹H NMR spectrum of **5** (500 MHz, CDCl₃).

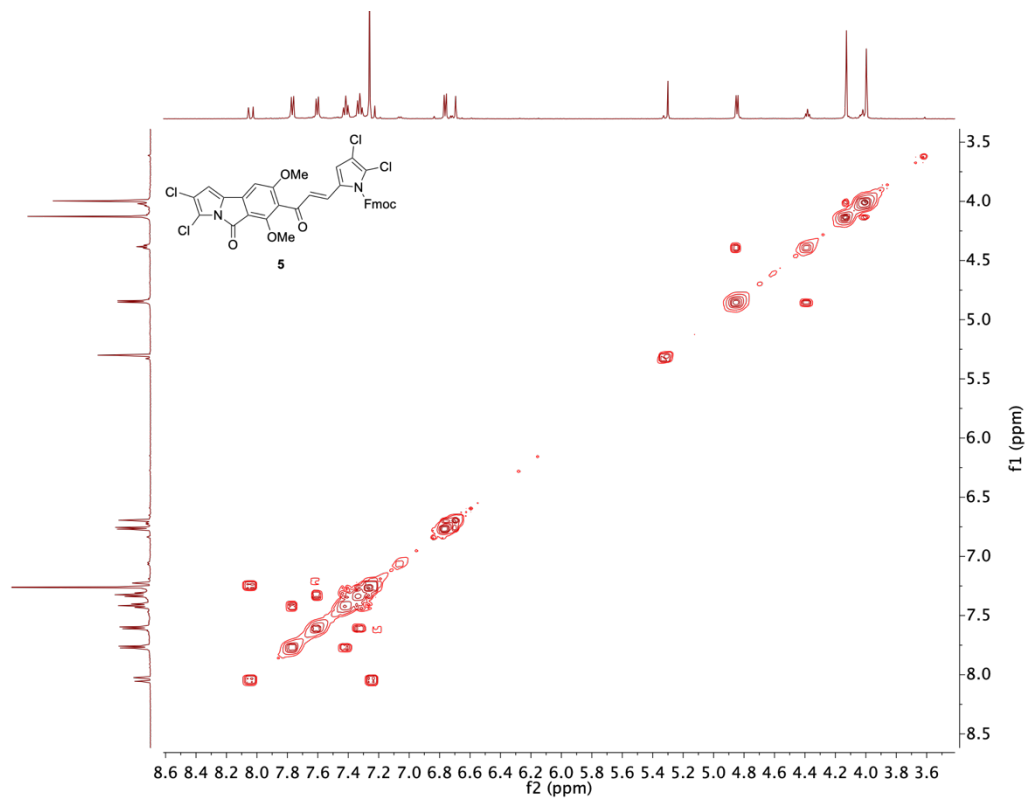


Figure S27: COSY NMR spectrum of **5** (125 MHz, CDCl_3).

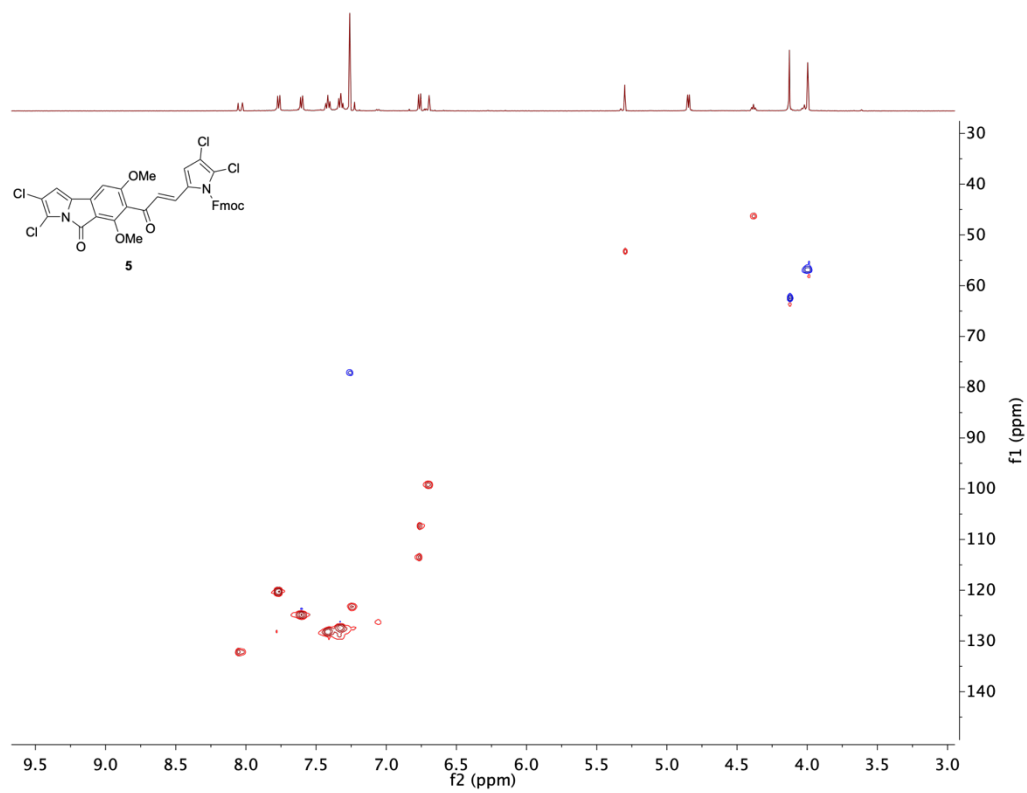


Figure S28: HSQC NMR spectrum of **5** (125 MHz, CDCl_3).

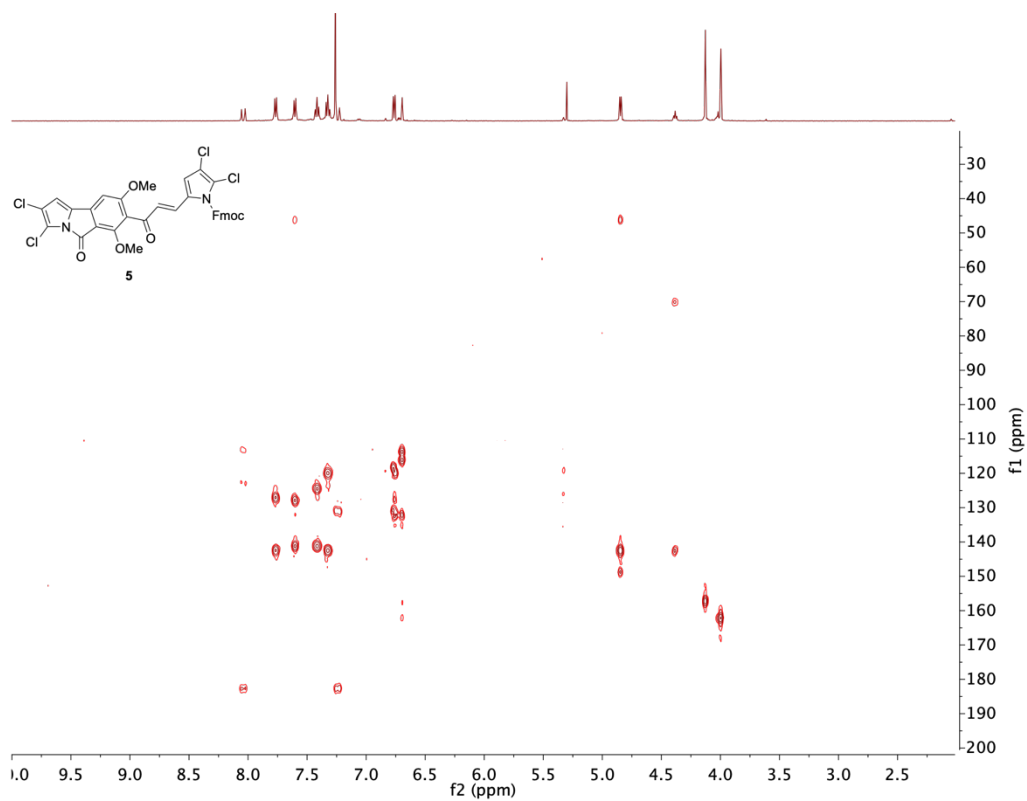


Figure S29: HMBC NMR spectrum of **5** (125 MHz, CDCl_3).

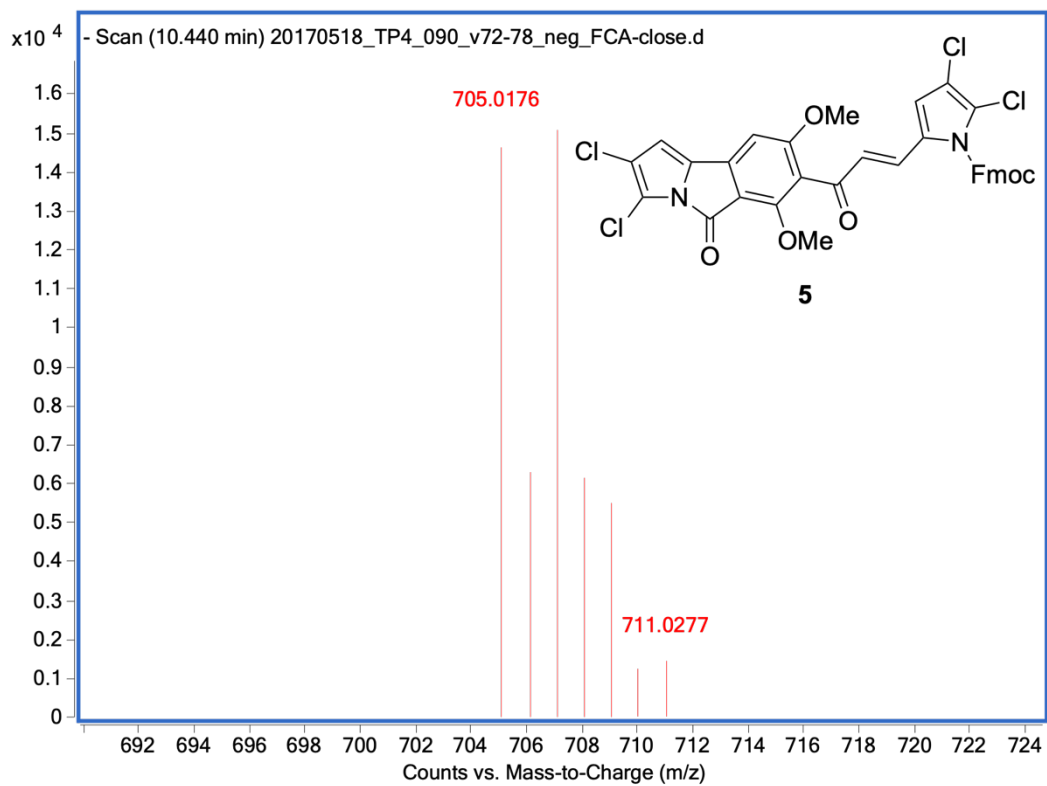


Figure S30: HR-ESI-TOFMS of **5**.

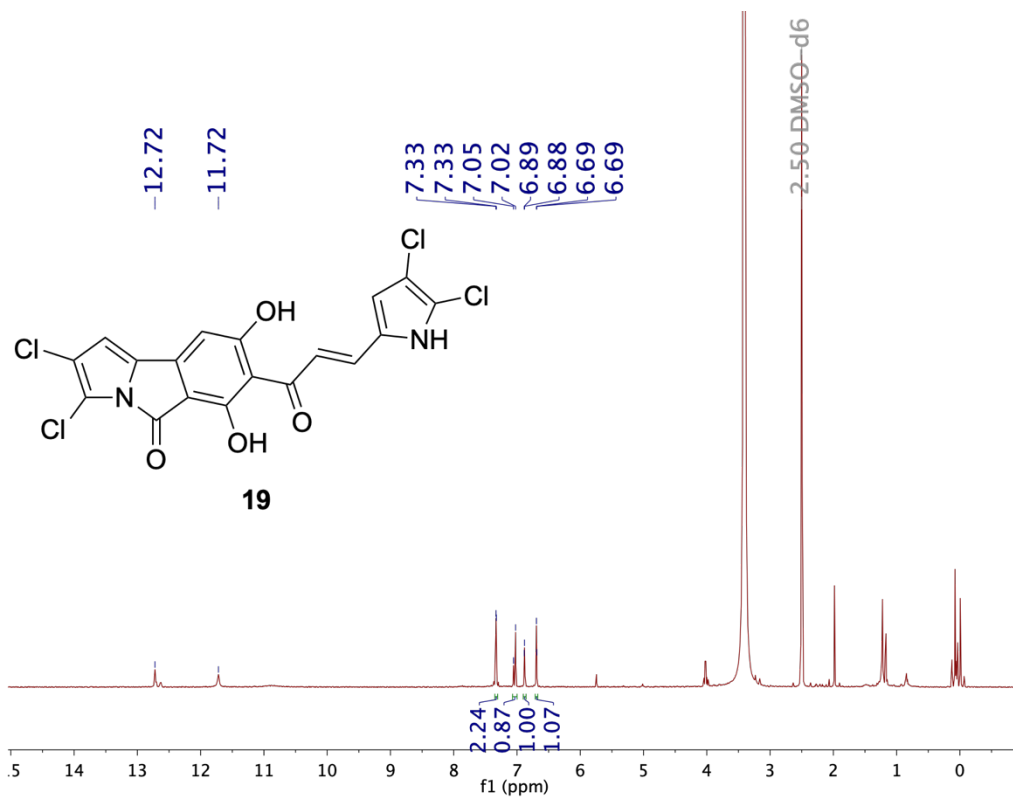


Figure S31: ¹H NMR spectrum of **19** (500 MHz, DMSO-d₆).

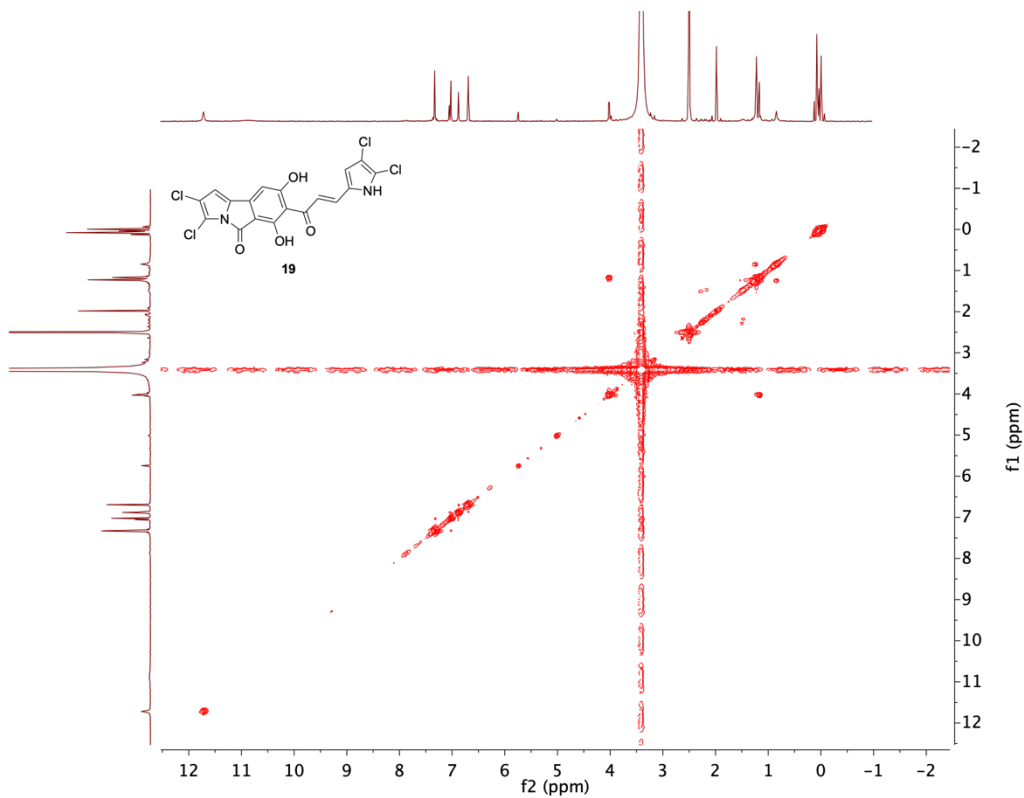
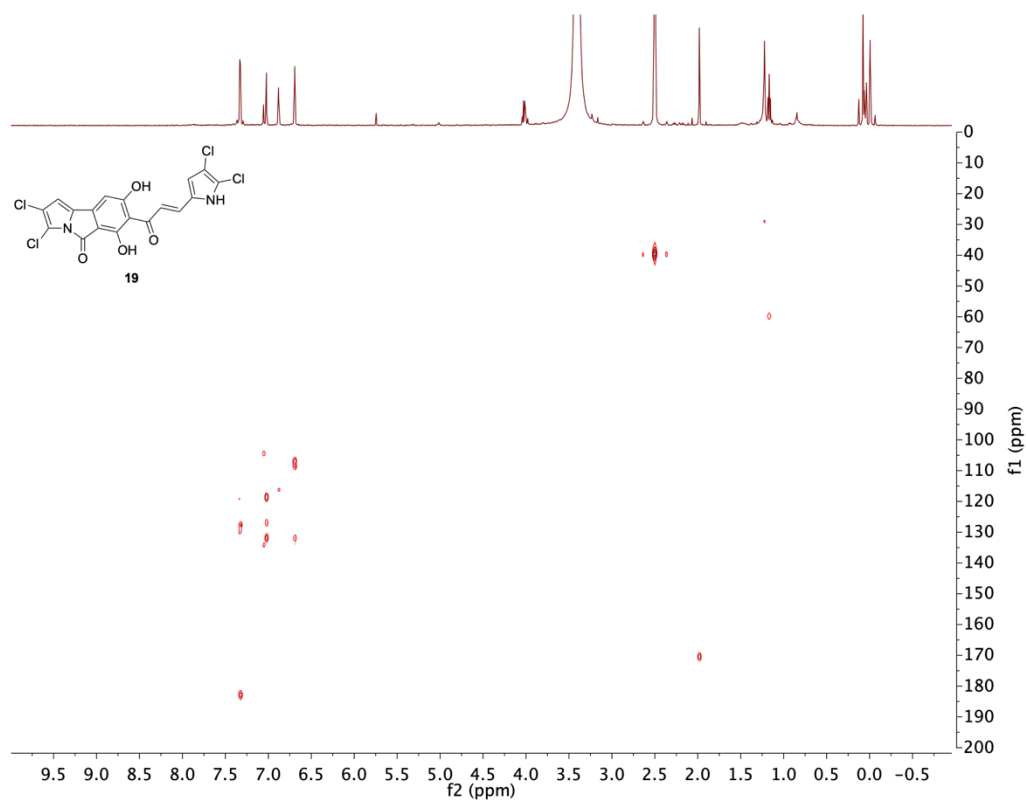
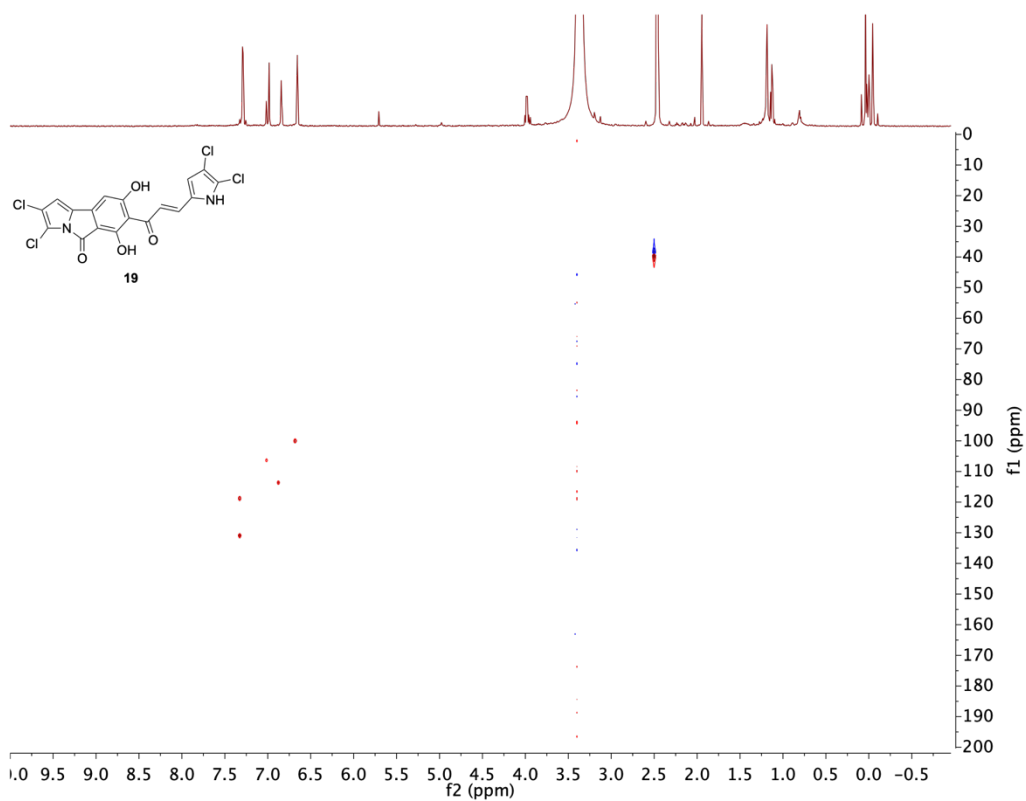


Figure S32: COSY NMR spectrum of **19** (125 MHz, DMSO-d₆).



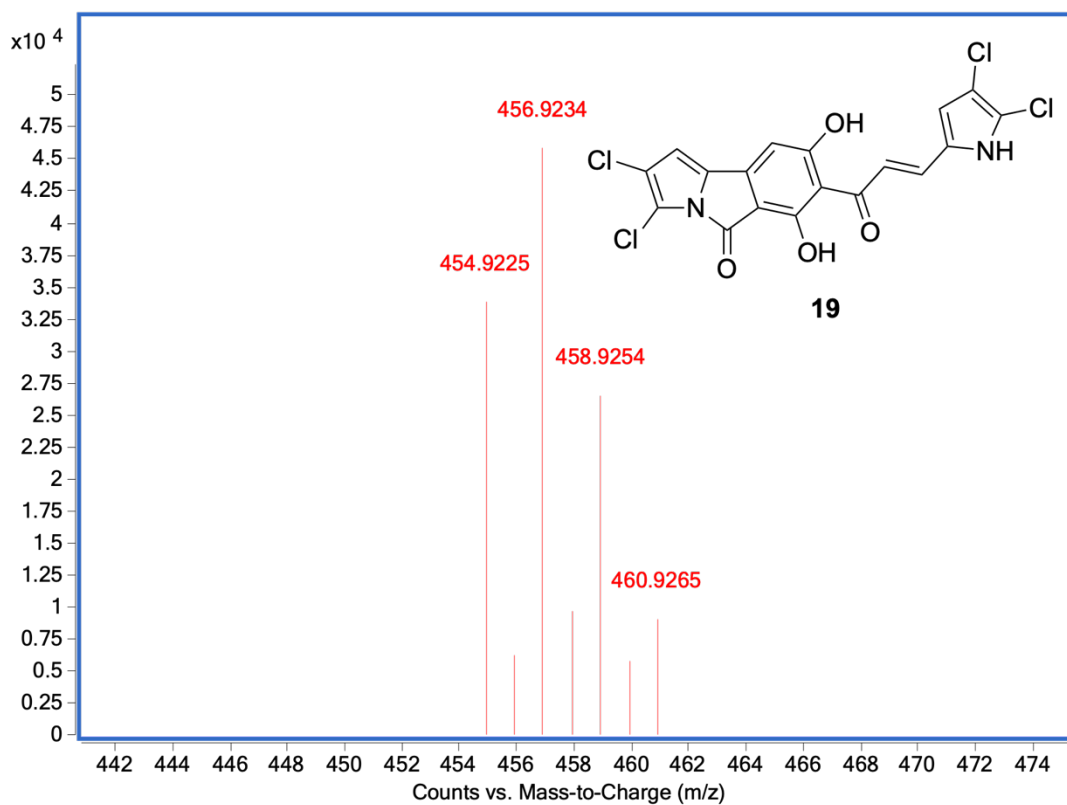


Figure S35: HR-ESI-TOFMS of **19**.

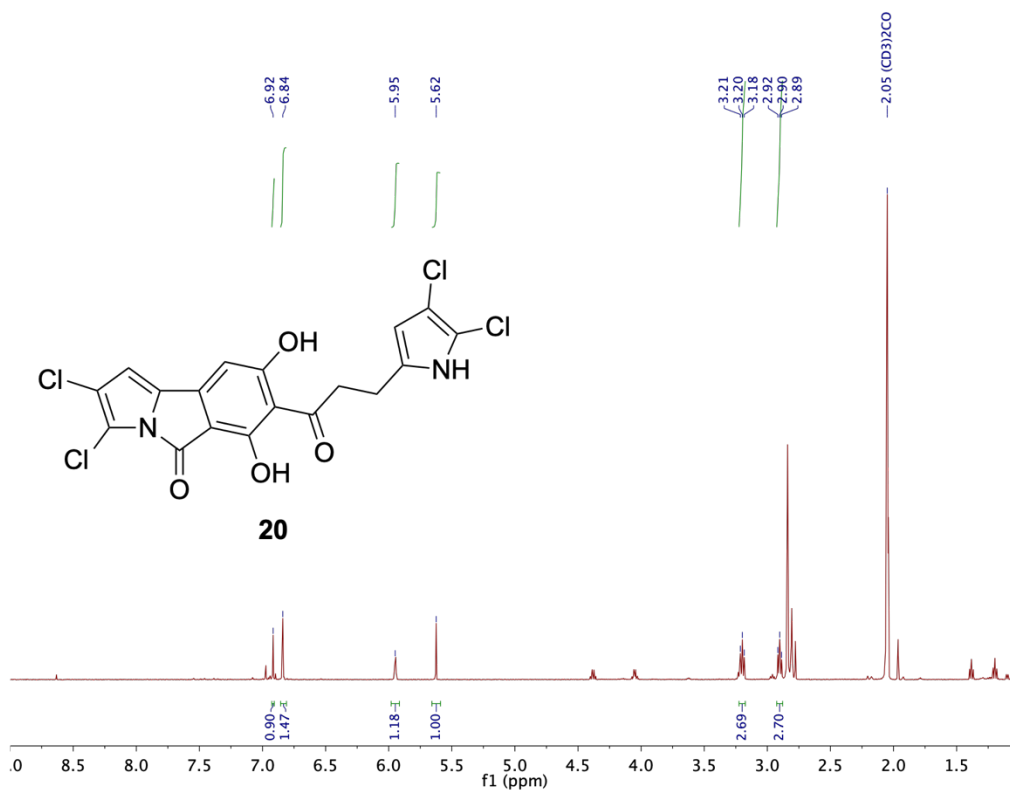


Figure S36: ^1H NMR spectrum of **20** (500 MHz, $(\text{CD}_3)_2\text{CO}$).

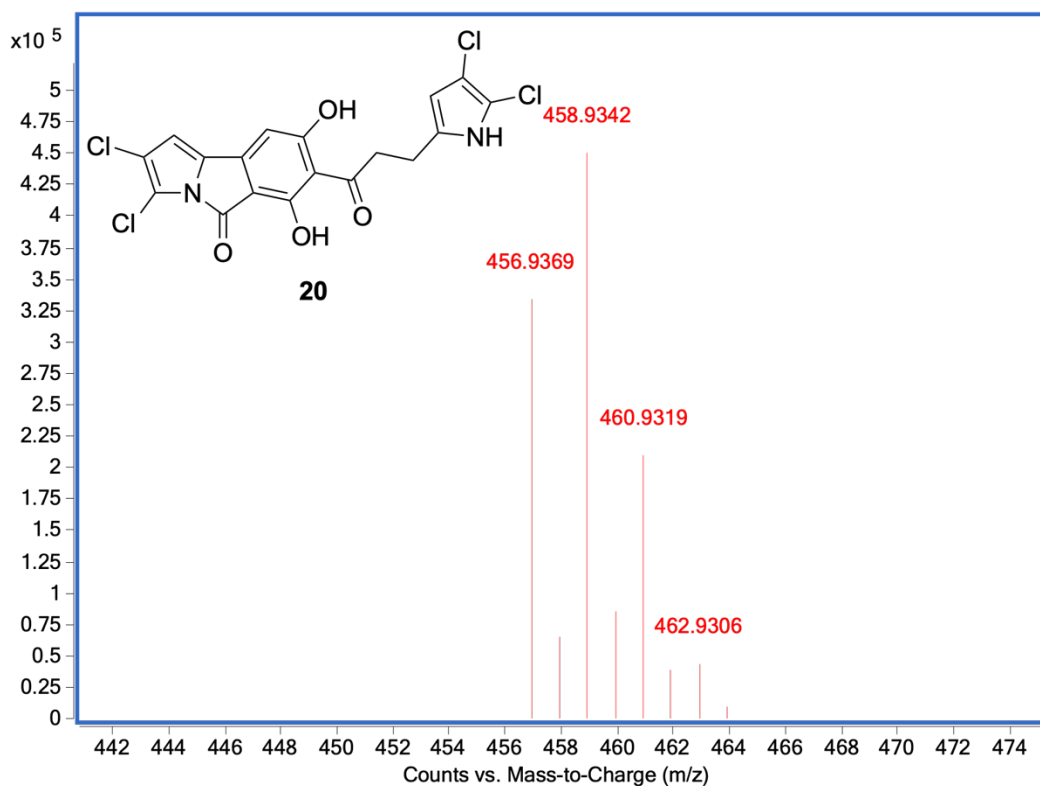


Figure S37: HR-ESI-TOFMS of **20**.

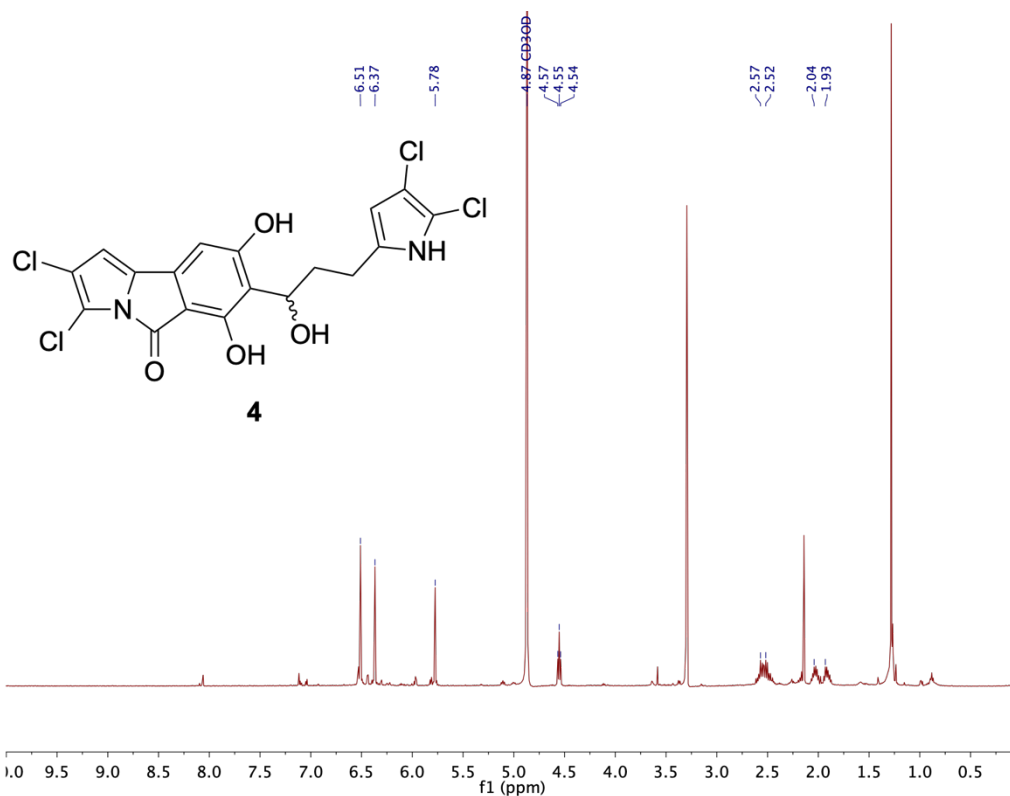


Figure S38: ¹H NMR spectrum of **4** (500 MHz, CD₃OD).

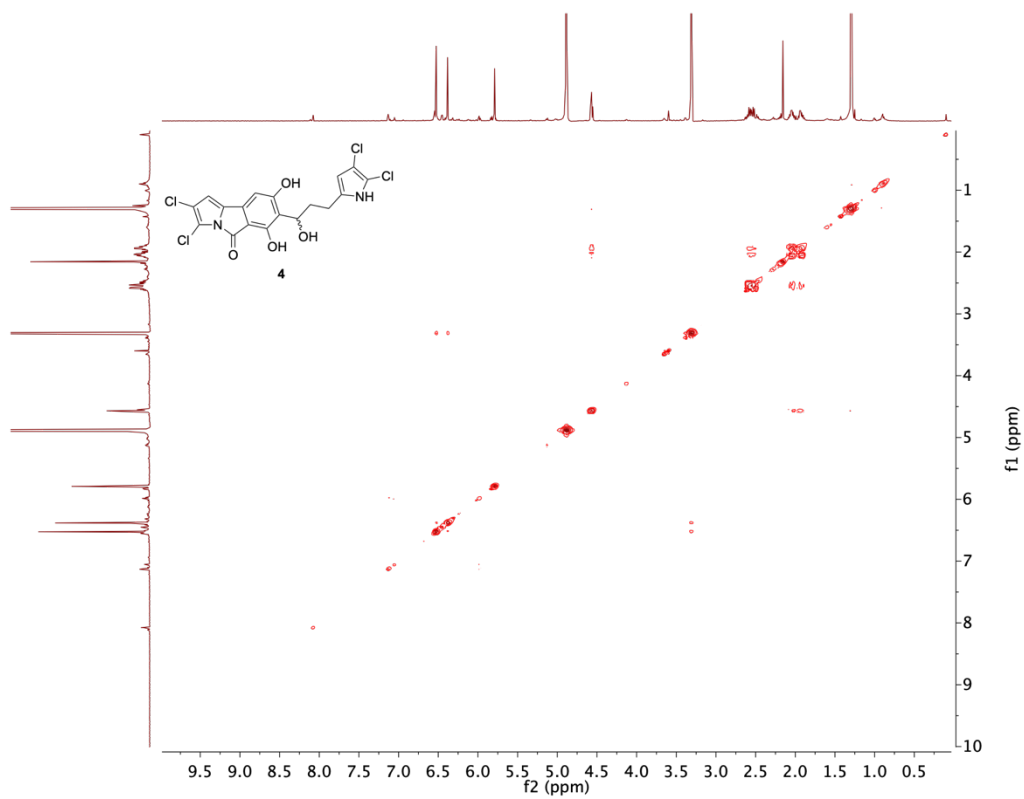


Figure S39: COSY NMR spectrum of **4** (125 MHz, CD₃OD).

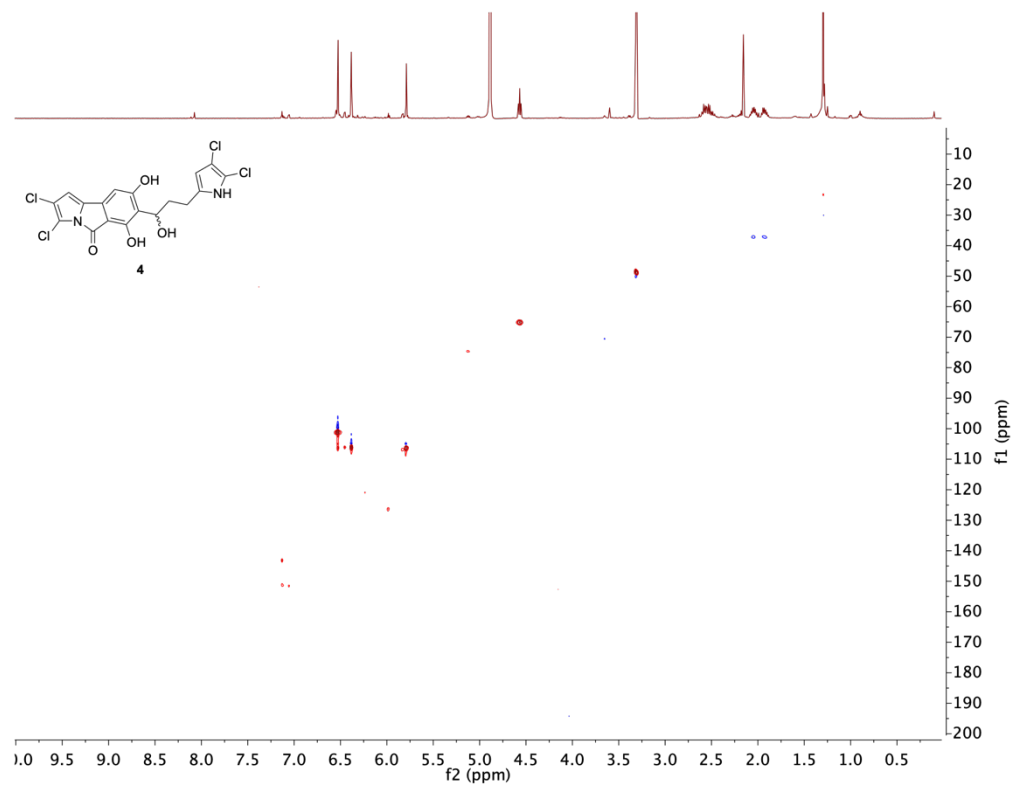


Figure S40: HSQC NMR spectrum of **4** (125 MHz, CD₃OD).

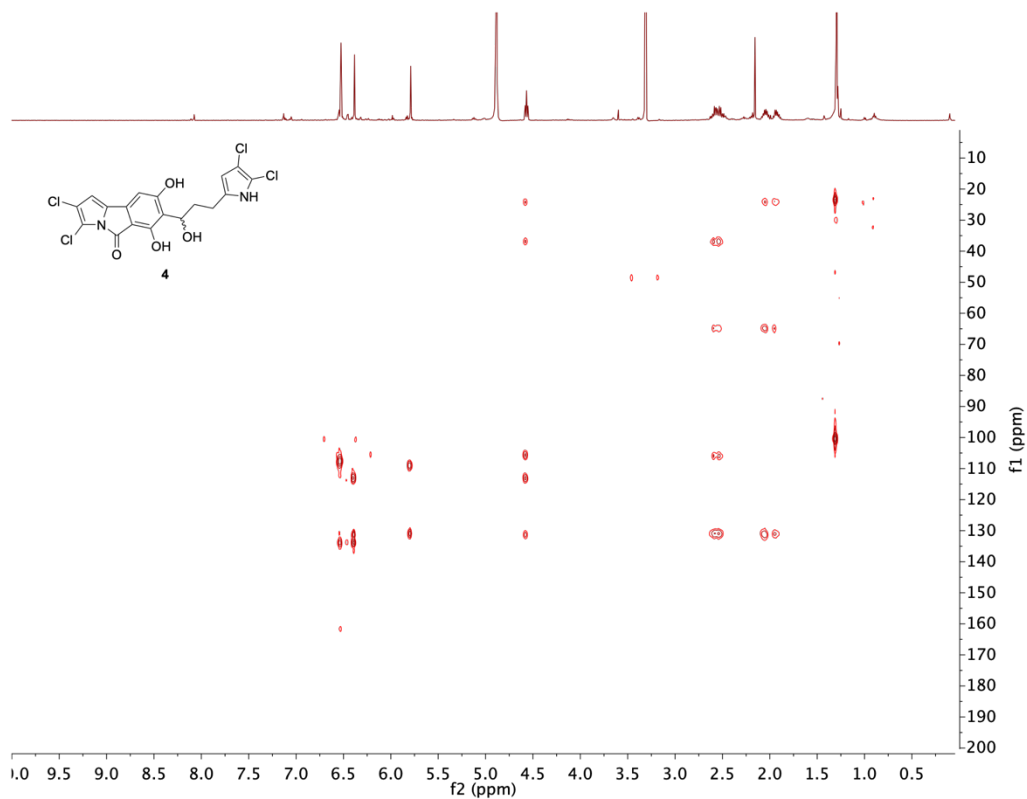


Figure S41: HMBC NMR spectrum of **4** (125 MHz, CD₃OD).

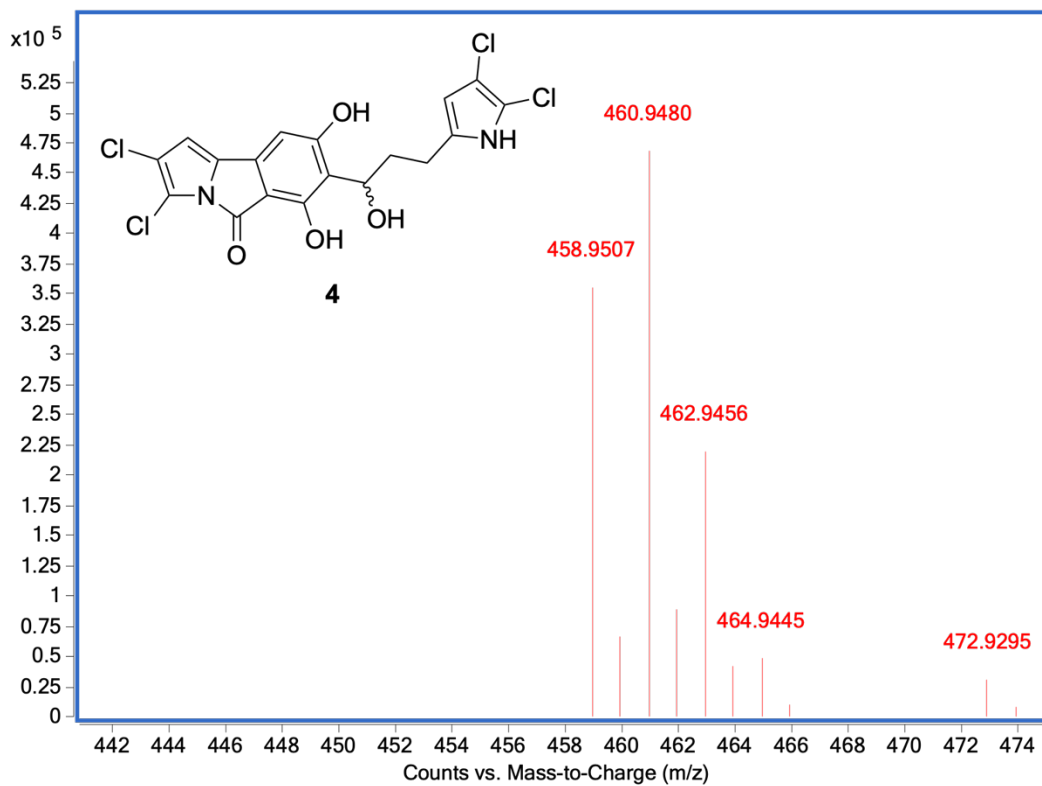


Figure S42: HR-ESI-TOFMS of **4**.

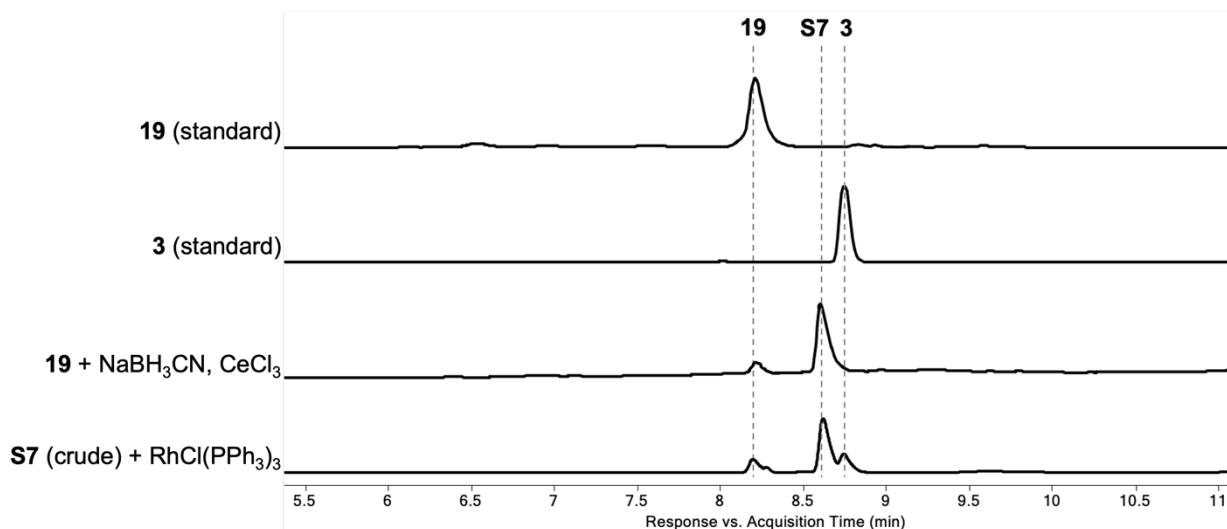


Figure S43: LC-MS chromatogram of alternative reduction sequence with **19**. From top to bottom: **19** (standard); **3** (standard); Luche reduction of **19** yields a new product with a mass indicative of a deoxygenated product; hydrogenation of proposed olefin **S7** shows partial conversion to a new product that matches **3** by retention time, UV, and HR-ESI-TOFMS. UV monitored at 350 nm.

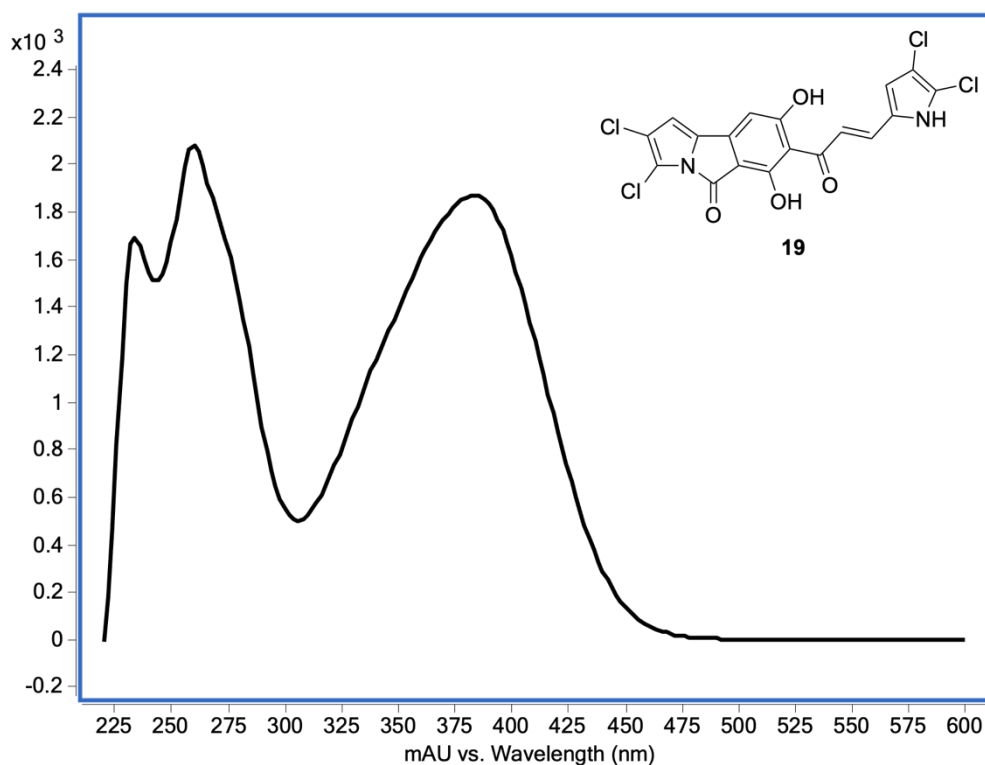


Figure S44: UV/Vis spectrum of **19**.

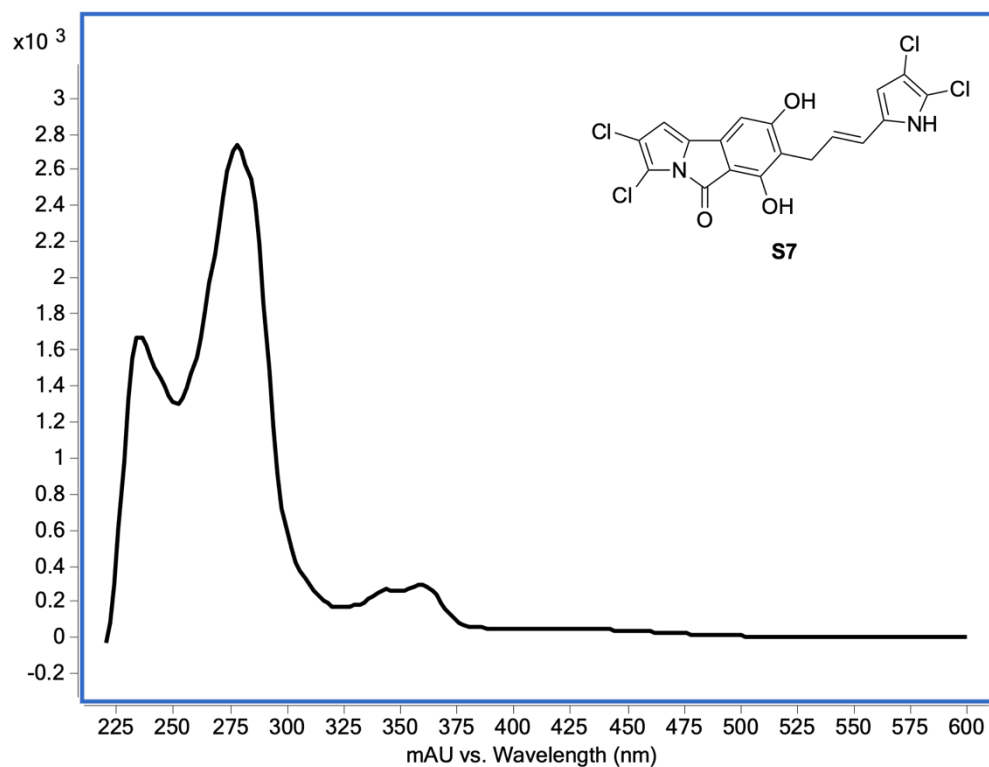


Figure S45: UV/Vis spectrum of **S7** and its proposed structure.

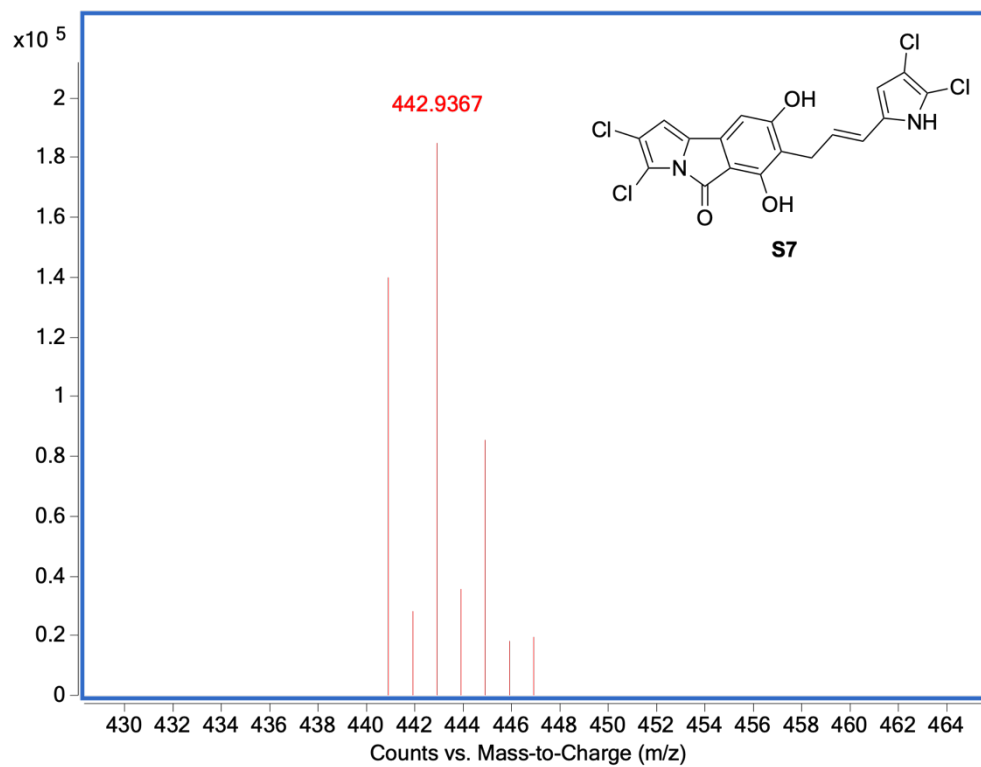


Figure S46: HR-ESI-TOFMS of **S7** and its proposed structure.

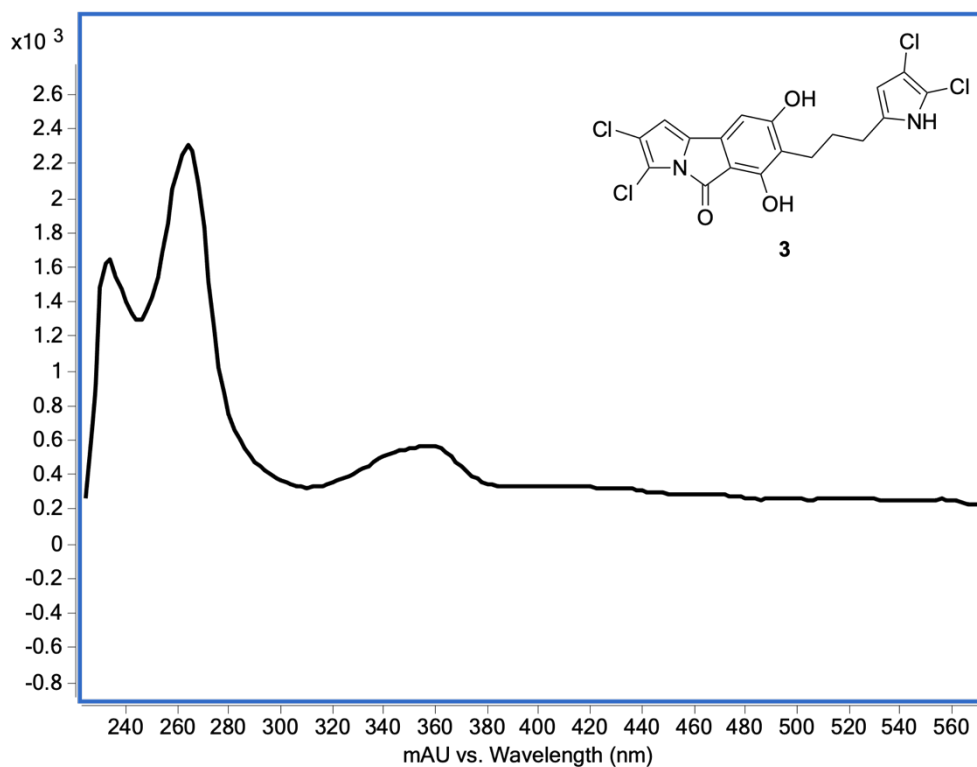


Figure S47: UV/Vis spectrum of new product and its proposed structure (**3**). Data matches the reported UV/Vis spectrum of **3**.³

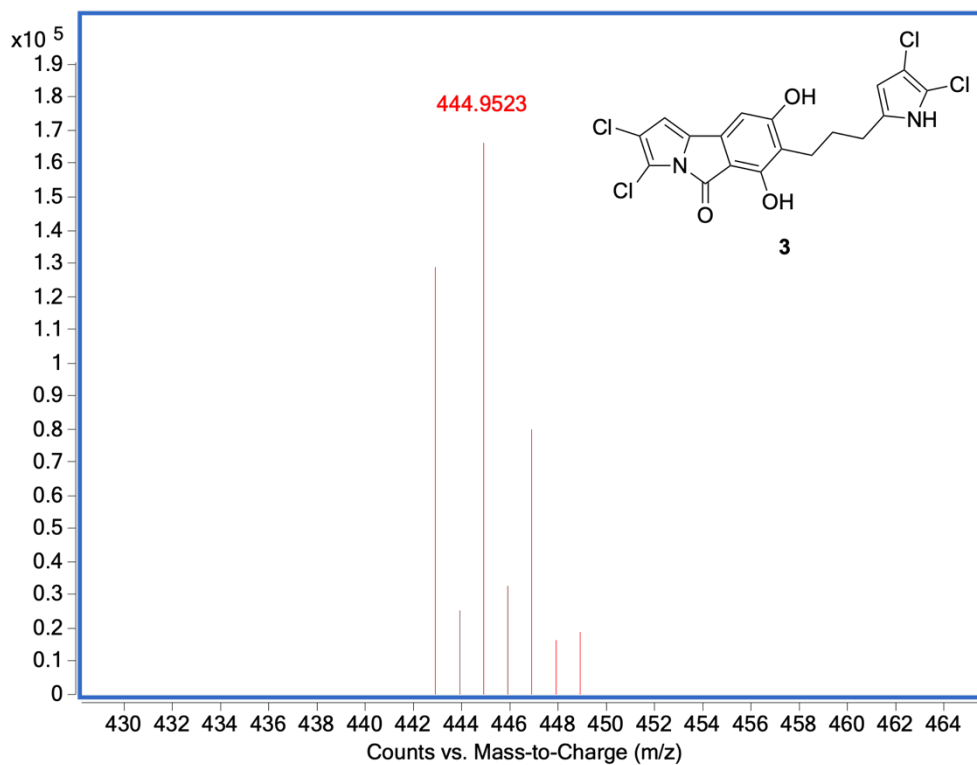


Figure S48: HR-ESI-TOFMS of new product and its proposed structure (**3**). Data matches the reported HR-MS data of **3**.³

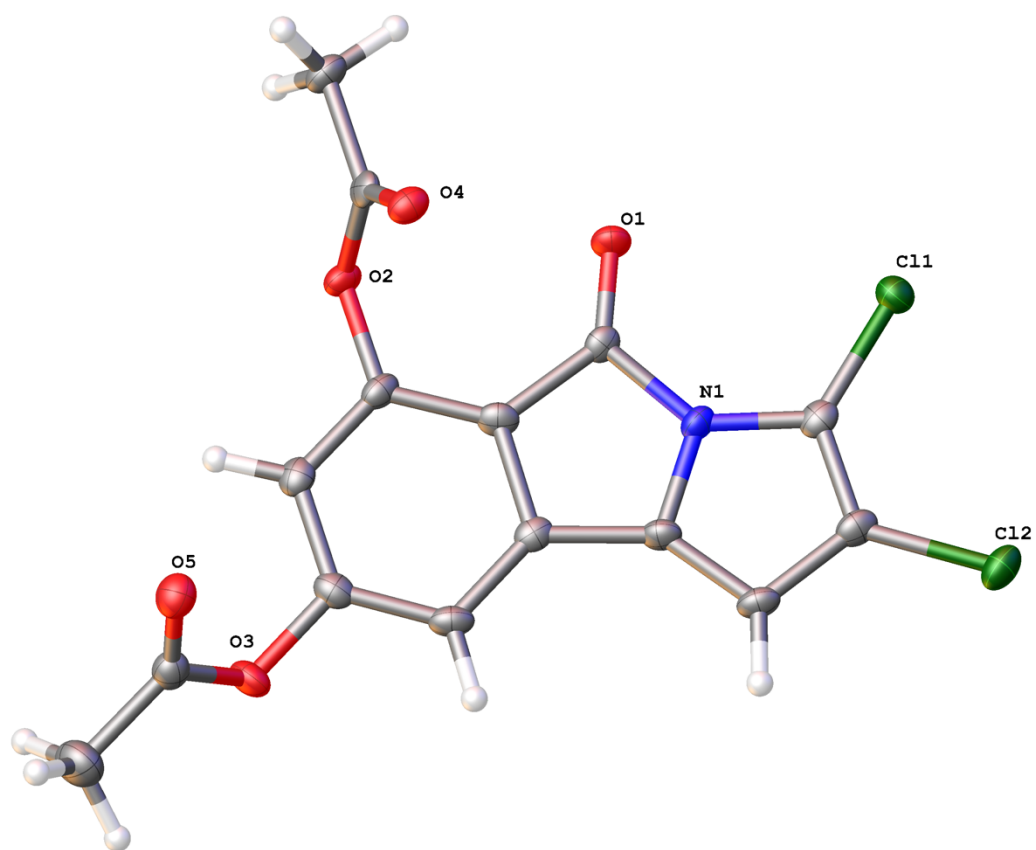


Figure S49: X-ray crystal structure of **16**.

Experimental Summary

The single crystal X-ray diffraction studies were carried out on a Bruker Kappa Photon CMOS CCD diffractometer equipped with Mo K α radiation ($\lambda = 0.71073 \text{ \AA}$). A 0.21 x 0.15 x 0.05 mm yellow plate was mounted on a Cryoloop with Paratone oil. Data were collected in a nitrogen gas stream at 100 (2) K using Φ and ω scans. Crystal-to-detector distance was 40 mm and exposure time was 60 seconds per frame using a scan width of 0.5°. Data collection was 99.3% complete to 25.00° in Θ . A total of 26133 reflections were collected covering the indices, $-9 \leq h \leq 9$, $-16 \leq k \leq 17$, $-17 \leq l \leq 17$. 5834 reflections were found to be symmetry independent, with a R_{int} of 0.0421. Indexing and unit cell refinement indicated a primitive, triclinic lattice. The space group was found to be $P-1$. The data were integrated using the Bruker SAINT software program and scaled using the TWINABS software program. Solution by direct methods (SHELXS) produced a complete phasing model consistent with the proposed structure.

All nonhydrogen atoms were refined anisotropically by full-matrix least-squares (SHELXL-97). All hydrogen atoms were placed using a riding model. Their positions were constrained relative to their parent atom using the appropriate HFIX command in SHELXL-97. Crystallographic data are summarized in Table S1.

Table S1. Crystal data and structure refinement for Chamb01 (16).

Identification code	IC12	
Empirical formula	C15 H9 Cl2 N O5	
Molecular formula	C15 H9 Cl2 N O5	
Formula weight	354.13	
Temperature	100(2) K	
Wavelength	0.71073 Å	
Crystal system	Triclinic	
Space group	P -1	
Unit cell dimensions	a = 7.8220(8) Å	$\alpha = 74.483(3)^\circ$.
	b = 13.9019(13) Å	$\beta = 89.752(3)^\circ$.
	c = 14.0299(15) Å	$\gamma = 87.505(3)^\circ$.
Volume	1468.6(3) Å ³	
Z	4	
Density (calculated)	1.602 Mg/m ³	
Absorption coefficient	0.467 mm ⁻¹	
F(000)	720	
Crystal size	0.210 x 0.150 x 0.050 mm ³	
Crystal color, habit	Yellow Plate	
Theta range for data collection	2.606 to 26.413°.	
Index ranges	-9<=h<=9, -16<=k<=17, 0<=l<=17	
Reflections collected	26133	
Independent reflections	5834 [R(int) = 0.0421]	
Completeness to theta = 25.000°	99.3 %	
Absorption correction	Semi-empirical from equivalents	
Max. and min. transmission	0.745376 and 0.599064	
Refinement method	Full-matrix least-squares on F ²	
Data / restraints / parameters	5834 / 0 / 420	
Goodness-of-fit on F ²	1.034	
Final R indices [I>2sigma(I)]	R1 = 0.0511, wR2 = 0.1067	
R indices (all data)	R1 = 0.0664, wR2 = 0.1142	
Extinction coefficient	n/a	
Largest diff. peak and hole	0.481 and -0.336 e.Å ⁻³	

Table S2. Atomic coordinates ($\times 10^4$) and equivalent isotropic displacement parameters ($\text{\AA}^2 \times 10^3$) for Chamb01. $U(\text{eq})$ is defined as one third of the trace of the orthogonalized U_{ij} tensor.

	x	y	z	$U(\text{eq})$
Cl(1)	1322(1)	-1194(1)	6856(1)	22(1)
Cl(2)	628(1)	-2029(1)	4784(1)	25(1)
O(1)	3152(4)	934(2)	6688(2)	20(1)
O(2)	4954(4)	2910(2)	5816(2)	19(1)
O(3)	5852(4)	3441(2)	2339(2)	23(1)
O(4)	2097(4)	3197(2)	5927(2)	21(1)
O(5)	3980(4)	4745(2)	2245(2)	26(1)
N(1)	2714(4)	219(2)	5384(2)	17(1)
C(1)	1887(6)	-669(3)	5668(3)	19(1)
C(2)	1649(6)	-972(3)	4831(3)	20(1)
C(3)	2328(5)	-265(3)	4004(3)	18(1)
C(4)	2975(6)	464(3)	4373(3)	18(1)
C(5)	3260(5)	967(3)	5825(3)	16(1)
C(6)	3954(5)	1726(3)	4973(3)	18(1)
C(7)	4706(5)	2614(3)	4955(3)	18(1)
C(8)	5307(5)	3200(3)	4074(3)	19(1)
C(9)	5128(5)	2884(3)	3216(3)	19(1)
C(10)	4358(6)	2010(3)	3203(3)	19(1)
C(11)	3785(5)	1421(3)	4100(3)	17(1)
C(12)	3499(6)	3170(3)	6271(3)	18(1)
C(13)	3951(6)	3415(3)	7215(3)	22(1)
C(14)	5206(6)	4398(3)	1931(3)	22(1)
C(15)	6310(7)	4902(3)	1087(3)	35(1)
Cl(1')	3870(1)	-1128(1)	11878(1)	22(1)
Cl(2')	4670(1)	-2074(1)	9865(1)	22(1)
O(1')	1717(4)	1025(2)	11630(2)	21(1)
O(2')	-399(4)	2965(2)	10696(2)	19(1)
O(3')	-1360(4)	3324(2)	7232(2)	22(1)
O(4')	2368(4)	3359(2)	10737(2)	27(1)

O(5')	291(4)	4658(2)	7080(2)	26(1)
N(1')	2267(4)	235(2)	10376(2)	15(1)
C(1')	3217(5)	-650(3)	10684(3)	16(1)
C(2')	3494(5)	-1005(3)	9881(3)	17(1)
C(3')	2696(5)	-319(3)	9026(3)	19(1)
C(4')	1963(5)	427(3)	9360(3)	15(1)
C(5')	1610(5)	1006(3)	10780(3)	18(1)
C(6')	797(5)	1740(3)	9909(3)	16(1)
C(7')	-90(5)	2637(3)	9849(3)	17(1)
C(8')	-800(5)	3188(3)	8960(3)	19(1)
C(9')	-565(6)	2819(3)	8131(3)	19(1)
C(10')	327(6)	1932(3)	8150(3)	18(1)
C(11')	994(5)	1390(3)	9060(3)	16(1)
C(12')	995(6)	3274(3)	11122(3)	19(1)
C(13')	514(6)	3470(3)	12078(3)	26(1)
C(14')	-832(6)	4261(3)	6770(3)	21(1)
C(15')	-1828(6)	4679(3)	5837(3)	29(1)

Table S3. Bond lengths [Å] and angles [°] for Chamb01 (**16**).

Cl(1)-C(1)	1.696(4)	Cl(1')-C(1')	1.700(4)
Cl(2)-C(2)	1.719(4)	Cl(2')-C(2')	1.718(4)
O(1)-C(5)	1.203(5)	O(1')-C(5')	1.202(5)
O(2)-C(12)	1.384(5)	O(2')-C(12')	1.384(5)
O(2)-C(7)	1.393(4)	O(2')-C(7')	1.400(5)
O(3)-C(14)	1.374(5)	O(3')-C(14')	1.372(5)
O(3)-C(9)	1.398(5)	O(3')-C(9')	1.401(5)
O(4)-C(12)	1.195(5)	O(4')-C(12')	1.197(5)
O(5)-C(14)	1.191(5)	O(5')-C(14')	1.199(5)
N(1)-C(1)	1.379(5)	N(1')-C(1')	1.376(5)
N(1)-C(4)	1.383(5)	N(1')-C(4')	1.397(5)
N(1)-C(5)	1.426(5)	N(1')-C(5')	1.418(5)
C(1)-C(2)	1.365(5)	C(1')-C(2')	1.359(5)
C(2)-C(3)	1.423(6)	C(2')-C(3')	1.442(5)
C(3)-C(4)	1.372(6)	C(3')-C(4')	1.353(6)
C(3)-H(3)	0.9500	C(3')-H(3')	0.9500
C(4)-C(11)	1.454(6)	C(4')-C(11')	1.468(5)
C(5)-C(6)	1.485(6)	C(5')-C(6')	1.491(5)
C(6)-C(7)	1.385(6)	C(6')-C(7')	1.383(6)
C(6)-C(11)	1.407(5)	C(6')-C(11')	1.407(5)
C(7)-C(8)	1.380(6)	C(7')-C(8')	1.382(5)
C(8)-C(9)	1.397(5)	C(8')-C(9')	1.399(5)
C(8)-H(8)	0.9500	C(8')-H(8')	0.9500
C(9)-C(10)	1.384(6)	C(9')-C(10')	1.385(6)
C(10)-C(11)	1.389(6)	C(10')-C(11')	1.389(5)
C(10)-H(10)	0.9500	C(10')-H(10')	0.9500
C(12)-C(13)	1.500(5)	C(12')-C(13')	1.483(5)
C(13)-H(13D)	0.9800	C(13')-H(13A)	0.9800
C(13)-H(13E)	0.9800	C(13')-H(13B)	0.9800
C(13)-H(13F)	0.9800	C(13')-H(13C)	0.9800
C(14)-C(15)	1.496(6)	C(14')-C(15')	1.490(6)
C(15)-H(15D)	0.9800	C(15')-H(15A)	0.9800
C(15)-H(15E)	0.9800	C(15')-H(15B)	0.9800
C(15)-H(15F)	0.9800	C(15')-H(15C)	0.9800

C(12)-O(2)-C(7)	116.6(3)	C(10)-C(11)-C(6)	120.6(4)
C(14)-O(3)-C(9)	118.3(3)	C(10)-C(11)-C(4)	132.6(4)
C(1)-N(1)-C(4)	109.3(3)	C(6)-C(11)-C(4)	106.8(4)
C(1)-N(1)-C(5)	137.9(3)	O(4)-C(12)-O(2)	122.7(3)
C(4)-N(1)-C(5)	112.6(3)	O(4)-C(12)-C(13)	126.6(4)
C(2)-C(1)-N(1)	106.7(4)	O(2)-C(12)-C(13)	110.8(4)
C(2)-C(1)-Cl(1)	130.7(3)	C(12)-C(13)-H(13D)	109.5
N(1)-C(1)-Cl(1)	122.6(3)	C(12)-C(13)-H(13E)	109.5
C(1)-C(2)-C(3)	109.6(4)	H(13D)-C(13)-H(13E)	109.5
C(1)-C(2)-Cl(2)	125.0(3)	C(12)-C(13)-H(13F)	109.5
C(3)-C(2)-Cl(2)	125.4(3)	H(13D)-C(13)-H(13F)	109.5
C(4)-C(3)-C(2)	105.7(3)	H(13E)-C(13)-H(13F)	109.5
C(4)-C(3)-H(3)	127.1	O(5)-C(14)-O(3)	123.0(4)
C(2)-C(3)-H(3)	127.1	O(5)-C(14)-C(15)	127.6(4)
C(3)-C(4)-N(1)	108.7(4)	O(3)-C(14)-C(15)	109.3(4)
C(3)-C(4)-C(11)	143.8(4)	C(14)-C(15)-H(15D)	109.5
N(1)-C(4)-C(11)	107.5(3)	C(14)-C(15)-H(15E)	109.5
O(1)-C(5)-N(1)	125.4(4)	H(15D)-C(15)-H(15E)	109.5
O(1)-C(5)-C(6)	131.6(4)	C(14)-C(15)-H(15F)	109.5
N(1)-C(5)-C(6)	103.0(3)	H(15D)-C(15)-H(15F)	109.5
C(7)-C(6)-C(11)	120.7(4)	H(15E)-C(15)-H(15F)	109.5
C(7)-C(6)-C(5)	129.3(3)	C(12')-O(2')-C(7')	116.8(3)
C(11)-C(6)-C(5)	110.0(3)	C(14')-O(3')-C(9')	117.6(3)
C(8)-C(7)-C(6)	119.5(3)	C(1')-N(1')-C(4')	108.4(3)
C(8)-C(7)-O(2)	118.7(3)	C(1')-N(1')-C(5')	138.3(3)
C(6)-C(7)-O(2)	121.7(3)	C(4')-N(1')-C(5')	113.3(3)
C(7)-C(8)-C(9)	119.0(4)	C(2')-C(1')-N(1')	107.5(3)
C(7)-C(8)-H(8)	120.5	C(2')-C(1')-Cl(1')	130.1(3)
C(9)-C(8)-H(8)	120.5	N(1')-C(1')-Cl(1')	122.3(3)
C(10)-C(9)-C(8)	123.1(4)	C(1')-C(2')-C(3')	109.1(3)
C(10)-C(9)-O(3)	118.1(3)	C(1')-C(2')-Cl(2')	125.9(3)
C(8)-C(9)-O(3)	118.7(4)	C(3')-C(2')-Cl(2')	125.0(3)
C(9)-C(10)-C(11)	117.2(3)	C(4')-C(3')-C(2')	105.5(3)
C(9)-C(10)-H(10)	121.4	C(4')-C(3')-H(3')	127.2
C(11)-C(10)-H(10)	121.4	C(2')-C(3')-H(3')	127.2
		C(3')-C(4')-N(1')	109.5(4)

C(3')-C(4')-C(11')	144.0(4)	C(10')-C(11')-C(4')	131.5(4)
N(1')-C(4')-C(11')	106.4(3)	C(6')-C(11')-C(4')	107.2(3)
O(1')-C(5')-N(1')	126.2(4)	O(4')-C(12')-O(2')	122.2(4)
O(1')-C(5')-C(6')	130.7(4)	O(4')-C(12')-C(13')	127.3(4)
N(1')-C(5')-C(6')	103.1(3)	O(2')-C(12')-C(13')	110.5(4)
C(7')-C(6')-C(11')	120.0(3)	C(12')-C(13')-H(13A)	109.5
C(7')-C(6')-C(5')	130.0(3)	C(12')-C(13')-H(13B)	109.5
C(11')-C(6')-C(5')	110.0(3)	H(13A)-C(13')-H(13B)	109.5
C(8')-C(7')-C(6')	120.3(3)	C(12')-C(13')-H(13C)	109.5
C(8')-C(7')-O(2')	118.7(4)	H(13A)-C(13')-H(13C)	109.5
C(6')-C(7')-O(2')	120.8(3)	H(13B)-C(13')-H(13C)	109.5
C(7')-C(8')-C(9')	118.0(4)	O(5')-C(14')-O(3')	123.7(4)
C(7')-C(8')-H(8')	121.0	O(5')-C(14')-C(15')	126.5(4)
C(9')-C(8')-H(8')	121.0	O(3')-C(14')-C(15')	109.8(3)
C(10')-C(9')-C(8')	124.0(4)	C(14')-C(15')-H(15A)	109.5
C(10')-C(9')-O(3')	116.3(3)	C(14')-C(15')-H(15B)	109.5
C(8')-C(9')-O(3')	119.6(4)	H(15A)-C(15')-H(15B)	109.5
C(9')-C(10')-C(11')	116.3(4)	C(14')-C(15')-H(15C)	109.5
C(9')-C(10')-H(10')	121.8	H(15A)-C(15')-H(15C)	109.5
C(11')-C(10')-H(10')	121.8	H(15B)-C(15')-H(15C)	109.5
C(10')-C(11')-C(6')	121.4(4)		

Table S4. Anisotropic displacement parameters ($\text{\AA}^2 \times 10^3$) for Chamb01(16). The anisotropic displacement factor exponent takes the form: $-2 \pi^2 [h^2 a^{*2} U^{11} + \dots + 2 h k a^* b^* U^{12}]$

	U11	U22	U33	U23	U13	U12
Cl(1)	23(1)	23(1)	20(1)	-5(1)	3(1)	-4(1)
Cl(2)	22(1)	23(1)	33(1)	-14(1)	-4(1)	-2(1)
O(1)	24(2)	23(2)	13(1)	-6(1)	-2(1)	-2(1)
O(2)	19(2)	22(2)	20(1)	-11(1)	0(1)	-3(1)
O(3)	26(2)	23(2)	16(1)	-1(1)	5(1)	-1(1)
O(4)	18(2)	23(2)	23(1)	-10(1)	-2(1)	1(1)
O(5)	26(2)	22(2)	30(2)	-7(1)	-1(1)	-1(1)
N(1)	17(2)	18(2)	19(2)	-9(1)	-2(1)	-2(2)
C(1)	17(2)	17(2)	23(2)	-8(2)	-3(2)	4(2)
C(2)	17(2)	24(2)	21(2)	-11(2)	-5(2)	2(2)
C(3)	19(2)	23(2)	15(2)	-9(2)	-5(2)	4(2)
C(4)	20(2)	21(2)	12(2)	-5(2)	-3(2)	3(2)
C(5)	12(2)	18(2)	19(2)	-6(2)	-5(2)	1(2)
C(6)	17(2)	23(2)	14(2)	-4(2)	-5(2)	4(2)
C(7)	14(2)	20(2)	22(2)	-11(2)	-2(2)	0(2)
C(8)	17(2)	16(2)	25(2)	-7(2)	0(2)	2(2)
C(9)	16(2)	22(2)	18(2)	-3(2)	1(2)	3(2)
C(10)	18(2)	27(2)	14(2)	-8(2)	-3(2)	5(2)
C(11)	13(2)	19(2)	19(2)	-7(2)	-3(2)	4(2)
C(12)	25(2)	9(2)	20(2)	-3(2)	1(2)	-1(2)
C(13)	23(2)	22(2)	24(2)	-12(2)	-5(2)	0(2)
C(14)	23(2)	21(2)	20(2)	-6(2)	-3(2)	-3(2)
C(15)	43(3)	32(2)	26(2)	-2(2)	4(2)	-2(2)
Cl(1')	24(1)	23(1)	17(1)	-3(1)	-4(1)	2(1)
Cl(2')	21(1)	19(1)	28(1)	-9(1)	2(1)	2(1)
O(1')	25(2)	26(2)	16(1)	-10(1)	1(1)	-2(1)
O(2')	16(2)	26(2)	19(1)	-12(1)	2(1)	-2(1)
O(3')	21(2)	23(2)	19(1)	-4(1)	-4(1)	0(1)
O(4')	25(2)	33(2)	28(2)	-15(1)	8(1)	-9(1)
O(5')	29(2)	18(1)	32(2)	-9(1)	4(1)	-2(1)

N(1')	16(2)	20(2)	11(2)	-6(1)	0(1)	-4(2)
C(1')	12(2)	19(2)	17(2)	-3(2)	-3(2)	1(2)
C(2')	14(2)	16(2)	24(2)	-10(2)	-2(2)	0(2)
C(3')	17(2)	22(2)	21(2)	-10(2)	3(2)	-6(2)
C(4')	12(2)	19(2)	15(2)	-5(2)	1(2)	-5(2)
C(5')	16(2)	20(2)	20(2)	-9(2)	2(2)	-4(2)
C(6')	13(2)	19(2)	18(2)	-7(2)	-1(2)	-4(2)
C(7')	17(2)	19(2)	18(2)	-8(2)	5(2)	-5(2)
C(8')	17(2)	17(2)	23(2)	-5(2)	1(2)	3(2)
C(9')	19(2)	19(2)	19(2)	-3(2)	-1(2)	-4(2)
C(10')	17(2)	18(2)	20(2)	-6(2)	1(2)	-3(2)
C(11')	13(2)	17(2)	19(2)	-8(2)	3(2)	-3(2)
C(12')	18(2)	16(2)	25(2)	-9(2)	2(2)	-2(2)
C(13')	28(3)	32(2)	22(2)	-16(2)	3(2)	-5(2)
C(14')	25(2)	17(2)	22(2)	-8(2)	5(2)	2(2)
C(15')	26(2)	28(2)	27(2)	4(2)	-1(2)	2(2)

Table S5. Hydrogen coordinates ($\times 10^4$) and isotropic displacement parameters ($\text{\AA}^2 \times 10^3$) for Chamb01 (**16**).

	x	y	z	U(eq)
H(3)	2333	-293	3335	22
H(8)	5833	3809	4050	23
H(10)	4226	1820	2606	23
H(13D)	3324	4031	7248	33
H(13E)	5184	3508	7234	33
H(13F)	3640	2866	7780	33
H(15D)	5697	5500	681	52
H(15E)	6589	4442	681	52
H(15F)	7369	5093	1345	52
H(3')	2687	-378	8367	22
H(8')	-1429	3800	8912	23
H(10')	475	1706	7571	22
H(13A)	1058	2955	12622	38
H(13B)	-732	3458	12151	38
H(13C)	899	4128	12093	38
H(15A)	-1546	5377	5552	44
H(15B)	-3055	4645	5981	44
H(15C)	-1539	4290	5366	44

References

1. Chen, J.; McNeil, A. J. *J. Am. Chem. Soc.* **2008**, *130*, 16496–16497.
2. Petriguet, J.; Inack Ngi, S.; Abarbri, M.; Thibonnet, J. *Tetrahedron Lett.* **2014**, *55*, 982–984.
3. Mantovani, S. M.; Moore, B. S. *J. Am. Chem. Soc.* **2013**, *135*, 18032–18035.

Chapter 3

Discovery and Biosynthesis of Tetrachlorizine Reveals Enzymatic Benzylic Dehydrogenation via an *ortho*-quinone methide

Trevor N. Purdy, Min Cheol Kim, Reiko Cullum, William Fenical, Bradley S. Moore

Abstract: *Ortho*-quinone methides (*o*-QMs) are reactive intermediates in biosynthesis that give rise to a variety of intra- and intermolecular cyclization/addition products in bacteria, fungi and plants. Herein, we report a new metabolic deviation of an *o*-QM intermediate in a benzylic dehydrogenation reaction that links the newly described marine bacterial natural products dihydrotetrachlorizine and tetrachlorizine. We discovered these novel dichloropyrrole-containing compounds from actinomycete strain AJS-327 that unexpectedly harbors in its genome a biosynthetic gene cluster (BGC) of striking similarity to that of chlorizidine, another marine alkaloid bearing a different carbon skeleton. Heterologous expression of the homologous flavin-dependent oxidoreductase enzymes Tcz9 and Clz9 revealed their native functions in tetrachlorizine and chlorizidine biosynthesis, respectively, supporting divergent oxidative dehydrogenation and pyrrolizine-forming reactions. Swapping these berberine bridge enzyme-like oxidoreductases, we produced cyclized and dehydrogenated analogs of tetrachlorizine and chlorizidine, including a dearomatized chlorizidine analog that stabilizes an *o*-QM via conjugation with a 3*H*-pyrrolizine ring.

In the post-genomics era, the discovery of natural product molecules not only provides opportunities to explore their native and applied biological functions, but also the occasion to relate their chemistry back to their encoding genes for further biotechnological innovations.¹⁻³ The ability to connect genes to molecules and vice versa through modern genome mining experimentation has transcended the field of microbial natural products chemistry and paved the way to new frontiers in synthetic biology,⁴ microbiome science,⁵ and biocatalysis,⁶ to name a few. Natural product biosynthetic enzymes are remarkable for their reaction diversity and plasticity, and as such, for their promise as biocatalysts to construct designer molecules.

Flavin adenine dinucleotide (FAD)-dependent oxidoreductases are one such family of enzymes that catalyze diverse chemical transformations with tremendous fidelity and biocatalytic utility.^{7,8} The berberine bridge enzyme (BBE)-like subfamily of flavoproteins are noteworthy for their ability to perform a variety of distinctive tailoring reactions in plants, fungi, and bacteria.⁹⁻¹² Notably, BBE-like enzymes are involved in nicotine, cannabinoid, and berberine alkaloid biosynthesis.¹³⁻¹⁵ Because so few BBE-like enzymes have been characterized, it is difficult for bioinformatic tools to predict the function of putative BBE-like enzymes without relying on their genomic context. The discovery of new BBE-like enzymes will yield new enzymatic reactions and improve bioinformatic predictions of biosynthetic gene clusters (BGCs) containing these fascinating enzymes (Figure S1).

Recently, we isolated a taxonomically distinct marine actinomycete bacterium (strain AJS-327) that harbors in excess of 27 putative BGCs, comprising approximately 17% of its genome.¹⁶ One of these BGCs exhibited high sequence and

architectural homology to the previously characterized *clz* BGC from *Streptomyces* sp. CNH-287, which is distinguished by the BBE-like enzyme Clz9 that catalyzes the formation of its unusual dihydropyrrolizine ring (Figure 3.1a).¹⁷ While strain AJS-327 is a prolific producer of cytotoxic secondary metabolites, including the recently discovered photopiperazines¹⁶ and ionostatin,¹⁸ we did not observe the production of chlorizidine A under several different media conditions. Instead, we identified two related tetrachlorinated metabolites in the organic extract by LC-MS analysis that were missing chlorizidine's distinctive heteroaromatic rings.

To characterize these new tetrachlorinated metabolites that did not match known compounds in various databases, we cultivated 20 L of strain AJS-327 and purified several milligrams of both metabolites. HR-MS data coupled with ¹³C NMR analysis revealed their molecular formulas as C₁₈H₁₀Cl₄N₂O₄ and C₁₈H₁₂Cl₄N₂O₄, which we have since named tetrachlorizine (**1**) and dihydrotetrachlorizine (**2**), respectively (Figure 3.1b). These molecules differ by one degree of unsaturation, which could be explained by the disappearance of high field methylenic protons in the ¹H NMR spectrum of **2** and the appearance of two olefinic doublets in the ¹H NMR spectrum of **1**. Key HMBC and NOE correlations were essential for determining the full connectivity between each ring system. Both of these metabolites are reminiscent of previously reported dichloropyrrole-containing secondary metabolites, such as chlorizidine A (**3**) (Figure 3.1c)¹⁷, pyoluteorin¹⁹, the armeniaspirols²⁰, marinopyrroles²¹, pyralomycins,²² and the pyrrolomycins²³ (Figure S2). To better understand the biosynthetic relationship of the tetrachlorizines and how they are related to **3**, we next turned our attention to the AJS-327 *clz*-like BGC and the role the putative BBE-like enzyme plays in **1** biosynthesis.

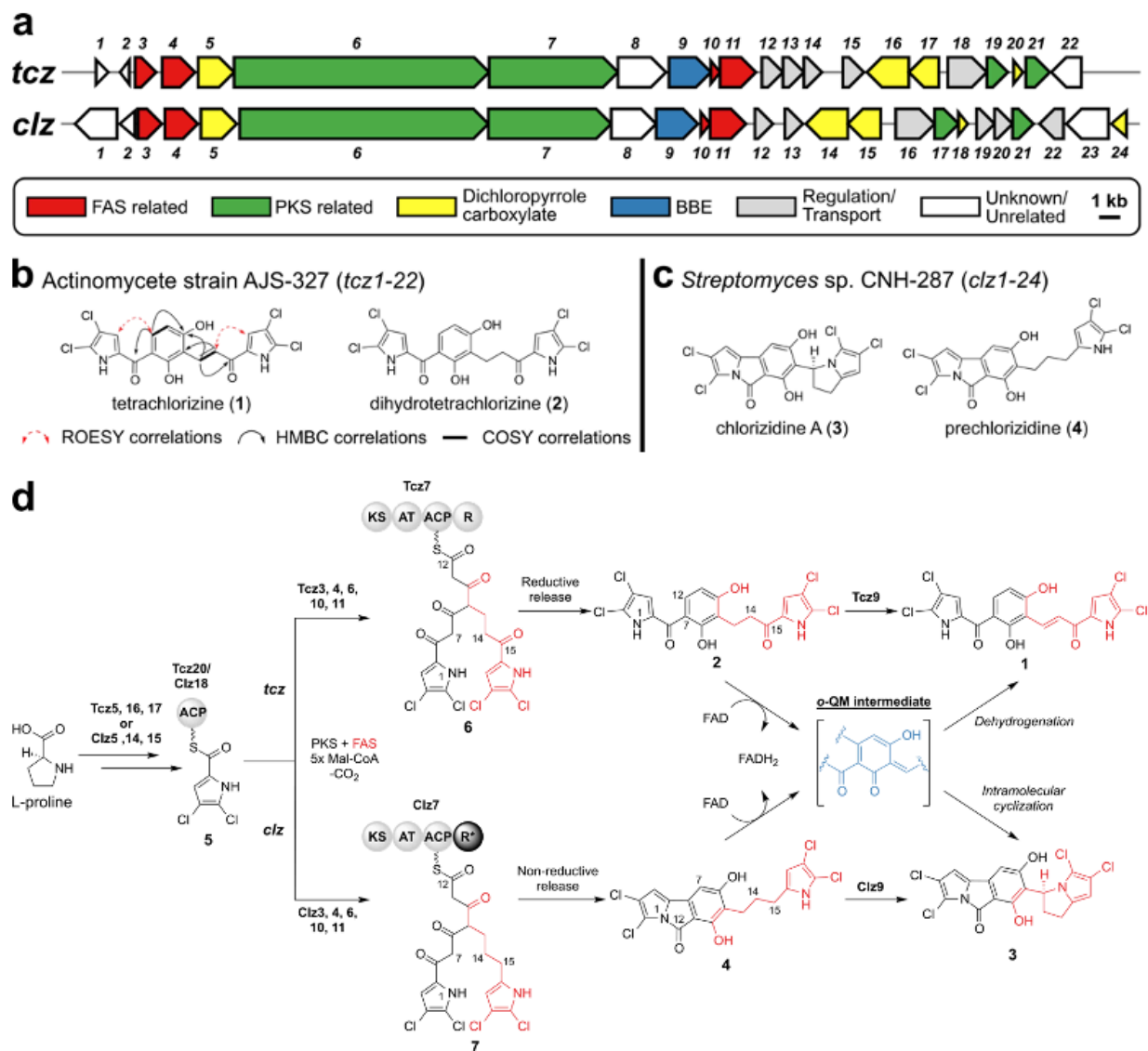


Figure 3.1. Molecular basis for tetrachlorizine biosynthesis. (a) Alignment of the tetrachlorizine (*tcz*) and chlorizidine A (*clz*) BGCs. Genes are color-coded by associated function. (b) Structures of novel dichloropyrrole-containing natural products, tetrachlorizine (1) and dihydrotetrachlorizine (2). Key 2D NMR correlations of 1 are depicted. (c) Structures of previously characterized chlorizidine A (3) and biosynthetic precursor, prechlorizidine (4). (d) Proposed polyketide biosynthesis of 1, in comparison with the previously reported biosynthesis of 3.¹⁷ The rare FAS-derived dichloropyrrolyl extender unit is colored red. The general structure of the *o*-QM intermediate generated by Tcz9 and Clz9 is colored blue. This *o*-QM intermediate represents one possible regio- and stereoisomer for both pathways. Abbreviations: ACP, acyl carrier protein; AT, acyl transferase; FAD, flavin adenine dinucleotide; FADH₂, reduced FAD (hydroquinone form); FAS, fatty acid synthase; KS, ketoacyl synthase; Mal-CoA, malonyl-coenzyme A; PKS, polyketide synthase; R, thioester reductase; *inactive domain.

Sequence analysis revealed a contiguous region of 33.7 kb containing 22 open reading frames (ORFs) that displayed extremely high similarity and organization to the

chlorizidine A BGC (*clz*) (Figure 3.1a).¹⁷ Remarkably, a homologue for every gene associated with **3** biosynthesis could be putatively annotated in strain AJS-327.²⁴ Every homologue in the tetrachlorizine BGC (*tcz*) shares 58-90% amino acid sequence similarity and 46-81% identity with its corresponding gene associated with **3** biosynthesis. As such, we envisioned a highly analogous polyketide synthase (PKS) assembly line pathway for **1** and the previously established **3**¹⁷ with subtle metabolic differences that could repurpose their biosyntheses to achieve different cyclization patterns (Figure 3.1d).

There are two key structural differences best exemplified in the penultimate pathway intermediates **2** and prechlorizidine (**4**) that are quite informative. Most significant is the oxidation state and connectivity of the terminal carbon C-12 in both molecules that derives from the fully mature PKS intermediates **6** and **7** (Figure 3.1d). In the case of **2**, **6** is reductively off-loaded by the terminal Tcz7 reductase (R) domain to an aldehyde intermediate that reacts with C-7 to generate the central tetrasubstituted benzene ring. This contrasts **4** in which we earlier envisaged that the PKS substrate **7** is nonreductively off-loaded and that C-12 rather forms an amide bond with N-1.¹⁷ The former mechanism is consistent with off-loading of similar PKS-extended, dichloropyrrole-containing secondary metabolites.^{20,21,25} The second structural difference is the oxidation state of C-15 which maintains the carbonyl of the dichloropyrrolyl-acyl carrier protein (**5**) substrate in **2** but is reduced to a methylene in **4**.

We previously showed that the flavoenzyme Clz9 catalyzes the final reaction in the chlorizidine pathway via an *o*-QM intermediate to install the dihydropyrrolizine ring (Figure 3.1d, highlighted in blue).¹⁷ Although tetrachlorizine does not have such a structure motif, its BGC encodes the FAD-linked oxidoreductase Tcz9 that shares 69% amino acid

sequence similarity and 53% identity with Clz9, suggesting a related enzymatic function. Sequence alignment of Tcz9 with Clz9 and other well characterized BBE family members confirmed the distinguishing active site motifs RSGGH and CxxI/V/LG necessary for bicovalent FAD attachment by the histidine and cysteine residues at positions 67 and 125, respectively (Figure S3).^{9,12,26} Given the high sequence homology to Clz9 and functional group similarity in **2**, we speculated that Tcz9 could generate a similar *o*-QM intermediate. However, instead of catalyzing nucleophilic attack via the dichloropyrrole-nitrogen as seen in **3** biosynthesis, Tcz9 would facilitate deprotonation at C-14 and subsequent formation of an α,β -unsaturated ketone (Figure 3.1d). To explore the suspected role of Tcz9 in tetrachlorizine biosynthesis, we overexpressed Tcz9 in *Escherichia coli* and purified the polyhistidine tagged, recombinant protein fused with a maltose binding protein

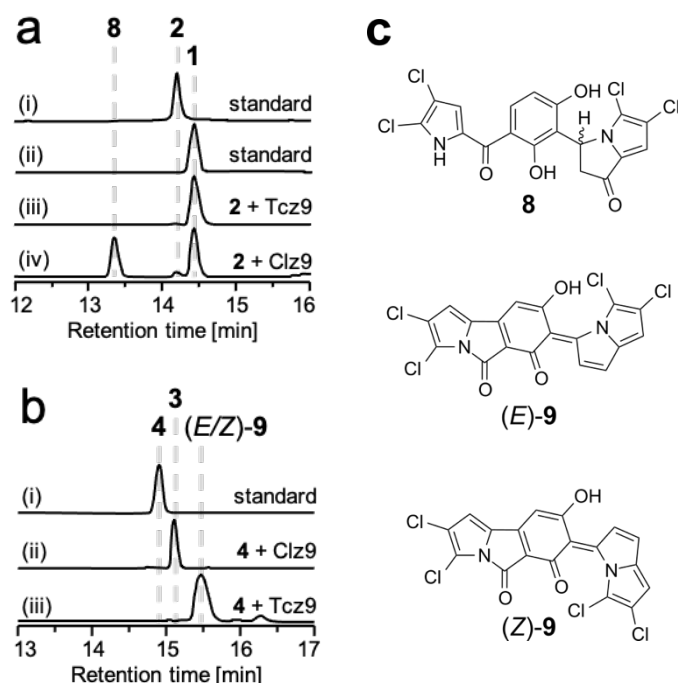
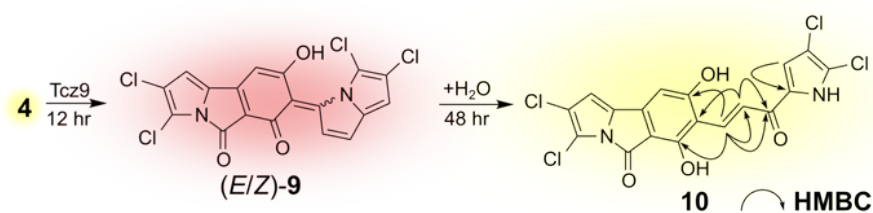


Figure 3.2. (a) HPLC analysis of the *in vitro* conversion with **2** and either Tcz9 or Clz9 after 12 hours: UV absorption monitored at 360 nm; (i) purified **2** standard; (ii) purified **1** standard. (iii) **2** + Tcz9, confirming Tcz9's role in **1** biosynthesis; (iv) **2** + Clz9, yielding the cyclized derivative **8** in addition to **1**. (b) HPLC analysis of the *in vitro* conversion with **4** and either Clz9 or Tcz9 after 12 hours: UV absorption monitored at 430 nm; (i) purified **4** standard; (ii) **4** + Clz9, as previously reported;¹⁷ (iii) **4** + Tcz9, yielding a mixture of stabilized *o*-QM isomers, (E)-**9** and (Z)-**9**. (c) Structures of enzymatic derivatives **8**, (E)-**9** and (Z)-**9**.

by affinity chromatography. Upon incubation with **2**, we observed the complete conversion to **1** (Figure 3.2a), thereby confirming the functional role of Tcz9 as a dehydrogenase in tetrachlorizine biosynthesis.

Upon confirming the role of Tcz9 in **1** biosynthesis, we were curious about the divergent reactivities of Clz9 and Tcz9 and whether the conversion of **2**→**1** and **4**→**3** were under enzyme or substrate control. We hypothesized that both BBE-like enzymes catalyzed the oxidative generation of similar *o*-QM intermediates, however, it was unclear how the C-15 carbonyl in the fatty acid synthase-derived extender unit of **2** influenced the dehydrogenation reaction catalyzed by Tcz9. Upon incubation of **2** with Clz9, we observed a mixture of two products (Figure 3.2a), one of which was **1**. The earlier eluting product exhibited an identical UV spectrum as **2**, but the same mass as **1**. NMR analysis revealed this product to be a cyclized analog of tetrachlorizine (**8**), indicating Tcz9 and Clz9 have preferential activity to perform dehydrogenation and cyclization reactions, respectively (Figure 3.2c). Protein structure models comparing Tcz9 and Clz9 could not unambiguously explain which residues are critical for Tcz9's dehydrogenation reactions. Future X-ray crystallography and mutagenesis experiments will be required to explain the difference in catalytic activity between Tcz9 and Clz9.



Scheme 3.1. Abbreviated reaction scheme depicting the enzymatic process for oxidation of **4** to (*E*)-**9** and (*Z*)-**9** catalyzed by Tcz9, which non-enzymatically coalesce to **10** in the presence of water. Key HMBC correlations for assigning the structure of **10** are included.

Next, we reversed roles to explore the fate of **4** with the mismatched Tcz9 (Figure 3.2b). Distinctively, the color of the reaction changed from yellow to a deep red over several hours, indicating the formation of a new product (Video S1). LC-MS analysis clearly showed the consumption of **4** and the appearance of two new products with mass 436.9058 ($[M - H]^-$; $C_{18}H_6Cl_4N_2O_3$) without any formation of **3**. NMR analysis revealed this new product to be the cyclized and twice dehydrogenated configurational isomers (*E*)-**9** and (*Z*)-**9** (Figure 3.2c). This result indicates that Tcz9 not only acts as a dehydrogenase in the absence of the C-15 carbonyl, but it can also act as a cyclase, catalyzing the same intramolecular cyclization reaction as Clz9. Moreover, we were surprised to find that Tcz9 is capable of catalyzing successive dehydrogenation reactions with **4**. The isolation of (*E*)-**9** and (*Z*)-**9** confirmed our hypothesis that the oxidation reaction proceeds via an *o*-QM intermediate. Both of these dearomatized compounds are stabilized via conjugation with the 3*H*-pyrrolizine ring and are stable at room temperature. However, (*E*)-**9** and (*Z*)-**9** slowly changed from red to yellow following purification, and NMR spectroscopic analysis indicated these two molecules coalesced to the same rearranged, water adduct with a mass of 454.9171 ($[M - H]^-$; $C_{18}H_8Cl_4N_2O_4$). We speculate that (*E*)-**9** and (*Z*)-**9** non-enzymatically react with water by 1,6-conjugate addition to generate the linear α,β -unsaturated ketone product, **10** (Scheme 3.1; a full proposed mechanism is provided in Scheme S1). Thus, Tcz9 is ultimately capable of dehydrogenation reactions with **2** and **4** that ultimately generate α,β -unsaturated ketones, **1** and **10**, but through two distinct mechanisms.

Numerous biosynthetic proposals feature *o*-QM intermediates founded on biomimetic total syntheses, non-enzymatic coupling of secondary metabolites, and

specific trapping reactions using biosynthetic precursors.^{28–30} These ephemeral intermediates react with various nucleophiles and can undergo inter- and intramolecular conjugate addition, cycloaddition, and spirolation reactions before they can be isolated and spectroscopically characterized.^{31–33} Several synthetic approaches have been developed to generate and stabilize natural product-derived *o*-QMs for spectroscopic analysis, typically by cooling these intermediates to extremely low temperatures.^{34,35} Here, we have not only demonstrated that Clz9 and Tcz9 catalyze benzylic functionalization reactions via an *o*-QM intermediate, but we were also able to isolate a stabilized *o*-QM conjugated with the 3*H*-pyrrolizine ring system. The unprecedented oxidation of the unactivated propyl chain in **4** to the α,β -unsaturated ketone **10** via a cyclized, twice dehydrogenated, and stabilized *o*-QM intermediate highlights the versatility and potential of the enzymes to perform challenging chemical transformations.

In conclusion, we established the genetic basis for the biosynthesis of two previously undescribed dichloropyrrole-containing marine natural products, tetrachlorizine and dihydrotetrachlorizine. Bioinformatic analysis revealed a gene cluster with striking similarity to the chlorizidine gene cluster, and further comparative *in vitro* studies revealed nuanced activity between the corresponding BBE-like tailoring enzymes Tcz9 and Clz9. The benzylic dehydrogenation reactions catalyzed by Tcz9 proceed via an *o*-QM intermediate. To our knowledge, this is the first example of a dehydrogenation reaction proceeding via an *o*-QM, expanding the reaction repertoire of these highly reactive intermediates. These findings epitomize the importance of connecting genes to the molecules and understanding the nuanced approaches nature has developed to perform powerful and selective chemical transformations. Further development of BBE-

like enzymes for biocatalytic applications may deliver chemoenzymatic solutions to challenging oxidative reactions in total synthesis efforts.

Acknowledgements

We kindly thank Brendan Duggan and Anthony Mrse for NMR assistance, and Alexander Smith for isolating strain AJS-327. Funding was generously provided by the NIH (R01-AI47818 to B.S.M.; R37-CA044848 to W.F.) and the NIH Marine Biotechnology Training Grant Predoctoral Fellowship (T32-GM067550) to T.N.P.

Chapter 3 is a reprint in full of the material as it appears in the *Journal of the American Chemical Society* **2021**, *143*, 3682-3686. Purdy, Trevor N.; Kim, Min C.; Cullum, Reiko; Fenical, William; Moore, Bradley S. The dissertation author was a co-primary investigator and author of this paper.

References

1. Doroghazi, J. R.; Albright, J. C.; Goering, A. W.; Ju, K. S.; Haines, R. R.; Tchalukov, K. A.; Labeda, D. P.; Kelleher, N. L.; Metcalf, W. W. A roadmap for natural product discovery based on large-scale genomics and metabolomics. *Nat. Chem. Biol.* **2014**, *10*, 963–968.
2. Ziemert, N.; Alanjary, M.; Weber, T. The evolution of genome mining in microbes – a review. *Nat. Prod. Rep.* **2016**, *33*, 988–1005.
3. Navarro-Muñoz, J. C.; Selem-Mojica, N.; Mullowney, M. W.; Kautsar, S. A.; Tryon, J. H.; Parkinson, E. I.; De, E. L. C.; Santos, L.; Yeong, M.; Cruz-Morales, P.; Abubucker, S.; Roeters, A.; Lokhorst, W.; Fernandez-Guerra, A.; Dias Cappelini, L. T.; Goering, A. W.; Thomson, R. J.; Metcalf, W. W.; Kelleher, N. L.; Barona-Gomez, F.; Medema, M. H. A computational framework to explore large-scale biosynthetic diversity. *Nat. Chem. Biol.* **2020**, *16*, 60–68.
4. Kim, E.; Moore, B. S.; Yoon, Y. J. Reinvigorating natural product combinatorial

- biosynthesis with synthetic biology. *Nat. Chem. Biol.* **2015**, *11*, 649–659.
5. Donia, M. S.; Fischbach, M. A. Small molecules from the human microbiota. *Science*. **2015**, *349*, 1254766.
 6. Huffman, M. A.; Fryszkowska, A.; Alvizo, O.; Borra-Garske, M.; Campos, K. R.; Canada, K. A.; Devine, P. N.; Duan, D.; Forstater, J. H.; Grosser, S. T.; Halsey, H. M.; Hughes, G. J.; Jo, J.; Joyce, L. A.; Kolev, J. N.; Liang, J.; Maloney, K. M.; Mann, B. F.; Marshall, N. M.; McLaughlin, M.; Moore, J. C.; Murphy, G. S.; Nawrat, C. C.; Nazor, J.; Novick, S.; Patel, N. R.; Rodriguez-Granillo, A.; Robaire, S. A.; Sherer, E. C.; Truppo, M. D.; Whittaker, A. M.; Verma, D.; Xiao, L.; Xu, Y.; Yang, H. Design of an *in vitro* biocatalytic cascade for the manufacture of islatravir. *Science*. **2019**, *366*, 1255–1259.
 7. Walsh, C. T.; Wencewicz, T. A. Flavoenzymes: Versatile catalysts in biosynthetic pathways. *Nat. Prod. Rep.* **2013**, *30*, 175–200.
 8. Teufel, R.; Agarwal, V.; Moore, B. S. Unusual flavoenzyme catalysis in marine bacteria. *Curr. Opin. Chem. Biol.* **2016**, *31*, 31–39.
 9. Huang, C. H.; Lai, W. L.; Lee, M. H.; Chen, C. J.; Vasella, A.; Tsai, Y. C.; Liaw, S. H. Crystal structure of glucooligosaccharide oxidase from *Acremonium strictum*: A novel flavinylation of 6-S-cysteinyl, 8 α -N1-histidyl FAD. *J. Biol. Chem.* **2005**, *280*, 38831–38838.
 10. Nielsen, C. A.; Folly, C.; Hatsch, A.; Molt, A.; Schröder, H.; O'Connor, S. E.; Naesby, M. The important ergot alkaloid intermediate chanoclavine-I produced in the yeast *Saccharomyces cerevisiae* by the combined action of EasC and EasE from *Aspergillus japonicus*. *Microb. Cell Fact.* **2014**, *13*, 1–11.
 11. Carlson, J. C.; Li, S.; Gunatilleke, S. S.; Anzai, Y.; Burr, D. A.; Podust, L. M.; Sherman, D. H. Tirandamycin biosynthesis is mediated by co-dependent oxidative enzymes. *Nat. Chem.* **2011**, *3*, 628–633.
 12. Daniel, B.; Konrad, B.; Toplak, M.; Lahham, M.; Messenlehner, J.; Winkler, A.; Macheroux, P. The family of berberine bridge enzyme-like enzymes: A treasure-trove of oxidative reactions. *Arch. Biochem. Biophys.* **2017**, *632*, 88–103.
 13. Taura, F.; Morimoto, S.; Shoyama, Y.; Mechoulam, R. First Direct Evidence for the Mechanism of Δ^9 -Tetrahydrocannabinolic Acid Biosynthesis. *J. Am. Chem. Soc.* **1995**, *117*, 9766–9767.
 14. Lewis, R. S.; Lopez, H. O.; Bowen, S. W.; Andres, K. R.; Steede, W. T.; Dewey, R. E. Transgenic and Mutation-Based Suppression of a *Berberine Bridge Enzyme-Like (BBL)* Gene Family Reduces Alkaloid Content in Field-Grown Tobacco. *PLoS One* **2015**, *10*, 1–17.

15. Shoyama, Y.; Tamada, T.; Kurihara, K.; Takeuchi, A.; Taura, F.; Arai, S.; Blaber, M.; Shoyama, Y.; Morimoto, S.; Kuroki, R. Structure and Function of Δ^1 -Tetrahydrocannabinolic Acid (THCA) Synthase, the Enzyme Controlling the Psychoactivity of *Cannabis sativa*. *J. Mol. Biol.* **2012**, *423*, 96–105.
16. Kim, M. C.; Cullum, R.; Machado, H.; Smith, A. J.; Yang, I.; Rodvold, J. J.; Fenical, W. Photopiperazines A–D, Photosensitive Interconverting Diketopiperazines with Significant and Selective Activity against U87 Glioblastoma Cells, from a Rare, Marine-Derived Actinomycete of the Family Streptomycetaceae. *J. Nat. Prod.* **2019**, *82*, 2262–2267.
17. Mantovani, S. M.; Moore, B. S. Flavin-Linked Oxidase Catalyzes Pyrrolizine Formation of Dichloropyrrole-Containing Polyketide Extender Unit in Chlorizidine A. *J. Am. Chem. Soc.* **2013**, *135*, 18032–18035.
18. Kim, M. C.; Winter, J. M.; Cullum, R.; Li, Z.; Fenical, W. Complementary Genomic, Bioinformatics, and Chemical Approaches Facilitate the Absolute Structure Assignment of Ionostatin, a Linear Polyketide from a Rare Marine-Derived Actinomycete. *ACS Chem. Biol.* **2020**, *23*, 32.
19. Nowak-Thompson, B.; Chaney, N.; Wing, J. S.; Gould, S. J.; Loper, J. E. Characterization of the Pyoluteorin Biosynthetic Gene Cluster of *Pseudomonas fluorescens* Pf-5. *J. Bacteriol.* **1999**, *181*, 2166–2174.
20. Qiao, Y.; Yan, J.; Jia, J.; Xue, J.; Qu, X.; Hu, Y.; Deng, Z.; Bi, H.; Zhu, D. Characterization of the Biosynthetic Gene Cluster for the Antibiotic Armeniaspirols in *Streptomyces armeniacus*. *J. Nat. Prod.* **2019**, *82*, 318–323.
21. Yamanaka, K.; Ryan, K. S.; Gulder, T. A. M.; Hughes, C. C.; Moore, B. S. Flavoenzyme-Catalyzed Atropo-Selective *N,C*-Bipyrrole Homocoupling in Marinopyrrole Biosynthesis. *J. Am. Chem. Soc.* **2012**, *134*, 12434–12437.
22. Flatt, P. M.; Wu, X.; Perry, S.; Mahmud, T. Genetic Insights into Pylalomycin Biosynthesis in *Nonomuraea spiralis* IMC A-0156. *J. Nat. Prod.* **2013**, *76*, 939–946.
23. Zhang, X.; Parry, R. J. Cloning and Characterization of the Pyrrolomycin Biosynthetic Gene Clusters from *Actinosporangium vitaminophilum* ATCC 31673 and *Streptomyces* sp. Strain UC 11065. *Antimicrob. Agents Chemother.* **2007**, *51*, 946–957.
24. There is one ORF associated with chlorizidine A biosynthesis that is absent in the tetrachlorizidine BGC - a flavin mononucleotide reductase gene. Putative FMN reductase genes have been identified elsewhere in the genome.
25. Nowak-Thompson, B.; Gould, S. J.; Loper, J. E. Identification and sequence

- analysis of the genes encoding a polyketide synthase required for pyoluteorin biosynthesis in *Pseudomonas fluorescens* Pf-5. *Gene* **1997**, *204*, 17–24.
26. Winkler, A.; Hartner, F.; Kutchan, T. M.; Glieder, A.; Macheroux, P. Biochemical Evidence That Berberine Bridge Enzyme Belongs to a Novel Family of Flavoproteins Containing a Bi-covalently Attached FAD Cofactor. *J. Biol. Chem.* **2006**, *281*, 21276–21285.
 27. Willis, N. J.; Bray, C. D. *ortho*-Quinone Methides in Natural Product Synthesis. *Chem. - A Eur. J.* **2012**, *18*, 9160–9173.
 28. Bai, W. J.; David, J. G.; Feng, Z. G.; Weaver, M. G.; Wu, K. L.; Pettus, T. R. R. The Domestication of *ortho*-Quinone Methides. *Acc. Chem. Res.* **2014**, *47*, 3655–3664.
 29. Singh, M. S.; Nagaraju, A.; Anand, N.; Chowdhury, S. *ortho*-Quinone methide (*o*-QM): a highly reactive, ephemeral and versatile intermediate in organic synthesis. *RSC Adv.* **2014**, *4*, 55924–55959.
 30. Spence, J. T. J.; George, J. H. Total Synthesis of Peniphenones A–D via Biomimetic Reactions of a Common *o*-Quinone Methide Intermediate. *Org. Lett.* **2015**, *17*, 5970–5973.
 31. Rodriguez, R.; Adlington, R. M.; Moses, J. E.; Cowley, A.; Baldwin, J. E. A New and Efficient Method for *o*-Quinone Methide Intermediate Generation: Application to the Biomimetic Synthesis of (±)-Alboatrin. *Org. Lett.* **2004**, *6*, 3617–3619.
 32. Feng, Z.-G.; Burnett, G. L.; Pettus, T. R. R. A Biomimetic Synthesis of *des*-Hydroxy Paecilospirone. *Synlett.* **2018**, *29*, 1517–1519.
 33. Cavitt, S. B.; Sarrafizadeh, H. R.; Gardner, P. D. The Structure of *o*-Quinoxine Methide Trimer. *J. Org. Chem.* **1962**, *27*, 1211–1216.
 34. Rosenau, T.; Potthast, A.; Elder, T.; Kosma, P. Stabilization and First Direct Spectroscopic Evidence of the *o*-Quinone Methide Derived from Vitamin E. *Org. Lett.* **2002**, *4*, 4285–4288.

Supporting Information

Materials

All chemicals were purchased from Fisher Scientific, Alfa Aesar, or MilliporeSigma without further purification. All solvents were of HPLC grade or higher. Preparative flash column chromatography was carried out on a Teledyne ISCO CombiFlash® Rf+ Lumen™ system using diatomaceous earth for crude extract loading and silica gel 60 (EMD, 40-63µm) for the stationary phase. Semi-preparative HPLC purification was carried out using a Phenomenex Luna C18 column (5 µm, 250 × 10 mm) at a flow rate of 3.0 mL/min, coupled with a Shimadzu SCL-10A system and Shimadzu SPD-M10A UV/Vis detector (Shimadzu Corp., Kyoto, Japan). Preparative HPLC purification was achieved using a Phenomenex Luna C18 column (5 µm, 100 × 2.0 mm) at a flow rate of 10.0 mL/min, coupled with an Agilent Technologies system composed of a PrepStar pump, a ProStar 410 autosampler, and a ProStar UV detector (Agilent Technologies Inc., CA, USA). UV spectra were measured with a Beckman Coulter DU800 spectrophotometer with a path length of 1 cm, and IR spectra were acquired on a JASCO FTIR-4100 spectrometer. NMR spectroscopic data were obtained either on a 500 MHz JEOL NMR spectrometer with a 3.0 mm probe, a 600 MHz Bruker NMR spectrometer with a 1.7 mm cryoprobe, or a 500 MHz Varian NMR spectrometer with a 5 mm, ¹³C optimized cold probe. The values of the chemical shifts are described in ppm and coupling constants are reported in Hz. NMR chemical shifts were referenced to the residual solvent peaks (d_H 2.50 and d_C 39.5 for DMSO- d_6 ; d_H 8.74, 7.58, and 7.21 and d_C 149.9, 135.5, and 123.5 for pyridine- d_5). High resolution LC-MS (HR-LC-MS) analysis was conducted on an Agilent 6530 Accurate-Mass Q-TOF MS (MassHunter software, Agilent) equipped with a dual electrospray

ionization (ESI) source and an Agilent 1260 LC system (ChemStation software, Agilent) with a diode array detector. Q-TOF MS settings during the LC gradient were as follows: acquisition - mass range acquisition m/z 100 – 1700, MS scan rate 10/s, MS/MS scan rate 2/s, fixed collision energy 20 eV; source - gas temperature 300 °C, gas flow 11 L/min; nebulizer 35 psig, ion polarity negative; scan source parameters - VCap 3000, Fragmentor 100, Skimmer 65, OctopoleRFPeak 750.

Plasmid DNA was isolated from an overnight culture using the QIAprep Spin miniprep Kit (Qiagen, Hilden, Germany) according to the manufacturer's protocol. DNA clean-up after PCR or agarose gel electrophoresis was performed with QIAquick PCR; Gel Cleanup Kit according to the manufacturer's protocol. DNA sequencing was carried out by the Genewiz Sequencing Facility in San Diego, CA.

Sonication of *E. coli* cells was performed using a 6 mm tip (Qsonica, CT, USA). Protein purification was performed on an ÄKTApurifier instrument (GE Healthcare, IL, USA) with the modules Box-900, UPC-900, R-900 and Frac-900 with all buffers filtered through a nylon membrane 0.2 μm GDWP (Merck, NJ, USA) prior to use. FPLC data was analyzed with UNICORN 5.31 (Built 743) software. All proteins were purified by Ni^{2+} affinity chromatography using a 5 mL HisTrap HP (GE Healthcare) column. Proteins were concentrated using Amicon Ultra filters with 50 kDa MWCO (MilliporeSigma). Buffer exchange was performed by size exclusion chromatography using a HiLoad 16 \times 60 cm Superdex 75 prep grade column (GE Healthcare).

Bacterial Strains and Growth Conditions

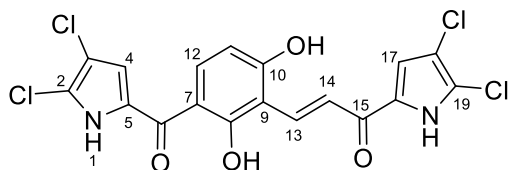
Cultivation and purification of tetrachlorizine (1) and dihydrotetrachlorizine (2)

Actinomycete sp. AJS-327 was previously isolated from a sponge fragment that washed ashore in La Jolla, CA.¹ Actinomycete sp. AJS-327 was cultured in 500 mL of a seawater-based A1 medium (10 g of starch, 4 g of yeast, 2 g of peptone, 300 mL of deionized water, and 700 mL of seawater), shaking at 180 rpm and 27 °C. After 4 days of cultivation, the culture medium was used to inoculate 20 × 2.8 L Fernbach flasks each containing 1 L of seawater-based A1 medium and shaken at 180 rpm and 27 °C. After an additional 7 days of cultivation, 20 g of Amberlite XAD-7 resin was added to each flask and shaking was continued at 180 rpm for 4 hours. The resin was collected by filtration through cheesecloth and washed with deionized water. The washed resin was extracted with acetone, and the solvent was removed under vacuum. The remaining solution was then extracted with ethyl acetate, and the ethyl acetate layer was collected and evaporated under reduced pressure to yield 3.8 g of organic extract.

The crude extract was fractionated using Lichroprep RP-18 (40-63 μ m, Merck) and a step gradient elution with H₂O and MeOH (20%, 40%, 60%, 80%, and 100%; each 200 mL) to give five subfractions. The 100% MeOH fraction (1.5 g) was subjected to re-fractionated by silica vacuum flash chromatography using a step gradient solvent system with DCM and MeOH (0%, 2%, 3%, 5%, 10%, 50%, and 100% MeOH; each 100 mL) to afford seven fractions. Fractions 2 (60 mg) and 3 (350 mg) were subjected to reversed-phase preparative HPLC (UV detection at 350 nm) using gradient elution from 10% to 100% aqueous MeCN in 0.02% TFA over 60 min to obtain compounds **1** (t_R 47.9 min) and **2** (t_R 46.8 min). Both compounds were further purified by reversed-phase semi-

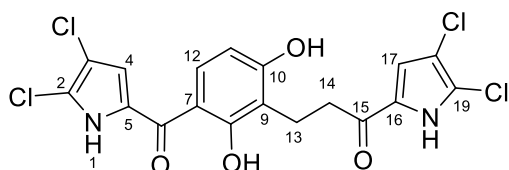
preparative HPLC (UV detection at 350 nm) with an MeCN/H₂O (in 0.02% TFA) gradient elution system from 60% to 100% for 30 min, which resulted in the isolation of **1** (6.5 mg) and **2** (2.8 mg).

Tetrachlorizine (**1**):



Dark orange gum; UV (MeOH) λ_{\max} (log ϵ) 354 (3.99) nm; IR (ZnSe) ν_{\max} 3221, 1685, 1585, 1414, 1262, 1208, 1138 cm⁻¹; ¹H and ¹³C NMR data, see Tables S2-3; HR-ESI-TOFMS: m/z = 456.9317 [M-H]⁻ (calcd. for C₁₈H₉³⁵Cl₄N₂O₄, 456.9301).

Dihydrotetrachlorizine (**2**):



Yellow gum; UV (MeOH) λ_{\max} (log ϵ) 227 sh (3.59), 244 (3.50), 297 (3.80), 350 (3.83) nm; IR (ZnSe) ν_{\max} 3218, 1601, 1563, 1490, 1420, 1301, 1251, 1174, 1136, 1082, 1025 cm⁻¹; ¹H and ¹³C NMR data, see Tables S2 and S4; HR-ESI-TOFMS: m/z = 458.9496 [M-H]⁻ (calcd. for C₁₈H₁₁³⁵Cl₄N₂O₄, 458.9472).

Purification of prechlorizidine (**4**)

Heterologous expression of the *clz* gene cluster and characterization of prechlorizidine has been previously reported.² Cultivation of the deletion mutant *Streptomyces coelicolor* M512_4B11 Δ clz9 and isolation of prechlorizidine (**4**) was performed following a modified procedure; briefly, colonies of *S. coelicolor* M512_4B11 Δ clz9 were inoculated in 2 \times 250 mL flasks containing 50 mL of TSB media supplemented with kanamycin (50 mg/mL⁻¹) and nalidixic acid (25 mg/mL) for 5 days and shaken at 180 rpm and 30 °C. The cultures were then transferred to 2.8 mL Fernbach flasks containing 1 L of R5 media supplemented with kanamycin (50 mg/mL) and shaken at 180 rpm and 30 °C. After an additional 7 days of cultivation, 800 mL of EtOAc was added to each flask and shaken for 1 additional hour. The cultures were combined and centrifuged. The supernatant was extracted, and the organic layer was separated and dried over MgSO₄. The solvent was then evaporated under reduced pressure and the crude extract was loaded onto diatomaceous earth. The crude extract was eluted onto silica for flash column purification using a gradient from 0–20% EtOAc in hexanes over 20 minutes. The solvent was evaporated under reduced pressure, which resulted in the isolation of **4** (22.4 mg).

Protein Expression, Purification, and *In Vitro* Assay Conditions

Cloning and expression of Clz9 and Tcz9

Cloning and expression of Clz9 has been previously reported.² Actinomycete sp. AJS-327 gDNA was isolated following standard procedures and concentrated using an isopropanol precipitation procedure.^{3,4} The gene coding for Tcz9 was amplified from gDNA using PrimeSTAR Max DNA polymerase (Takara Bio Inc., Kyoto, Japan) and oligonucleotides Tcz9_MBP_F (CTGTACTTCCAATCCGGATCCATGGCCACCCCATC CGCATTC) and Tcz9_MBP_R (GGTGGTGGTGGTGGTCTCGAGTCAGTCCAGCGGTCC GTCGA). The resulting 1.5-kb PCR product was cloned into a PCR amplified pET28a_MBP vector using oligonucleotides Tcz9_MBP_F and Tcz9_MBP_R by Gibson Assembly using HiFi DNA Assembly Master Mix (New England Biosciences, MA, USA). The resulting construct, Tcz9_MBP, was isolated from *E. coli* DH10B, verified by DNA sequencing and then transformed into *E. coli* BL21 (DE3) cells for protein expression. Expression of Tcz9 was started by inoculating an overnight culture at 200 rpm and 37 °C with a single colony of *E. coli* BL21 (DE3) harboring Tcz9_MBP, in Luria-Bertani (LB) broth supplemented with kanamycin (50 µg/mL) and chloramphenicol (12.5 µg/mL). The cultures were then transferred to 2.8 mL Fernbach flasks containing 1 L of terrific broth (TB) media supplemented with kanamycin (50 µg/ml), chloramphenicol (12.5 µg/mL), and riboflavin (~100 mg/L). After incubation at 200 rpm and 30 °C until an OD₆₀₀ = 0.8 was reached (approximately 4 hours), the temperature was lowered to 18 °C and protein expression was induced by the addition of IPTG (0.1 mM final concentration). The culture was incubated at 200 rpm and 18 °C for 20 hours until stopped by harvesting the cells via centrifugation (7,500g, 4 °C, 30 min). The cell pellet was stored at –80 °C.

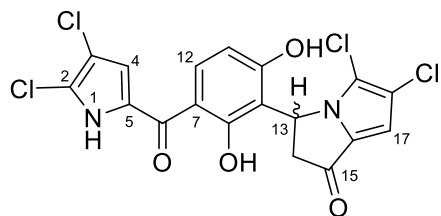
Purification of Clz9 and Tcz9

The purification of Clz9 and Tcz9 was performed following a modified procedure that was previously reported.² Frozen cell pellets were thawed and then suspended in lysis buffer (2 mL/g cells, 20 mM Tris-HCl pH 8.0, 500 mM NaCl, 10% glycerol). The cells were then sonicated at 40% amplitude for 20 cycles of 15 seconds on and 45 seconds off while remaining chilled on ice. The lysate was recovered by centrifugation (10,000g, 4 °C, 30 min) and purified by Ni²⁺ affinity chromatography over a 30 minute gradient from 10–100% elution buffer (20 mM Tris, 200 mM NaCl, 30 mM imidazole, pH 8.0) in wash buffer (20 mM Tris, 200 mM NaCl, 250 mM imidazole, pH 8.0). Eluting fractions were evaluated for purity by SDS-PAGE, and pure fractions were collected and concentrated using a 50 kDa MWCO spin filter. The protein was further purified by size exclusion chromatography preequilibrated with a 100 mM potassium phosphate buffer (5% glycerol, pH 7.5). Clz9 and Tcz9 were concentrated to approximately 20 mg/mL prior to aliquoting and storage at –80 °C.

General Procedure for *in vitro* Assays with Clz9 and Tcz9

The *in vitro* assays were performed following a modified procedure that was previously reported.² A solution containing **2** or **4** (1 mM) in DMSO was suspended in potassium phosphate buffer (5 mL, pH 7.5, with 0.2 mg/mL catalase and 10% DMSO). The reaction was initiated with addition of Clz9 or Tcz9 (50 μM final concentration) and incubated for 12 hours at 37 °C.

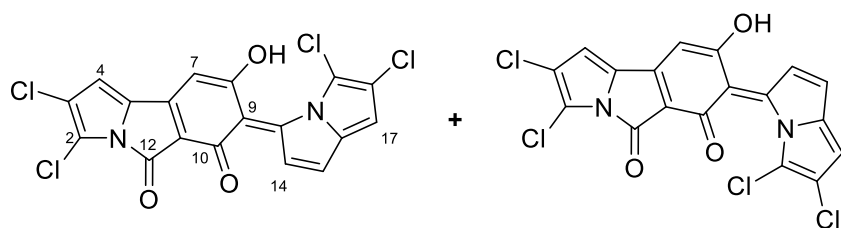
5,6-dichloro-3-(3-(4,5-dichloro-1H-pyrrole-2-carbonyl)-2,6-dihydroxyphenyl)-2,3-dihydro-1H-pyrrolizin-1-one (8):



Following incubation for 12 hours, the reaction was transferred to a 15 mL falcon tube and extracted with three times with EtOAc. The organic layer was washed with brine and dried using MgSO₄. The crude mixture was then concentrated and loaded onto celite for normal phase flash chromatography using a gradient from 0 – 20% MeOH in DCM. The solvent was evaporated under reduced pressure, which resulted in the isolation of 4 (300 µg).

UV (MeOH) λ_{max} 227, 244, 297, 354 nm; ¹H and ¹³C NMR data, see Tables S5-6; HR-ESI-TOFMS: m/z = 456.9333 [M-H]⁻ (calcd. for C₁₈H₉³⁵Cl₄N₂O₄, 456.9317).

(E)- and (Z)-2,3-dichloro-7-(5,6-dichloro-3H-pyrrolizin-3-ylidene)-8-hydroxy-5H-pyrrolo[2,1-a]isoindole-5,6(7H)-dione ((E)-9) and ((Z)-9) (unable to unambiguously differentiate geometric isomers):



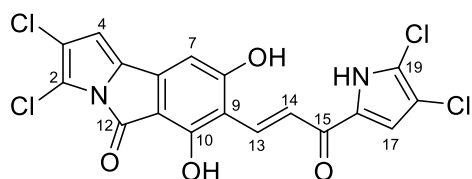
Over the course of the reaction, a red precipitate slowly precipitated out of solution. This precipitate was vacuum filtered over Celite and rinsed with three times with water to

remove residual DMSO. The precipitate was resuspended in MEOH and loaded onto Celite for normal phase flash chromatography using a gradient from 0 – 8%, then flushed with 20% MEOH in DCM. The solvent was evaporated under reduced pressure, which resulted in the isolation of (*E*)-**9** and (*Z*)-**9** (100 µg and 800 µg).

The desired product strongly binds to MgSO₄; thus, certain drying agents should be avoided when removing water from organic solvent solutions containing this product. Compounds (*E*)-**9** and (*Z*)-**9** have very limited solubility in common organic solvents, including EtOAc, DCM, MeCN, and acetone.

UV (MeOH) λ_{max} 246, 280, 370, 426, 452, 481, 510, 535 nm; ¹H data, see Table S7; HR-ESI-TOFMS: *m/z* = 436.9058 and 436.9065 [M-H]⁻ (calcd. for C₁₈H₅³⁵Cl₄N₂O₃, 436.9055).

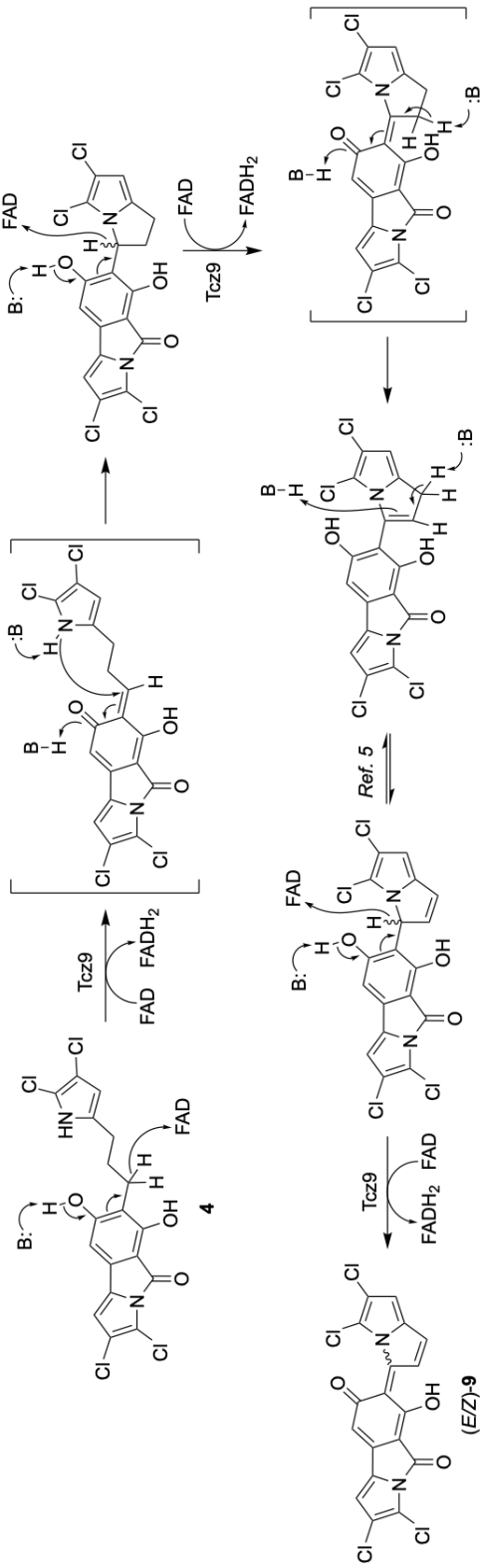
(*E*)-2,3-dichloro-7-(3-(4,5-dichloro-1*H*-pyrrol-2-yl)-3-oxoprop-1-en-1-yl)-6,8-dihydroxy-5*H*-pyrrolo[2,1-*a*]isoindol-5-one (10**):**



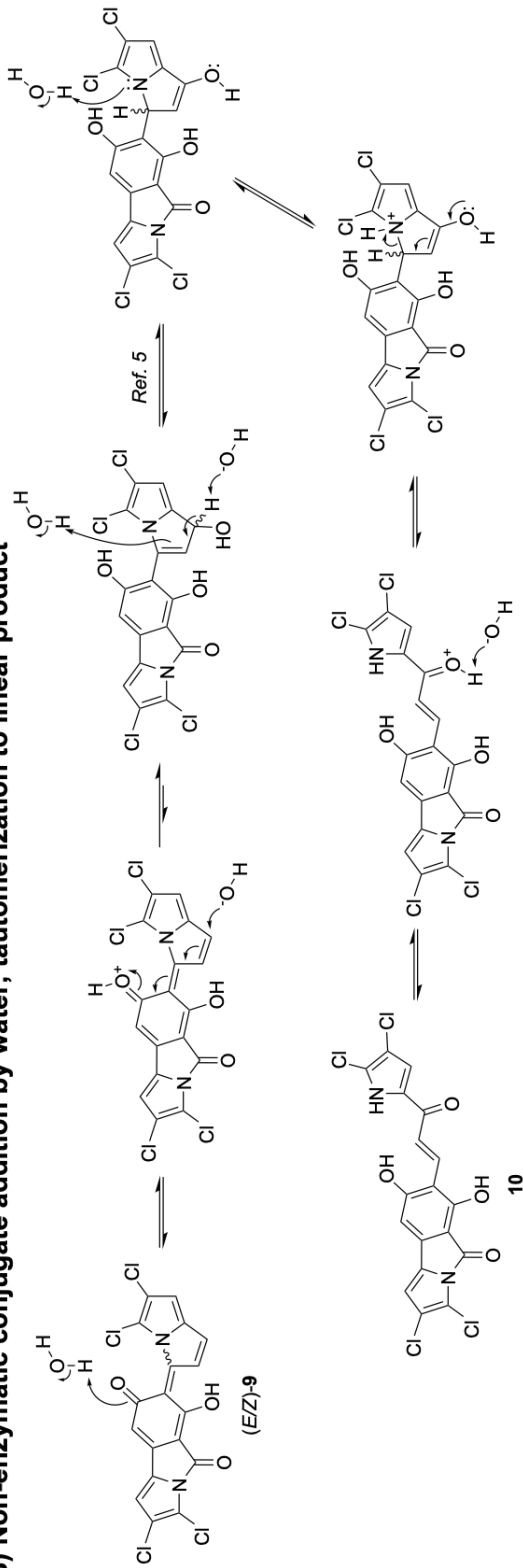
Over the course of 24 – 48 hours, isomers (*E*)-**9** and (*Z*)-**9** slowly converged to the same yellow product (**10**) while dissolved in DMSO-*d*₆. The product was further characterized by NMR. ¹H and ¹³C chemical shifts at C-13, C-14, and C15 closely matched the corresponding atoms in **1** to help confirm the absolute structure.

UV (MeOH) λ_{\max} 224, 263, 354, 420 nm; ^1H and ^{13}C NMR data, see Tables S8-9; HR-ESI-TOFMS: $m/z = 454.9171$ $[\text{M}-\text{H}]^-$ (calcd. for $\text{C}_{18}\text{H}_7^{35}\text{Cl}_4\text{N}_2\text{O}_4$, 454.9160).

A) Step 1: Enzymatic Oxidation by Tcz9



B) Non-enzymatic conjugate addition by water; tautomerization to linear product



Scheme S1: Proposed mechanism for conversion of **4** to **10**. **(A)** Enzymatic oxidation by Tcz9, which includes an intramolecular cyclization reaction and two subsequent dehydrogenation reactions. Tautomerization for the 3H-pyrroline intermediate to the 1H-pyrroline intermediate⁵ is required prior to the final dehydrogenation reaction. **(B)** Non-enzymatic conjugate addition by water to (E/Z)-9, generating the linear product **10**.

Supplementary Tables

Table S1. Putative functions of the genes in the BGC associated with **2** and sequence comparisons with *clz* genes² or closest homologues.

Gene	Size (a.a.)	Predicted Function	<i>clz</i> ² or closest homolog (% Protein Identity)	GenBank Accession Number
<i>tcz1</i>	146	MarR family transcriptional regulator	<i>S. cacaoi</i> (84)	WP_171394890.1
<i>tcz2</i>	131	Putative sterol carrier protein	<i>clz2</i> (62)	WP_158692259.1
<i>tcz3</i>	262	Enoyl-ACP reductase	<i>clz3</i> (73)	WP_027747159.1
<i>tcz4</i>	392	2-alkenoyl-CoA carboxylase/reductase	<i>clz4</i> (78)	WP_106965699.1
<i>tcz5</i>	448	FAD-dependent halogenase	<i>clz5</i> (81)	WP_027747161.1
<i>tcz6</i>	3015	Type I PKS	<i>clz6</i> (54)	WP_051262040.1
<i>tcz7</i>	1515	Type I PKS	<i>clz7</i> (57)	WP_051262041.1
<i>tcz8</i>	560	FAD-dependent halogenase (inactive)	<i>clz8</i> (46)	WP_027747162.1
<i>tcz9</i>	477	FAD-dependent oxidoreductase (BBE-like)	<i>clz9</i> (53)	WP_051262042.1
<i>tcz10</i>	91	ACP	<i>clz10</i> (67)	WP_027747163.1
<i>tcz11</i>	436	KS type II	<i>clz11</i> (65)	WP_051262043.1
<i>tcz12</i>	246	Transporter ATP-binding protein	<i>S. varsoviensis</i> (77)	WP_030877486.1
<i>tcz13</i>	257	ABC transporter permease	<i>S. varsoviensis</i> (84)	WP_030877482.1
<i>tcz14</i>	210	TetR family regulator	<i>clz12</i> (60)	WP_078512405.1
<i>tcz15</i>	225	LuxR family regulator	<i>clz13</i> (59)	WP_158692260.1
<i>tcz16</i>	490	Adenyltransferase	<i>clz14</i> (69)	WP_027747166.1
<i>tcz17</i>	378	Acyl-CoA dehydrogenase	<i>clz15</i> (70)	WP_027747167.1
<i>tcz18</i>	451	Na ⁺ /H ⁺ exchanger	<i>clz16</i> (66)	WP_051262045.1
<i>tcz19</i>	248	PPTase	<i>clz17</i> (51)	WP_051262046.1
<i>tcz20</i>	97	ACP	<i>clz18</i> (62)	WP_027747168.1
<i>tcz21</i>	263	Thioesterase	<i>clz19</i> (58)	WP_051262049.1
<i>tcz22</i>	335	Hypothetical Protein	<i>S. coeruleorubidus</i> (57)	WP_150481289.1

Abbreviations: ACP (acyl carrier protein); CoA (coenzyme A); FAD (flavin adenine dinucleotide); PKS (polyketide synthase); BBE-like (berberine bridge enzyme-like); KS (ketoacyl synthase); ATP (adenosine triphosphate); PPTase (phosphopantetheinyl transferase)

Table S2. ^1H and ^{13}C NMR spectroscopic data for **1** and **2**.

position	1 ((CD_3) $_2\text{SO}$)		2 ((CD_3) $_2\text{SO}$)		2 ($\text{C}_5\text{D}_5\text{N}$)	
	δ_{C} , type ^a	δ_{H} , mult (<i>J</i> in Hz) ^b	δ_{C} , type ^a	δ_{H} , mult (<i>J</i> in Hz) ^b	δ_{C} , type ^a	δ_{H} , mult (<i>J</i> in Hz) ^b
2	120.4, C ^e		119.7, C ^e		120.5, C ^e	
3	110.1, C ^e		109.8, C ^e		110.9, C ^e	
4	117.7, CH	7.20, d (2.8)	117.1, CH	7.10, d (2.9)	117.9, CH	7.21, m ^{c,d}
5	127.1, C		127.4, C		128.9, C	
6	184.1, C		184.2, C		185.3, C	
7	110.9, C		111.0, C		112.3, C	
8	164.9, C		162.5, C		164.0, C	
9	109.7, C		114.0, C		115.6, C	
10	164.4, C		162.3, C		163.8, C	
11	108.2, CH	6.65, d (9.0)	107.8, CH	6.54, d (9.0)	108.2, CH	6.82, d (8.9)
12	134.8, CH	7.99, d (9.0)	131.0, CH	7.79, d (9.0)	131.5, CH	8.01, d (8.9)
13	132.6, CH	8.07, d (15.8)	18.2, CH ₂	2.86, m ^c	19.5, CH ₂	3.63, m
14	123.2, CH	7.85, d (15.8)	36.2, CH ₂	2.86, m ^c	37.4, CH ₂	3.37, m
15	178.1, C		188.6, C		189.5, C	
16	131.0, C		129.3, C		130.6, C	
17	115.0, CH	7.18, d (2.3)	115.4, CH	7.13, d (2.7)	116.0, CH	7.22, s
18	109.6, C ^f		109.2, C ^f		110.3, C ^f	
19	120.0, C ^f		119.4, C ^f		120.1, C ^f	
1-NH		13.36, br d (2.8)		13.05, br s		
8-OH		13.70, br s		13.25, br s		
10-OH		11.79, br s		10.76, br s		
20-NH		13.24, br d (2.3)		12.70, br s		

^a125 MHz. ^b500 MHz. ^cOverlapping signals. ^dconfirmed by HSQC. ^{e,f}Signals may be switched.

Table S3. COSY, HMBC, and ROESY NMR data for **1** (500 MHz, (CD₃)₂SO).

1				
position	δ_H/δ_C	COSY	HMBC	ROESY
4	7.20/117.7	H-1-NH	C-2, C-5	H-12
11	6.65/108.2	H-12	C-7, C-9	
12	7.99/134.8	H-11	C-6, C-8, C-10	H-4
13	8.07/132.6	H-14	C-10, C-15	
14	7.85/123.2	H-13	C-9, C-15	H-17
17	7.18/115.0	H-20-NH	C-16, C-19	H-14
1-NH	13.36/-	H-4	C-3	
8-OH	13.70/-		C-7, C-8, C-9	
10-OH	11.79/-		C-9, C-10	
20-NH	13.24/-	H-17	C-19	

Table S4. COSY, HMBC, and ROESY NMR data for **2** (500 MHz).

2 ((CD₃)₂SO)				
position	δ_H/δ_C	COSY	HMBC	
4	7.10/117.1	H-1-NH	C-2, C-5	
11	6.54/107.8	H-12	C-7, C-9	
12	7.79/131.0	H-11	C-6, C-8, C-10	
13	2.86/18.2	H-14	C-10, C-15	
14	2.86/36.2	H-13	C-9, C-15	
17	7.13/115.4	H-20-NH	C-16, C-19	
1-NH	13.05/-	H-4		
8-OH	13.25/-			
10-OH	10.76/-		C-9, C-10, C-11	
20-NH	12.70/-	H-17		

2 (C₅D₅N)				
position	δ_H/δ_C	COSY	HMBC	ROESY
4	7.21/117.9		C-2, C-5	H-12
11	6.82/108.2	H-12	C-7, C-9	
12	8.01/131.5	H-11	C-6, C-8, C-10	H-4
13	3.63/19.5	H-14	C-8, C-9, C-10, C-14, C-15	
14	3.37/37.4	H-13	C-9, C-13, C-15	H-17
17	7.22/116.0		C-16, C-19	H-14
1-NH	-			
8-OH	-			
10-OH	-			
20-NH	-			

Table S5. ^1H and ^{13}C NMR spectroscopic data for **8** and **8'** (CD_3OD).

position	8 and 8'	
	δ_{C} , type ^a	δ_{H} , mult (<i>J</i> in Hz) ^b
2 / 2'	120.1, C ^c / 120.2, C ^d	
3 / 3'	127.6, C ^c / 127.3, C ^d	
4 / 4'	104.8, CH / 104.8, CH	7.01, s / 6.98, s
5 / 5'	N.O. ^f	
6 / 6'	184.4, C / 184.5, C	
7 / 7'	110.2, C ^g / 110.2, C ^h	
8 / 8'	N.O. ^f	
9 / 9'	111.6, C ^g / 111.2, C ^h	
10 / 10'	163.0, C / 163.5, C	
11 / 11'	106.3, CH / 106.7, CH	6.57, d (9.0) / 6.43, d (9.0)
12 / 12'	132.5, CH / 132.3, CH	7.97, m ^e / 7.96, m ^e
13 / 13'	18.5, CH / 48.9, CH	6.37, dd (8.3, 3.2) / 6.32, dd, (8.3, 3.2)
14a / 14a'	43.3, CH / 43.4, CH	3.49, m ^e / 3.46, m ^e
14b / 14b'		3.16, dd (18.1, 3.2) / 3.10, dd (18.1, 3.2)
15 / 15'	190.6, C / 190.6, C	
16 / 16'	130.4, C / N.O. ^f	
17 / 17'	116.1, CH / 116.2, CH	6.76, s / 6.75, s
18 / 18'	116.6, C ⁱ / 116.8, C ^j	
19 / 19'	N.O. ⁱ / N.O. ^j	

^a125 MHz. ^b500 MHz. ^{c,d,g,h,i,j}Signals may be switched. ^eOverlapping signals. ^fNot observed (N.O.).

Table S6. COSY, HMBC, and NOESY NMR data for **8** and **8'** (500 MHz, CD₃OD).

8 and 8'			
position	$\delta_{\text{H}}/\delta_{\text{C}}$	COSY / NOESY	HMBC
4	7.01/104.8	- / H-12	120.1, 127.6
4'	6.98/104.8	- / H-12	120.2, 127.3
11	6.57/106.3	H-12 / H-12	110.2, 111.6
11'	6.43/106.7	H-12' / H-12'	111.2
12	7.97/132.5	H-11 / H-4, H-11	C-6, C-10
12'	7.96/132.3	H-11' / H-4', H-11'	C-6', C-10'
13	6.37/48.5	H-14a, H-14b / H-14a, H-14b	
13'	6.32/48.9	H-14a', H-14b' / H-14a', H-14b'	
14a	3.49/43.3	H-13, H-14b / H-13, H-14b	C-15
14a'	3.46/43.4	H-13', H-14b' / H-13', H-14b'	C-15'
14b	3.16/43.3	H-13, H-13a / H-13, H-14a	
14b'	3.10/43.4	H-13', H-13a' / H-13', H-14a'	
17	6.76/116.1		C-16, 116.6
17'	6.75/116.2		116.8

Table S7. ¹H NMR spectroscopic data for (**E**)-**9** and (**Z**)-**9** ((CD₃)₂SO).

position	(E)-9/(Z)-9	(E)-9/(Z)-9
	δ_{H} , mult (<i>J</i> in Hz) ^a	δ_{H} , mult (<i>J</i> in Hz) ^a
4	7.57, s ^a	7.36, br. s ^c
7	6.91, s ^a	7.20, br. s ^c
14	8.16, d (7.6) ^b	7.99, br. s ^c
15	7.51, d (7.6) ^b	6.89, br. s ^c
17	6.84, s ^a	6.52, br. s ^c

^a500 MHz. ^{a,b,c}Signals may be switched.

Table S8. ^1H and ^{13}C NMR spectroscopic data for **10** ($(\text{CD}_3)_2\text{SO}$).

position	10	
	δ_{C} , type ^a	δ_{H} , mult (<i>J</i> in Hz) ^b
2, 3, 5, 6, 18, 19 ^c		
4	108.0, CH	6.85, s
7	101.5, CH	6.66, s
8	158.6, C ^d	
9	110.7, C ^d	
10	166.2, C ^d	
11	105.2, C	
12	160.3, C	
13	132.8, CH	7.98, d (15.8)
14	122.7, CH	7.75, d (15.8)
15	178.1, C	
16	131.0, C	
17	114.7, CH	7.09, s

^a125 MHz. ^b500 MHz. ^c δ_{C} = 109.6, 112.4, 116.2, 120.0, 131.0, 131.6, 136.5. ^d Signals may be switched.

Table S9. COSY and HMBC NMR spectroscopic data for **10** (500 MHz, $(\text{CD}_3)_2\text{SO}$).

10			
position	$\delta_{\text{H}}/\delta_{\text{C}}$	COSY	HMBC
4	6.85/108.0		112.4, 131.6
7	6.66/101.5		131.6, C-8, C-9, C-10, C-11
13	7.98/132.8	H-14	C-8, C-10, C-14, C-15
14	7.75/122.7	H-13	C-9, C-15
17	7.09/114.7		120.0, C-16

Supplementary Figures

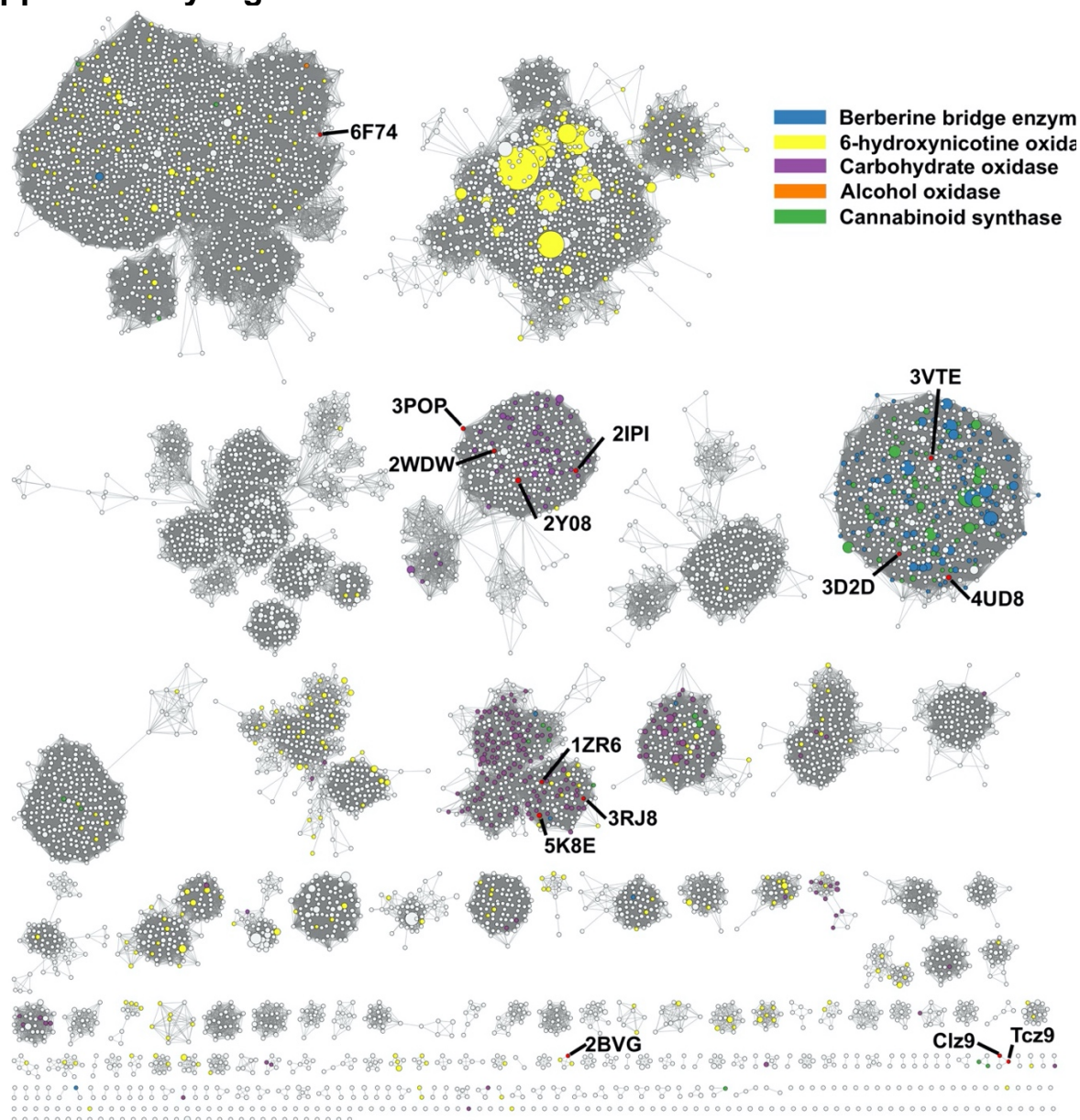


Figure S1. Sequence similarity network (SSN) of BBE-like oxidoreductases (Pfam PF08031 supplemented with Tcz9). SSN was generated by the EFI-EST⁶ server at an E-value of 5 and alignment score of 85. The SSN was visualized using Cytoscape v3.8.0.⁷ Proteins are colored by their putative function. Representative examples of BBE-like oxidoreductases include: 6F74, VAO-type oxidase (MtVAO713); 3POP, pregilvocarcin V oxidase (GilR); 2WDW, hexose oxidase (Dbv29); 2Y08, tirandamycin oxidase (TamL); 2IPI, aclacinomycin oxidoreductase (AknOx); 3VTE, tetrahydrocannabinolic acid synthase (THCA synthase); 3D2D, berberine bridge enzyme (EcBBE); 4UD8, monolignol oxidase (AtBBE); 1ZR6, glucooligosaccharide oxidase (GOOX); 5K8E, xylooligosaccharide oxidase (XylIO); 3RJ8, carbohydrate oxidase; 2BVG, 6-hydroxy-D-nicotine oxidase (6-HDNO).

```

1 1 110
Tcz9 MATPSAFESGSLTPGDGEEAAGVWVWVCHDAAVAEAVR SVRERGLPFRVRSGLGHSMCMGLSNLDDG--
2 Clz9 MTADPSESERSDMNEADEVNEVDELSLETGQTSGTKRPFTRVITGPADGEFDEARVWNECFARPKKEIIVYCADTRVAVRVRQRGGPFRVRSGLGHSM5GLSNLDDG--
3 TamL MGSHHHHHHHSSDYDIP TTEENLYFQGSEFMKHIDSVAPGD IYEDLRGGENLRYGDEPEEHLVSGSAEEIQVLSRAVRSCKRVAARSGGHCYEDFVANSQVYR--
4 GilR GSHMTASVPP-----F TVGRDPRYIELSHDNHREYVPEEEFFPATDDVAASLQKAVTEGRGVACRSGLGHCCGDFVGTPRRD-
5 EcBBE MENTKPIFFLSLIFLLNCAEAGNDLLSCLTFNGVRNHTVFSADSDSDFNRFHLHSIQNPLFQNSLISKPSAIIILPGSKEEENITIRCKRGSWTIRLSRSGGHSYEGLSYSDTTF
6 THCAS ANPRENLFKCF5KHIPNNVANPKLVYTOHQDQIYMSILNSTIQNLRREISDITTPKPLVIVTPSNNSHIGATILCSKRVGLQIRIRSRSGGHDAEGMSYISQVFPF

120 130 140 150 160 170 180 190 200 210 220 230
Tcz9 VVLDLGGGGVVELTDPDRQTVRIGGGARADVYNTIWDHR--LTVPAAGTCTPRCGVGGHVI GCGGGLSRSRGAIVDHIITALEMVDAGEGR-----L LRVSEDENPDIETWACRGGGGG
2 Clz9 VMLDYSQDDEIQQMSEDA5TVVGGGATIGDIFRARWARG--VTLPAGGFCPEIGIAGHMLGGGAGIIVRSRGLSDEHIVALEMVDSEGR-----I VVADHDSHHEELWASRGGGGG
3 TamL MWMMSRLSAGFDEBERGFAVEAGATIGAVYKTLFGRVWG-VTLPAGGFCPEIGIAGHMLGGGAGIIVRSRGLSDEHIVALEMVDSEGR-----I VVADHDSHHEELWASRGGGGG
4 GilR VVLDHNLHAIIGPAAADGAGVYVGSATVDQVQKALERRWN-AAALPLGACSAVGGGLVAGGGYGLISRGLVYHAAVEVAVDA5GAR TVIATREP SDNHIIDETWAWAHTGGGGG
5 EcBBE ILLDILVNNRYSIDLLHSETAWVESGSLGELYVAITESSKLGFTAGMCTVGTGGHISGCGGFGMSRKYGLAABVDAI LIDANGA-----I LDRQAMGEBDYAWAIRGGGGG
6 THCAS VAVDIBRNHSHIKIKIDVHSQTAWVEAGATIGEVYVYVINEKNEHLSFPGGYPCTVGVGGHIFSGGGYGAIVRNYGLAABNII DAHVNVDGK-----V LDRKSMGEBDIETWAI RGGGGG

240 250 260 270 280 290 300 310 320 330 340 350
Tcz9 NFGIATAYELR-----PTPIIDDVTTIFWISWTMSQIPDAVRA-----WQRWLSAESRINSFLSLEPQQQDMVAVFQVFDGPAADFRP LLAPELTAEVAPEAEVV--
2 Clz9 NFGIATAYELR-----TQPIIGDVTIFWAWDWRGABA IKA-----WQEWLATADGRINTLFIAPQDDMF AALGCFEGDAEELP IAPLVHAEVPTKVA--
3 TamL NFGVYRVMIRTAEDVPPGRLLPRPAEVLNITVWPGEDDEAAFLVRNHGRVFEQNSGPDSPCDLSVLAALTRSQSGALAMTTQLDADTGDPAEKRLLEYLAAVSEVGV
4 GilR NFGVYRVMIRTAEDVPPGRLLPRPAEVLNITVWPGEDDEETSFVVMRRFFWHERHSEPGSPESL FATLFVNHVSSGVLQVMQQDADVDPEGE IIAREFVASL TEGTGV
5 EcBBE VVGAIIYAWKIKLLPVEKVTYFR-VTKNVAIDEATSLHKWQVWABELEEDFTLS-----V LGGADEKQVWLTMLG-----FHFGLKTVAKSTFDLLFPELGLVEEDYLEIWSWG
6 THCAS NFGIIAAWKIKLVAVPSKSTIF5-VKKNMEIGHVVKVFNKQNKIAYKYDKDLVMTHTITKNI TDNHGKNKTTVHGQVFS5-----IFHGGVD5LVDLMNK5FPELGLIKKTDCKE5F5WI

360 370 380 390 400 410 420 430 440 450 460
Tcz9 -----EVPFIIQAVDTEALQGEAAAEEQVRAEGSSAIIANPEINDEALATIQEFITDIPPSHRAEAVYGMGGVGERERGDFAFVHRT-GIIAFEFRIIDMDSPE--DDRINIDWYIT
2 Clz9 -----TTPMII EAL5FEVWQGEAMKAT5VRAGKGNLSFVTEPLGDRAVEEIKKALAQAP5SHRAE5VBYGLGGVWAAKGRRETAFAVQRD-APVALIN5HIDMDEA--QDDPLNFAWIIQ
3 TamL QPHSDTRRILPWHHS TRWPGIAGDDMTG-RAK IIAAYARRSFDORIGTLYRLTSDYDNPAGVWAI IAYGGVWNAVPADETAQQRD-5 IILKIIVTMEDEA--QDDPLNFAWIIQ
4 GilR VGI PRGGVMSMII TGRYMSQADCGDVMGAR5AS5K5AYHRAATDEQL5VLRHLLH-ADIPGQAS5WYAF5GGI5NRRGPD5AA5VPPQRD-55VAK55M5S5AQD5AE--LDELHI5WIIQ
5 EcBBE ES5FALAGIETV5QLNRRKLF5DER-----AFIKTVKDLTKEPIL5K5FYGLERL5K5EPN--GFI5A5NG5FGG5M5SKIS5D5E5P5P5HR5SGTR5M5VE5V5AM5NQ5E5OK5K5TE5ED5WIE
6 THCAS DTTIFYS5GVVNF5NTAN5FRK5EIL5DR5AG5K5TAF5IK5LD5Y5V5K5IP5ET5AV5K5II5LE5K5Y5ED5V5GAG5M5Y5B5Y5GGI5M5EEI5ESA5I5P5E5P5HR5AG5IM5Y5EL5M5Y5T5AS5WE5K5Q5ED5NEK--5HIN5WVR

470 480 490 500 510 520 530 540 550 560 570 580 585
Tcz9 RIRHMAEHTTG-----AAAVATIDIALEN-----MLWAVYEEIIPRIWAVKRRYDPEINVEHHPHSTIPGSLTAEAAARAHGVPEATLKR IHHDDGLIDGLD
2 Clz9 NRASAAHTTGER-----GSVYNTIDITVEH-----MLWDYEEIIPRIWAVKRYDPEIDVFRHPQ5IPVSLTEAAEALGIPPHIAEELRAARQLR
3 TamL ELYRDWYADTGGVVPVGGAADGAVYVYDVIDIADDEEWNTSGV-----P5SELYVKDAPRITQAVKARWDPKINVERHIAL5VRVPP5A
4 GilR GLYEEF5AGTGGVPTGGRTDGCYIN5P5DADILD5PARNR5GE-----P5HHL5YKDN5YARL5R5SAK5RAMD5P5N5H5H5W5S5IGL
5 EcBBE KVIYEFMKPFV5KNP-----RLGVANHIDIDLGGIDWGNKTVYNNAIEISR5M5GE5VE5L5N5YERL5IRAKTLIDP5N5VE5N5P5C5I5PP5M5AN5FD5Y5L5E5K5TL5G5D5G5G5EV5V
6 THCAS SVYINFTTPYV5QNP-----RLAVL5N5R5D5ID5IG-----KTNH5ASPNNY5TQAR I5G5E5K5Y5G5K5N5R5L5V5K5K5V5K5V5D5P5N5F5FR5N5EQ5S5I5P5L5P5PHH5

```

Figure S2. Sequence comparison of Tcz9 with related BBE-like oxidoreductases. The conserved histidine and cysteine residues responsible for bivalent attachment with FAD are colored blue. Tcz9 from *Actinomyces* sp. AJ5-327; Clz9 from *Streptomyces* sp. CNH-287; TamL, 10-hydroxydehydrogenase in tirandamycin biosynthesis from *Streptomyces* sp. 307-9 (2Y08); GilR, pregilvocarin V oxidase in gilvocarin biosynthesis from *Streptomyces griseoflavus* Gö 3592 (3POP); EcBBE, berberine bridge enzyme from *Eschscholzia californica* (3D2D); THCA_synthase, tetrahydrocannabinolic acid synthase from *Cannabis sativa* (3VTE). The alignment was performed using ClustalW[®] and Geneious Pro 2019.1.3 (<https://www.geneious.com>) for visualization of the results.

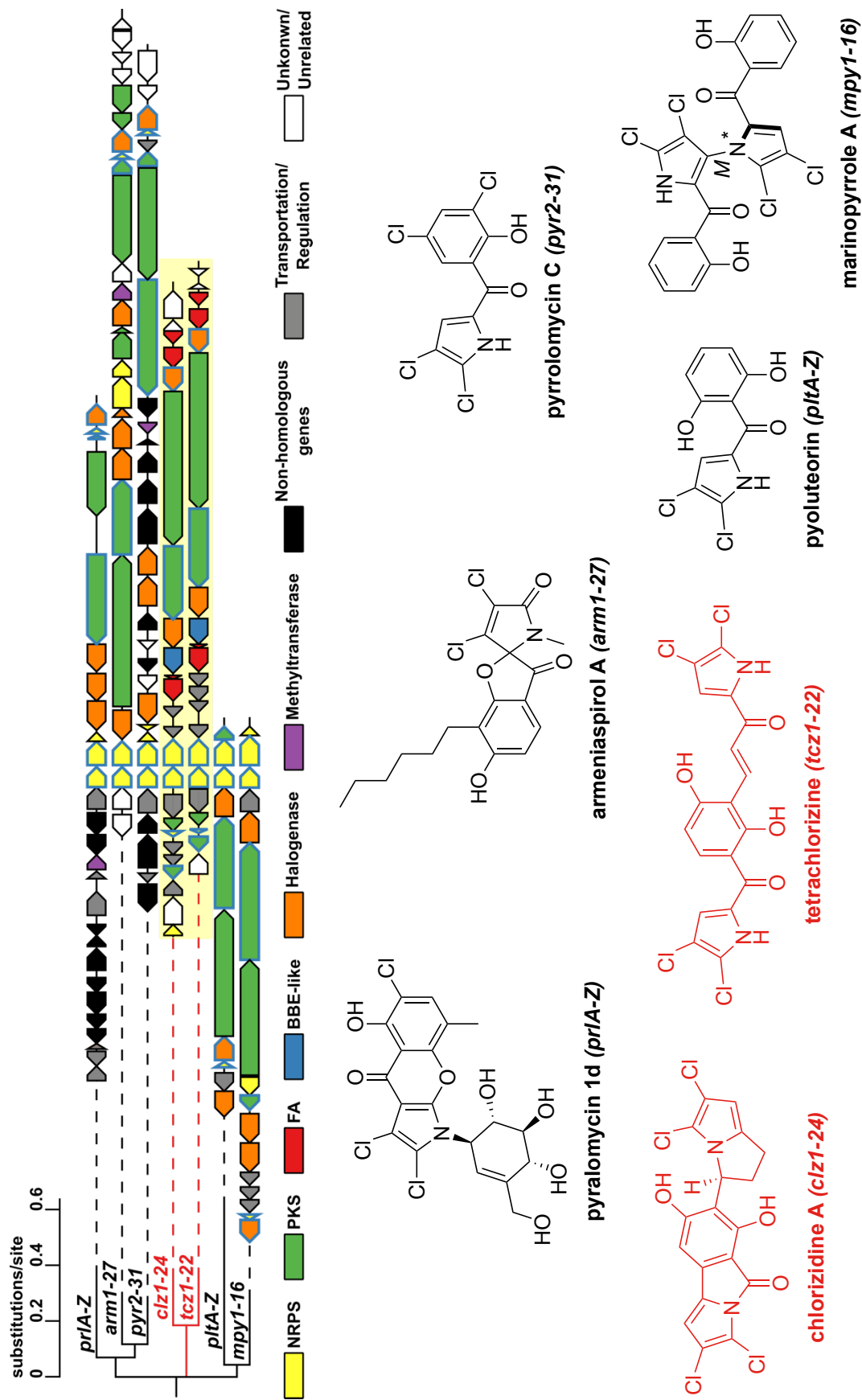


Figure S3. Alignment of characterized BGCs associated with dichloropyrrole-containing natural products using CORASON.⁹ BGCs compared in this study (*tcz* and *clz*) are highlighted in yellow. Biosynthetic genes conserved across each BGC (core genes) are outlined in blue. BGCs are aligned by the conserved adenylytransferase (AT) gene and referenced to the *clz* gene cluster. Branch length is calculated by concatenation and alignment of the conserved biosynthetic genes. E-value is 40.

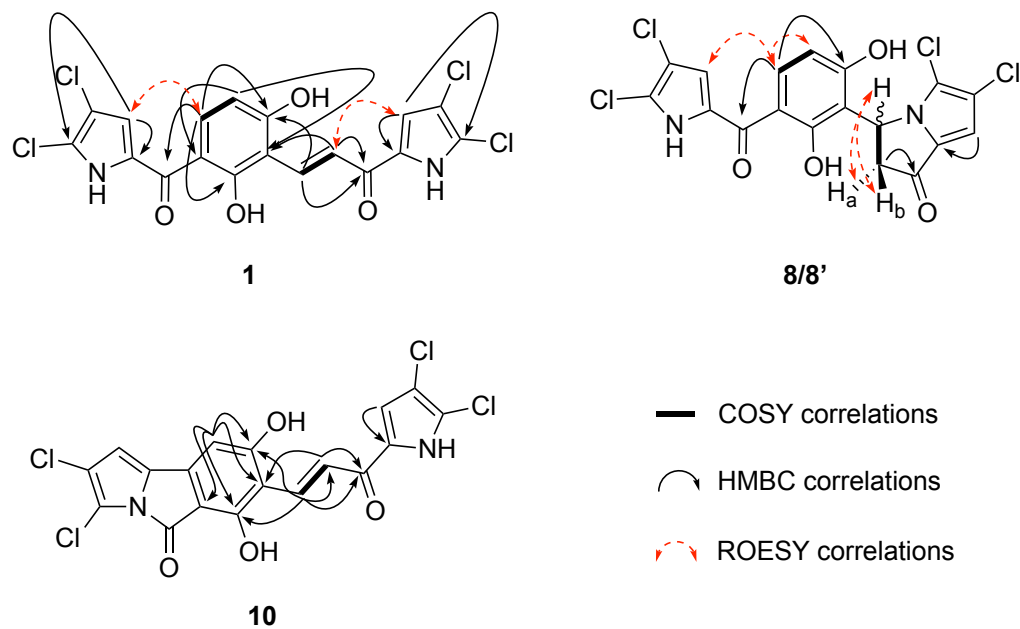


Figure S4. Key absolute COSY, ROESY, and HMBC correlations for **1**, **8**, and **10**. Correlations between protons and ambiguous carbons are listed in Tables S6 and S9.

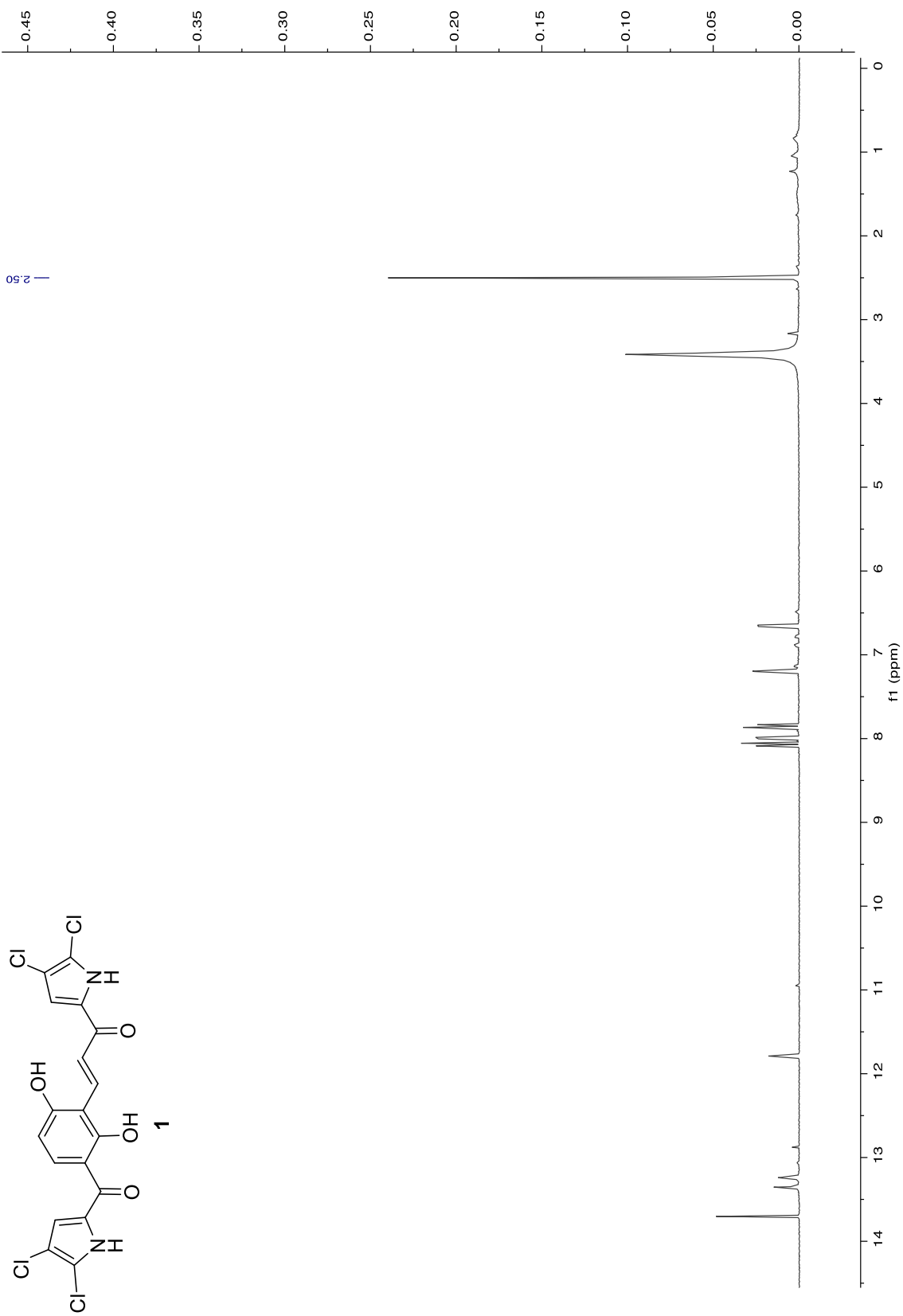


Figure S5. ¹H NMR spectrum of tetrachlorizine (1) in (CD₃)₂SO (500 MHz).

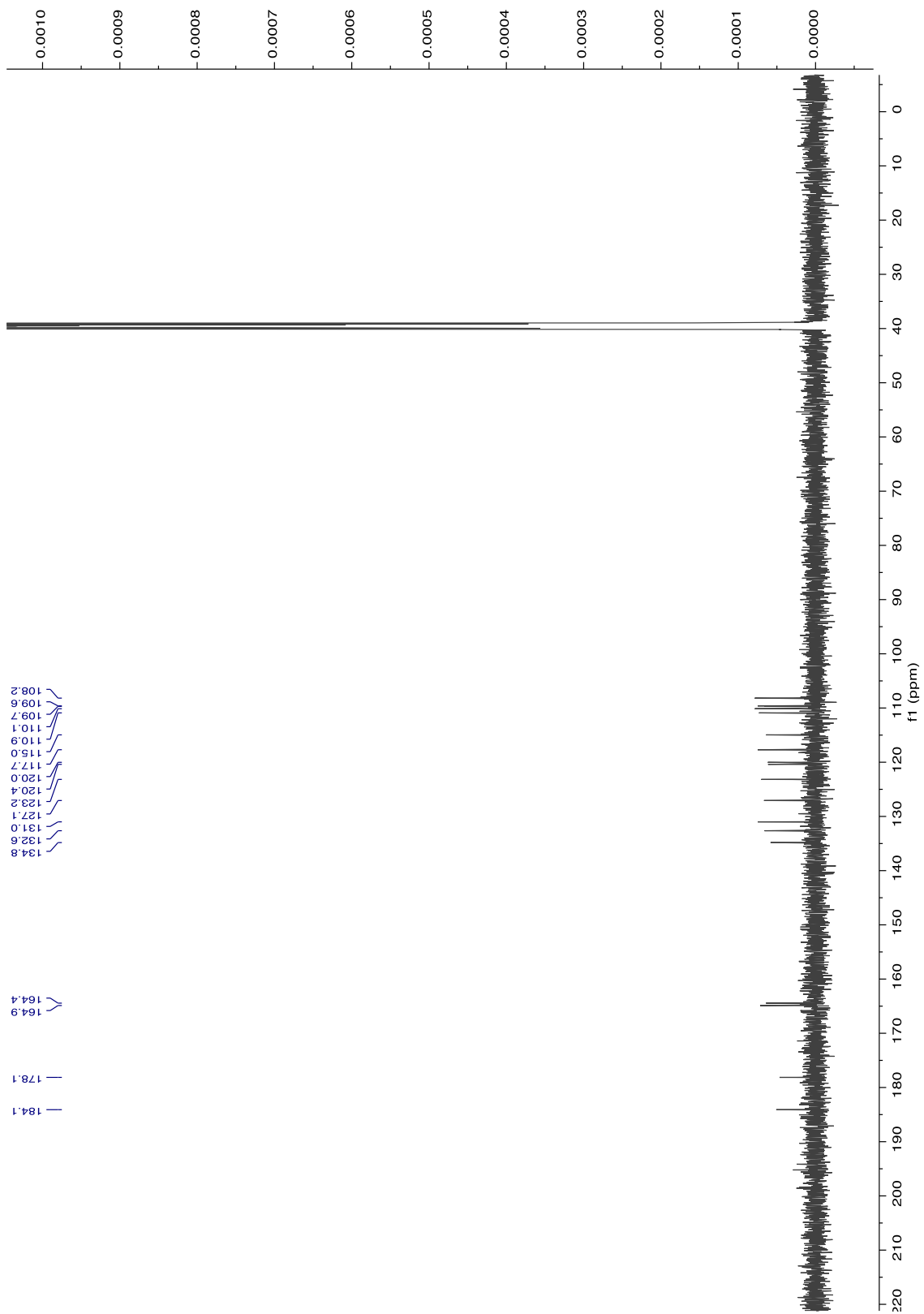


Figure S6. ^{13}C NMR spectrum of tetrachlorizine (1) in $(\text{CD}_3)_2\text{SO}$ (125 MHz).

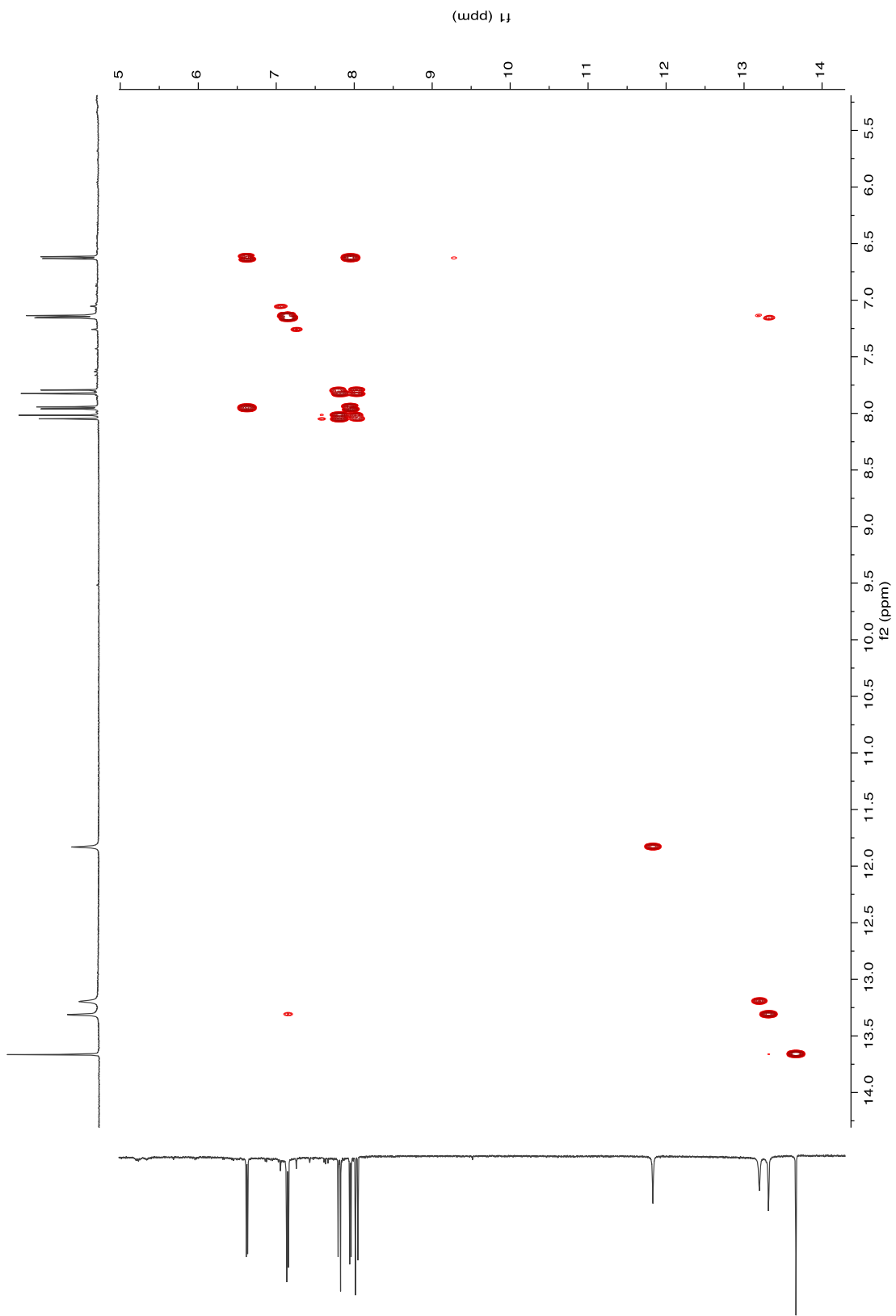


Figure S7. COSY NMR spectrum of tetrachlorizine (**1**) in $(\text{CD}_3)_2\text{SO}$ (500 MHz).

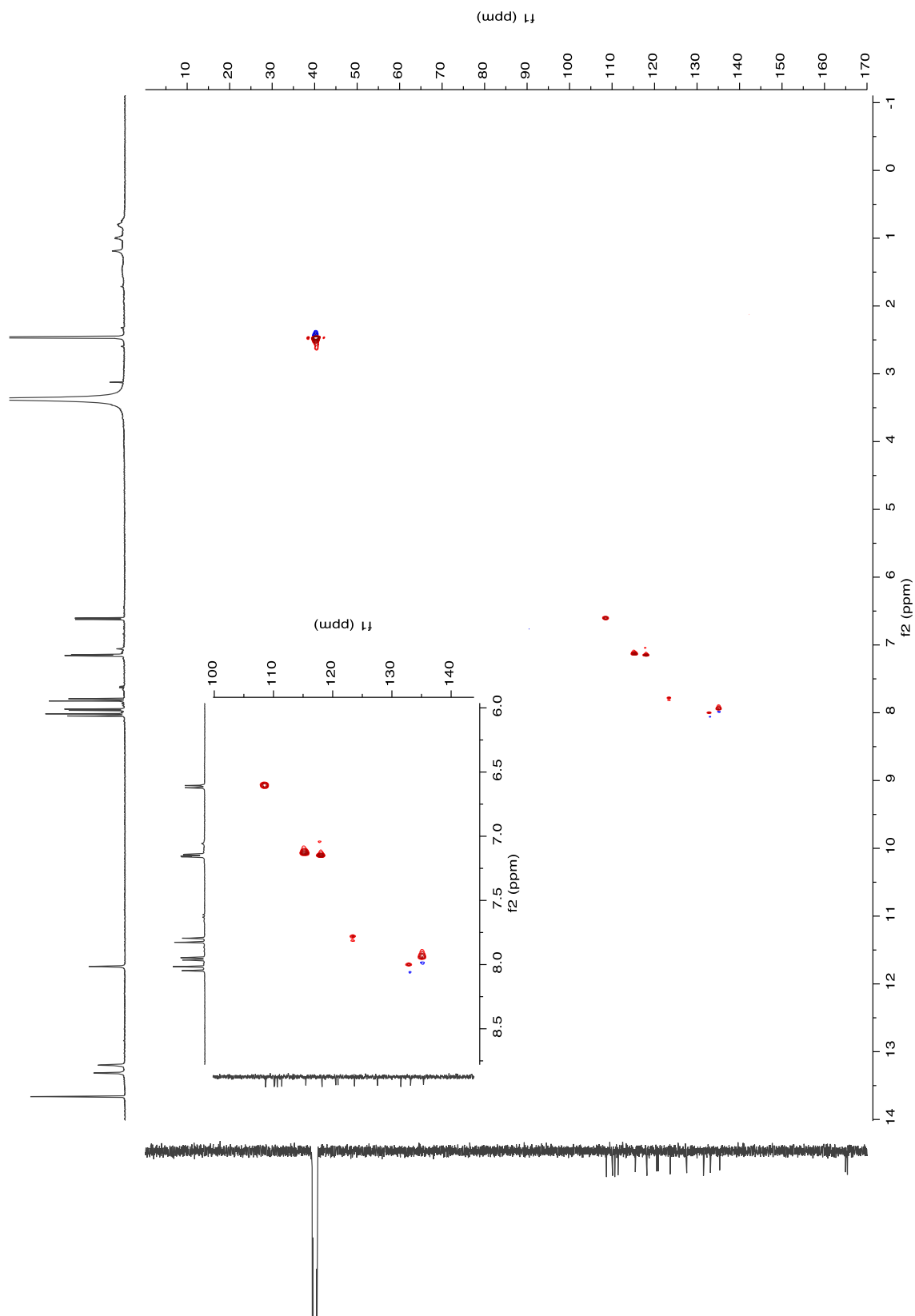


Figure S8. HSQC NMR spectrum of tetrachlorizine (**1**) in $(\text{CD}_3)_2\text{SO}$ (500 MHz).

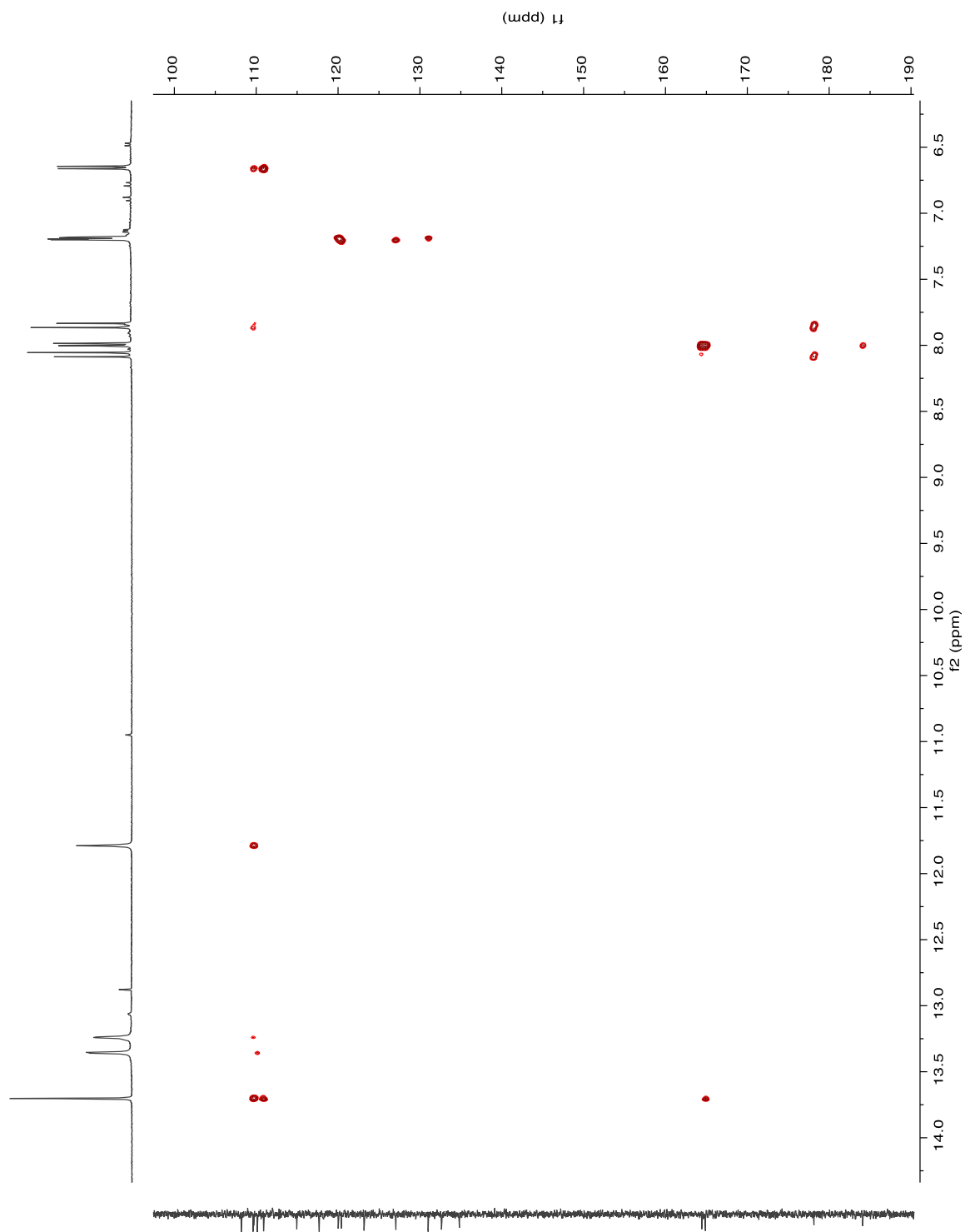


Figure S9. HMBC NMR spectrum of tetrachlorizine (1) in $(\text{CD}_3)_2\text{SO}$ (500 MHz).

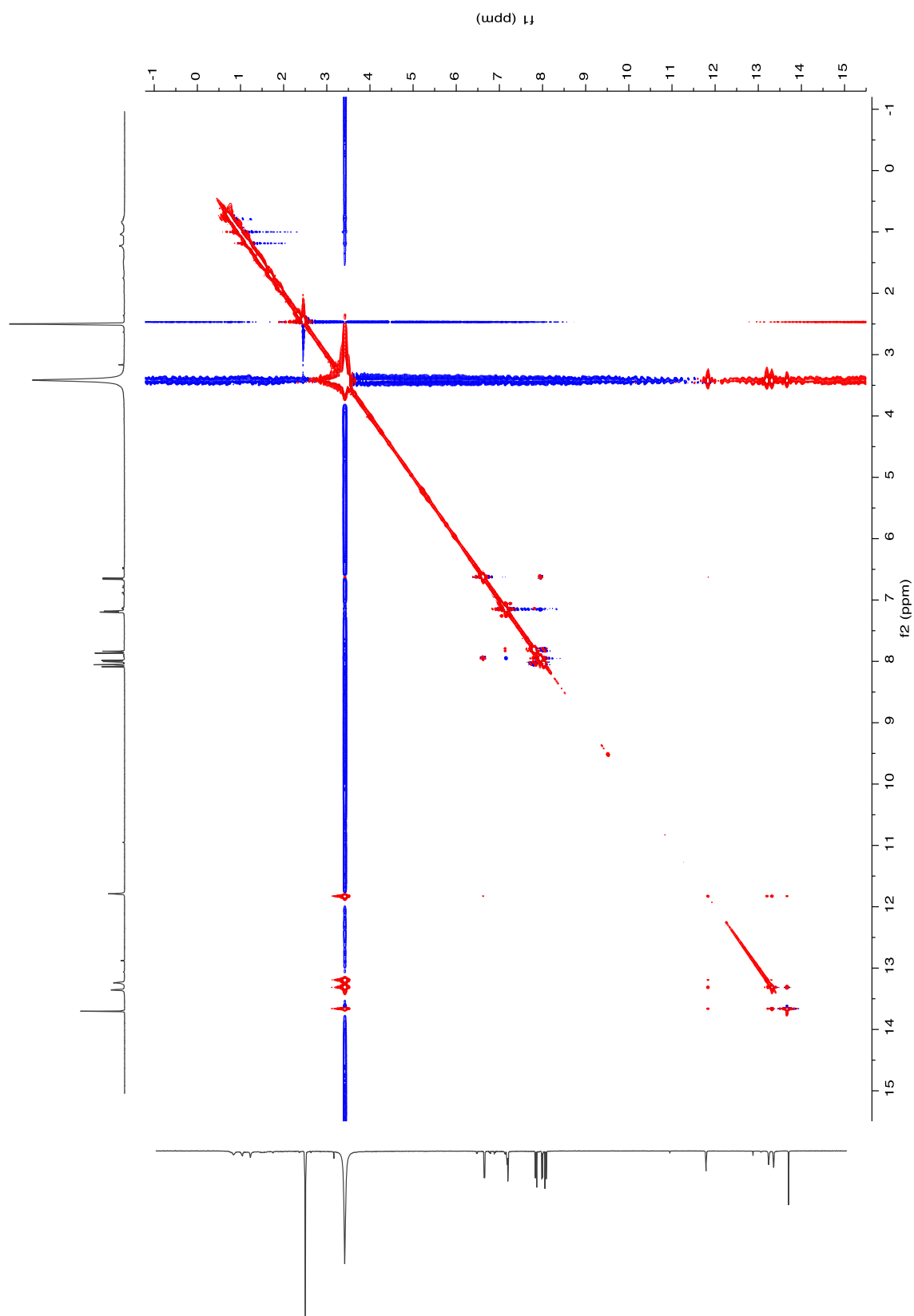


Figure S10. ROESY NMR spectrum of tetrachlorizine (**1**) in $(\text{CD}_3)_2\text{SO}$ (500 MHz).

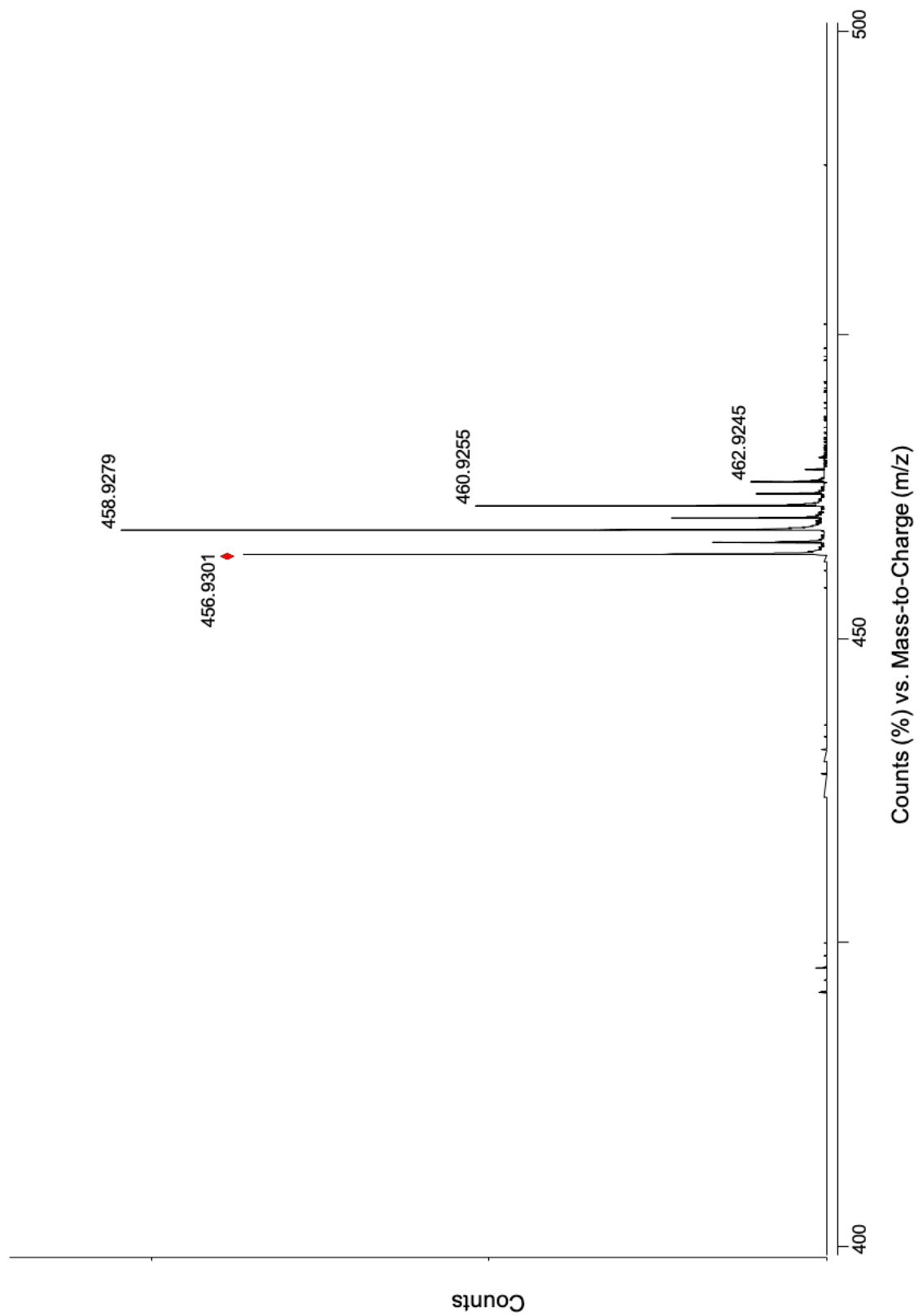


Figure S11. HR-ESI-TOF-MS spectrum of tetrachlorizine (1).

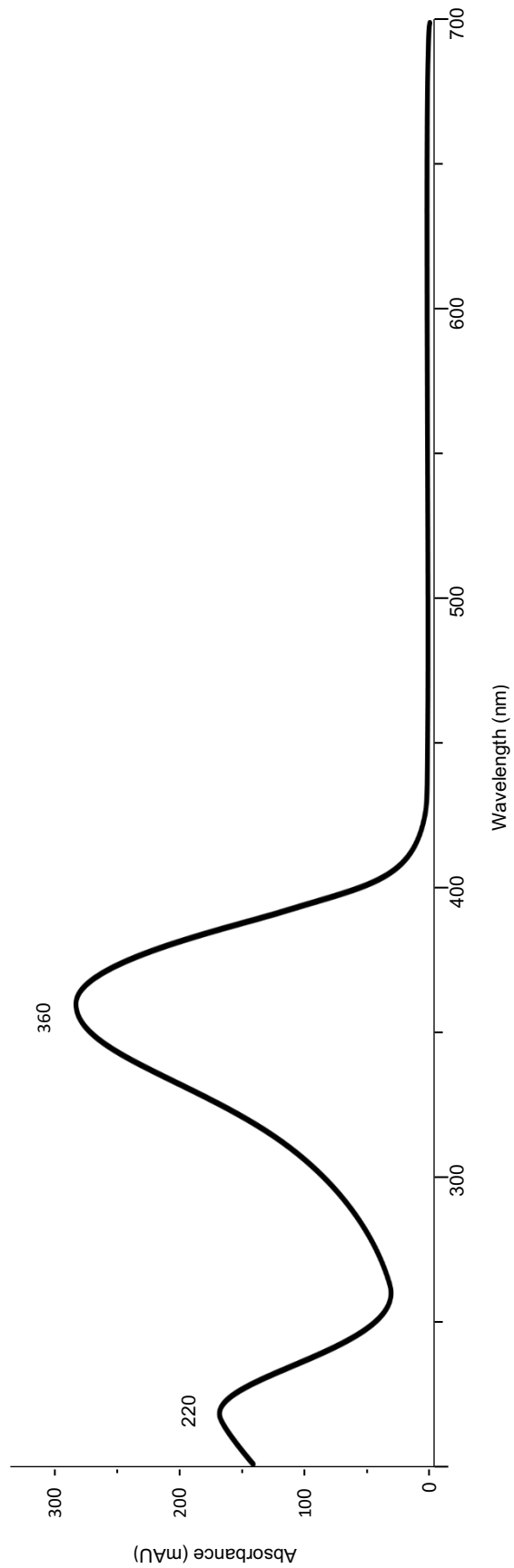


Figure S12. UV/vis spectrum of tetrachlorizine (**1**).

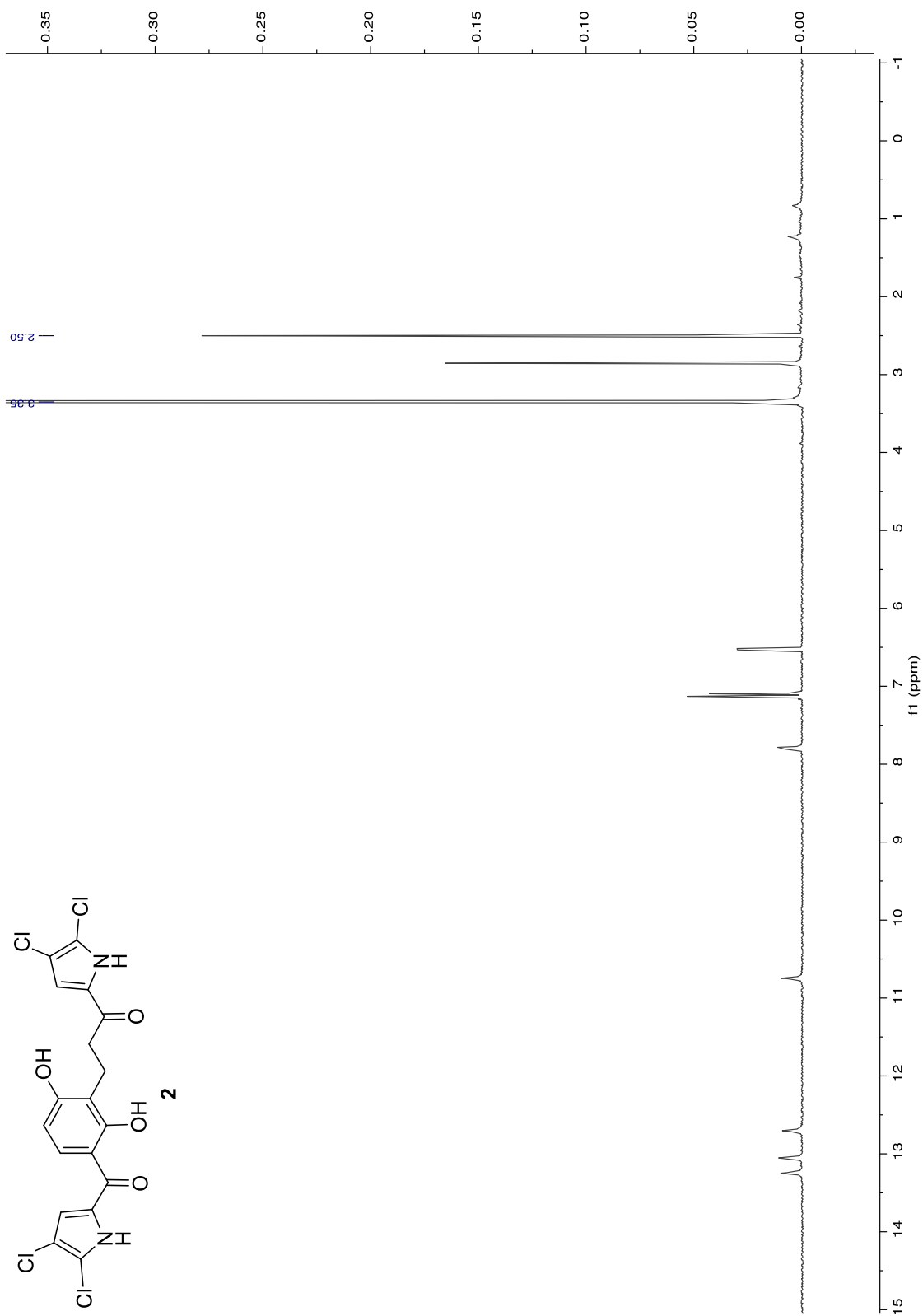


Figure S13. ¹H NMR spectrum of dihydrotrichlorizine (**2**) in (CD₃)₂SO (500 MHz).

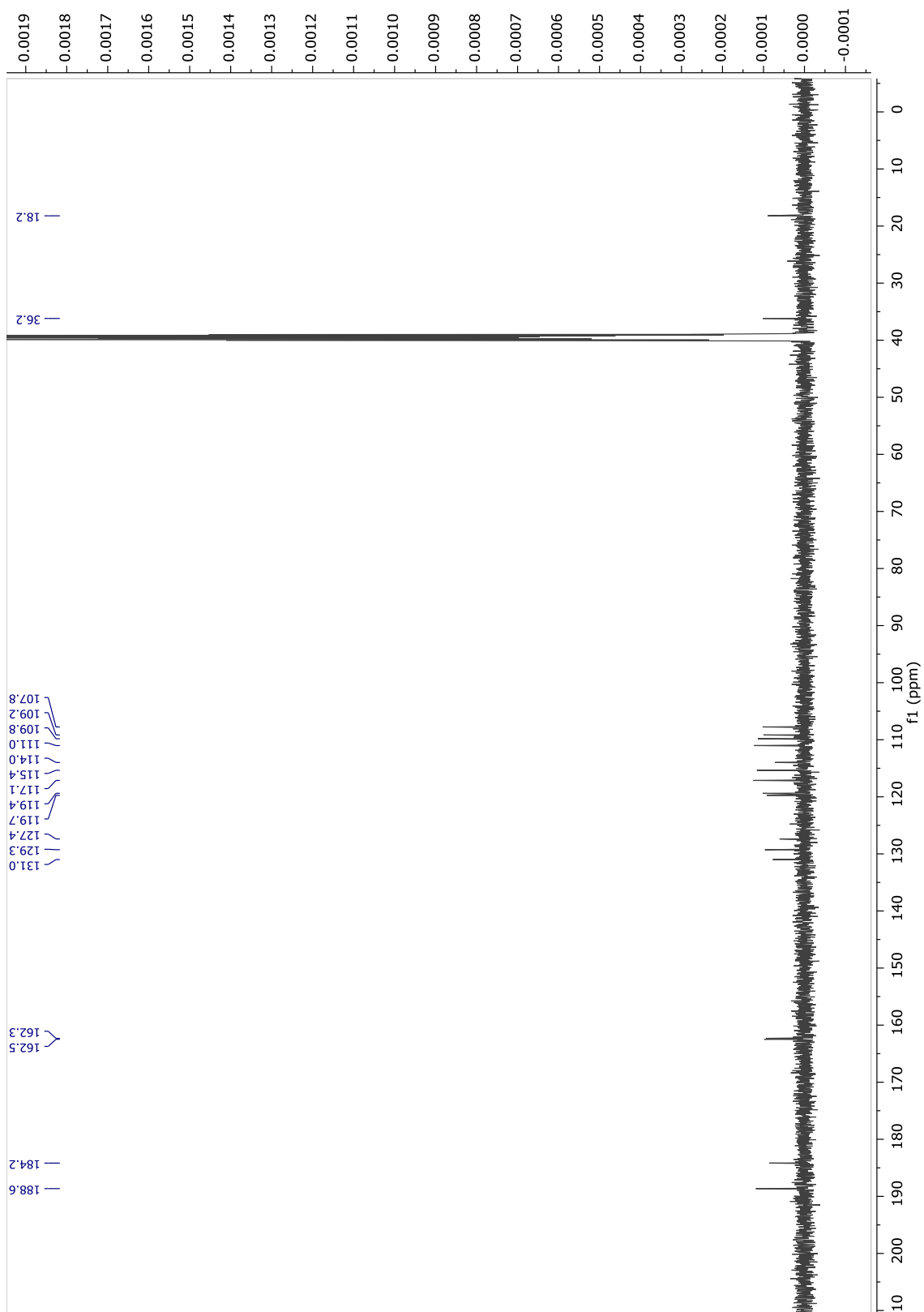


Figure S14. ¹³C NMR spectrum of dihydrotetrachlorizine (**2**) in (CD₃)₂SO (125 MHz).

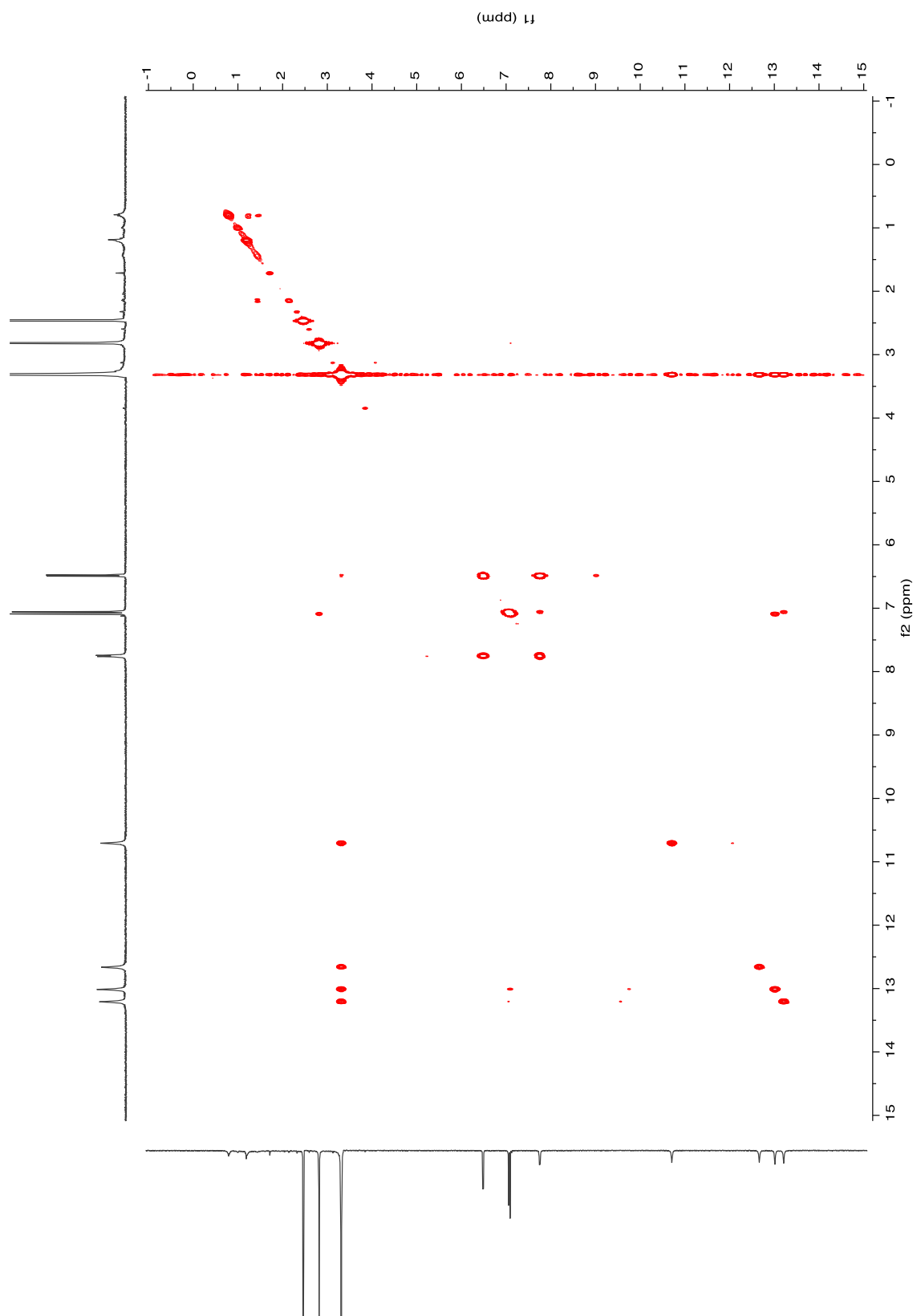


Figure S15. COSY NMR spectrum of dihydrotetrachlorizine (**2**) in (CD₃)₂SO (500 MHz).

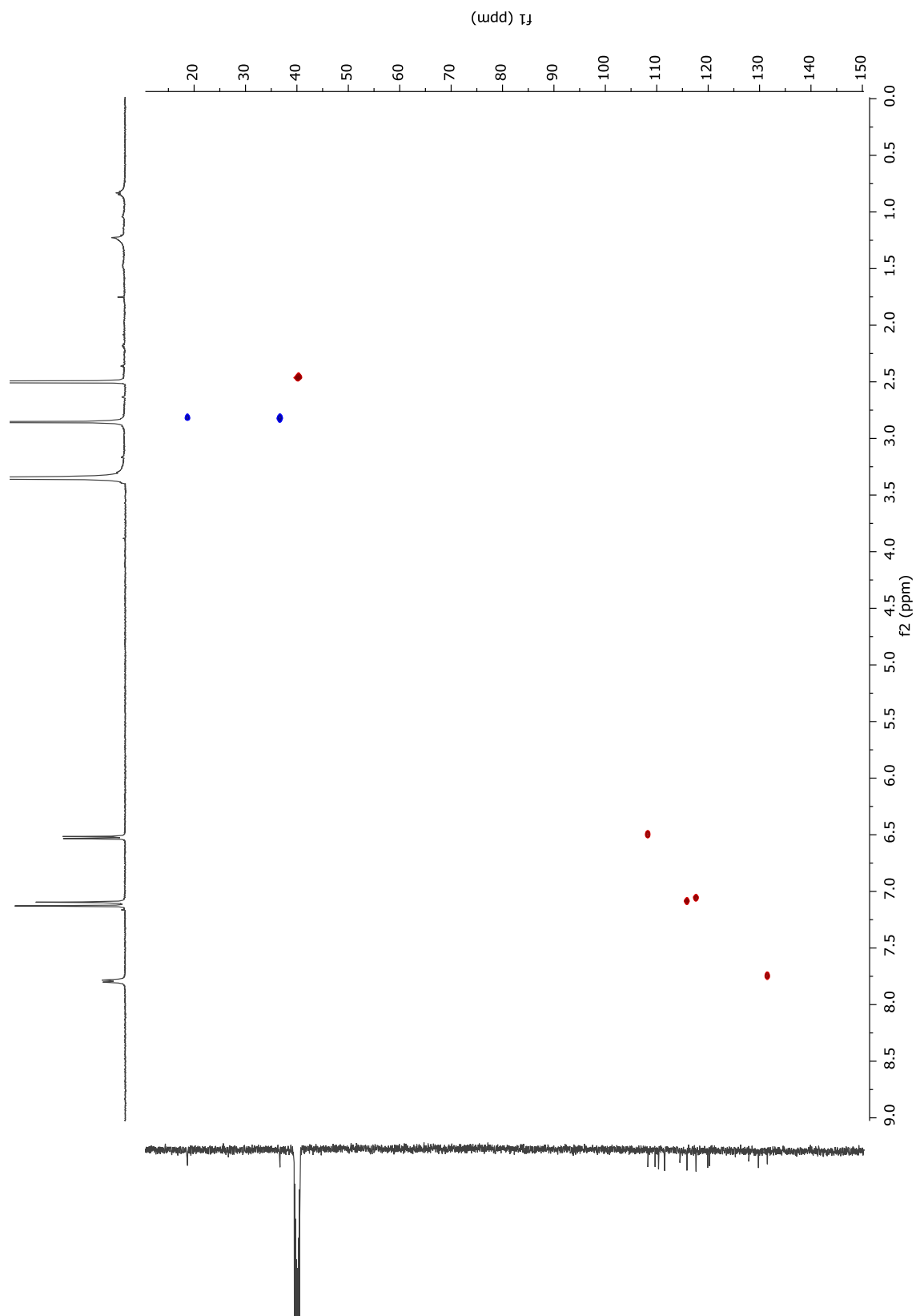


Figure S16. HSQC NMR spectrum of dihydrotetrachlorizine (**2**) in $(\text{CD}_3)_2\text{SO}$ (500 MHz).

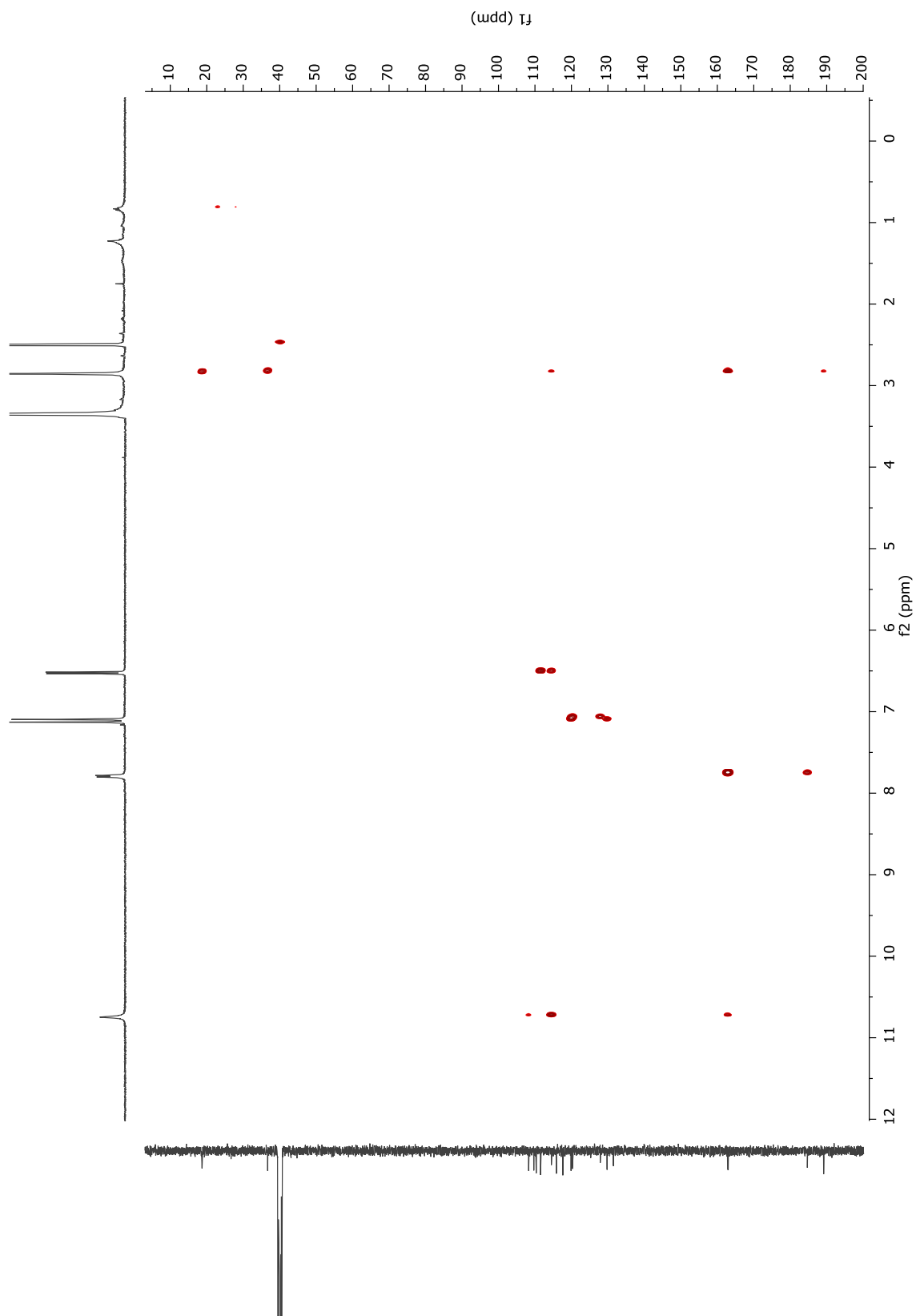


Figure S17. HMBC NMR spectrum of dihydrotetrachlorizine (**2**) in $(\text{CD}_3)_2\text{SO}$ (500 MHz).

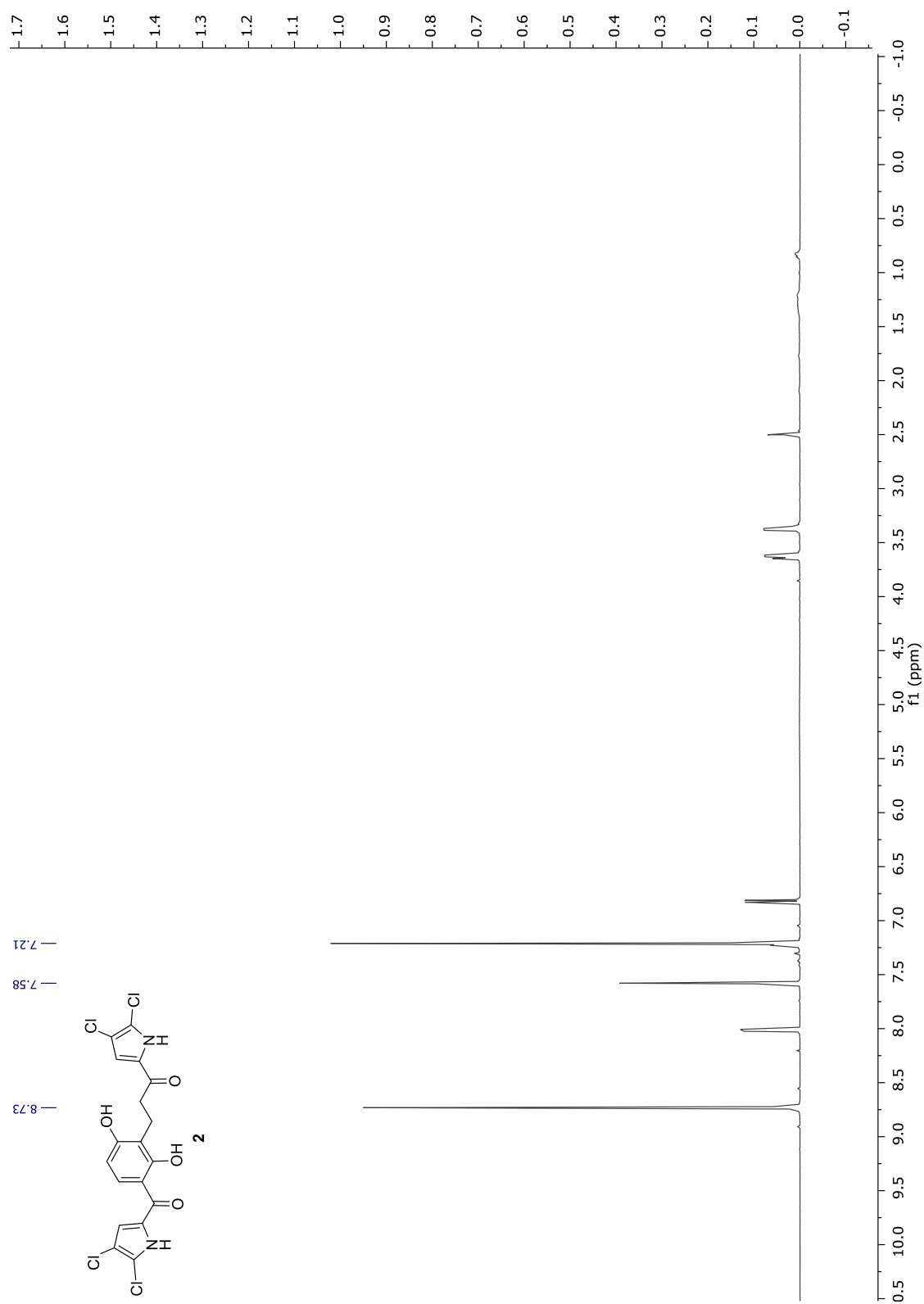


Figure S18. ¹H NMR spectrum of dihydrotrichlorizine (**2**) in C₅D₅N (500 MHz).

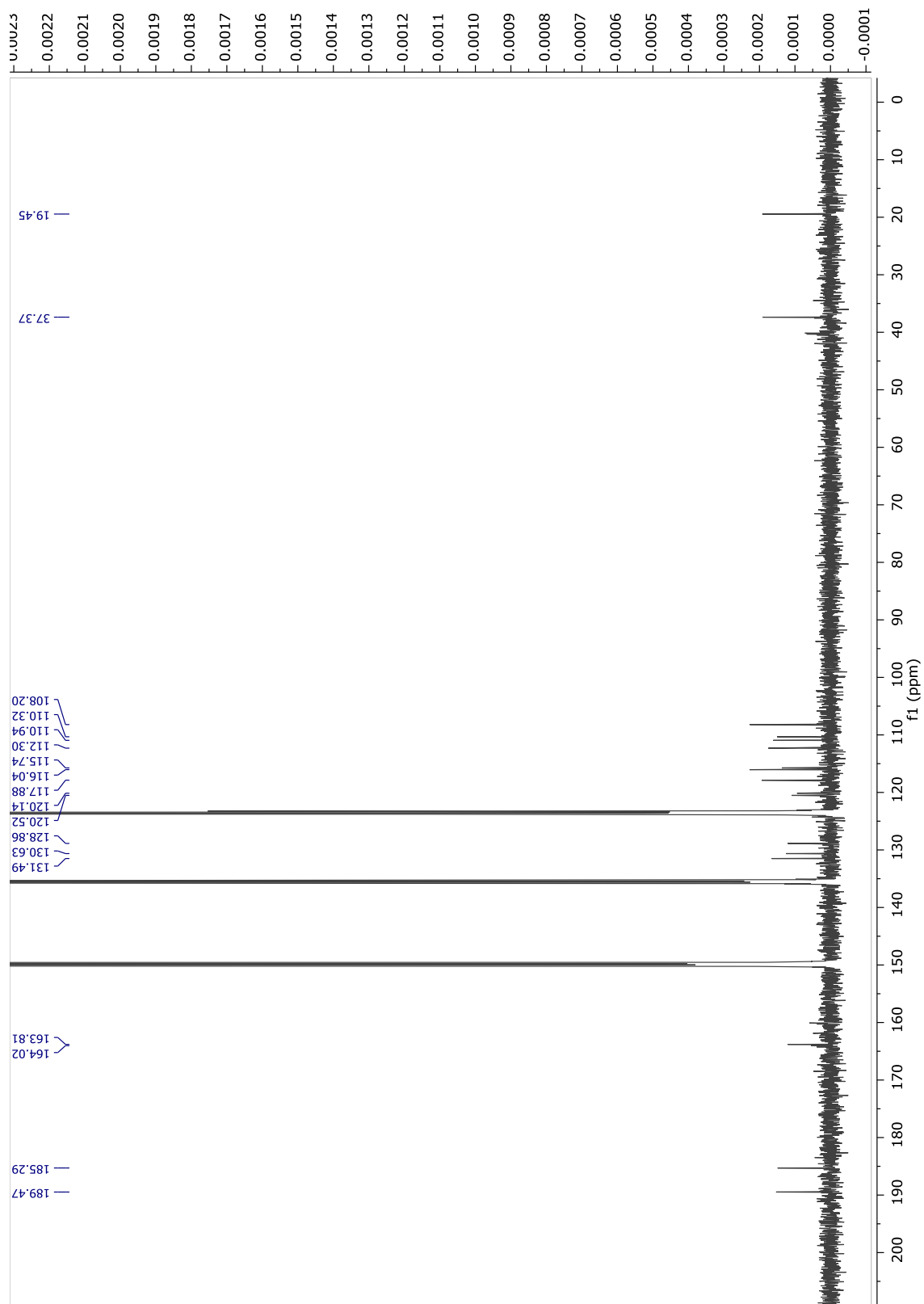


Figure S19. ^{13}C NMR spectrum of dihydrotetrachlorizine (2) in $\text{C}_5\text{D}_5\text{N}$ (125 MHz).

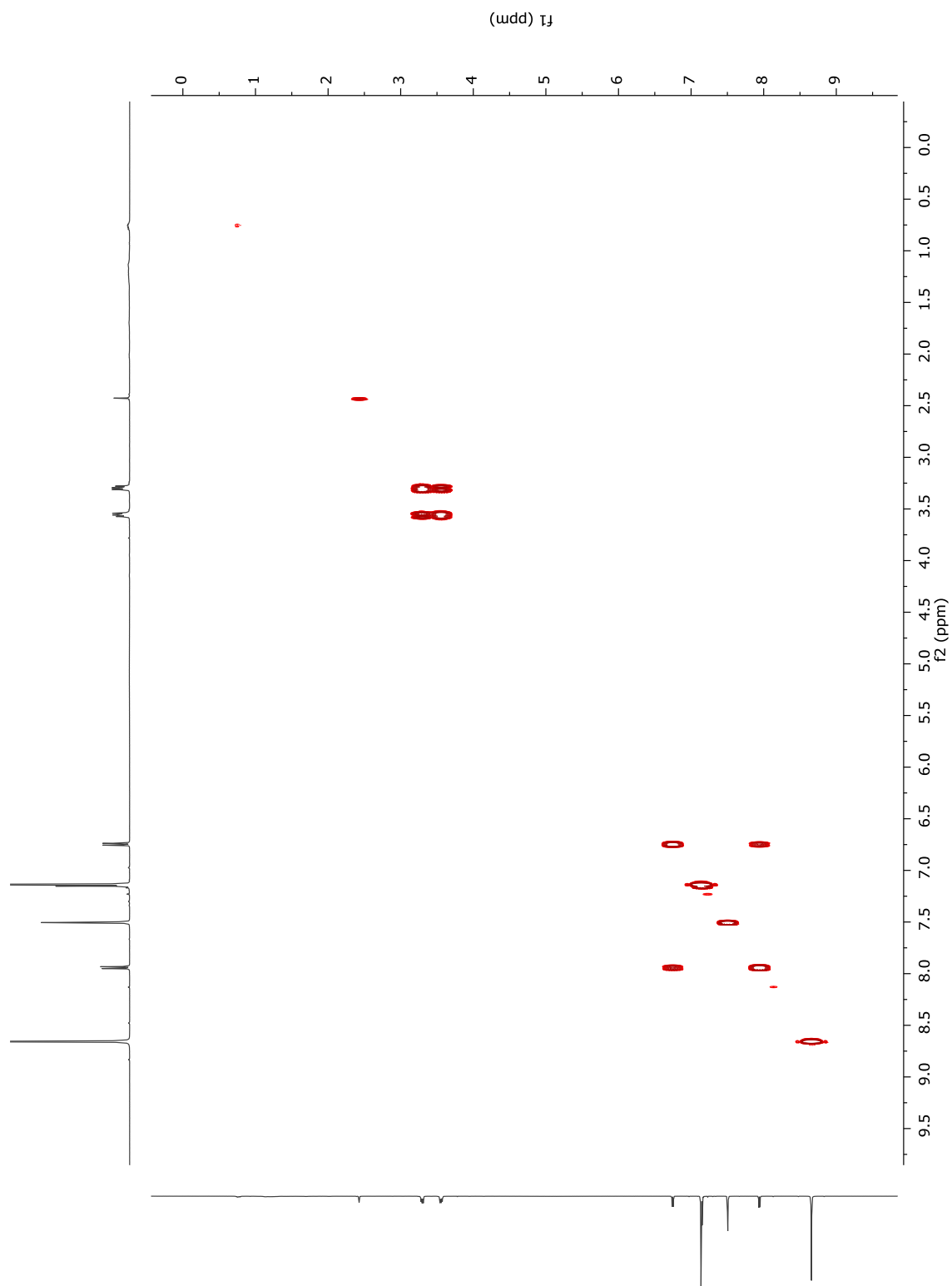


Figure S20. COSY NMR spectrum of dihydrotetrachlorizine (**2**) in C₅D₅N (500 MHz).

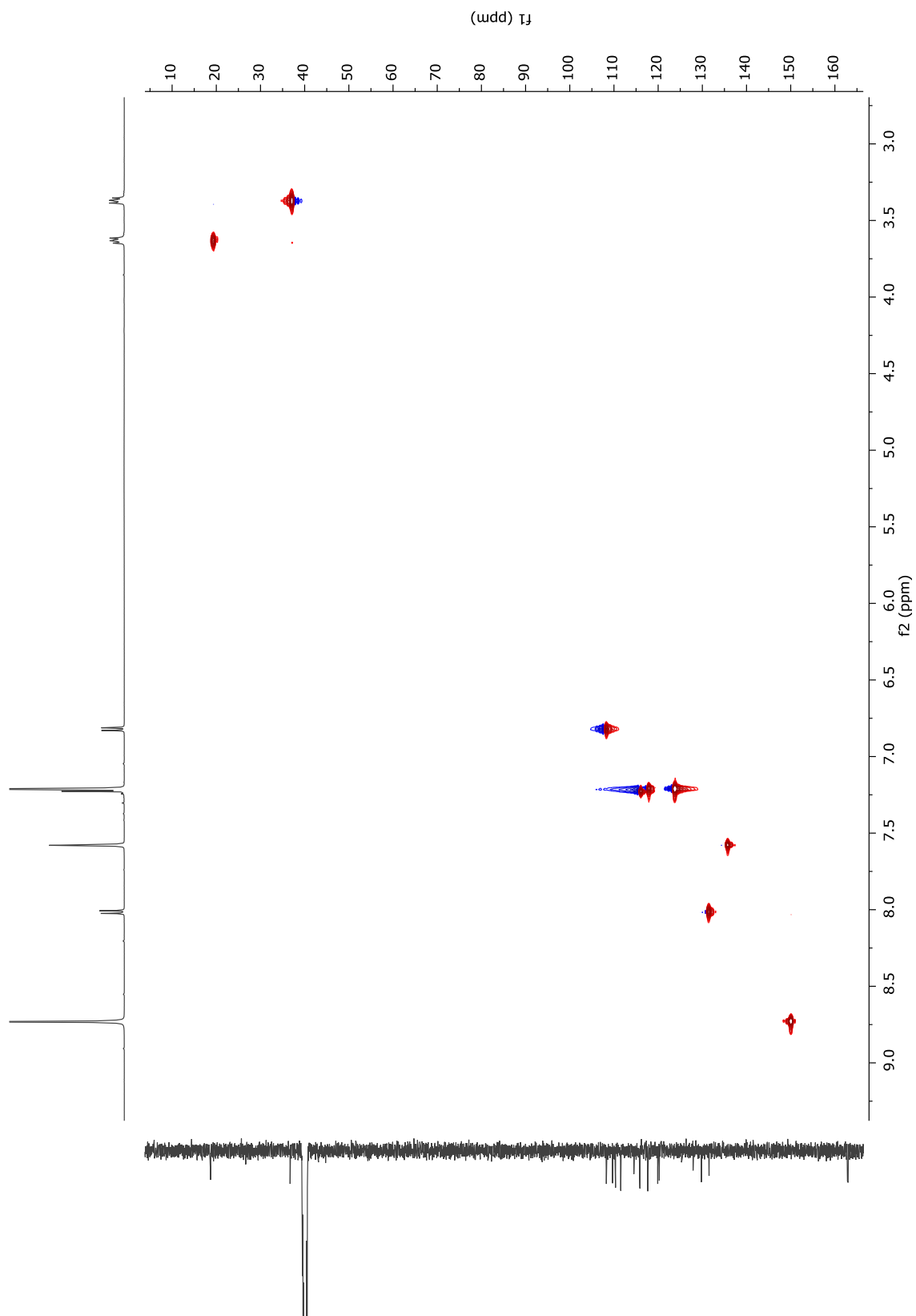


Figure S21. HSQC NMR spectrum of dihydrotetrachlorizine (**2**) in C₅D₅N (500 MHz).

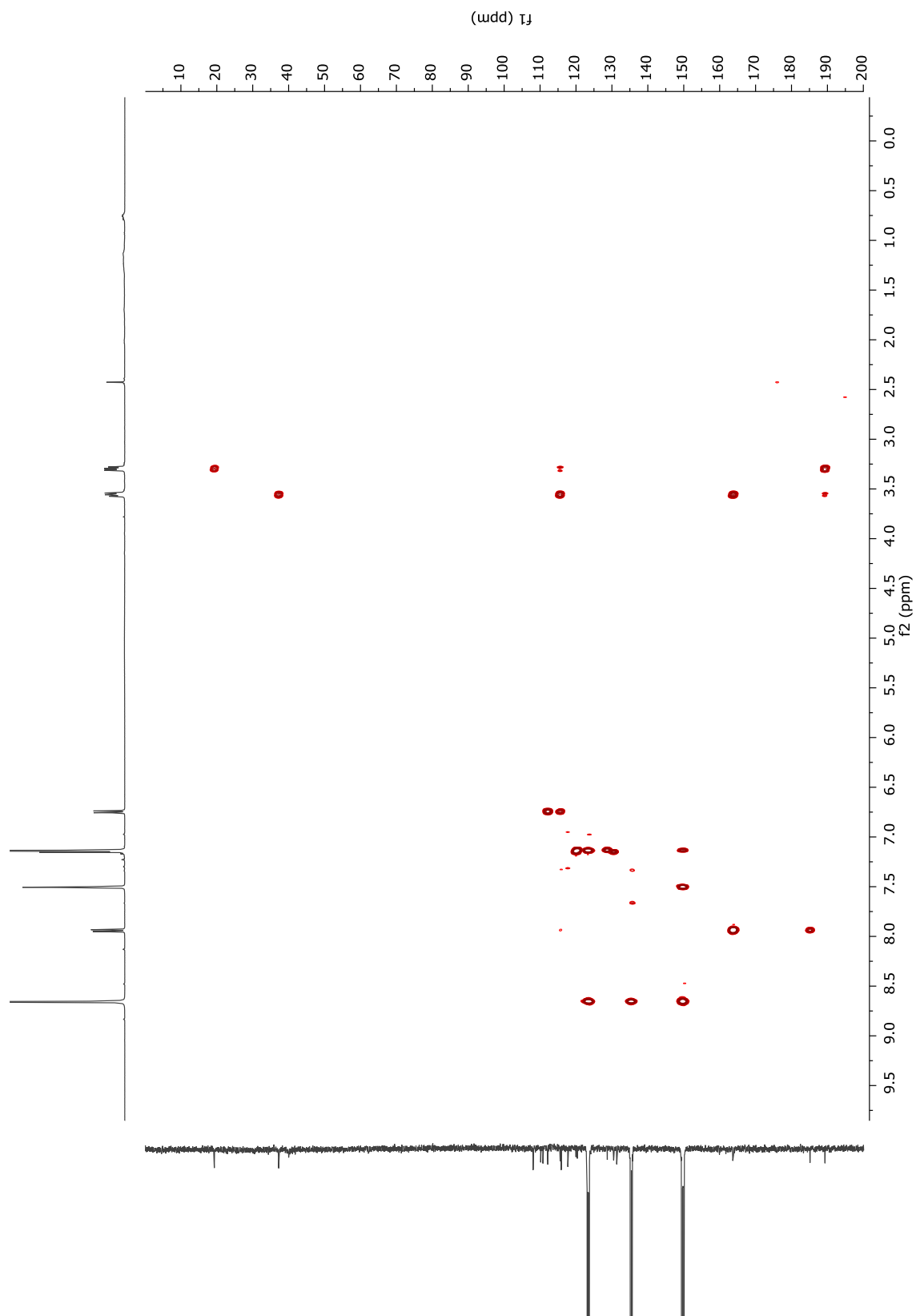


Figure S22. HMBC NMR spectrum of dihydrotetrachlorizine (2) in C₅D₅N (500 MHz).

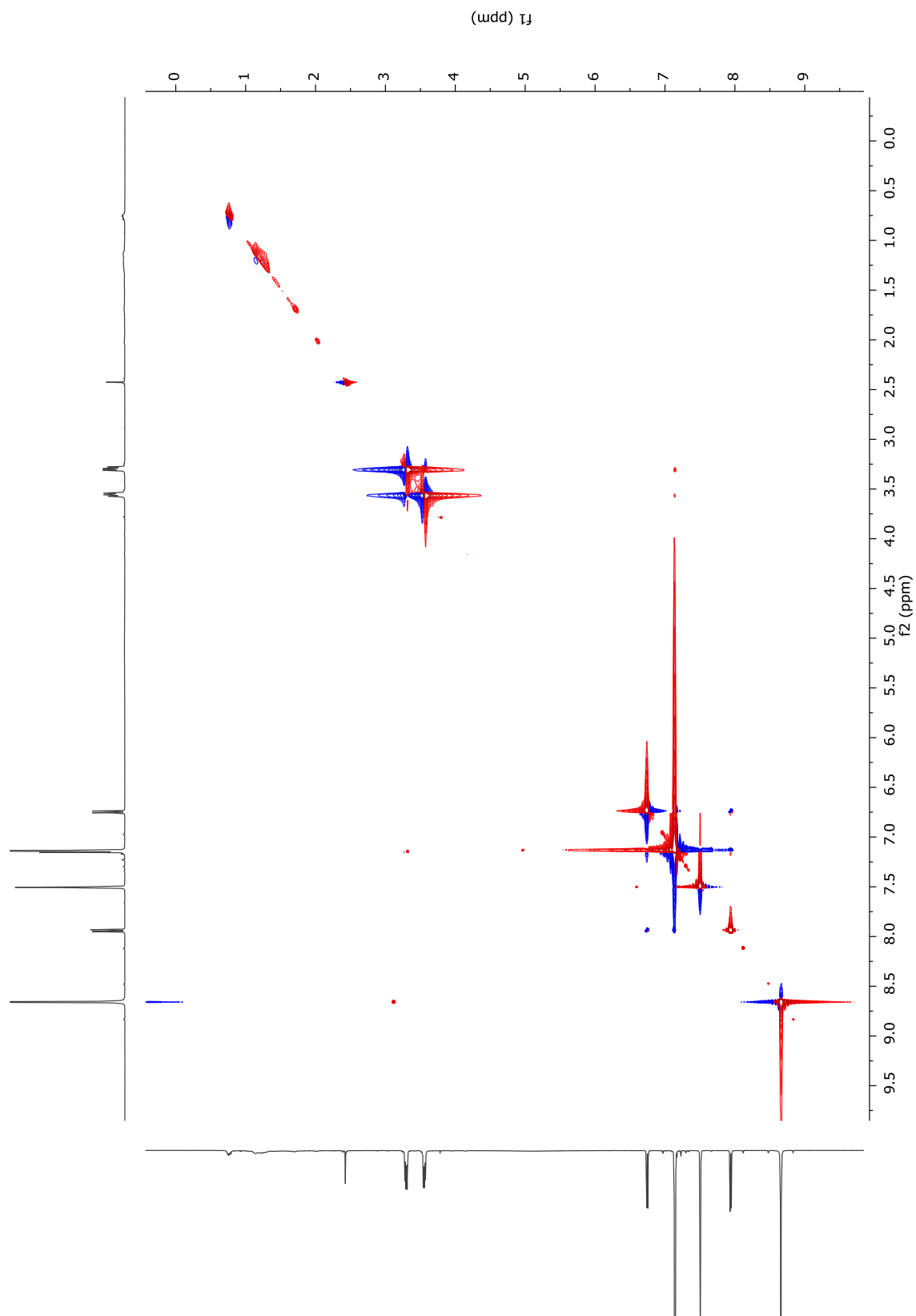


Figure S23. ROESY NMR spectrum of dihydrotetrachlorizine (**2**) in C₅D₅N (500 MHz).

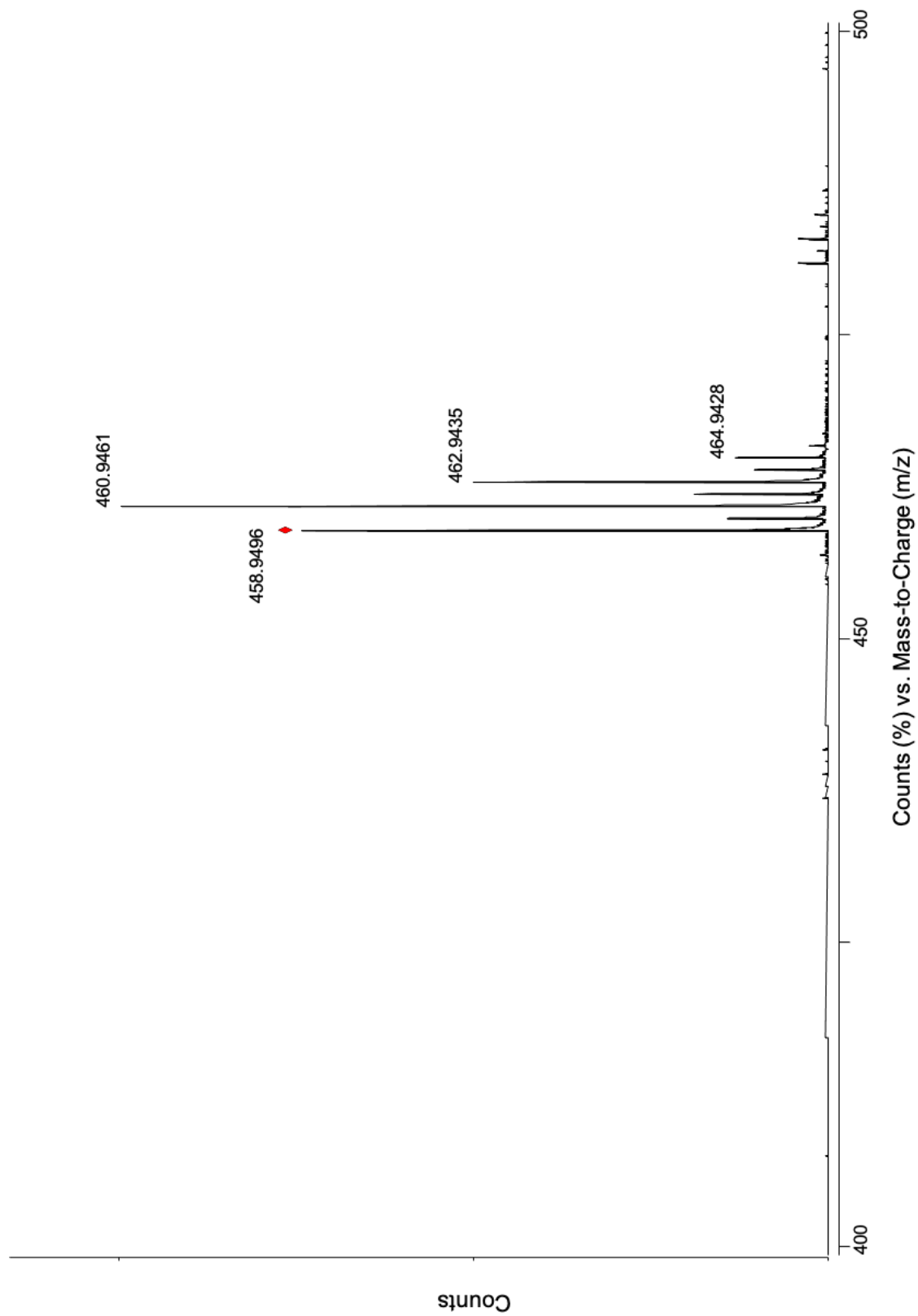


Figure S24. HR-ESI-TOF-MS spectrum of dihydrotetrachlorizine (**2**).

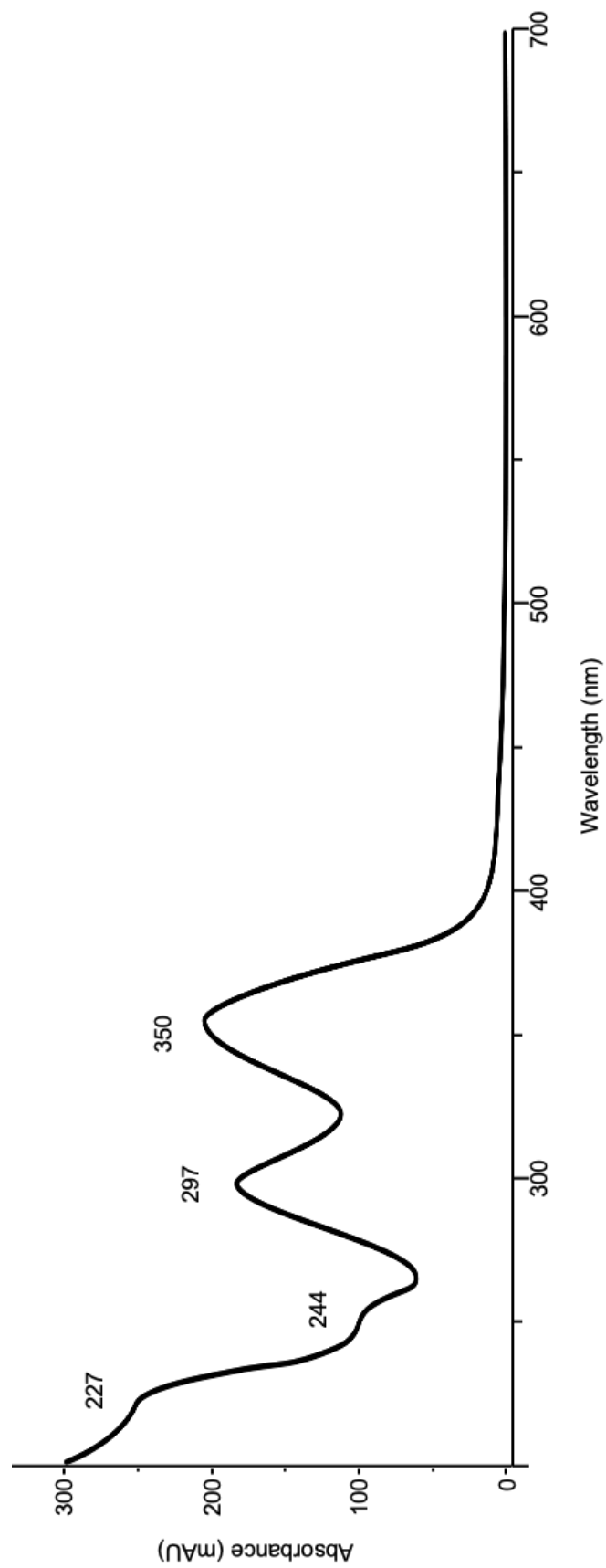


Figure S25. UV/vis spectrum of dihydrotetrachlorizine (**2**).

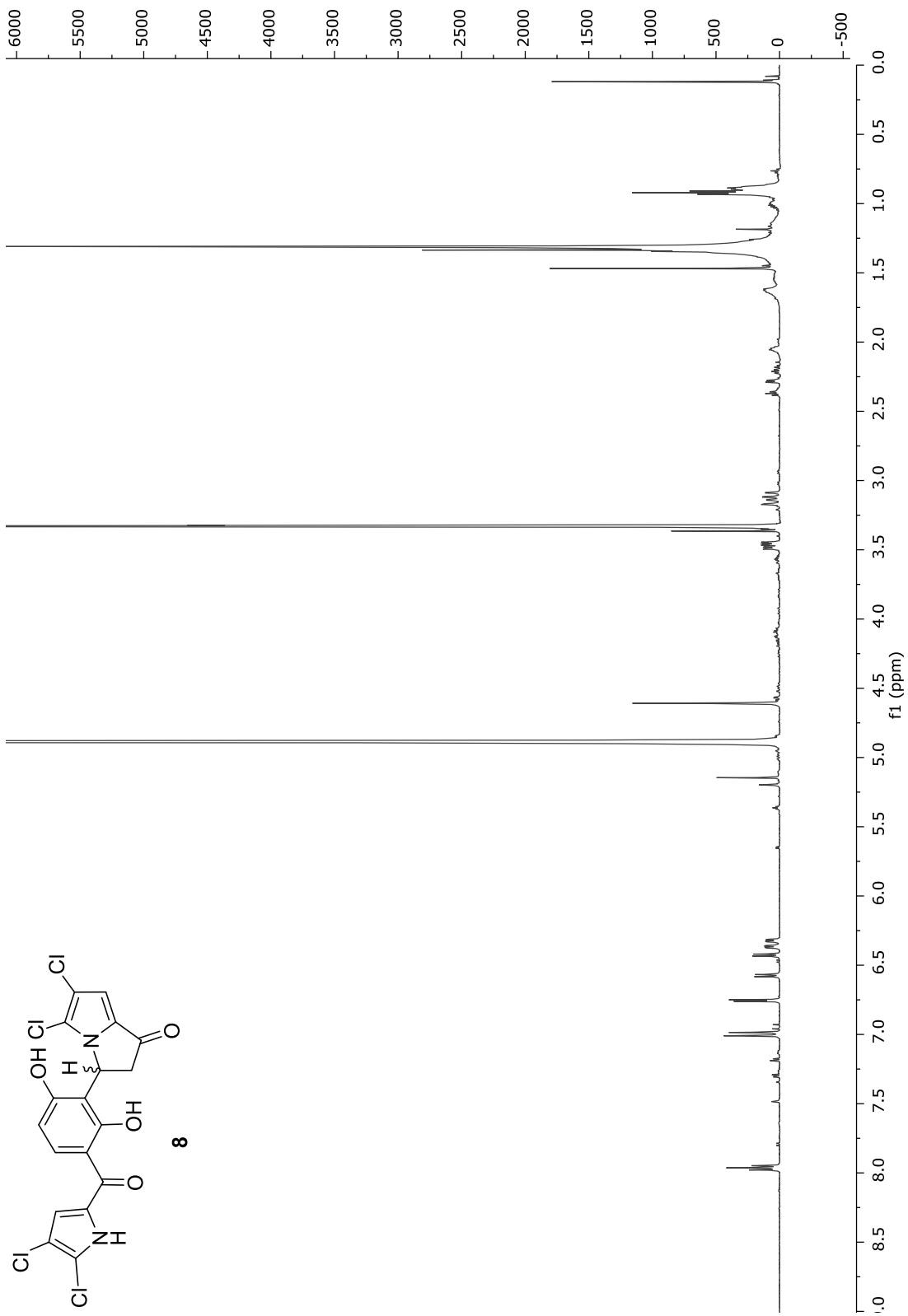


Figure S26. ^1H NMR spectrum of **8** in CD_3OD (500 MHz).

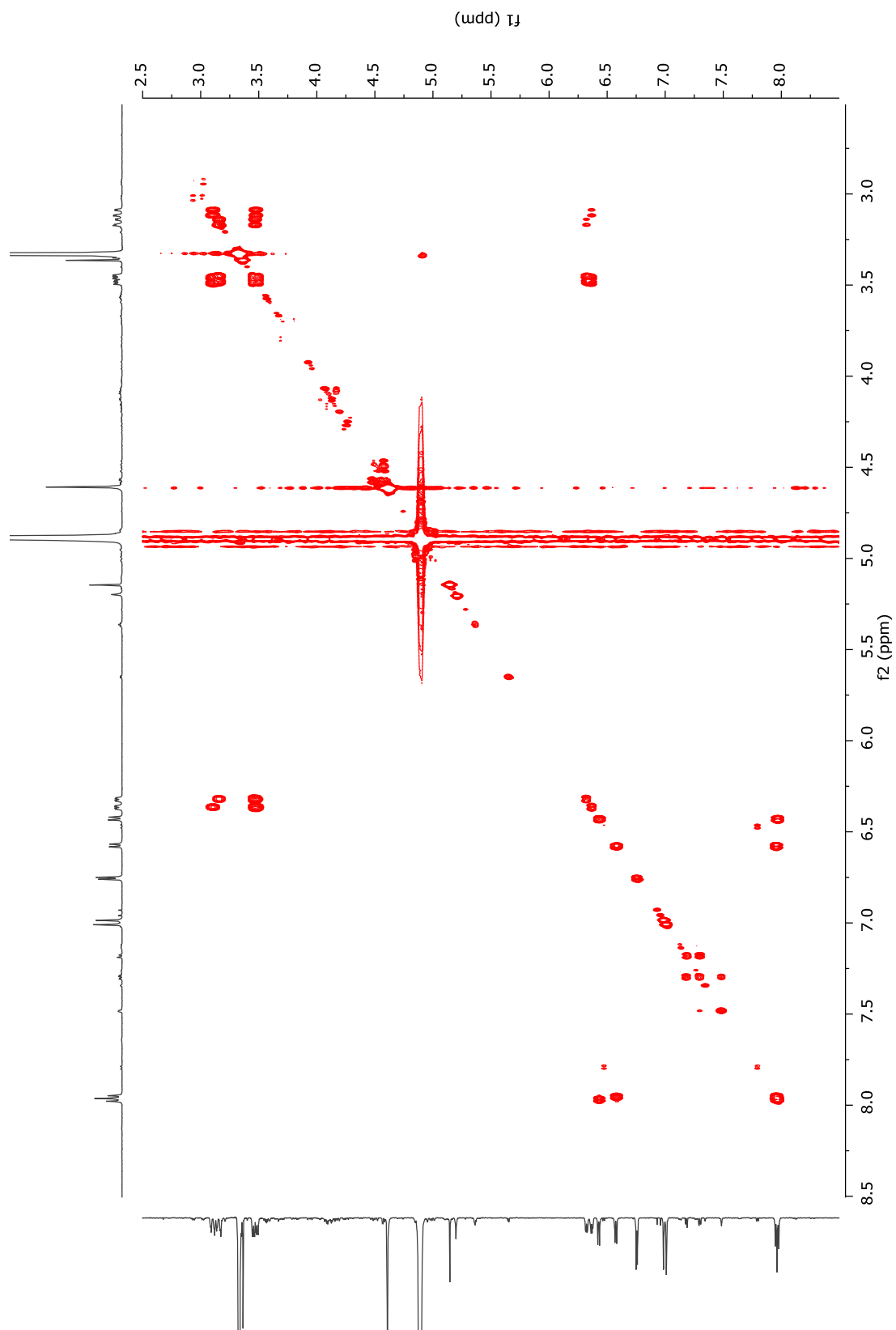


Figure S27. COSY NMR spectrum of **8** in CD₃OD (500 MHz).

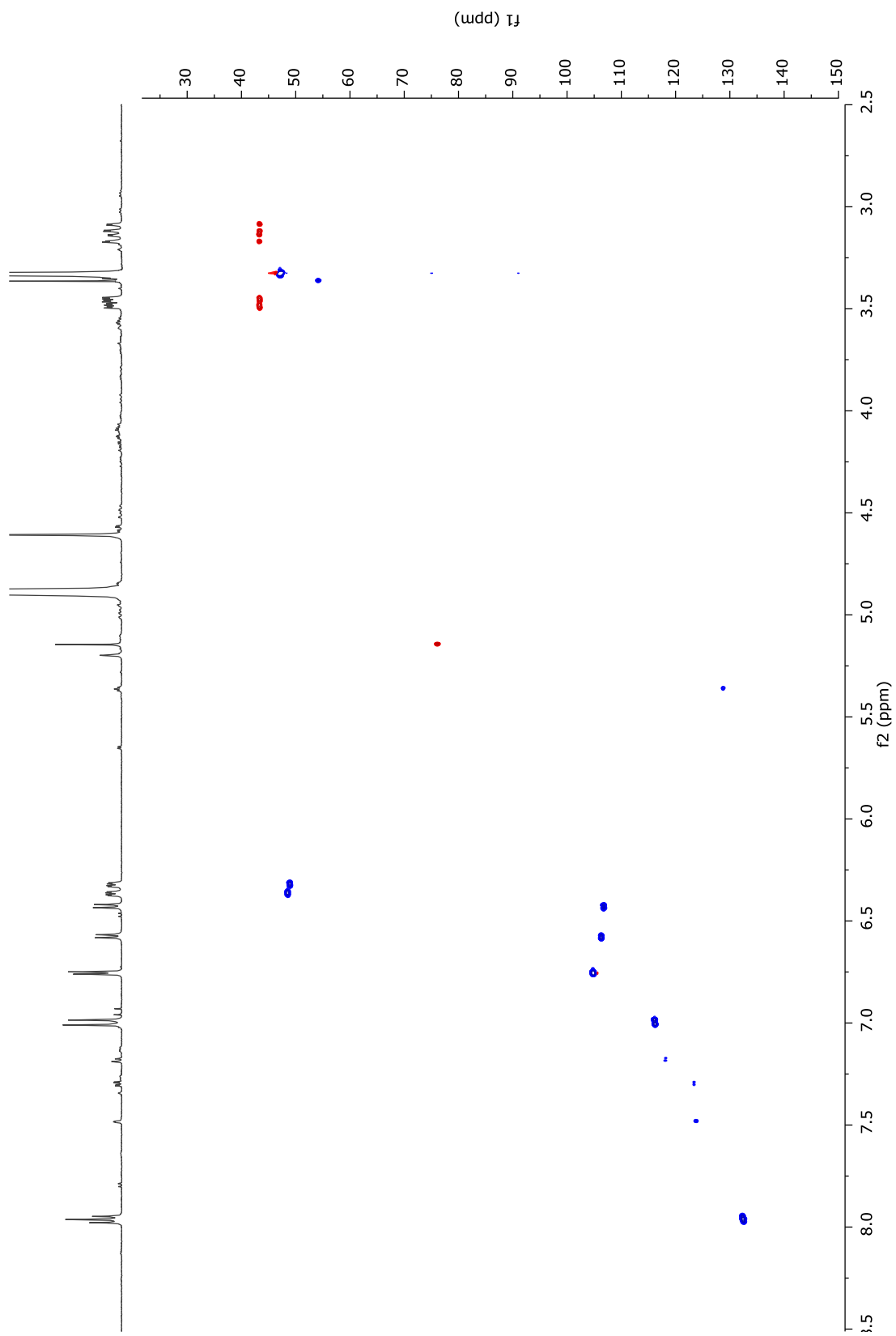


Figure S28. HSQC NMR spectrum of **8** in CD₃OD (500 MHz).

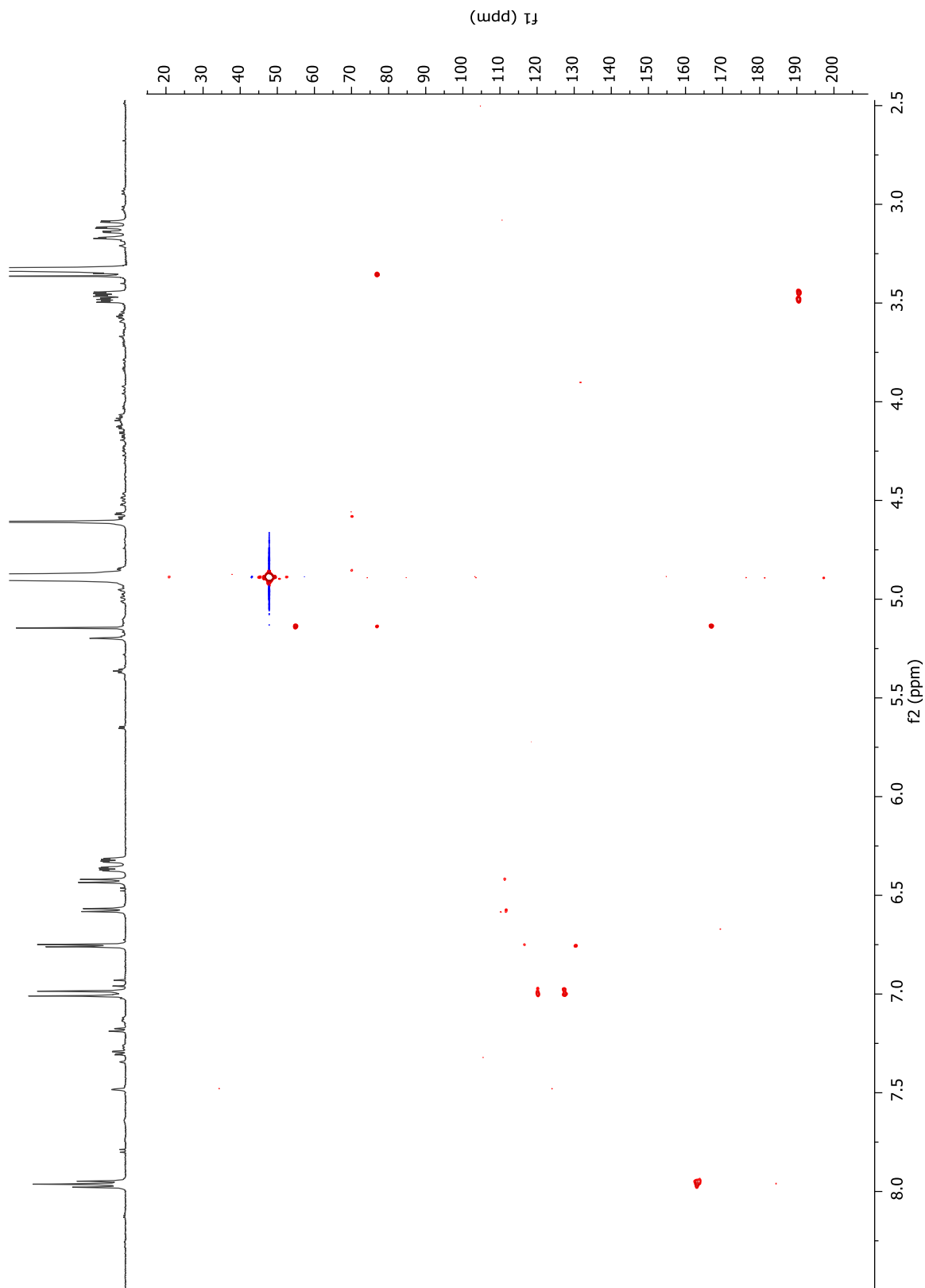


Figure S29. HMBC NMR spectrum of **8** in CD₃OD (500 MHz).

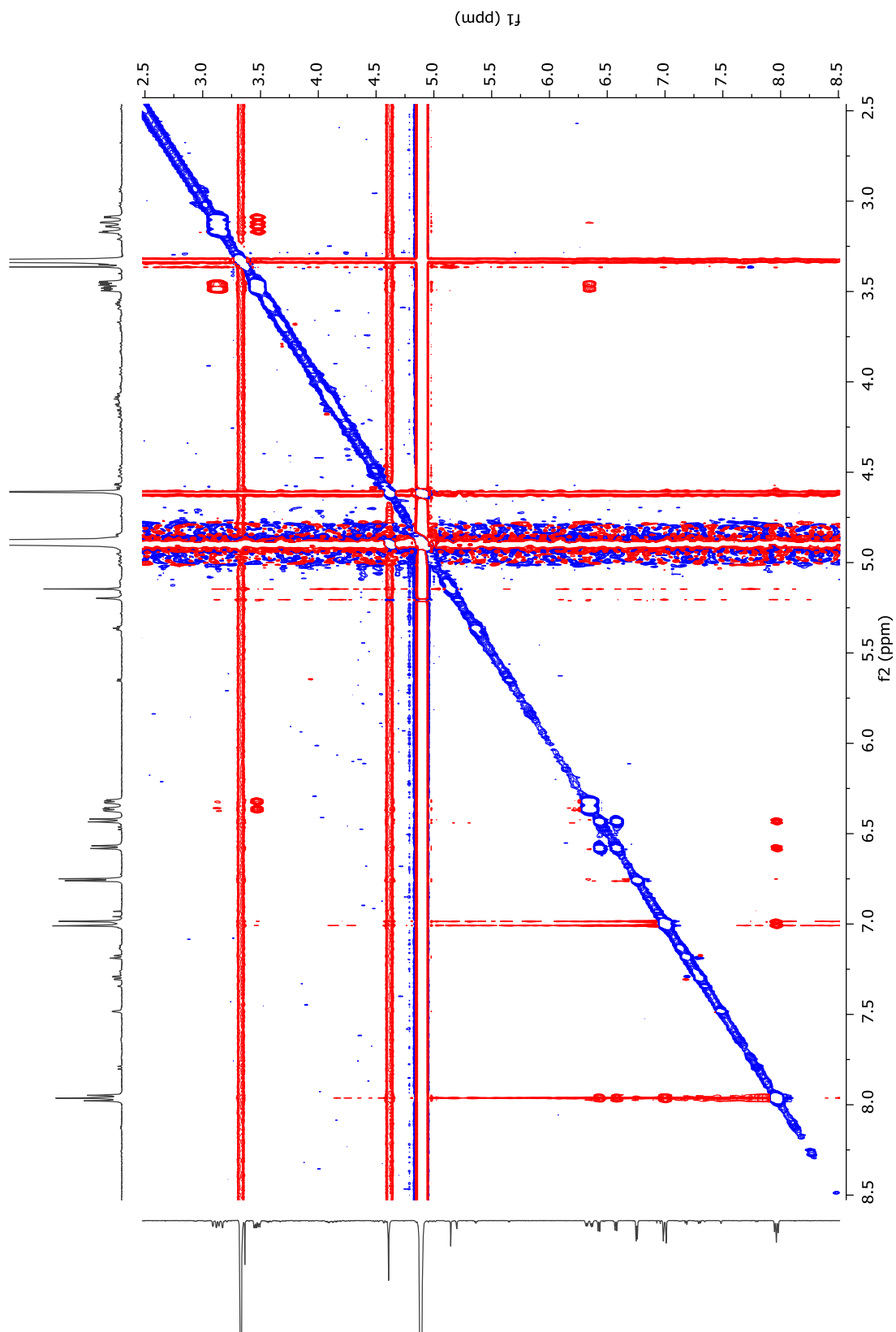


Figure S30. NOESY NMR spectrum of **8** in CD₃OD (500 MHz).

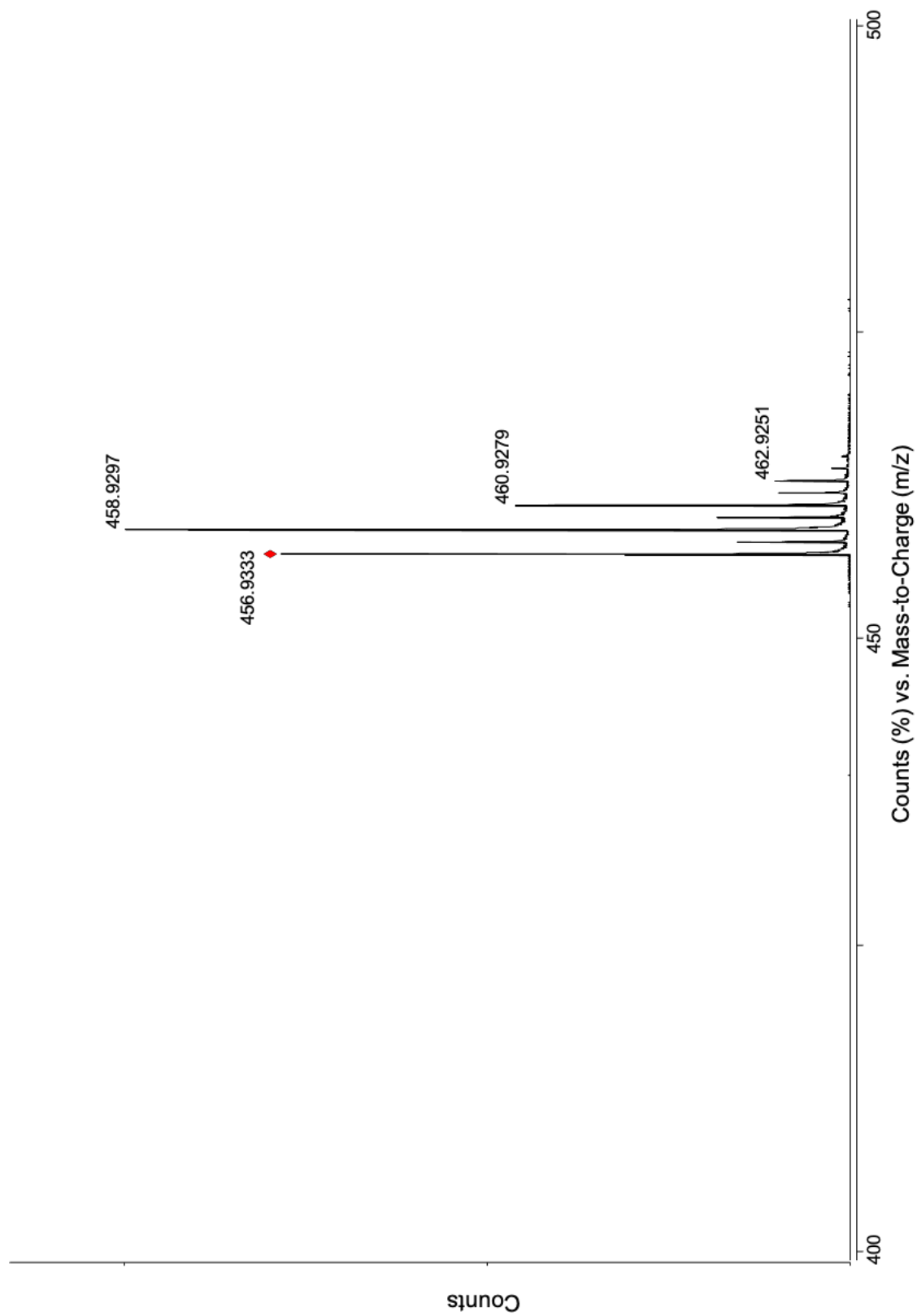


Figure S31. HR-ESI-TOF-MS spectrum of **8**.

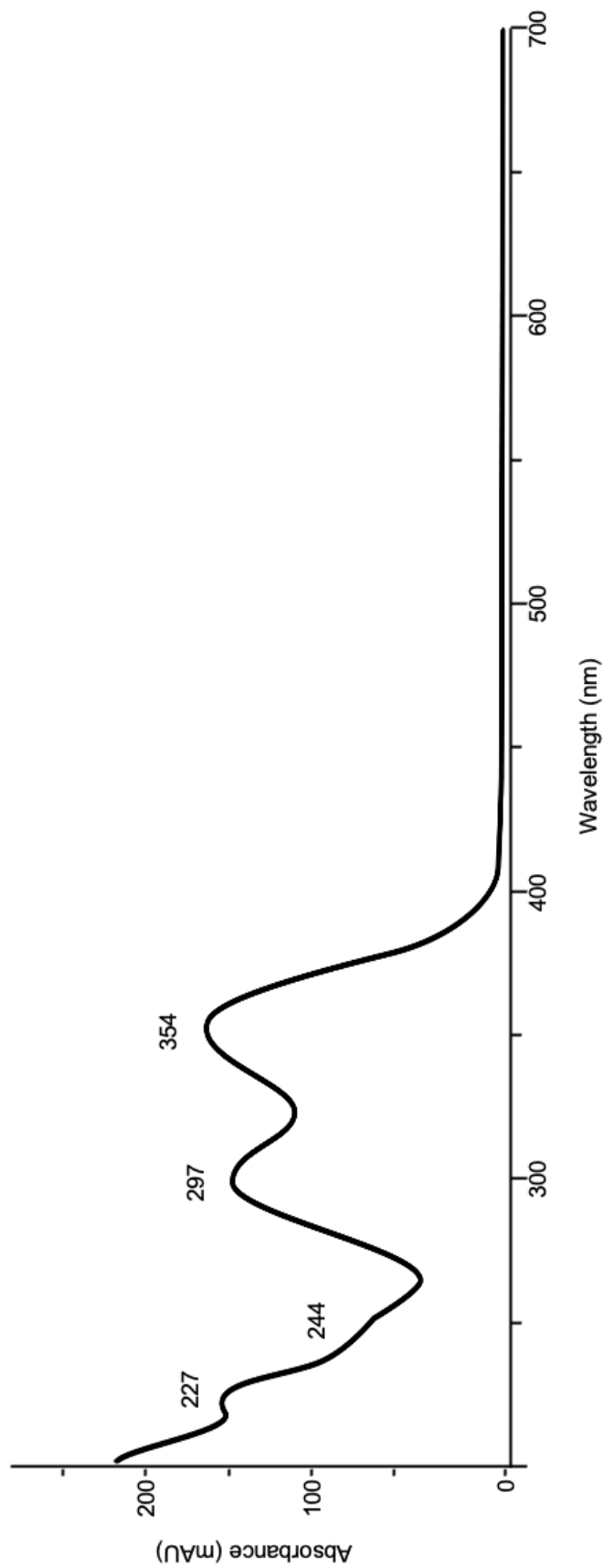


Figure S32. UV/vis spectrum of **8**.

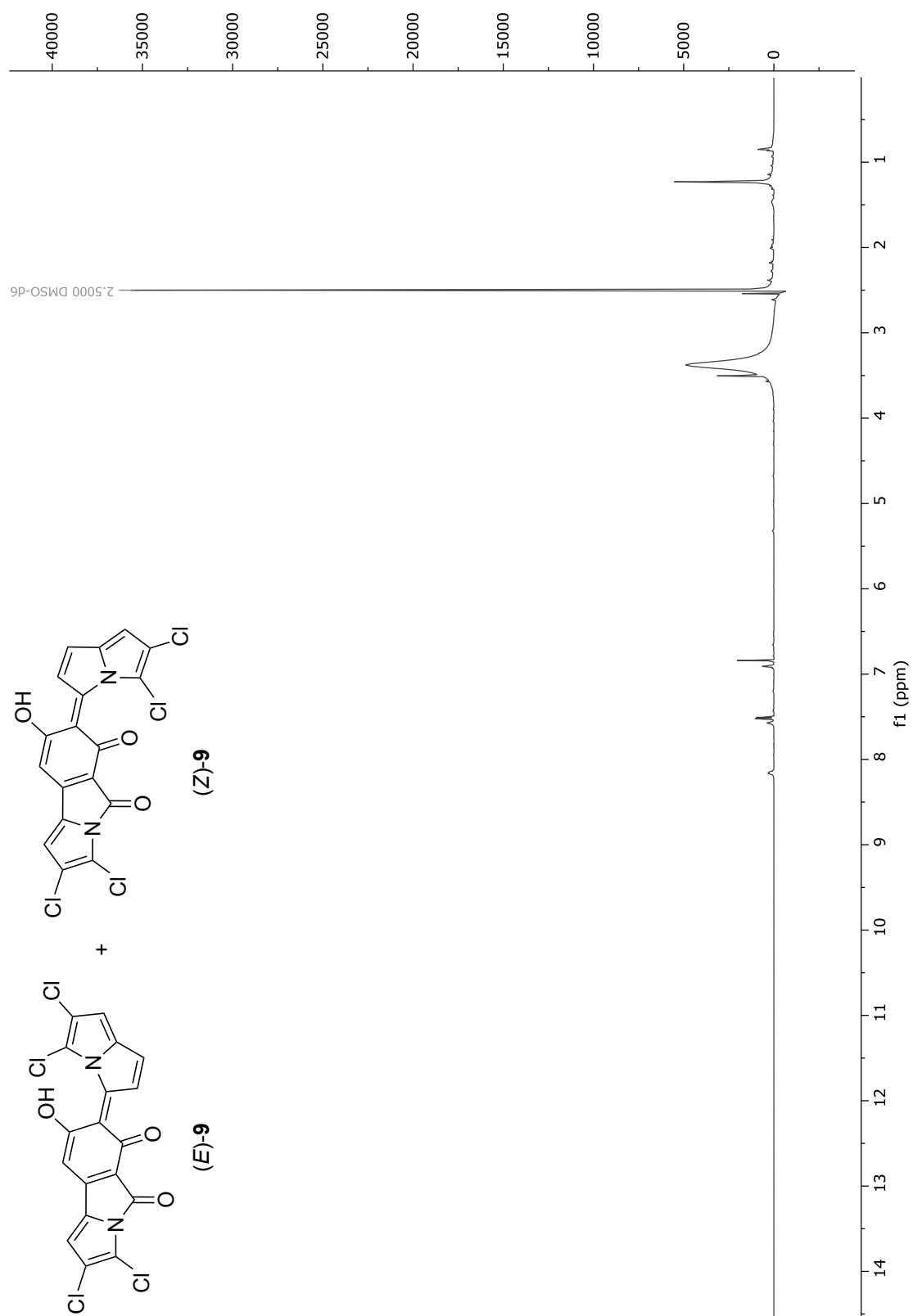


Figure S33. ¹H NMR spectrum of *(E/Z)*-9 after 5 minutes in (CD₃)₂SO (500 MHz).

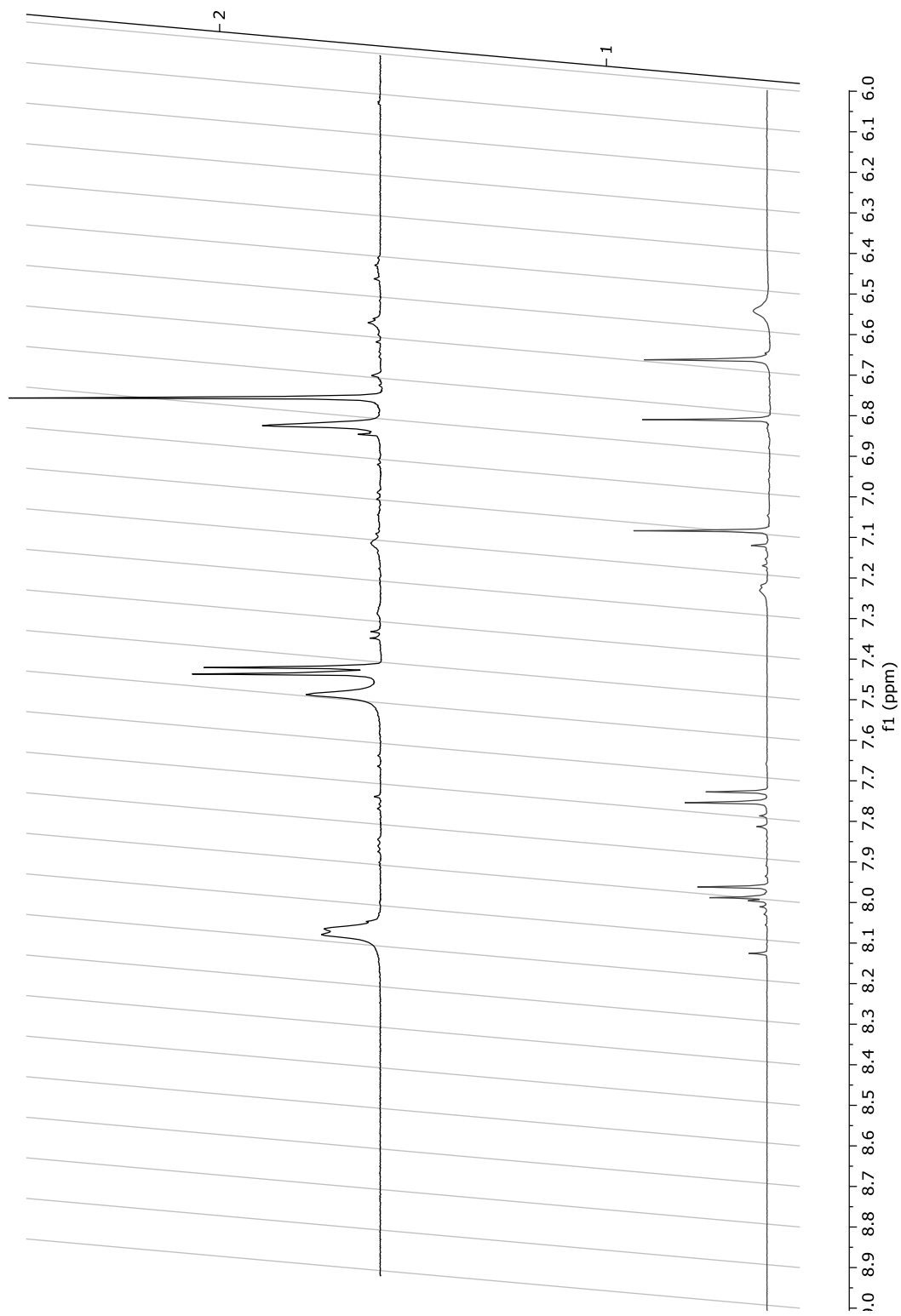


Figure S34. ¹H NMR time course comparison of (E/Z)-9 after 5 minutes (top) and 36 hours (bottom) in (CD₃)₂SO (500 MHz).

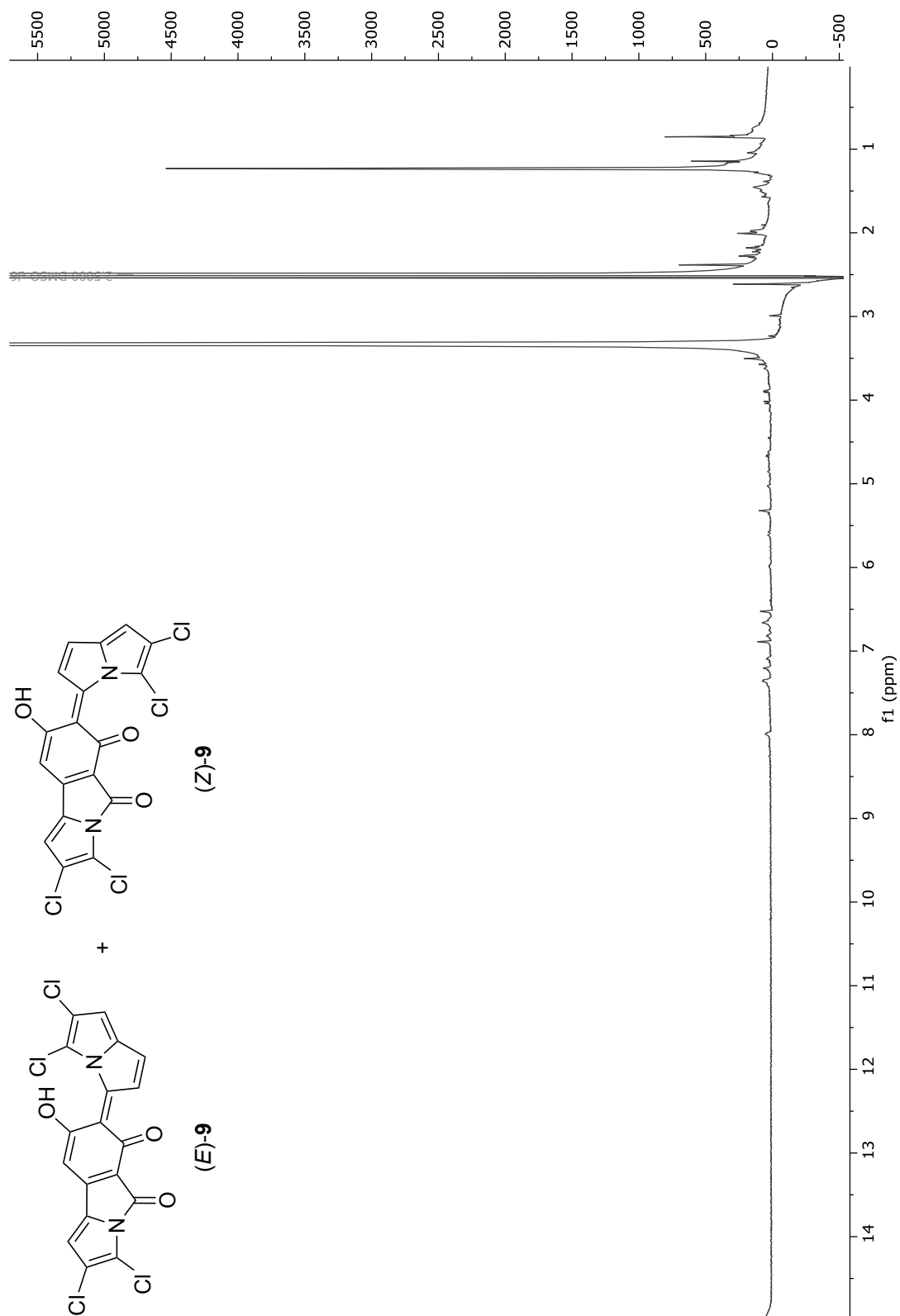


Figure S35. ¹H NMR spectrum of (E/Z)-9 after 5 minutes in (CD₃)₂SO (500 MHz).

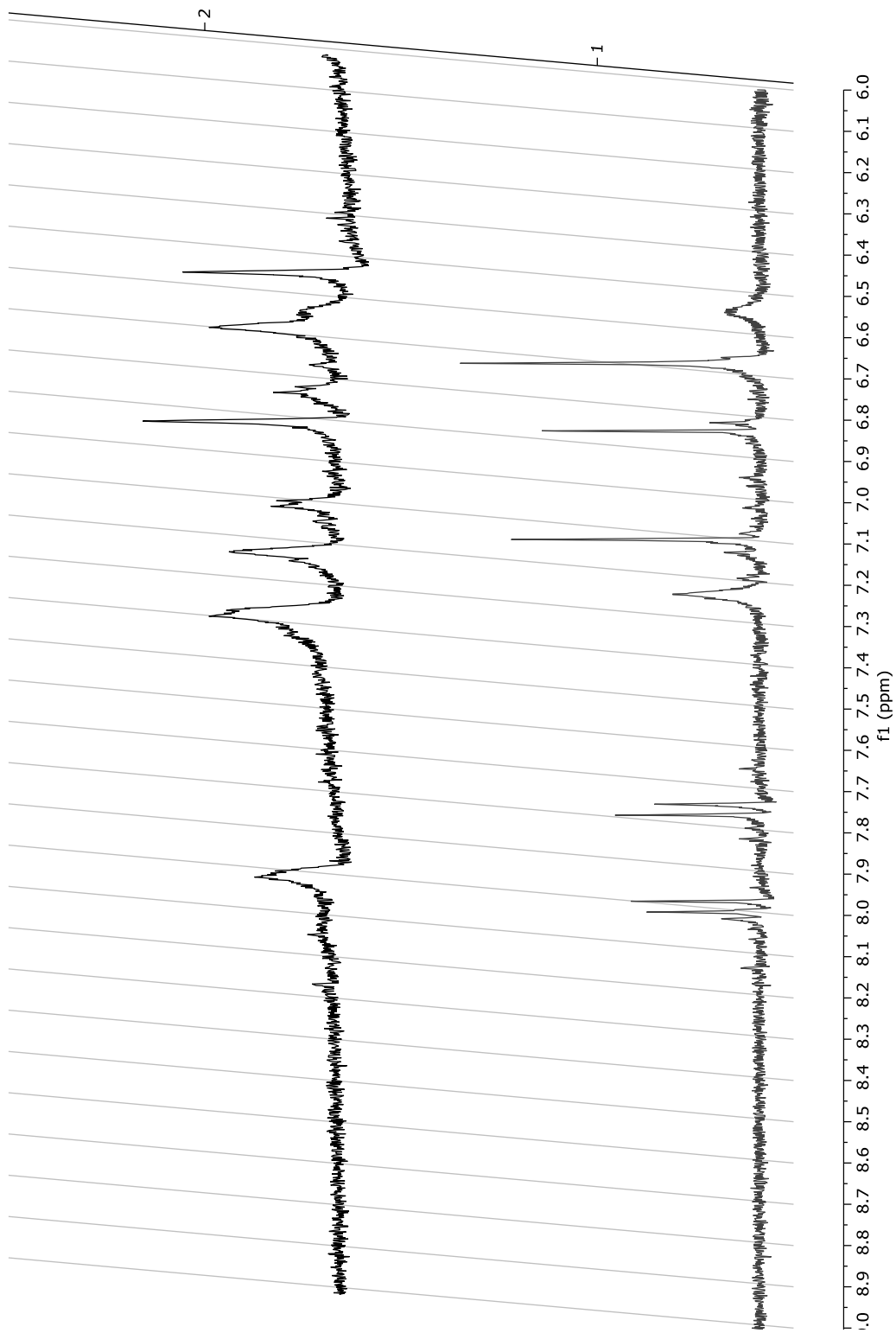


Figure S36. ¹H NMR time course comparison of (E/Z)-9 after 5 minutes and 36 hours in (CD₃)₂SO (500 MHz).

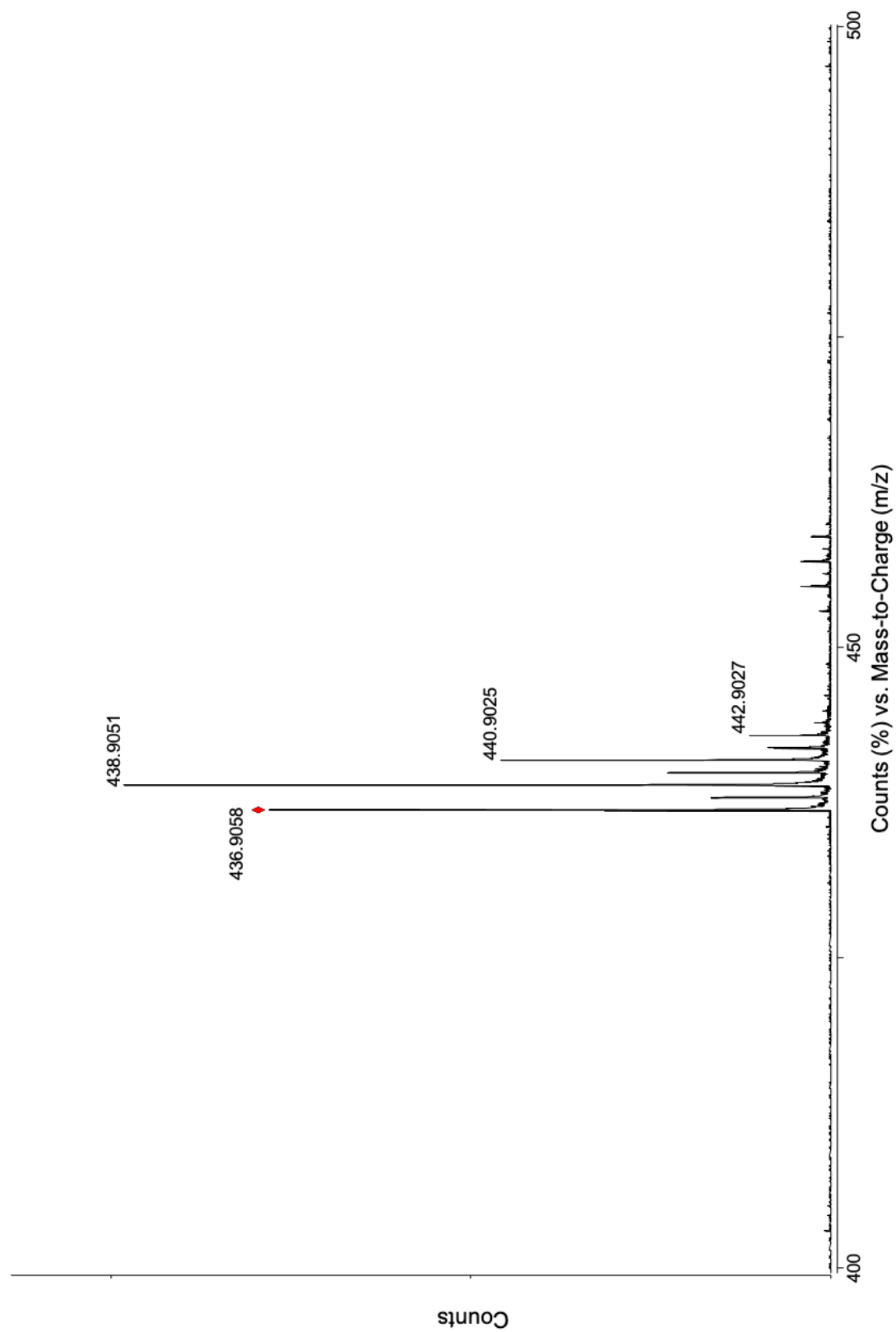


Figure S37. HR-ESI-TOF-MS spectrum of (E/Z)-9.

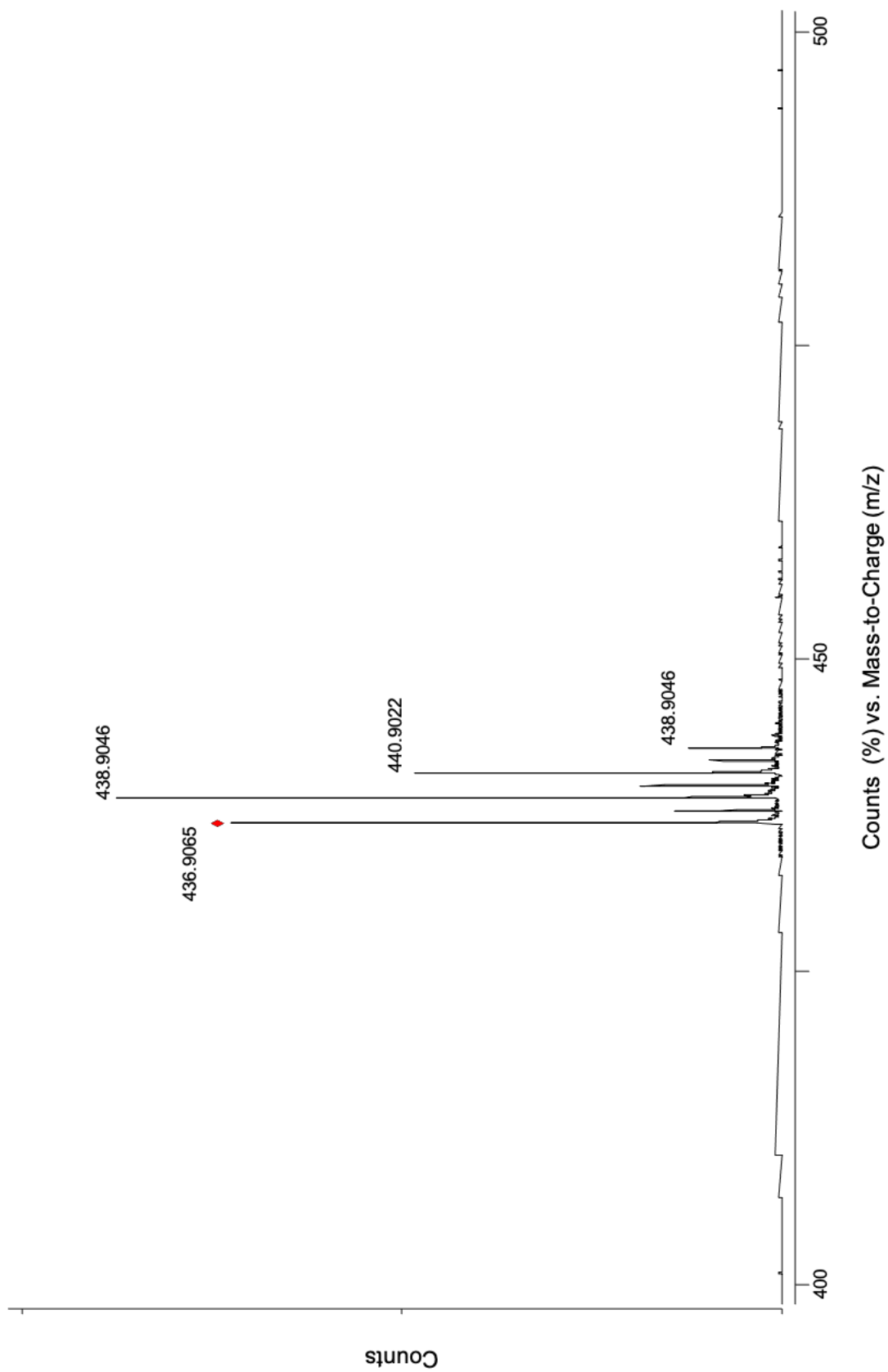


Figure S38. HR-ESI-TOF-MS spectrum of (E/Z)-9.

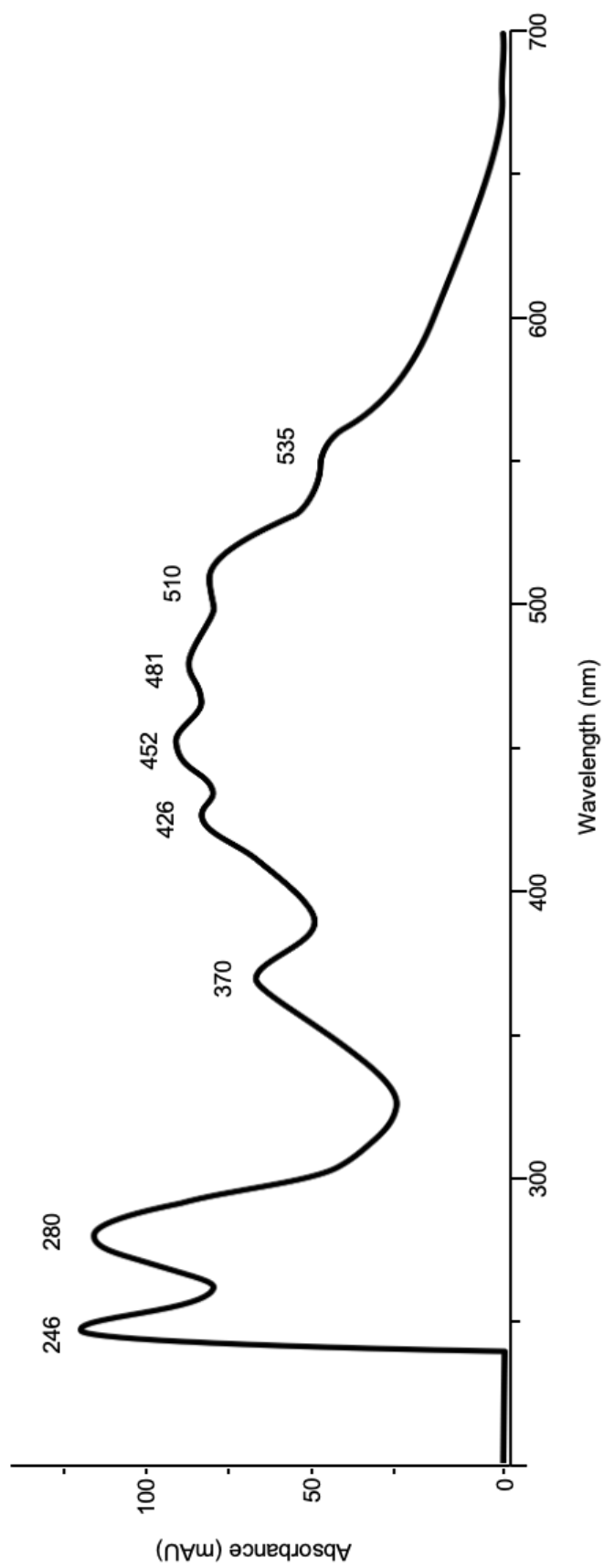


Figure S39. UV/vis spectrum of (E)- and (Z)-9.

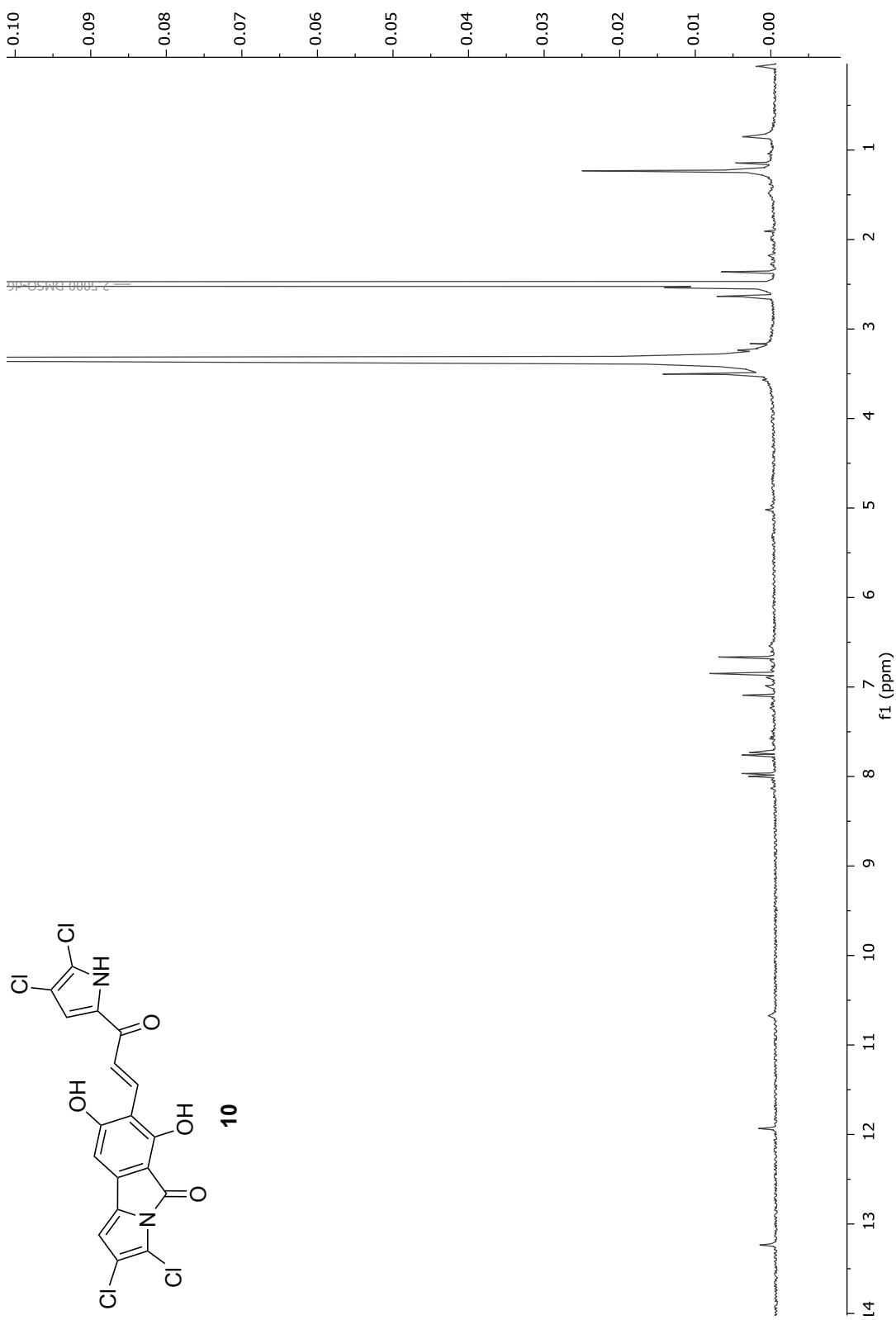


Figure S40. ¹H NMR spectrum of **10** in (CD₃)₂SO (500 MHz).

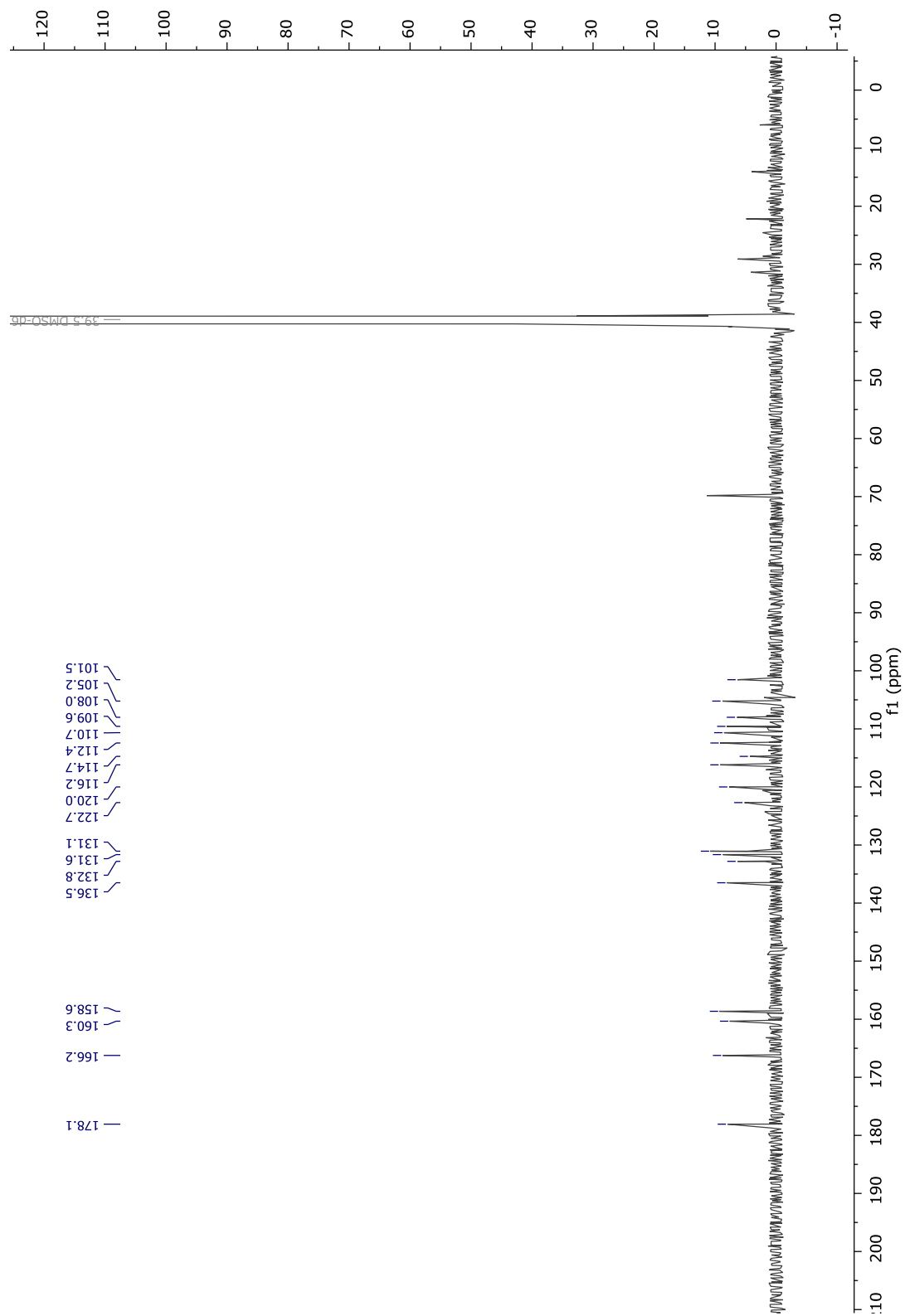


Figure S41. ^{13}C NMR spectrum of **10** in $(\text{CD}_3)_2\text{SO}$ (125 MHz).

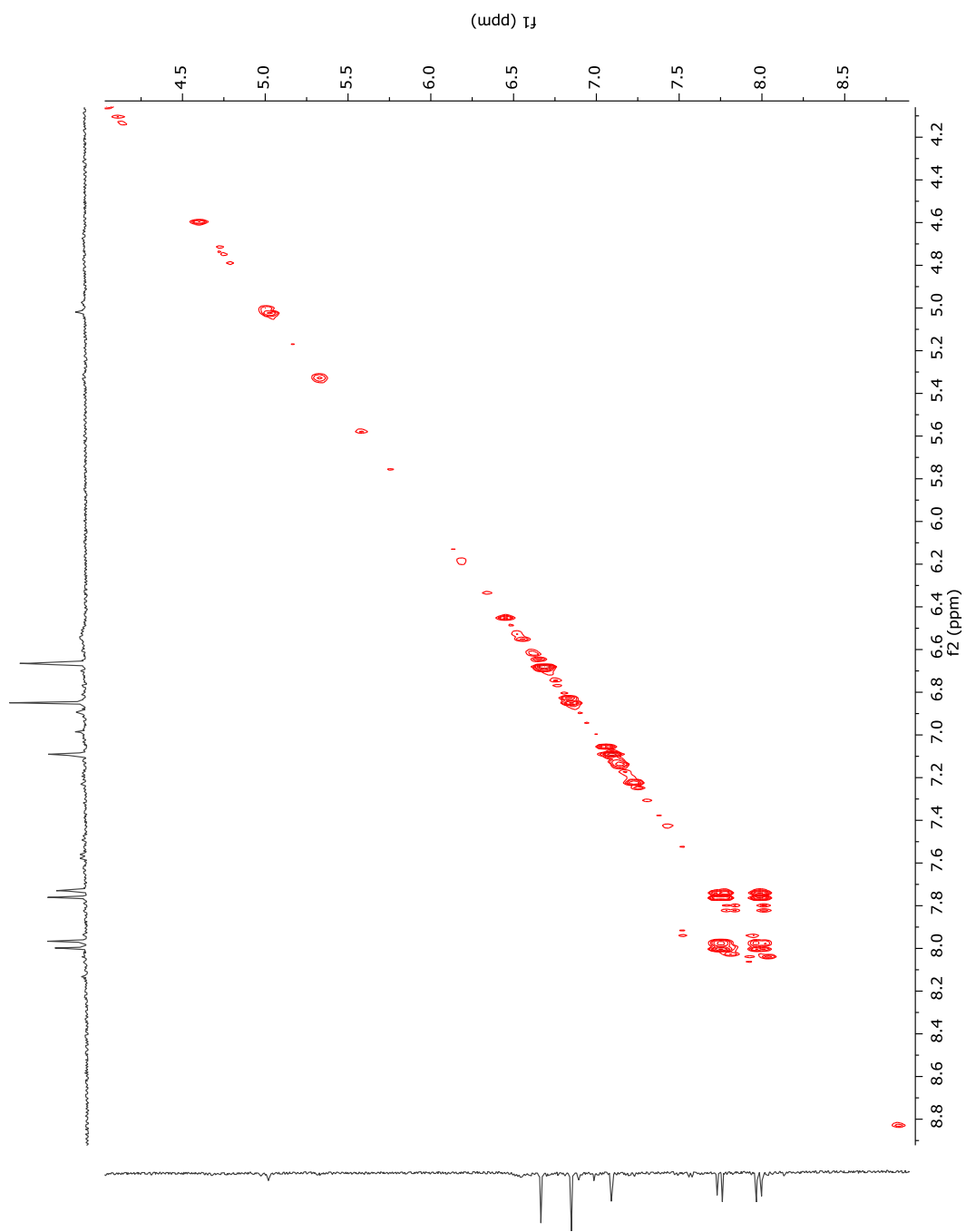


Figure S42. COSY NMR spectrum of **10** in (CD₃)₂SO (500 MHz).

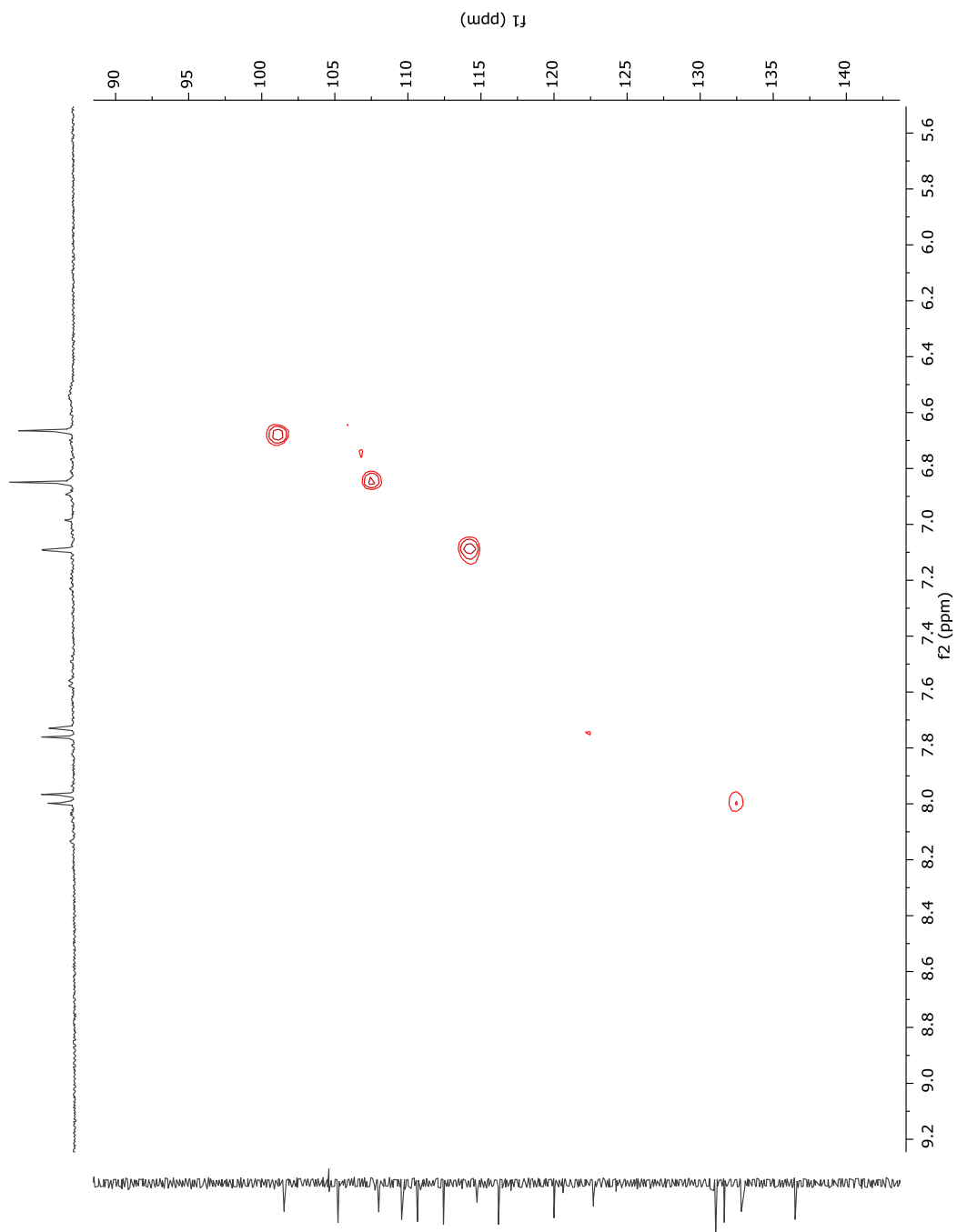


Figure S43. HSQC NMR spectrum of **10** in $(\text{CD}_3)_2\text{SO}$ (500 MHz).

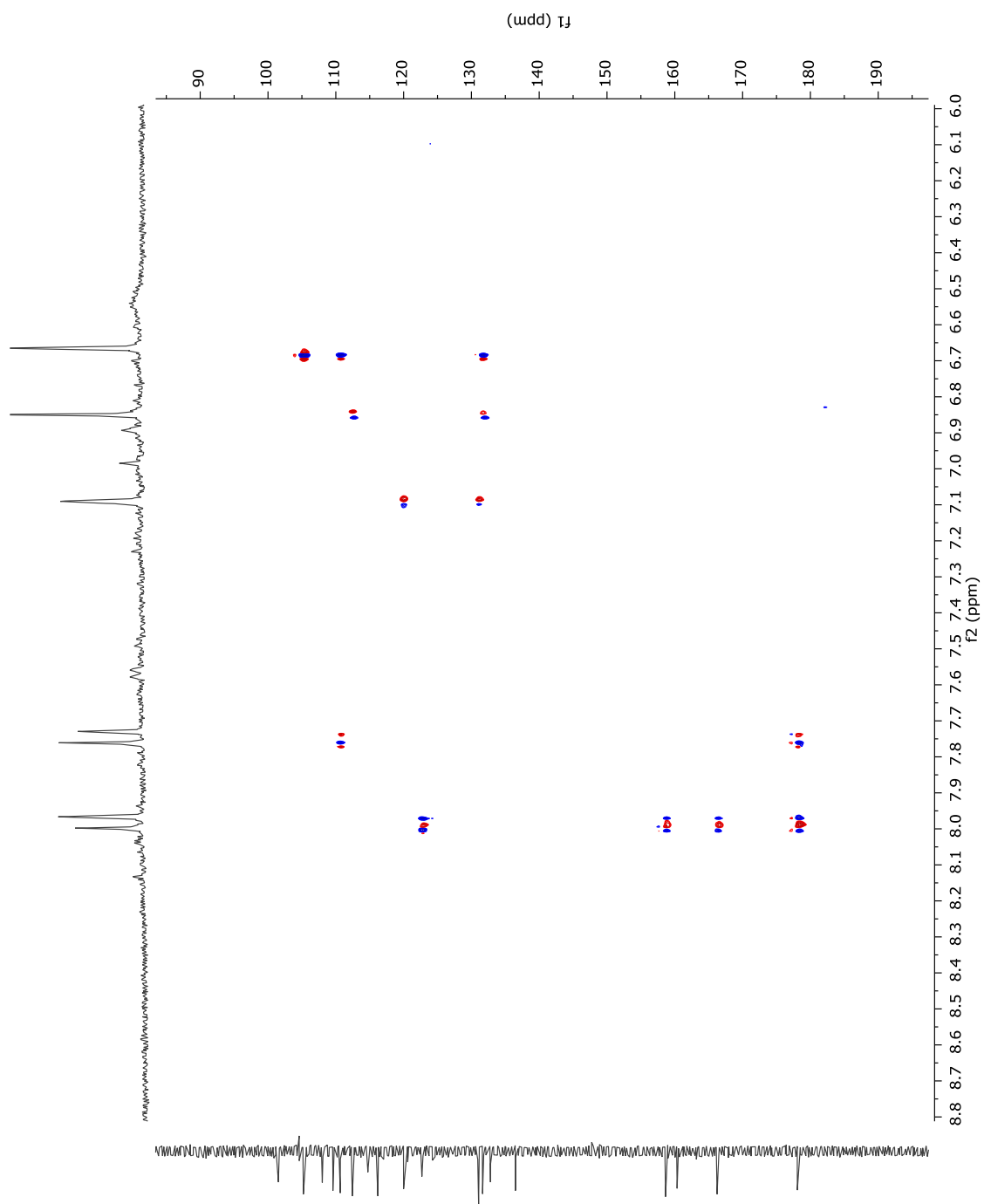


Figure S44. HMBC NMR spectrum of **10** in $(\text{CD}_3)_2\text{SO}$ (500 MHz).

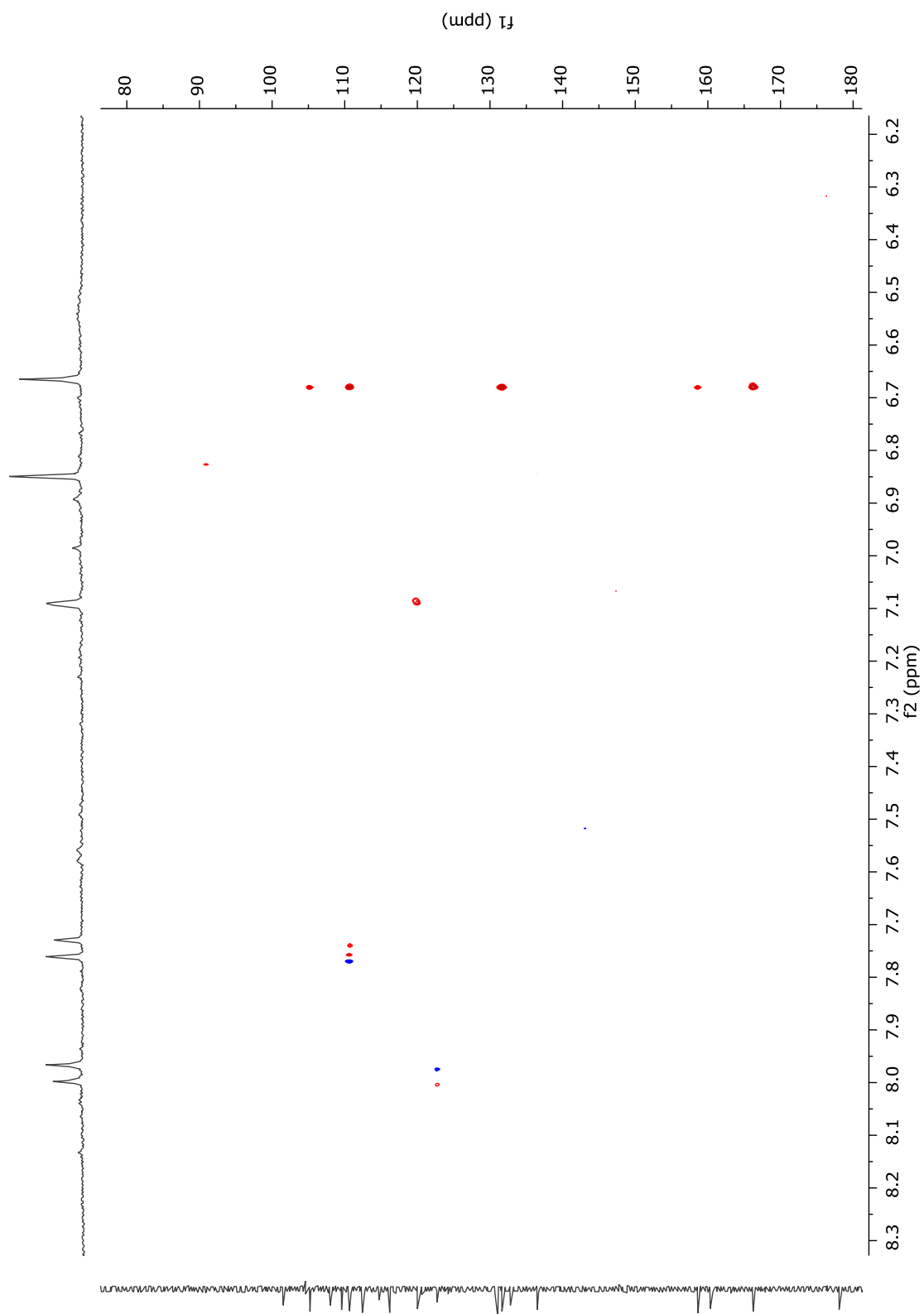


Figure S45. Long-range HMBC NMR spectrum of **10** in (CD₃)₂SO (500 MHz).

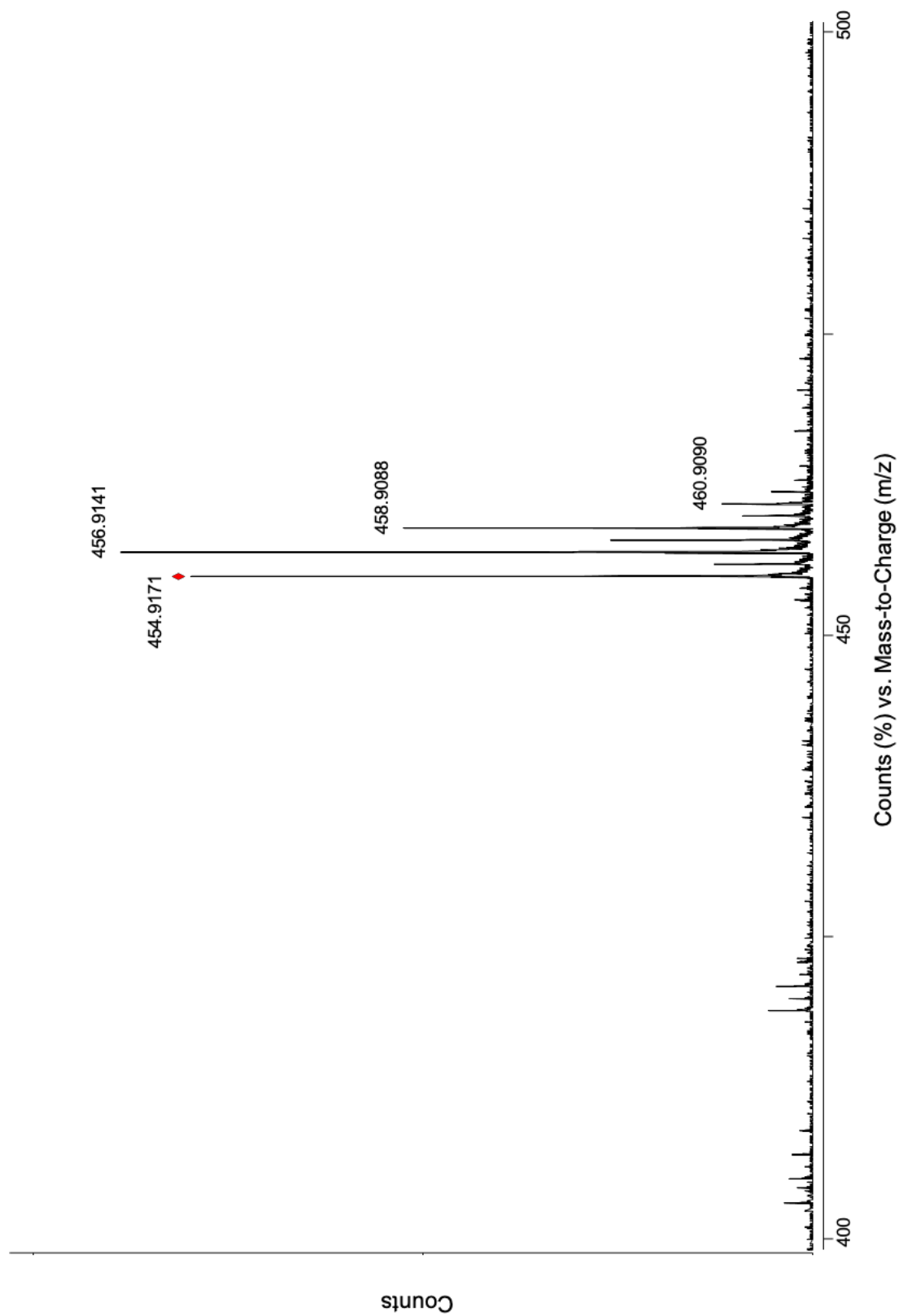


Figure S46. HR-ESI-TOF-MS spectrum of **10**.

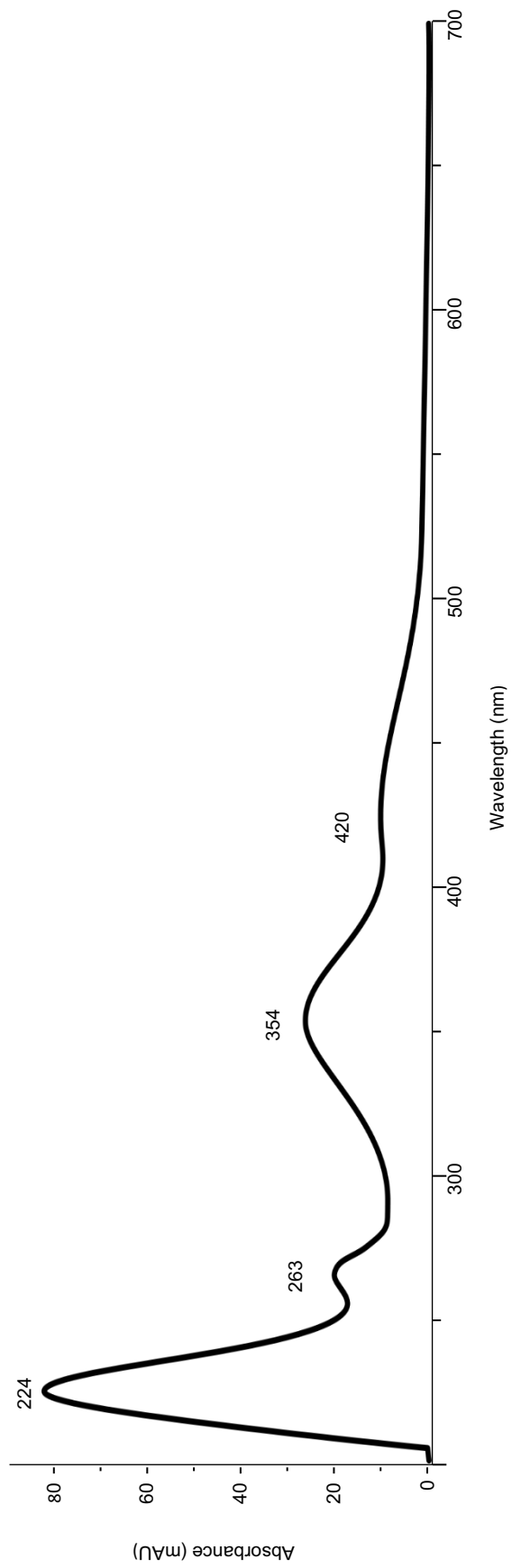


Figure S47. UV/vis spectrum of **10**.

1. Supplementary References

1. Kim, M. C.; Cullum, R.; Machado, H.; Smith, A. J.; Yang, I.; Rodvold, J. J.; Fenical, W. J. *Nat. Prod.* **2019**, *82*, 2262–2267.
2. Mantovani, S. M.; Moore, B. S. *J. Am. Chem. Soc.* **2013**, *135*, 18032–18035.
3. Kieser, T.; Bibb, M. J.; Buttner, M. J.; Chater, K. F.; Hopwood, D. A. *Practical Streptomyces genetics*; The John Innes Foundation: Norwich, 2000.
4. Green, M. R.; Sambrook, J. *Cold Spring Harb. Protoc.* **2017**, *2017* (8), 673–674.
5. Flitsch, W.; Jones, G. *Adv. Heterocycl. Chem.* **1984**, *37*, 1–66.
6. Zallot, R.; Oberg, N.; Gerlt, J. A. *Biochemistry* **2019**, *58* (41), 4169–4182.
7. Shannon, P.; Markiel, A.; Ozier, O.; Baliga, N. S.; Wang, J. T.; Ramage, D.; Amin, N.; Schwikowski, B.; Ideker, T. *Genome Res.* **2003**, *13* (11), 2498–2504.
8. Goujon, M.; McWilliam, H.; Li, W.; Valentin, F.; Squizzato, S.; Paern, J.; Lopez, R. *Nucleic Acids Res.* **2010**, *38* (SUPPL. 2), W695–W699.
9. Navarro-Muñoz, J. C.; Selem-Mojica, N.; Mullowney, M. W.; Kautsar, S. A.; Tryon, J. H.; Parkinson, E. I.; De, E. L. C.; Santos, L.; Yeong, M.; Cruz-Morales, P.; Abubucker, S.; Roeters, A.; Lokhorst, W.; Fernandez-Guerra, A.; Dias Cappelini, L. T.; Goering, A. W.; Thomson, R. J.; Metcalf, W. W.; Kelleher, N. L.; Barona-Gomez, F.; Medema, M. H. *Nat. Chem. Biol.* **2020**, *16*, 60–68.

Chapter 4

Exploring the Structure-Function Relationship of Clz9 and Tcz9 for Benzylic(sp³) C–H Functionalization Applications

Trevor N. Purdy, Bradley S. Moore

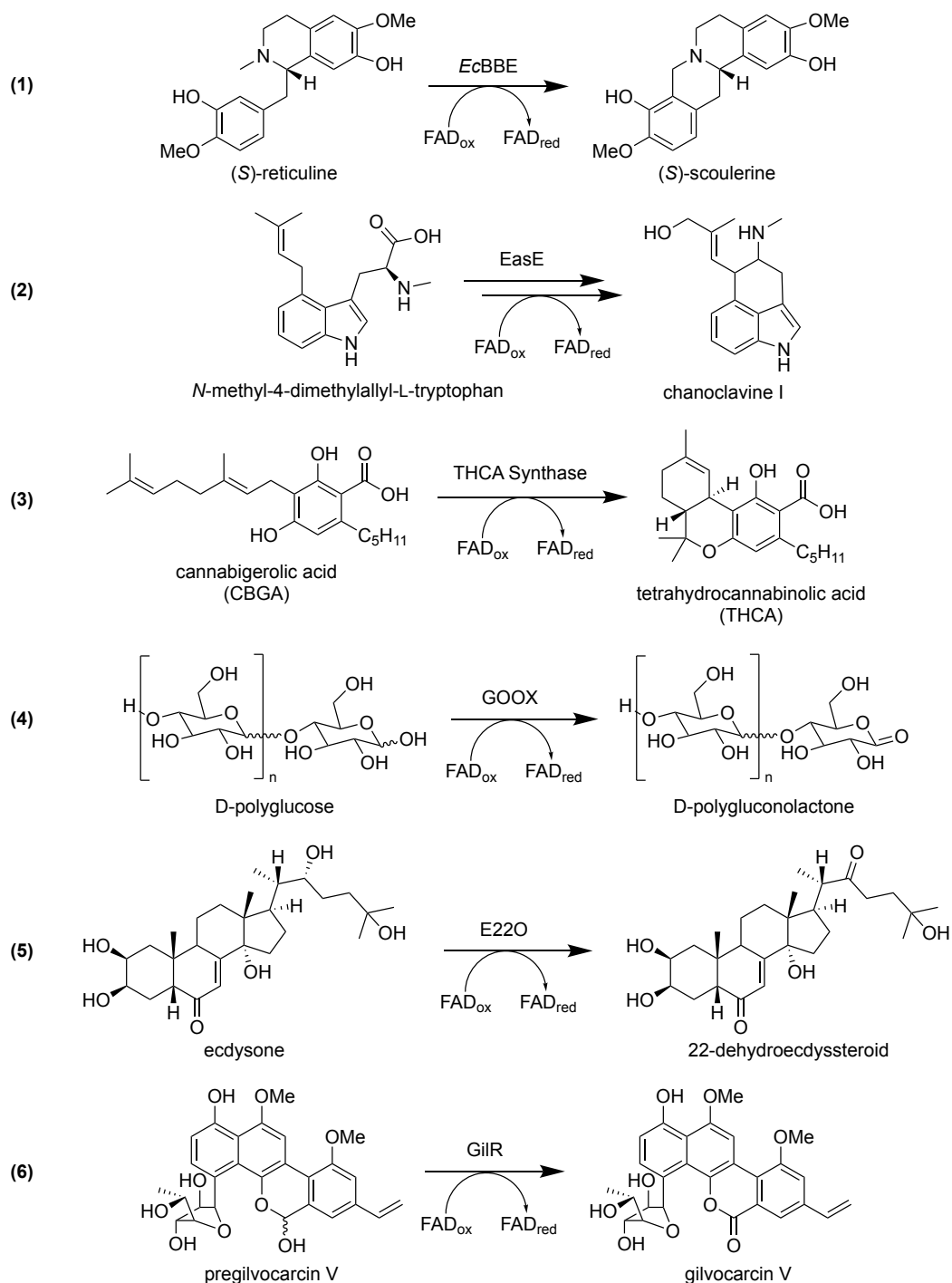
Abstract: The selective functionalization of benzylic(sp³) C–H bonds remains a formidable task in natural product total synthesis. However, certain enzymes have evolved the ability to perform these reactions under mild reaction conditions. We recently reported the function of a novel berberine bridge enzyme-like (BBE-like) oxidase, Tcz9, that catalyzed a benzylic functionalization reaction via a highly reactive *ortho*-quinone methide intermediate. We have since identified a key active site residue that differentiates Tcz9 from Clz9, a homolog with preferential cyclase activity. We have also expanded the substrate scope of Tcz9 and Clz9 to perform benzylic hydroxylation and cycloaddition reactions, including *in vitro* and *in vivo* cannabinoid production. Given their favorable biocatalytic properties, Tcz9 and Clz9 highlight new opportunities for engineering related BBE-like enzymes to perform challenging chemo-, regio-, and stereoselective benzylic functionalization reactions.

1. Introduction

Total synthesis has been routinely employed over the past two decades to supply pharmaceutical drugs, fine chemicals, and agrochemicals on an industrial scale.¹ However, most of these industrial processes require toxic reagents, harsh reaction conditions, and routinely struggle to match the selectivity and atom efficiency already designed by Nature. Breakthroughs in next generation sequencing, synthetic biology, and bioinformatics have accelerated the process to identify enzymes that can be developed as biocatalytic tools to augment total synthetic routes.^{2–5} Furthermore, rational design and directed evolution strategies have expanded the breadth of reactions enzymes can perform, enabling efficient one-pot cascade processes for manufacturing complex designer molecules and improving the accessibility of non-natural chemicals once considered to be biologically intractable.^{6–10} We are now entering the golden age of biocatalysis.

Enzymes belonging to the berberine bridge enzyme (BBE)-like oxidase subfamily are known to catalyze a variety of tailoring redox reactions in carbohydrate, steroid, meroterpenoid, polyketide, and alkaloid biosynthesis.^{11–16} These reactions not only limited to dehydrogenation reactions, but also include challenging carbon-carbon bond forming reactions, such as the namesake berberine bridge forming reaction in berberine-type alkaloids (Scheme 4.1). BBE-like oxidases share the distinct attribute of bicovalent attachment to flavin adenine dinucleotide (FAD) at the 6- and 8 α -positions of the isoalloxazine ring by conserved cysteine and histidine residues, respectively. This feature increases the redox potential of the FAD cofactor, enabling BBE-like oxidases to perform reactions not accessible by other FAD-dependent enzymes. Furthermore, structure-

function relationship studies have demonstrated that the bivalent attachment of FAD is essential for enzymatic activity.^{17,18}

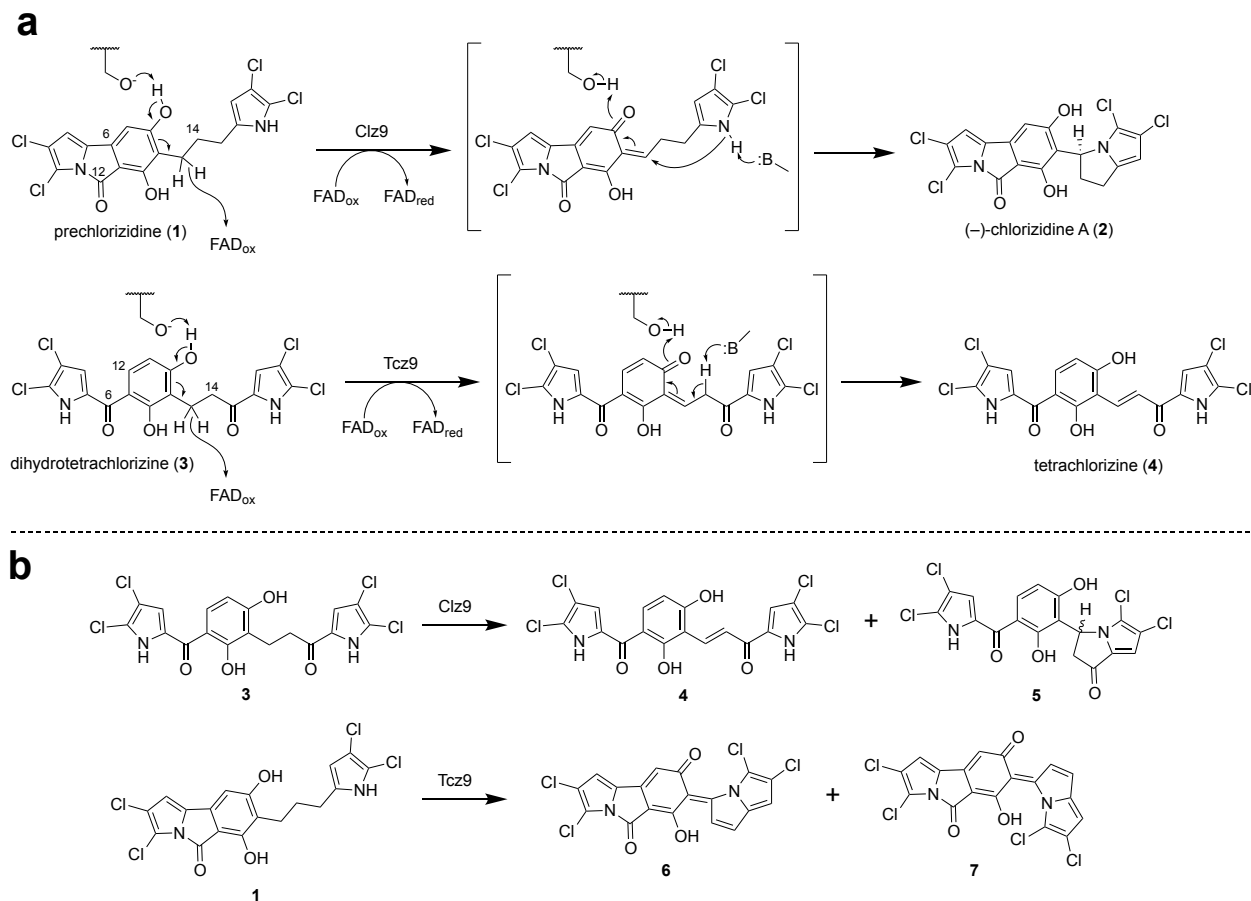


Scheme 4.1. Representative examples of characterized FAD-dependent BBE-like enzymes catalyzing C–C bond forming reactions (1-3) and dehydrogenation reactions (4-6) in natural product biosynthesis.

Carbon(sp³)-hydrogen (C–H) bond functionalization is one of the most valuable reactions to install new functionality into the framework of complex natural product scaffolds.^{19–21} However, synthetic approaches have faced challenges in overcoming the high bond dissociation energy of C–H bonds (~100 kcal·mol⁻¹), poor regioselective and stereoselective control, and potential over-oxidation. Benzylic C–H functionalization reactions are slightly more accessible due to their lower bond dissociation energy (~90 kcal·mol⁻¹) and have attracted both synthetic and biocatalytic interest.^{22–27} One benzylic C–H functionalization strategy leverages the reactivity of dearomatized *ortho*-quinone methide (*o*-QM) intermediates to regioselectively form new benzylic carbon-carbon or carbon-heteroatom bonds.²⁸ While their existence was questioned until direct observations were made in the 1960's, *o*-QMs now play an important role in total synthesis.^{29–31} However, their full synthetic potential has been limited due to the requirements of prefunctionalization, protecting group manipulations, high reaction temperatures, and transition metal catalysts. Alternatively, *o*-QMs have been implicated in numerous biosynthetic routes and recent biochemical discoveries have unveiled several families of enzymes capable of generating these highly reactive intermediates under mild conditions.^{18,32–34} Several of these enzymes also exhibit promising biocatalytic utility; however, the vast majority of examples are derived from plant or fungal sources, limiting scalability due to reduced protein expression levels and overall stability.^{35–38} Herein, we repurpose two previously characterized microbial BBE-like oxidases capable of directly generating *o*-QMs to perform chemoselective dehydrogenation, hydroxylation, and cyclization reactions with an impressive array of non-native substrates.

We recently reported the discovery of a novel tetrachlorinated natural product, tetrachlorizine (**4**), produced by a taxonomically distinct Actinomycete sp.³⁹ Bioinformatic analysis revealed a biosynthetic gene cluster architecturally similar to a previously reported dichloropyrrole containing natural product, (–)-chlorizidine A (**2**). The final biosynthetic step in chlorizidine and tetrachlorizine biosynthesis involves the BBE-like oxidases Clz9 and Tcz9, respectively, which share 48% amino acid sequence identity. These two enzymes facilitate hydride abstraction by the oxidized flavin cofactor and phenolic deprotonation by basic residues in the active site, generating a highly reactive *o*-QM intermediate. It is difficult to determine whether this mechanism is concerted, but there is evidence suggesting this may be the case.⁴⁰ Prechlorizidine (**1**) is converted to (–)-chlorizidine A (**2**) by intramolecular nucleophilic addition of the dichloropyrrole nitrogen, generating a rare dihydropyrrolizine ring enantioselectively, while dihydrotetrachlorizine (**3**) is converted to tetrachlorizine (**4**) by benzylic dehydrogenation. Our initial experiments exploring this difference in catalytic function began by incubating **3** with Clz9, yielding a 1:1 mixture of **4** and a new cyclized derivative (**5**), indicating that dehydrogenation can still occur, but Clz9 preferentially acts as a cyclase (Scheme 4.2b). In contrast, incubation of **1** with Tcz9 generated two triply oxidized, stabilized *o*-QM isomers (**6** and **7**) that were unexpectedly stable in aqueous solutions at room temperature. The production of **6** and **7** indicates Tcz9 is also capable of both intramolecular cyclization and dehydrogenation reactions with non-native substrates, however, the additional dehydrogenation activity with prechlorizidine distinguishes Tcz9 from Clz9. It was also the first time we observed products that seemingly undergo multiple iterations of oxidation by either BBE-like enzyme. We hypothesize the C-15 carbonyl of

3 lowers the pKa of the α -protons attached to facilitate deprotonation and subsequent dehydrogenation by Tcz9 and Clz9 following *o*-QM formation. In addition, we anticipate that a key active site residue in Tcz9 is capable of deprotonating C-14 without the C-15 carbonyl due to the absence of any cyclized product with **3** and the production of triply dehydrogenated products **6** and **7**. Given the curious results with two substrates and differences in activity between Clz9 and Tcz9, we sought to further explore the structure-function relationships of these two enzymes and assess their substrate promiscuity to functionalize a broader range of substrates.



Scheme 4.2. Benzylic functionalization reactions with microbial BBE-like enzymes Clz9 and Tcz9 via an *o*-QM intermediate. (a) Clz9 catalyzes intramolecular cyclization, while Tcz9 catalyzes a dehydrogenation. (b) Clz9 exhibits selectivity as a cyclase not observed with Tcz9 and **3**, while Tcz9 has preferential dehydrogenation activity not observed with Clz9.

2. Results

2.1. Site-directed mutagenesis of Clz9 and Tcz9

Our attempts to crystallize Clz9 and Tcz9 and confirm the structural differences between these two enzymes have proven unsuccessful. Therefore, we created 3D protein homology models of Clz9 and Tcz9 using AlphaFold and overlaid them with the published crystal structure of FAD-bound tetrahydrocannabinolic acid (THCA) synthase, a plant BBE-like homolog that shares approximately 25% sequence identity with Clz9 and Tcz9.^{18,41} This allowed us to predict the relative positioning of FAD in the active site of Clz9 and Tcz9 and evaluate proximal residues that would be critical for catalytic functions. Indeed, both models accurately predict the conserved histidine and cysteine residues necessary for bicovalent attachment (Figure 4.1a). Structural analysis of the models reveals three potential residues within the active site of Tcz9 that could be involved in C-14 deprotonation. One of these three residues in Tcz9, Y374, is conserved in Clz9. The two remaining basic residues in Tcz9, T124 and E368, are F156 and N400 in Clz9, respectively, and are hypothesized to play a role in the deprotonation. Thus, we prepared two Tcz9 mutants and two Clz9 mutants to reflect the natural variation observed at these two positions. Clz9 N400E and Tcz9 E368N did not exhibit any noticeable changes compared to the wild type enzymes, other than decreased activity with their non-native substrates (Figure 4.1b). Although Clz9 F156T and Tcz9 T124F lowered activity with both substrates, Clz9 F156T did produce a mixture of chlorizidine and the triply oxidized *o*-QM isomers **6** and **7**. Given this result, the T124 residue in Tcz9 may play a role in differentiating the activity of Clz9 and Tcz9. Additional structure-function relationship

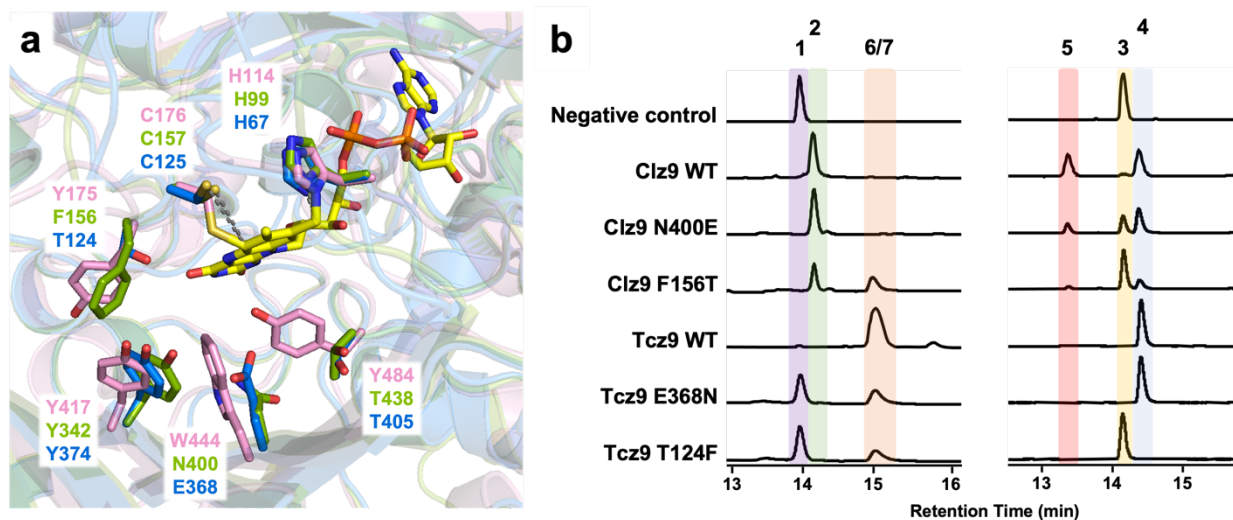


Figure 4.1. Investigation of active site residues that may be involved in the deprotonation event that differentiates the catalytic function of Tcz9 from Clz9. (a) Model overlay of Clz9 (green) and Tcz9 (blue) with THCA synthase (pink; 3VTE). The bicovalently attached FAD cofactor is yellow. (b) HPLC analysis of the *in vitro* conversion with **1** (left) or **3** (right) comparing the activity of two Clz9 and Tcz9 mutants with their respective wild-type enzymes after 12 hours. UV absorption monitored at 450nm (left) and 350 nm (right).

experiments will be necessary to fully evaluate additional residues that affect the cyclization and dehydrogenation capabilities of these two enzymes.

2.2. Benzylic hydroxylation reactions with non-native substrates

Two recent publications have rigorously examined the utility of *o*-QMs in biocatalytic applications.^{36,38} Both of these examples employ fungal α -ketoglutarate-dependent (α -KG) non-heme iron oxidases, CitB or ClaD, to perform chemo- and regioselective benzylic hydroxylation reactions. Wild-type CitB and ClaD display impressive promiscuity, hydroxylating more than 20 derivatives of clavatul containing various aromatic substituents. Upon hydroxylation by the α -KG non-heme iron oxygenases, these products undergo non-enzymatic dehydration to generate an *o*-QM intermediate, which can further react with additional nucleophiles present in solution, including primary and secondary alcohols, secondary amines, thiols, olefins, and indoles,

forming new benzylic C–O, C–N, C–S, and C–C bonds. So far, only methyl groups have been reported to be hydroxylated with these α -KG non-heme iron oxygenases, limiting their utility to enantioselectively functionalize prochiral substrates. We envisioned that BBE-like oxidases Clz9 and Tcz9 could provide an orthogonal approach to functionalize benzylic carbons enantioselectively via direct formation of an *o*-QM species within the active site of the enzyme.

Our next goal was to expand the role of Clz9 and Tcz9 past their cyclization and dehydrogenation functions. To do this, we prepared truncated derivatives of dihydrotetrachlorizine (**3**) that replaced the pendant dichloropyrrole moiety with a methyl substituent to see if benzylic functionalization would still occur. To our surprise, both Tcz9 and Clz9 were able to hydroxylate both **8** and **9** after 12 hours at room temperature, albeit in low quantities (Figure 4.2a). Furthermore, we realized that the reaction could be performed with the clarified cell lysate, eliminating the requirement for time-consuming protein purification. Although benzylic hydroxylation is the same reaction outcome as the α -KG non-heme iron oxygenases CitB and ClaD, the mechanism for benzylic hydroxylation with our BBE-like oxidases is fundamentally different. With α -KG non-heme iron oxidases CitB and ClaD, the initial oxygen source is molecular oxygen, which can then undergo non-enzymatic reversible dehydration to reform the *o*-QM and react with water present in solution;³³ with BBE-like oxidases Clz9 and Tcz9, the oxygen is believed to be sourced directly from water by nucleophilic addition into the enzymatically generated *o*-QM.

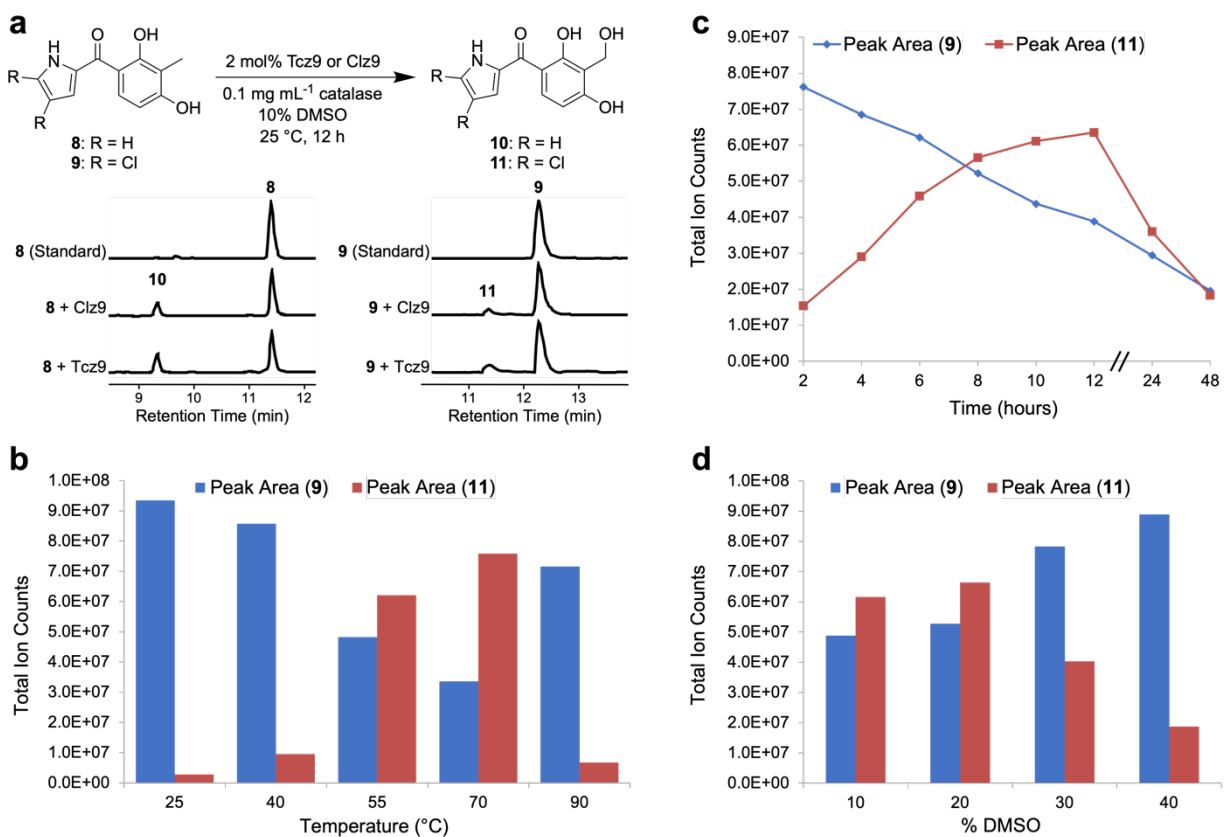


Figure 4.2. Biocatalytic properties of Tcz9. (a) Initial HPLC analysis of benzylic hydroxylation reaction *in vitro* with 2 mol% Clz9 or Tcz9 and **8** or **9** after 12 hours at 37 °C. Combined extracted ion chromatogram (EIC) for $m/z = 216.1, 232.1$ $[M-H]^-$ (left); $m/z = 284.0, 300.0$ $[M-H]^-$ (right). (b) Temperature profile for *in vitro* reaction with Tcz9 crude cell lysate and **9** at pH = 7.5 after 8 hours. (c) Time course experiment reveals optimal production formation after 8-12 hours at 55 °C before significant degradation of the product. (d) Effects of 10-40% DMSO on Tcz9 with **9** at 55 °C after 8 hours. Peak area is calculated by integrating the EIC for **9** and **11** in each sample.

2.3. Temperature and solvent effects on Tcz9 activity

Building upon these results, we examined several reaction parameters that might improve the conversion of **9** to **11** with Tcz9. We had previously observed the *in vitro* reactions with Clz9 and Tcz9 and their native substrates were slightly faster by performing these reactions in a 37 °C incubator, rather than at room temperature. Much to our surprise, wild-type Tcz9 significantly increased the production of **11** between 55-70 °C, compared to 25 °C (Figure 4.2b). Unfortunately, there also appeared to be more substrate

consumed above 70 °C without more desired product forming. This is explained by the observation that elevated temperatures promote spontaneous dehydration of the benzylic alcohol product to regenerate the *o*-QM, which could then degrade or react with other nucleophiles present in solution from the crude cell lysate. Accordingly, the disappearance of substrate at 90 °C with very little product observed could also be explained by possible degradation of the substrate, as no additional significant products could be detected that signified any side reactions were occurring. This pronounced stability at elevated temperatures is unexpected for wild type enzymes from a marine organism, but the bicovalent attachment of the protein to the FAD cofactor might play a role in reinforcing the structural integrity of the active site. This enhanced activity has also been documented with THCA synthase.⁴²

2.4. Time course analysis monitoring reaction progress of Tcz9 with 9

Guided by these results, we next monitored the progress of the reaction every few hours to track substrate consumption and possible product degradation at 55 °C (Figure 4.2c). The reaction rate decreases after approximately 8 hours, while substrate concentration continued to decline. After 48 hours, ~66% of the maximum benzyl alcohol product observed had degraded. Due to the hydrophobic nature of the substrates, we also examined Tcz9's stability in DMSO (Figure 4.2d). We initially used 10% DMSO as a carrier solvent for the substrate, but preliminary data suggests that Tcz9 can withstand upwards of 20% DMSO before activity is significantly affected. Overall, these experiments indicate that optimal reactions should be performed at approximately 55 °C for 8-10 hours in the presence of 10-20% DMSO. Although we could not develop a set of conditions that

reached full substrate consumption, the unreacted substrate can be recycled for subsequent *in vitro* reactions. Further experiments to optimize the reaction conditions will investigate the effects of pH, as well as optimal substrate and enzyme concentrations. Additionally, a small library of 10-15 additional substrates with various acyl and alkyl substituents will be used to probe the substrate scope for these enzymes.

2.5. *In vitro* cannabinoid production with Clz9 and Tcz9

The 2-alkylresorcinol scaffold of dihydrotetrachlorizine (**3**) and prechlorizidine (**1**) is shared by other well-known classes of natural products, including phytocannabinoids (commonly known as cannabinoids). In congruence with tetrachlorizine and chlorizidine biosynthesis, the terminal biosynthetic reaction in cannabinoid biosynthesis is also catalyzed by BBE-like enzymes that generate *o*-QM intermediates. Three enzymes have been characterized from *Cannabis sativa* L. that catalyze the oxidative cyclization reactions with cannabigerolic acid (CBGA, **12a**) to produce THCA (**13**), cannabidiolic acid (CBDA, **14**), and cannabichromenic acid (CBCA, **15a**) by their respective THCA, CBDA, and CBCA synthases.^{12,43,44} Given the therapeutic and commercial value of cannabinoids, in addition to the uncanny structural, enzymatic, and mechanistic parallels, we were curious if our bacterial BBE-like enzymes associated with marine alkaloid natural products could accept the cannabinoid precursor **12a**. Indeed, both wild type Clz9 and Tcz9 showed activity with CBGA at 5 mol% after 12 hours at 37 °C (Figure 4.3). The major product generated by both Clz9 and Tcz9 at pH 7.5 is **15a**, but they also produce uncharacterized products **16a** and **17a**. Interestingly, **16a** is exclusively produced by the Clz9 variants, while **17a** is produced exclusively by the Tcz9 variants. High-resolution

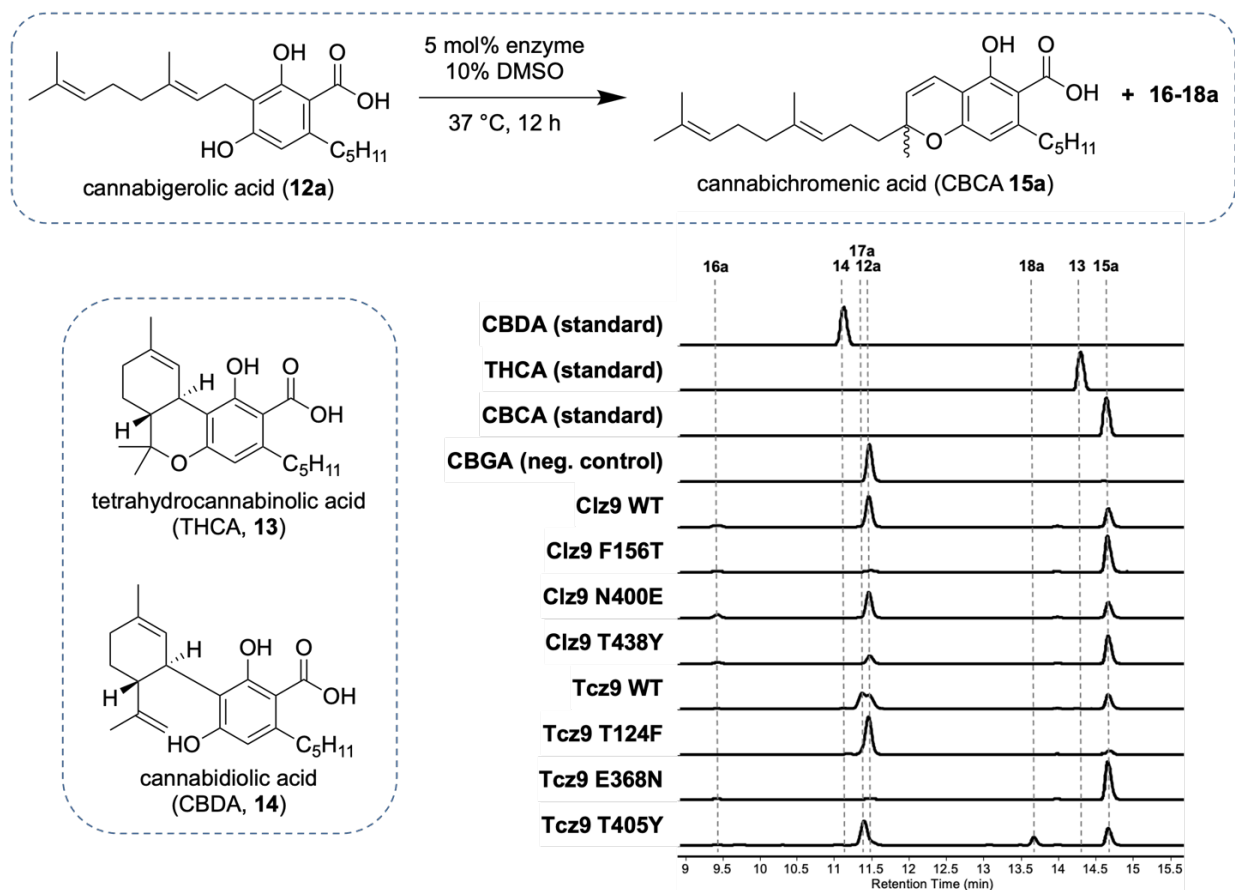


Figure 4.3. HPLC analysis of the *in vitro* reactions of CBGA (**12a**) with Clz9 or Tcz9 variants after incubation for 12 hours at pH 7.5 and 37 °C. No production of THCA (**13**) or CBDA (**14**) was detected at this pH. The major product observed was CBCA (**15a**). **16-18a** have yet to be structurally characterized. UV absorption monitored at 300 nm.

mass spectrometry confirmed **16a** and **17a** have the same exact mass as THCA, CBDA, and CBCA ($[M-H]^-$ $m/z = 357.205$; $C_{27}H_{38}O_4$), indicating oxidation of **12a** has taken place. However, the retention times of **16a** and **17a** differ most significantly from naturally occurring cannabinoids THCA and CBCA, suggesting these uncharacterized products are most likely structurally related to CBDA. We are currently scaling up production of the relevant Tcz9 and Clz9 variants to isolate and verify the structures of these two unknown products.

Given these promising results, we decided to screen our four Clz9 and Tcz9 variants and probe the effect of the F156/T124 and N400/E368 substitutions on catalytic

activity with **12a**. Clz9 N400E exhibited similar activity to the wild-type enzyme, and the F156T mutant nearly consumed all **12a** to produce **15a** with minor traces of **16a** (Figure 4.4a). In contrast, the Tcz9 E368N variant consumed all **12a** to produce **15a** exclusively, while the T124F variant abolished activity. We also prepared two additional variants, Clz9 T438Y and Tcz9 T405Y, that reflect the THCA synthase Y484 residue that is crucial for catalytic activity in cannabinoid biosynthesis (Figure 4.1a).¹⁸ Clz9 T438Y produced **15a** exclusively, while the Tcz9 T405Y variant produced a 1:1 mixture of **15a** and **17a**. Tcz9 T405Y also produced a third product **18a** with mass 355.1907 ([M-H]⁻; C₂₇H₄₀O₄) suggestive of a doubly oxidized product; however, this mass does not match any known cannabinoids. Overall, these results suggest that the F156/T124 and N400/E368 residues play a role in substrate binding or positioning within the active site and could be targeted positions for further mutagenesis experiments. Additionally, both Clz9 T438Y and Tcz9 T405Y variants reflecting the tyrosine residue conserved across plant cannabinoid synthases increased conversion of **12a**, suggesting that the tyrosine hydroxyl group may be better positioned for phenolic deprotonation of the cannabinoid substrates, compared to the threonine residue in the bacterial BBE-like oxidases.

All isolated cannabinoids from *C. sativa* L. share a common C10 geranyl chain *para* to a pentyl or propyl alkyl chain, derived from hexanoyl-CoA or butanoyl-CoA, respectively.⁴⁵ However, cannabinoids with C15 farnesyl chains and methyl substituents have been isolated from other plants and even fungi.^{46,47} There are several reports that the *C. sativa* cannabinoid synthases accept substrates with various alkyl substituents,^{37,48} but no information has been reported on the effects of altering the prenyl chain length with these enzymes. Biochemical investigations with the recently characterized homolog

daurichromenic acid (DCA) synthase from *Rhododendron dauricum* report this homolog can accept not only geranyl and farnesyl prenylated substrates, but also C20 geranylgeranyl prenylated analogs.⁴⁹ However, DCA synthase is selective for methyl-substituted alkyl groups, exhibiting no activity with **12a**. We decided to screen our wild-type Clz9 and Tcz9 enzymes and their variants with three linear cannabinoids with various alkyl and prenyl substituents. Cannabigerovarinic acid (CBGVA, **12b**), the propyl analog of **12a**, exhibited a similar activity profile compared to **12a** with wild type Clz9, Tcz9 and all six mutants, producing what we anticipate is cannabichromevarinic acid (CBCVA, **15b**) as the major product (Figure 4.4). Similar to the reaction with **12a**, the Clz9 enzymes exclusively produce an unknown product **16b**, and the Tcz9 enzymes exclusively producing **17b** (Figure 4.4). Based on the relative retention times, **15b** and **16b** are most likely the propyl analogs of **15a** and **16a**.

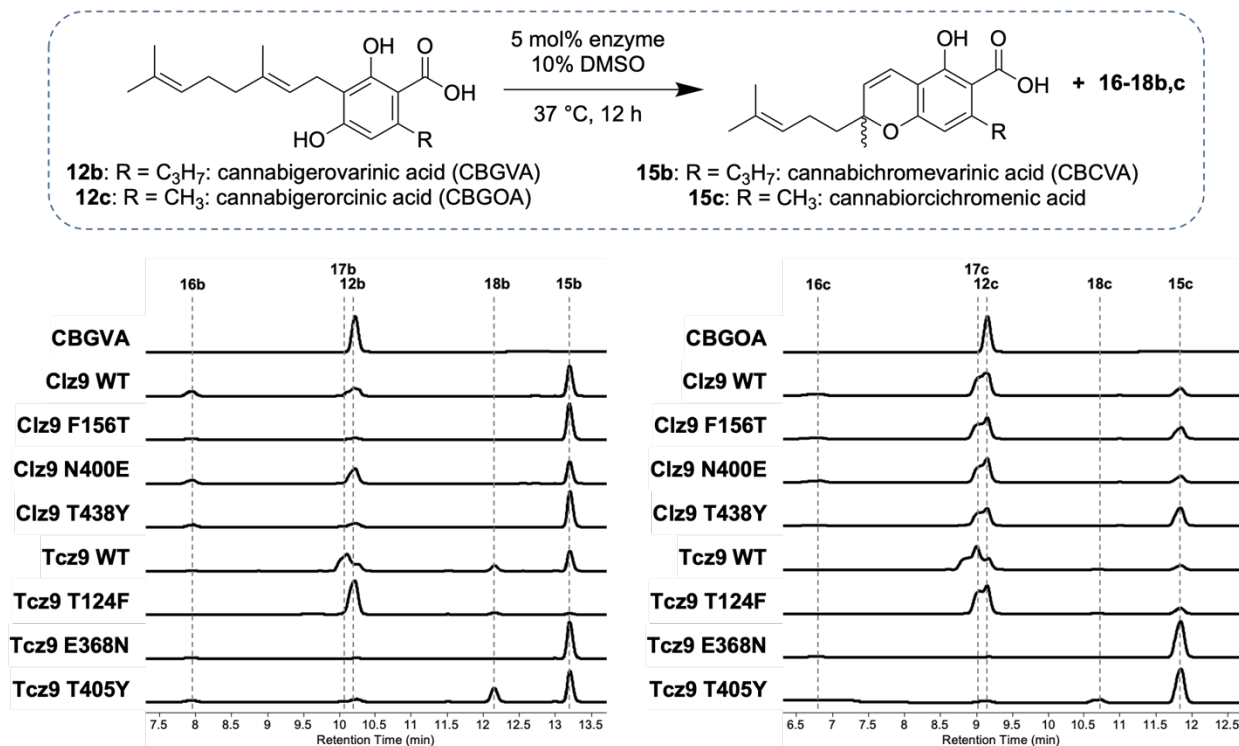


Figure 4.4. HPLC analysis of the *in vitro* reactions of **12b** (left) or **12c** (right) with Clz9 and Tcz9 variants after incubation for 12 hours at pH 7.5 and 37 °C. **16-18b-c** have yet to be structurally characterized. UV absorption monitored at 300 nm.

The methyl derivative of **12a**, cannabigerorcinic acid (CBGOA, **12c**), exhibited a slightly different activity profile than **12b** and **12a** (Figure 4.4). Tcz9 E368N and T405Y produced **15c**, which we anticipate is cannabiorichromenic acid, the methyl analog of **15a**. Wild-type Tcz9 and Tcz9 T124F produced **17c**, what is most likely the methyl analog of **17a** and **17b** (Figure 4.5c). Wild type Clz9 and its three variants displayed an activity profile that resembled wild type Tcz9 and its variants, producing a mixture of **15c** and **17c** with traceable amounts of **16c**. The final cannabinoid we screened was grifolic acid (**19**), the only substrate screened at this time with a farnesyl chain. **19** exhibited no activity with any of the Clz9 enzymes, but three of the four Tcz9 enzymes fully consumed grifolic acid (**19**) to produce what we anticipate is DCA (**20**), given its relative retention time to **19** and the related chromene-containing analogs **15a-c** (Figure 4.5). Isolating and characterizing these products will be critical to understanding the difference in activity between substrate and enzymes.

Given the lack of structural information regarding the relationships between THCA synthase, CBDA synthase, and CBCA synthase, it is difficult to predict which residues influence the difference in cyclization and site specificity. However, the fact that Tcz9 T124F completely abolished activity with grifolic acid (**19**) suggests that the longer farnesyl chain may be embedded in the active site and the larger phenyl group may interfere with substrate binding. It is unclear at this time which residues differentiate CBCA synthase from THCA and CBDA synthases, but recent biochemical investigations have determined THCA synthase and CBDA synthase produce higher amounts of THCA (**13**) and CBDA (**14**), respectively, at pH values below pH 5.5. At pH values between 5.5 and 8.0, there was greater production of CBCA (**15a**).⁴² Given that the *in vitro* reactions with

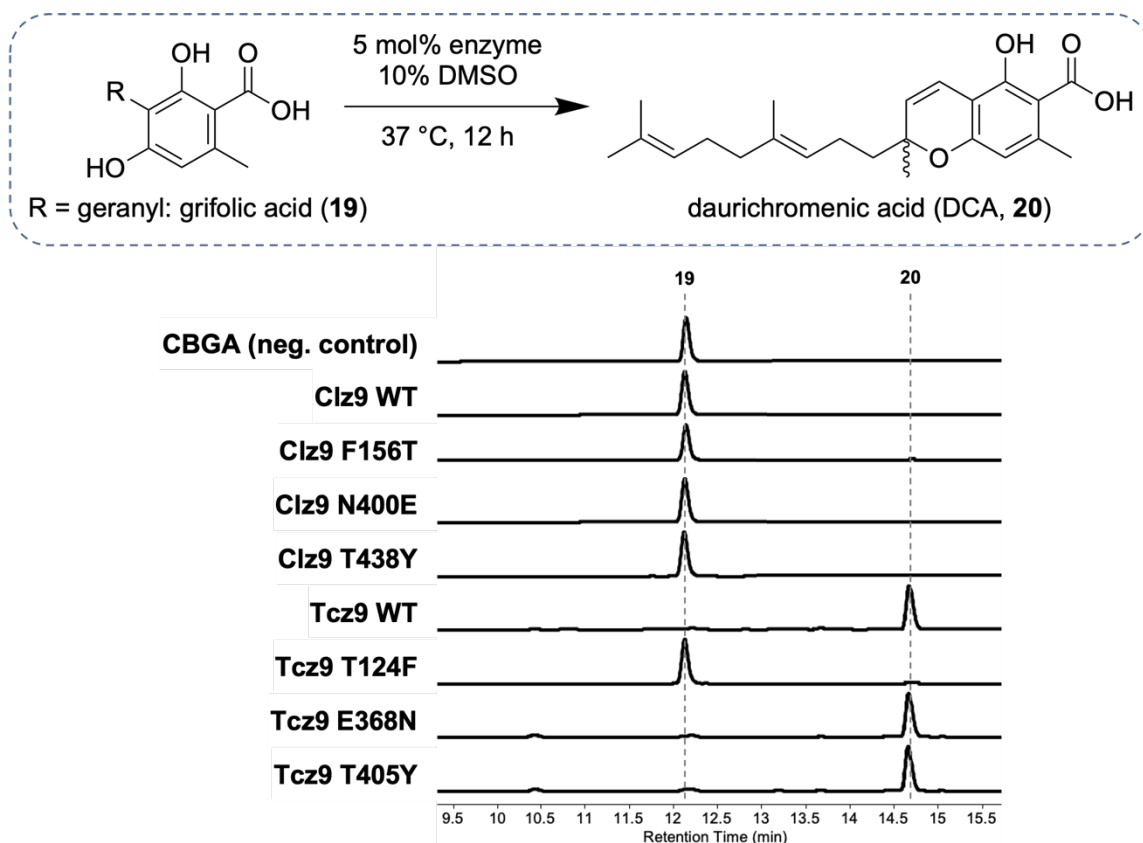


Figure 4.5. HPLC analysis of the *in vitro* reactions of **19** with Clz9 and Tcz9 variants after incubation for 12 hours at pH 7.5 and 37 °C. UV absorption monitored at 300 nm.

the Clz9 and Tcz9 enzymes have only been screened at pH 7.5, further analysis at lower pH values may reveal additional cannabinoid products.

2.6. *In vivo* cannabinoid production with Tcz9 T405Y

One of the biggest challenges remaining for this project is structural confirmation of all the products generated by the four cannabinoid substrates. Commercially available cannabinoids are typically sold in their decarboxylated forms, which are more stable and have more therapeutic value. The propyl, methyl, and farnesyl derivatives of THCA (**13**), CBDA (**14**), and CBCA (**15a**) are produced in extremely low quantities or sourced from other organisms and are not produced for commercial purposes at this time, and total

synthesis routes are prohibitively difficult. The few carboxylated cannabinoids that are commercially available cost several hundred dollars per milligram. Therefore, the most cost-effective approach to verify the identities of these products will be to scale-up reactions to a ten- or hundred-milligram scale and characterize each product by NMR. To streamline the scale-up process, we attempted a whole-cell biotransformation by adding 1 mM CBGA (**12a**) to a 1L culture of *E. coli* BL21(DE3) cells overexpressing Tcz9 T405Y. On our first attempt, we were able to convert approximately 80% of the CBGA (**12a**) to the two desired products **15a** and **17a** over 48 hours (Figure S1) with 5x more substrate than we had previously attempted *in vitro*. This reaction needs to be further optimized, but it is a promising start to scale-up production. To date, THCA synthase has only been successfully heterologously expressed in insect cells or yeast, but not in any bacterial systems.^{18,37,50,51} The biotransformation reactions described herein lay the foundation for developing the first bacterial systems capable of producing a diverse catalog of cannabinoid derivatives.

3. Discussion and Conclusions

BBE-like enzymes are a relatively small family of characterized enzymes that are only starting to be recognized for their biocatalytic utility.^{42,52,53} The distinctive bicovalent tethering to FAD has profound electronic and structural implications for the functions of these enzymes, allowing them to be manipulated to perform a multitude of oxidative reactions with a diverse range of complex substrates found in plants, fungi, and bacteria.⁵³ This plasticity and versatility is enabled by subtle active site variations, as demonstrated by the different activity profiles amongst the plant cannabinoid synthases and two

bacterial oxidases, Clz9 and Tcz9. These two groups of BBE-like oxidases are found in completely unrelated organisms and catalyze different reactions with substrates derived from unrelated biosynthetic pathways. Mechanistically, these cannabinoid synthases and bacterial oxidases facilitate hydride abstraction by FAD and phenolic deprotonation within the active site to generate a highly reactive *o*-QM intermediate. *o*-QMs typically react with any nucleophile present, but these enzymes direct the *o*-QM to perform transformative benzylic functionalization reactions chemo-, regio-, and stereoselectively. The delicate balance of promiscuity and selectivity that these enzymes display, coupled with their impressive stability makes them ideal candidates for biocatalytic development. We anticipate that further genome mining efforts will uncover more BBE-like enzymes capable of unprecedented oxidation transformations and homologs of previously characterized enzymes that access more diverse substrate and products.

Overall, the work completed in this chapter demonstrates the remarkable biocatalytic potential of two bacterial BBE-like oxidases, Clz9 and Tcz9. These two enzymes are promiscuous and versatile, performing several different benzylic functionalization reactions beyond their native function on substrates derived from completely unrelated biosynthetic pathways. The Clz9 and Tcz9 F156/T124 substitution appears to have influence on the difference in reaction selectivity between these two enzymes, but additional studies are required to fully understand the structure-function relationship between these two enzymes. Not only can these enzymes catalyze intramolecular nucleophilic addition reactions and dehydrogenations, but we have demonstrated they are capable of benzylic hydroxylation and cycloaddition reactions as well. Furthermore, the wild-type enzymes exhibit favorable biocatalytic properties,

withstanding temperatures as high as 70 °C and more than 20% DMSO. The most exciting prospect for these enzymes is their biomanufacturing potential to produce rare or unnatural cannabinoids in a bacterial heterologous system, a feat yet to be achieved with the plant-derived cannabinoid synthases. Future work will focus on optimizing the reaction conditions by studying the effects of pH, temperature, substrate concentration, and then scaling up these conditions to confirm the structures of all the observed products. Additional rational engineering studies may also improve the selectivity of these enzymes to produce desired cannabinoids

Chapter 4 is coauthored by Purdy, Trevor N. and Moore, Bradley S. The dissertation author was the primary investigator and author of this paper.

References

1. Nicolaou, K. C. The Emergence of the Structure of the Molecule and the Art of Its Synthesis. *Angew. Chemie Int. Ed.* **2013**, *52*, 131–146.
2. Madhavan, A.; Sindhu, R.; Parameswaran, B.; Sukumaran, R. K.; Pandey, A. Metagenome Analysis: a Powerful Tool for Enzyme Bioprospecting. *Appl. Biochem. Biotechnol.* **2017**, *183*, 636–651.
3. Badenhorst, C. P. S.; Bornscheuer, U. T. Getting Momentum: From Biocatalysis to Advanced Synthetic Biology. *Trends Biochem. Sci.* **2018**, *43*, 180–198.
4. Devine, P. N.; Howard, R. M.; Kumar, R.; Thompson, M. P.; Truppo, M. D.; Turner, N. J. Extending the application of biocatalysis to meet the challenges of drug development. *Nat. Rev. Chem.* **2018**, *2*, 409–421.
5. de Rond, T.; Asay, J. E.; Moore, B. S. Co-occurrence of enzyme domains guides the discovery of an oxazolone synthetase. *Nat. Chem. Biol.* **2021**, *17*, 794–799.
6. Schwizer, F.; Okamoto, Y.; Heinisch, T.; Gu, Y.; Pellizzoni, M. M.; Lebrun, V.; Reuter, R.; Köhler, V.; Lewis, J. C.; Ward, T. R. Artificial Metalloenzymes: Reaction Scope and Optimization Strategies. *Chem. Rev.* **2017**, *118*, 142–231.
7. Huffman, M. A.; Fryszkowska, A.; Alvizo, O.; Borra-Garske, M.; Campos, K. R.; Canada, K. A.; Devine, P. N.; Duan, D.; Forstater, J. H.; Grosser, S. T.; Halsey, H. M.; Hughes, G. J.; Jo, J.; Joyce, L. A.; Kolev, J. N.; Liang, J.; Maloney, K. M.; Mann, B. F.; Marshall, N. M.; McLaughlin, M.; Moore, J. C.; Murphy, G. S.; Nawrat, C. C.; Nazor, J.; Novick, S.; Patel, N. R.; Rodriguez-Granillo, A.; Robaire, S. A.; Sherer, E. C.; Truppo, M. D.; Whittaker, A. M.; Verma, D.; Xiao, L.; Xu, Y.; Yang, H. Design of an in vitro biocatalytic cascade for the manufacture of islatravir. *Science* **2019**, *366*, 1255–1259.
8. Winkler, C. K.; Schrittwieser, J. H.; Kroutil, W. Power of Biocatalysis for Organic Synthesis. *ACS Cent. Sci.* **2021**, *7*, 55–71.
9. Yang, Y.; Arnold, F. H. Navigating the Unnatural Reaction Space: Directed Evolution of Heme Proteins for Selective Carbene and Nitrene Transfer. *Acc. Chem. Res.* **2021**, *54*, 1209–1225.
10. Nazor, J.; Liu, J.; Huisman, G. Enzyme evolution for industrial biocatalytic cascades. *Curr. Opin. Biotechnol.* **2021**, *69*, 182–190.
11. Rink, E.; Böhm, H. Conversion of reticuline into scoulerine by a cell free preparation from *Macleaya microcarpa* cell suspension cultures. *FEBS Lett.* **1975**, *49*, 396–399.
12. Taura, F.; Morimoto, S.; Shoyama, Y.; Mechoulam, R. First Direct Evidence for the

Mechanism of Δ^1 -Tetrahydrocannabinolic Acid Biosynthesis. *J. Am. Chem. Soc.* **1995**, *117*, 9766–9767.

13. Lee, M. H.; Lai, W. L.; Lin, S. F.; Hsu, C. S.; Liaw, S. H.; Tsai, Y. C. Structural characterization of glucooligosaccharide oxidase from *Acremonium strictum*. *Appl. Environ. Microbiol.* **2005**, *71*, 8881–8887.

14. Noinaj, N.; Bosserman, M. A.; Schickli, M. A.; Piszczek, G.; Kharel, M. K.; Pahari, P.; Buchanan, S. K.; Rohr, J. The crystal structure and mechanism of an unusual oxidoreductase, GilR, involved in gilvocarcin V biosynthesis. *J. Biol. Chem.* **2011**, *286*, 23533–23543.

15. Kamimura, M.; Saito, H.; Niwa, R.; Niimi, T.; Toyoda, K.; Ueno, C.; Kanamori, Y.; Shimura, S.; Kiuchi, M. Fungal Ecdysteroid-22-oxidase, a New Tool for Manipulating Ecdysteroid Signaling and Insect Development. *J. Biol. Chem.* **2012**, *287*, 16488–16498.

16. Nielsen, C. A.; Folly, C.; Hatsch, A.; Molt, A.; Schröder, H.; O'Connor, S. E.; Naesby, M. The important ergot alkaloid intermediate chanoclavine-I produced in the yeast *Saccharomyces cerevisiae* by the combined action of EasC and EasE from *Aspergillus japonicus*. *Microb. Cell Fact.* **2014**, *13*, 1–11.

17. Winkler, A.; Kutchan, T. M.; Macheroux, P. 6-S-Cysteinylation of Bi-covalently Attached FAD in Berberine Bridge Enzyme Tunes the Redox Potential for Optimal Activity. *J. Biol. Chem.* **2007**, *282*, 24437–24443.

18. Shoyama, Y.; Tamada, T.; Kurihara, K.; Takeuchi, A.; Taura, F.; Arai, S.; Blaber, M.; Shoyama, Y.; Morimoto, S.; Kuroki, R. Structure and function of Δ^1 -tetrahydrocannabinolic acid (THCA) synthase, the enzyme controlling the psychoactivity of *Cannabis sativa*. *J. Mol. Biol.* **2012**, *423*, 96–105.

19. Newhouse, T.; Baran, P. S. If C-H Bonds Could Talk: Selective C-H Bond Oxidation. *Angew. Chemie Int. Ed.* **2011**, *50*, 3362–3374.

20. Abrams, D. J.; Provencher, P. A.; Sorensen, E. J. Recent applications of C–H functionalization in complex natural product synthesis. *Chem. Soc. Rev.* **2018**, *47*, 8925–8967.

21. Guillemard, L.; Kaplaneris, N.; Ackermann, L.; Johansson, M. J. Late-stage C–H functionalization offers new opportunities in drug discovery. *Nat. Rev. Chem.* **2021**, *5*, 522–545.

22. Liégault, B.; Renaud, J.-L.; Bruneau, C. Activation and functionalization of benzylic derivatives by palladium catalysts. *Chem. Soc. Rev.* **2008**, *37*, 290–299.

23. Chen, Y.; Lie, F.; Li, Z. Enantioselective benzylic hydroxylation with *Pseudomonas monteilii* TA-5: A simple method for the syntheses of (*R*)-benzylic alcohols containing

reactive functional groups. *Adv. Synth. Catal.* **2009**, *351*, 2107–2112.

24. Genovino, J.; Sames, D.; Hamann, L. G.; Touré, B. B. Accessing Drug Metabolites via Transition-Metal Catalyzed C–H Oxidation: The Liver as Synthetic Inspiration. *Angew. Chemie Int. Ed.* **2016**, *55*, 14218–14238.

25. Yazaki, R.; Ohshima, T. Recent strategic advances for the activation of benzylic C–H bonds for the formation of C–C bonds. *Tetrahedron Lett.* **2019**, *60*, 1–11.

26. Tanwar, L.; Börgel, J.; Ritter, T. Synthesis of Benzylic Alcohols by C–H Oxidation. *J. Am. Chem. Soc.* **2019**, *141*, 17983–17988.

27. Betori, R. C.; May, C. M.; Scheidt, K. A. Combined Photoredox/Enzymatic C–H Benzylic Hydroxylations. *Angew. Chemie* **2019**, *131*, 16642–16646.

28. Bai, W. J.; David, J. G.; Feng, Z. G.; Weaver, M. G.; Wu, K. L.; Pettus, T. R. R. The domestication of *ortho*-quinone methides. *Acc. Chem. Res.* **2014**, *47*, 3655–3664.

29. Van de Water, R. W.; Pettus, T. R. R. *o*-Quinone methides: Intermediates underdeveloped and underutilized in organic synthesis. *Tetrahedron* **2002**, *58*, 5367–5405.

30. Willis, N. J.; Bray, C. D. *ortho*-Quinone methides in natural product synthesis. *Chem. - A Eur. J.* **2012**, *18*, 9160–9173.

31. Singh, M. S.; Nagaraju, A.; Anand, N.; Chowdhury, S. *ortho*-Quinone methide (*o*-QM): A highly reactive, ephemeral and versatile intermediate in organic synthesis. *RSC Adv.* **2014**, *4*, 55924–55959.

32. Ohashi, M.; Liu, F.; Hai, Y.; Chen, M.; Tang, M.; Yang, Z.; Sato, M.; Watanabe, K.; Houk, K. N.; Tang, Y. SAM-dependent enzyme-catalysed pericyclic reactions in natural product biosynthesis. *Nature* **2017**, *549*, 502–506.

33. Fan, J.; Liao, G.; Kindinger, F.; Ludwig-Radtke, L.; Yin, W. B.; Li, S. M. Peniphenone and Penilactone Formation in *Penicillium crustosum* via 1,4-Michael Additions of *ortho*-Quinone Methide from Hydroxyclovatol to γ -Butyrolactones from Crustosic Acid. *J. Am. Chem. Soc.* **2019**, *141*, 4225–4229.

34. Chen, Q.; Gao, J.; Jamieson, C.; Liu, J.; Ohashi, M.; Bai, J.; Yan, D.; Liu, B.; Che, Y.; Wang, Y.; Houk, K. N.; Hu, Y. Enzymatic Intermolecular Hetero-Diels–Alder Reaction in the Biosynthesis of Tropolonic Sesquiterpenes. *J. Am. Chem. Soc.* **2019**, *141*, 14052–14056.

35. Asai, T.; Tsukada, K.; Ise, S.; Shirata, N.; Hashimoto, M.; Fujii, I.; Gomi, K.; Nakagawara, K.; Kodama, E. N.; Oshima, Y. Use of a biosynthetic intermediate to explore the chemical diversity of pseudo-natural fungal polyketides. *Nat. Chem.* **2015**, *7*, 737–

743.

36. Doyon, T. J.; Perkins, J. C.; Baker Dockrey, S. A.; Romero, E. O.; Skinner, K. C.; Zimmerman, P. M.; Narayan, A. R. H. Chemoenzymatic *o*-Quinone Methide Formation. *J. Am. Chem. Soc.* **2019**, *141*, 20269–20277.

37. Luo, X.; Reiter, M. A.; D'Espaux, L.; Wong, J.; Denby, C. M.; Lechner, A.; Zhang, Y.; Grzybowski, A. T.; Harth, S.; Lin, W.; Lee, H.; Yu, C.; Shin, J.; Deng, K.; Benites, V. T.; Wang, G.; Baidoo, E. E. K.; Chen, Y.; Dev, I.; Petzold, C. J.; Keasling, J. D. Complete biosynthesis of cannabinoids and their unnatural analogues in yeast. *Nature* **2019**, *567*, 123–126.

38. Wu, G.; Yu, G.; Yu, Y.; Yang, S.; Duan, Z.; Wang, W.; Liu, Y.; Yu, R.; Li, J.; Zhu, T.; Gu, Q.; Li, D. Chemoreactive-Inspired Discovery of Influenza A Virus Dual Inhibitor to Block Hemagglutinin-Mediated Adsorption and Membrane Fusion. *J. Med. Chem.* **2020**, *63*, 6940.

39. Purdy, T. N.; Kim, M. C.; Cullum, R.; Fenical, W.; Moore, B. S. Discovery and Biosynthesis of Tetrachlorizine Reveals Enzymatic Benzylic Dehydrogenation via an *ortho*-Quinone Methide. *J. Am. Chem. Soc.* **2021**, *143*, 3682–3686.

40. Winkler, A.; Łyskowski, A.; Riedl, S.; Puhl, M.; Kutchan, T. M.; Macheroux, P.; Gruber, K. A concerted mechanism for berberine bridge enzyme. *Nat. Chem. Biol.* **2008**, *4*, 739–741.

41. Jumper, J.; Evans, R.; Pritzel, A.; Green, T.; Figurnov, M.; Ronneberger, O.; Tunyasuvunakool, K.; Bates, R.; Žídek, A.; Potapenko, A.; Bridgland, A.; Meyer, C.; Kohl, S. A. A.; Ballard, A. J.; Cowie, A.; Romera-Paredes, B.; Nikolov, S.; Jain, R.; Adler, J.; Back, T.; Petersen, S.; Reiman, D.; Clancy, E.; Zielinski, M.; Steinegger, M.; Pacholska, M.; Berghammer, T.; Bodenstein, S.; Silver, D.; Vinyals, O.; Senior, A. W.; Kavukcuoglu, K.; Kohli, P.; Hassabis, D. Highly accurate protein structure prediction with AlphaFold. *Nature* **2021**, *596*, 583–589.

42. Zirpel, B.; Kayser, O.; Stehle, F. Elucidation of structure-function relationship of THCA and CBDA synthase from *Cannabis sativa* L. *J. Biotechnol.* **2018**, *284*, 17–26.

43. Taura, F.; Morimoto, S.; Shoyama, Y. Purification and Characterization of Cannabidiolic-acid Synthase from *Cannabis sativa* L. *J. Biol. Chem.* **1996**, *271*, 16411–17416.

44. Morimoto, S.; Komatsu, K.; Taura, F.; Shoyama, Y. Purification and characterization of cannabichromenic acid synthase from *Cannabis sativa*. *Phytochemistry* **1998**, *49*, 1525–1529.

45. Gülck, T.; Møller, B. L. Phytocannabinoids: Origins and Biosynthesis. *Trends Plant Sci.* **2020**, *25*, 985–1004.

46. Kashiwada, Y.; Yamazaki, K.; Ikeshiro, Y.; Yamagishi, T.; Fujioka, T.; Mihashi, K.; Mizuki, K.; Cosentino, L. M.; Fowke, K.; Morris-Natschke, S. L.; Lee, K. H. Isolation of rhododaurichromanolic acid B and the anti-HIV principles rhododaurichromanolic acid A and rhododaurichromenic acid from *Rhododendron dauricum*. *Tetrahedron* **2001**, *57*, 1559–1563.
47. Hashimoto, T.; Ngoc Quang, D.; Nukada, M.; Asakawa, Y. Isolation, Synthesis and Biological Activity of Grifolic Acid Derivatives from the Inedible Mushroom *Albatrellus Dispersus*. *Heterocycles* **2005**, *65*, 2431–2439.
48. Peet, R.; Kavarana, M. J.; Winnicki, R.; Donsky, M.; Sun, M. Chemical Engineering Processes and Apparatus for the Synthesis of Compounds. **US 10,472**, 1–19 (2019).
49. Iijima, M.; Munakata, R.; Takahashi, H.; Kenmoku, H.; Nakagawa, R.; Kodama, T.; Asakawa, Y.; Abe, I.; Yazaki, K.; Kurosaki, F.; Taura, F. Identification and characterization of daurichromenic acid synthase active in anti-HIV biosynthesis. *Plant Physiol.* **2017**, *174*, 2213–2230.
50. Carvalho, Â.; Hansen, E. H.; Kayser, O.; Carlsen, S.; Stehle, F. Designing microorganisms for heterologous biosynthesis of cannabinoids. *FEMS Yeast Res.* **2017**, *17*, 1-11.
51. Thomas, F.; Schmidt, C.; Kayser, O. Bioengineering studies and pathway modeling of the heterologous biosynthesis of tetrahydrocannabinolic acid in yeast. *Appl. Microbiol. Biotechnol.* **2020**, *104*, 9551–9563.
52. Schrittwieser, J. H.; Resch, V.; Wallner, S.; Lienhart, W.-D.; Sattler, J. H.; Resch, J.; Macheroux, P.; Kroutil, W. Biocatalytic Organic Synthesis of Optically Pure (S)-Scoulerine and Berberine and Benzylisoquinoline Alkaloids. *J. Org. Chem.* **2011**, *76*, 6703–6714.
53. Daniel, B.; Konrad, B.; Toplak, M.; Lahham, M.; Messenlehner, J.; Winkler, A.; Macheroux, P. The family of berberine bridge enzyme-like enzymes: A treasure-trove of oxidative reactions. *Arch. Biochem. Biophys.* **2017**, *632*, 88–103.

Supplementary Information

Materials

All solvents purchased from Fisher Scientific were of HPLC grade or higher. Preparative flash column chromatography was carried out on a Teledyne ISCO CombiFlash® Rf+ Lumen™ system using diatomaceous earth for crude extract loading and silica gel 60 (EMD, 40-63µm) for the stationary phase. Preparative HPLC purification was achieved using a Phenomenex Luna C18 column (5 µm, 100 x 2.0 mm) at a flow rate of 10.0 mL/min, coupled with an Agilent Technologies system composed of a PrepStar pump, a ProStar 410 autosampler, and a ProStar UV detector (Agilent Technologies Inc., CA, USA). NMR spectroscopic data were obtained on a 500 MHz JEOL NMR spectrometer with a 3.0 mm probe. The values of the chemical shifts are described in ppm and coupling constants are reported in Hz. NMR chemical shifts were referenced to the residual solvent peaks (d_H 7.26 for $CDCl_3$). High resolution LC-MS (HR-LC-MS) analysis was conducted on an Agilent 6530 Accurate-Mass Q-TOF MS (MassHunter software, Agilent) equipped with a dual electrospray ionization (ESI) source and an Agilent 1260 LC system (ChemStation software, Agilent) with a diode array detector. Q-TOF MS settings during the LC gradient were as follows: acquisition - mass range acquisition m/z 100 – 1700, MS scan rate 10/s, MS/MS scan rate 2/s, fixed collision energy 20 eV; source - gas temperature 300 °C, gas flow 11 L/min; nebulizer 35 psig, ion polarity negative; scan source parameters - VCap 3000, Fragmentor 100, Skimmer 65, OctopoleRFPeak 750.

Plasmid DNA was isolated from an overnight culture using the QIAprep Spin miniprep Kit (Qiagen, Hilden, Germany) according to the manufacturer's protocol. DNA

clean-up after PCR or agarose gel electrophoresis was performed with QIAquick PCR & Gel Cleanup Kit according to the manufacturer's protocol. DNA sequencing was carried out by the Genewiz Sequencing Facility in San Diego, CA.

Sonication of *E. coli* cells was performed using a 6 mm tip (Qsonica, CT, USA). Protein purification was performed on an ÄKTApurifier instrument (GE Healthcare, IL, USA) with the modules Box-900, UPC-900, R-900 and Frac-900 with all buffers filtered through a nylon membrane 0.2 µm GDWP (Merck, NJ, USA) prior to use. FPLC data was analyzed with UNICORN 5.31 (Built 743) software. All proteins were purified by Ni²⁺ affinity chromatography using a 5 mL HisTrap HP (GE Healthcare) column. Proteins were concentrated using Amicon Ultra filters with 50 kDa MWCO (MilliporeSigma). Buffer exchange was performed using an Econo-Pac 10DG desalting column (Bio-rad).

Site-directed mutagenesis procedures

All Clz9 variants were generated by single primer site-directed mutagenesis of pET-MBP-*clz9* plasmid.¹ 50 µL PCR reactions were prepared with 1 ng/µL pET-MBP-*clz9* plasmid, 0.2 µM primer designated for each mutation (see Table S1), 200 µM dNTPs, 3% (v/v) DMSO, 1X Buffer HF, and 1 U Phusion polymerase. PCR amplification was performed following the procedure outlined in Table S2. Following amplification, 1 µL (20 U) DpnI restriction enzyme (New England Biolabs) was added to the PCR mixture and incubated at 37 °C for 1 h. 2 µL of the digestion mixture was transformed into chemically competent DH10B *E. coli* cells.

All Tcz9 variants were generated with tandem single primer site-directed mutagenesis on pET-MBP-*tcz9*² and subsequent annealing of amplification products

following the procedure outlined by Edelheit 000.³ Briefly, 25 μ L PCR reactions were prepared with 70 ng pET-MBP-*tcz9* plasmid, 0.2 μ M primer (forward or reverse for a designated mutant, see Table S1), 200 μ M dNTPs, 1X Buffer GC, and 1 U Phusion polymerase. PCR amplification was performed following the procedure outlined in Table S2, and the complementary forward and reverse reactions were combined to a final volume of 50 μ L. The combined reactions were denatured and slowly annealed in a thermocycler using the following program: 95 °C for 5 min, 90 °C for 1 min, 80 °C for 1 min, 70 °C for 30 s, 60 °C for 30 s, 50 °C for 30 s, 40 °C for 30 s, hold at 37 °C. Following annealing, 1.5 μ L (30 U) DpnI restriction enzyme was added and the mixture was incubated at 37 °C for 2 h. To improve the efficiency of transformation, the DpnI-digested samples were processed with a PCR clean-up kit (Qiagen), phosphorylated, and ligated prior to transformation. The PCR clean-up consisted of combining the DpnI-digested sample with 3 V Buffer QG + 1 V isopropanol, loading onto a micro spin column (Epoch Life Sciences), washing with Buffer PB followed by two washes with Buffer PE, and eluting with 10 μ L of warm PCR-grade water. 4 μ L of this cleaned and concentrated material was phosphorylated with 0.5 μ L T4 polynucleotide kinase (T4 PNK, New England Biolabs) and 1X T4 ligase buffer in a final volume of 5 μ L by incubating at 37 °C for 30 min and cooling to room temperature. This mixture was brought to a final volume of 10 μ L by treating with 0.5 μ L T4 DNA ligase (New England Biolabs), 0.5 μ L 10X T4 ligase buffer, and 4 μ L water and incubated at room temperature for 1 h. The entire 10 μ L mix was transformed into 80 μ L of chemically competent *E. coli* DH10B cells.

Over-expression and purification of Clz9 and Tcz9 variants

Each Clz9 variant-containing plasmid was transformed into *Escherichia coli* BL21 (DE3). A starter culture was grown overnight in 10 mL of LB media containing 40 µg/mL of kanamycin at 37 °C with overnight agitation. 1 L of TB media containing 40 µg/mL of kanamycin and 100 mg/L of riboflavin was inoculated with the 10 mL starter culture. The cells were grown at 37 °C with shaking (220 rpm) until the culture reached an OD₆₀₀ of 0.6. The flasks were then incubated at 4°C for ~30 min without shaking. Then the cultures were induced by adding IPTG to a final concentration of 0.5 mM, the temperature was lowered to 18 °C and the cells were allowed to grow with shaking (200 rpm) for an additional 20 hours. The cells were then harvested by centrifugation at 10,000 × g for 10 min at 4 °C.

The cell pellet from 1 L of culture was re-suspended in 30 mL binding buffer (50 mM KH₂PO₄, 150 mM NaCl, 10 mM imidazole, pH 8.0) containing approximately 10 mg of lysozyme. The cells were then lysed by sonication (pulse 'on' time 1.0 sec, pulse 'off' time 1.0 sec, output level 60%, 30 sec x6 cycles) on ice. The cell debris was removed by centrifugation at 39,000g for 40 minutes at 4 °C. The clarified supernatant was loaded onto a 5 mL Ni-NTA-affinity column pre-equilibrated with binding buffer kept at 4°C. The Ni-NTA-affinity column was then washed with 50 ml wash buffer (50 mM KH₂PO₄, 150 mM NaCl, 20 mM imidazole, pH 8.0). The protein was eluted from the column with elution buffer (50 mM KH₂PO₄, 150 mM NaCl, 250 mM imidazole, pH 8.0) at 4°C. The fractions containing protein were pooled and concentrated using an Amicon ultracentrifugal filter (10kDa MWCO) at 5000 × g to a final volume of 2.5 mL. The concentrated sample was buffer exchanged into 100 mM phosphate buffer at pH 7.5 containing 100 mM NaCl and glycerol to a final concentration of 15% using an Econo-Pac 10DG desalting column.

Finally, protein aliquots were subjected to flash freezing and stored at -80 °C for future use.

Overexpression and purification protocol for Tcz9 variants were same as that of Clz9. The only difference being Tcz9 variants contain N-terminal MBP tag in addition of His-tag.²

General procedure for *in vitro* assays with Clz9 and Tcz9 variants

The *in vitro* assays were performed following a modified procedure that was previously reported.¹ Assays (0.1 mL) contained 100 mM potassium phosphate buffer pH 7.5, 0.1 mg/mL⁻¹ catalase, 10 µL DMSO, 1 µL of a 20 mM stock solution of substrate and were initiated by addition of 20 µM wild type Clz9 or Tcz9 or their respective variants, unless otherwise altered to investigate the thermal and solvent effects on enzyme activity or product stability during time course experiments. Assays were allowed to incubate for 12 h at 37 °C before quenching with 150 µL acetonitrile. Assays were then centrifuged at 14000 × *g* for 30 minutes and passed through a 0.2 µm filter before injecting 50 µL of the solution for LC-MS analysis at a flow rate of 0.75 mL/min with a mobile phase combination of water + 0.1% formic acid (A) and acetonitrile + 0.1% formic acid (B) using a gradient as follows: 50% (B), 0 to 2 minutes; 50 to 100% (B), 2 to 10 min; 100% (B), 10 to 17 min; 100% to 50% (B), 17 to 18 min; 50% (B), 18 to 20 minutes.

***In vivo* conversion of CBGA to 15a and 17a with Tcz9_T405Y**

A starter culture of *Escherichia coli* BL21 (DE3) containing the pET-MBP-*tcz9_T405Y* plasmid was grown overnight in 10 mL of LB media containing 40 µg/mL of

kanamycin at 37 °C with overnight agitation. 1 L of TB media containing 40 µg/mL of kanamycin and 100 mg/L of riboflavin was inoculated with this starter culture. The cells were grown at 37 °C with shaking (220 rpm) until the culture reached an OD₆₀₀ of 0.6. The flask was then cooled to 18 °C with continuous shaking. Protein expression was induced by adding IPTG to a final concentration of 0.5 mM and 360 mg of CBGA dissolved in 20 mL DMSO was added to the culture (1 M final concentration). The cells were allowed to grow with shaking (200 rpm) for an additional 48 hours. At this time, 500 mL EtOAc was added to the culture and shaken for an additional 2 hours before extracting the organic layer. The aqueous layer was extracted with 500 mL two additional times. The organic layers were pooled, washed with brine, and concentrated under reduced pressure to yield 360 mg of crude extract. The crude mixture was resuspended in 4 mL acetonitrile and filtered prior to preparative HPLC purification at a flow rate of 10 mL/min with a mobile phase combination of water + 0.1% formic acid (A) and acetonitrile + 0.1% formic acid (B) using a gradient as follows: 80% (B), 0 to 8 minutes; 80 to 100% (B), 8 to 16 min; 100% (B), 16 to 21 min; 100% to 80% (B), 21 to 22 min; 80% (B), 22 to 25 minutes. The solvent was removed to yield 30.1 mg CBCA (**15a**, 8.3% yield) and 3.7 mg **17a** (1.0% yield) as clear oils. Spectral data for CBCA matches the reported literature.⁴

15a: ¹H (500 MHz, CDCl₃) δ 11.71 (br. s, 1H); 6.73 (d, 1H, J = 10.1 Hz); 6.24 (s, 1H); 5.48 (d, 1H, J = 10.1 Hz); 5.09 (t, 1H, J = 7.1 Hz); 2.88 (dd, 1H, J = 9.7, 7.7); 2.09 (m, 2H); 1.70 (m, 2H); 1.66 (s, 3H); 1.57 (m, 2H); 1.57 (s, 3H); 1.41 (s, 3H); 1.35 (m, 2H); 1.35 (m, 2H); 0.90 (t, 3H).

17a: ¹H (500 MHz, CDCl₃) δ 6.67 (d, 1H, J = 10.1 Hz); 6.32 (s, 1H); 5.61 (d, 1H, 10.1 Hz); 5.07 (t, 1H, J = 7.4 Hz); 2.93 (dd, 2H, J = 7.8, 11.1 Hz); 2.11 (2H, m); 1.80, (m, 2H);

1.65 (s, 3H); 1.56 (m, 2H); 1.55 (s, 3H); 1.48 (s, 3H); 1.33 (m, 2H); 1.33 (m, 2H); 0.88 (t, 3H).

Table S1. Site-directed mutagenesis primers. Mutant codons are highlighted in red.

Primer Name	Sequence (5'-3')
Clz9_F156T	ggccggc ACC tgcccggag
Clz9_N400E	cgtcgctc GAA taccacaccgac
Clz9_N400L	cgtcgctc CTG taccacaccgac
Clz9_T438Y	gcagctacgtcaac TAT atcgacctgaccgtcg
Tcz9_T124F_F	ccggccggc TTT tgcccgcg
Tcz9_T124F_R	cgcgggca AAA gccggccgg
Tcz9_E368N_F	ctgatggccttc AACT accgcaccgactg
Tcz9_E368N_R	cagtcggtgcggt GTT gaaggccatcag
Tcz9_T405Y_F	ccgcctacgtcaac TAT atcgacctggcc
Tcz9_T405Y_R	ggccaggtcgat ATA gttgacgtaggcgg

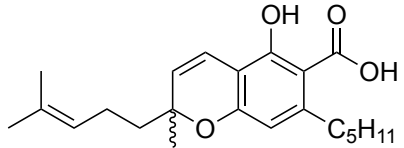
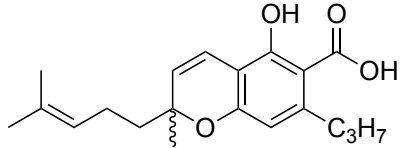
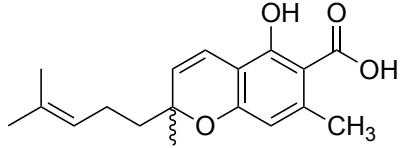
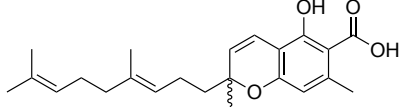
Table S2. PCR cycle for *clz9* mutagenesis.

Temperature	Duration	Cycle(s)
98 °C	30 s	1
98 °C	10 s	
65 °C	30 s	30
72 °C	4 min	
72 °C	10 min	
4 °C	∞	1

Table S3. PCR cycle for *tcz9* mutagenesis.

Temperature	Duration	Cycle(s)
98 °C	30 s	1
98 °C	40 s	
55 °C	40 s	30
72 °C	5 min	
72 °C	10 min	
4 °C	∞	1

Table S4: List of products identified by HPLC analysis from the reactions with **12a**, **12b**, **12c**, and **20**.

Name	#	Structure	Retention Time (min)	[M-H] ⁻ m/z =	UV/Vis (λ _{max})
cannabi-chromenic acid (CBCA) ^a	15a		11.4	357.2058	260, 292, 328
TBD	16a	TBD	9.5	357.2053	260, 281, 324
TBD ^a	17a	TBD	14.6	357.2056	274, 294, 310, 332
TBD	18a	TBD	13.7	355.1907	260, 329
cannabi-chromevarinic acid (CBCVA)	15b		10.1	329.1745	258, 292, 327
TBD	16b	TBD	8.0	329.1738	256, 281, 321
TBD	17b	TBD	13.3	329.1744	275, 298, 314, 340
TBD	18b	TBD	12.2	327.1585	259, 328
cannabiorci-chromenic acid	15c		9.0	301.1426	256, 290, 325
TBD	16c	TBD	6.8	301.1436	258, 278, 321
TBD	17c	TBD	11.9	301.1439	275, 300, 310, 338
TBD	18c	TBD	10.7	299.1290	259, 326
dauri-chromenic acid (DCA)	20		14.7	369.2050	258, 290, 325

^aPurified by preparative HPLC. ¹H NMR data acquired.

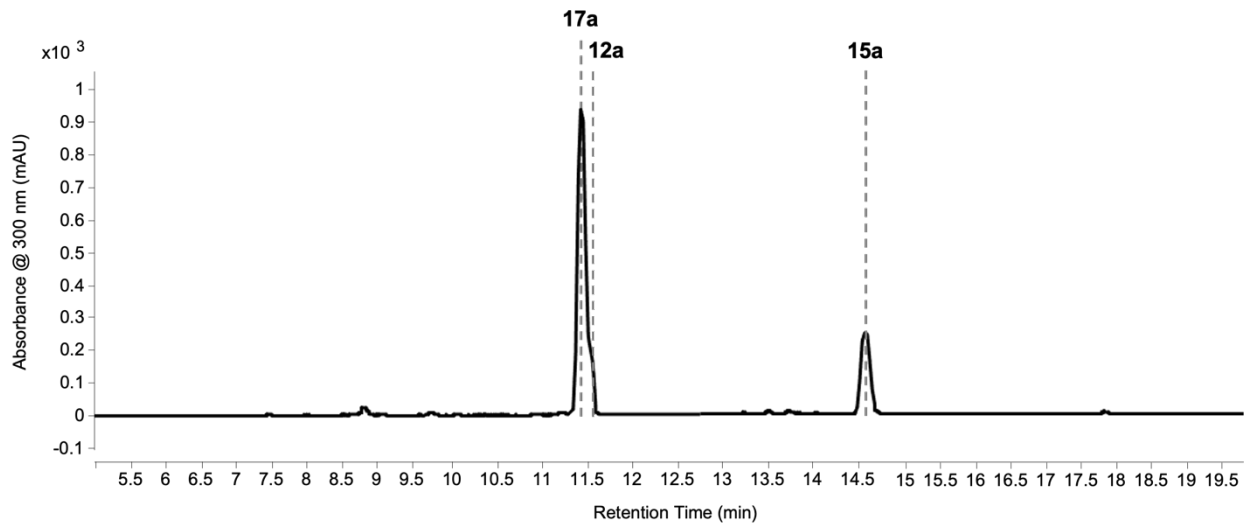


Figure S1: HPLC chromatogram for *in vivo* conversion of **12a** to **15a** and **17a** over 48 hours at 18 °C.

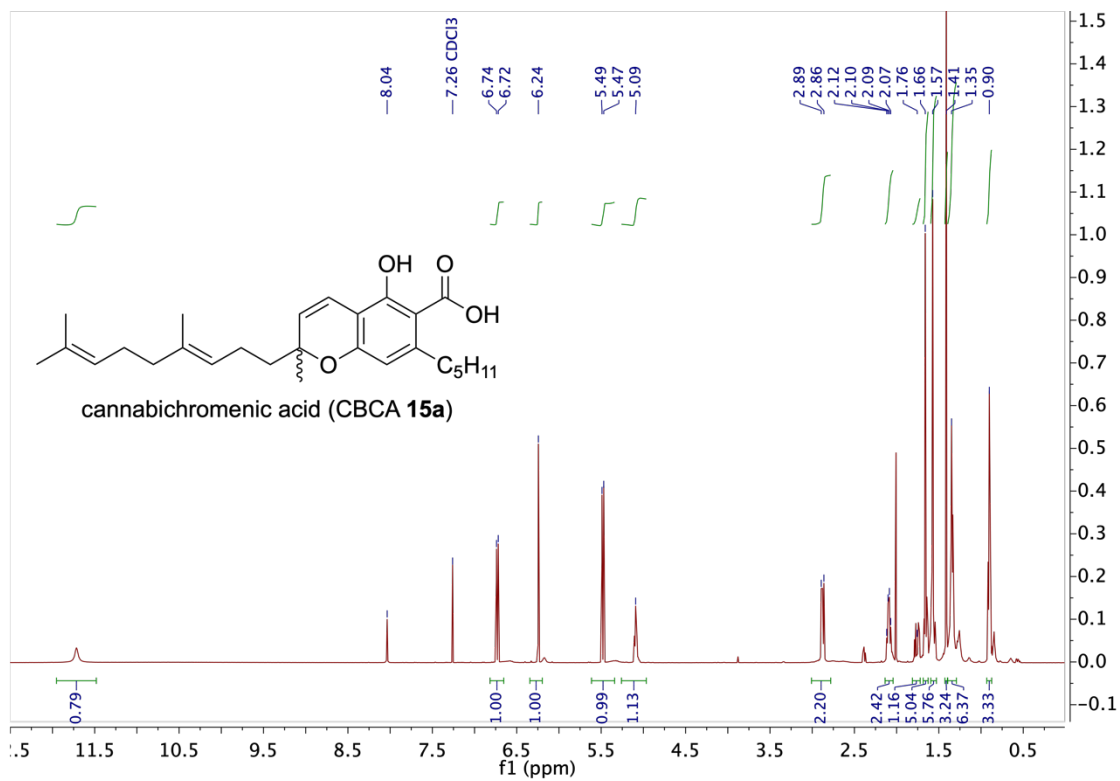


Figure S2: ^1H NMR spectrum of **15a** (500 MHz, CDCl_3).

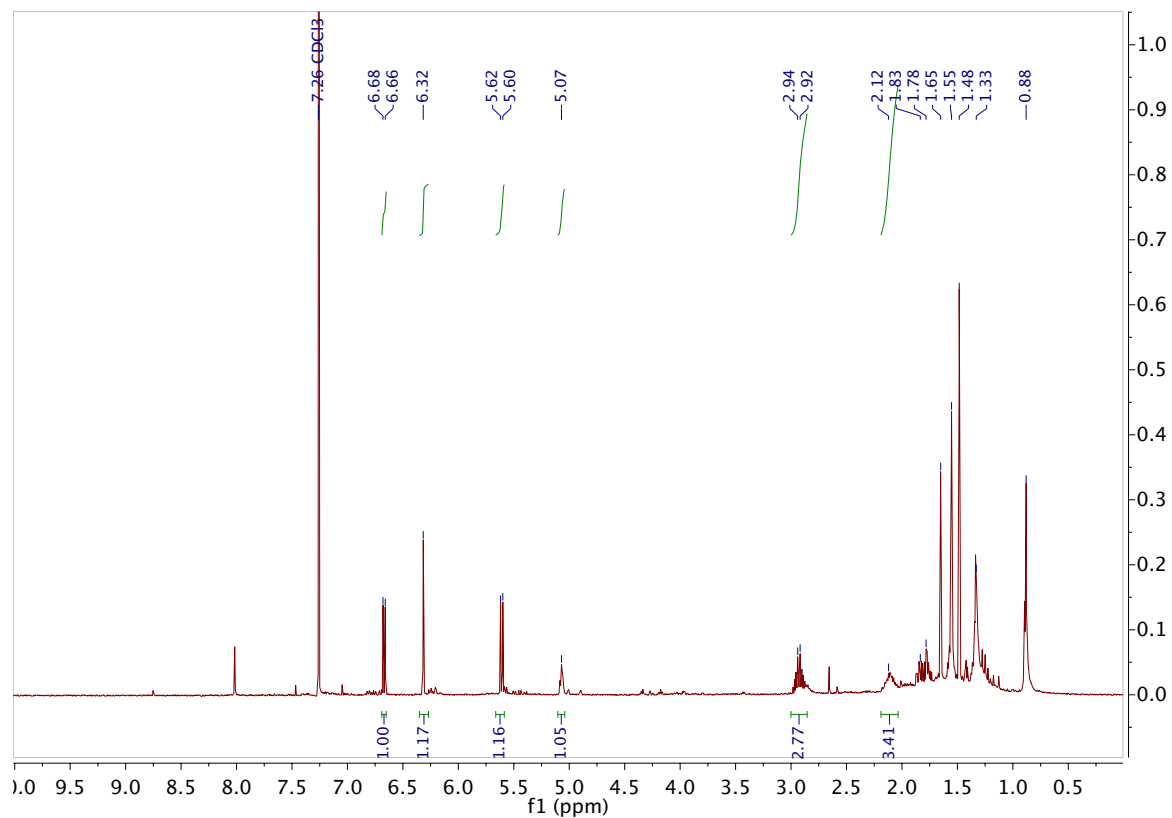


Figure S3: ^1H NMR spectrum of **17a** (500 MHz, CDCl_3).

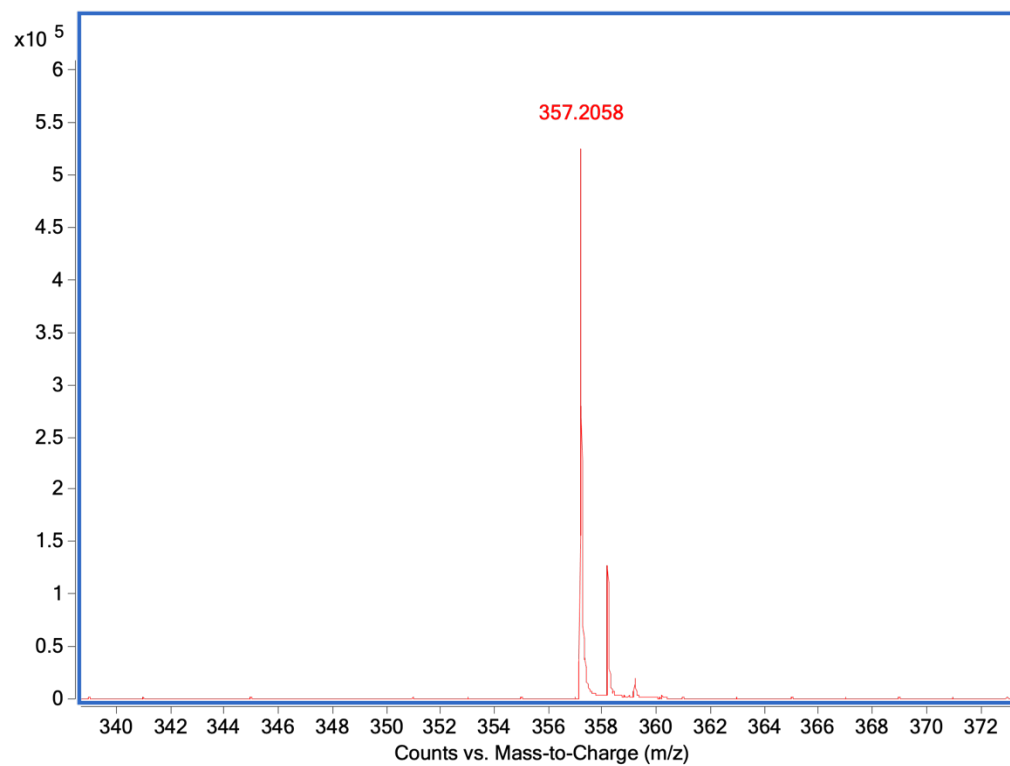


Figure S4: HR-LC-MS of **15a** ($[\text{M}-\text{H}]^-$; $\text{C}_{22}\text{H}_{30}\text{O}_4$).

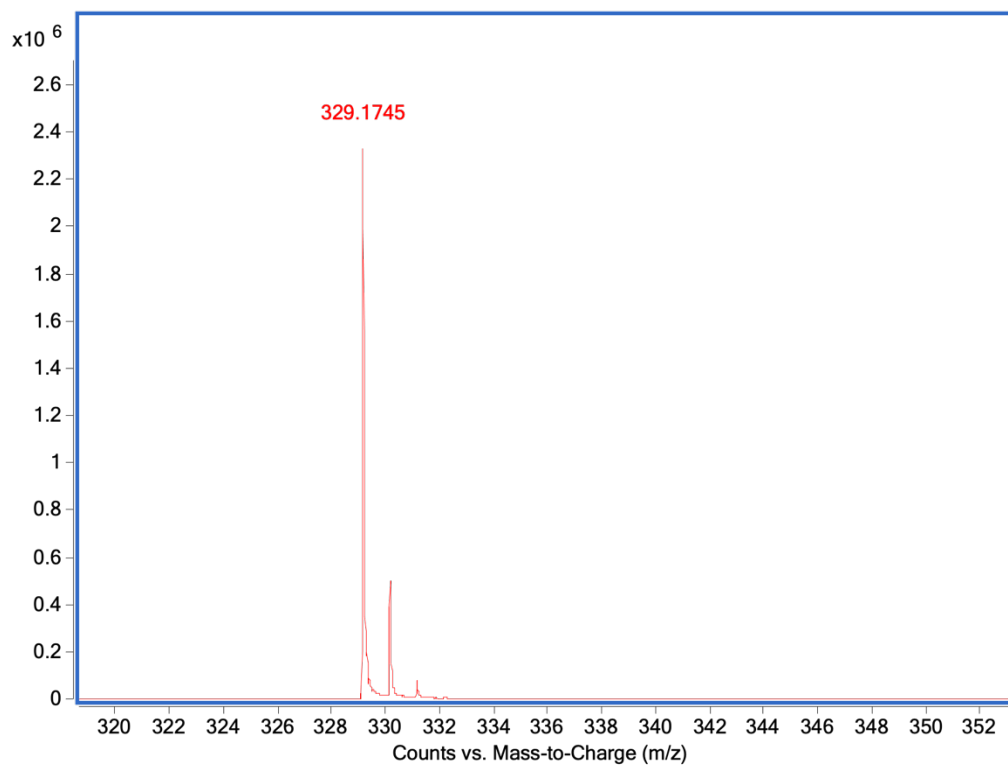


Figure S5: HR-LC-MS of **15b** ($[M-H]^-$; $C_{20}H_{26}O_4$).

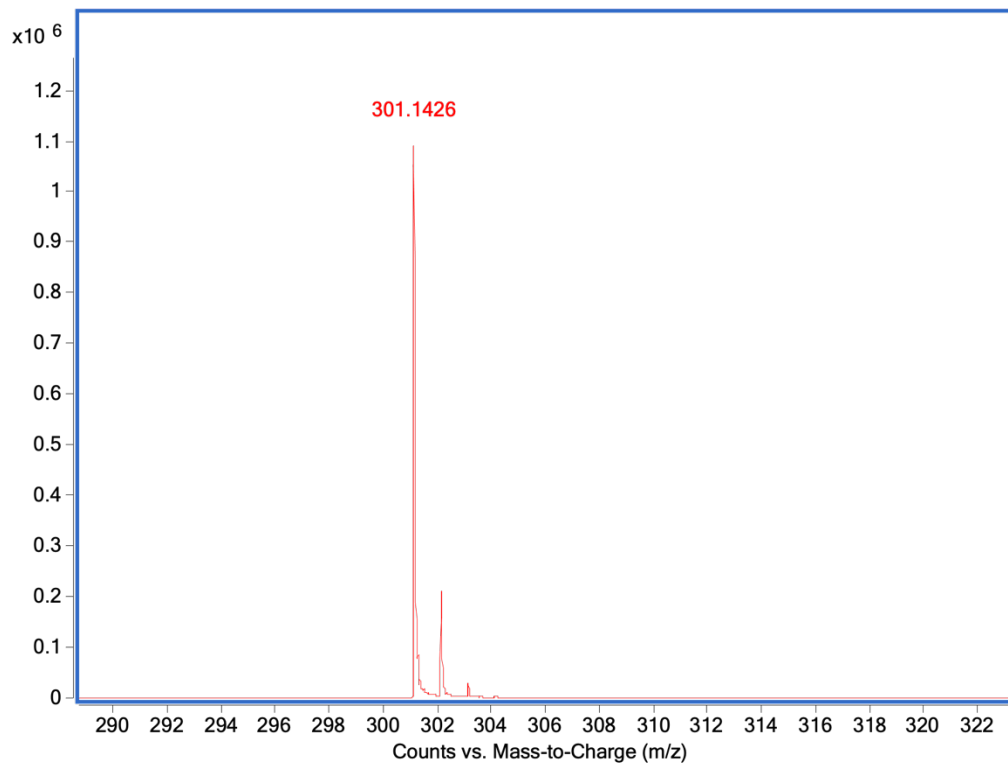


Figure S6: HR-LC-MS of **15c** ($[M-H]^-$; $C_{18}H_{22}O_4$).

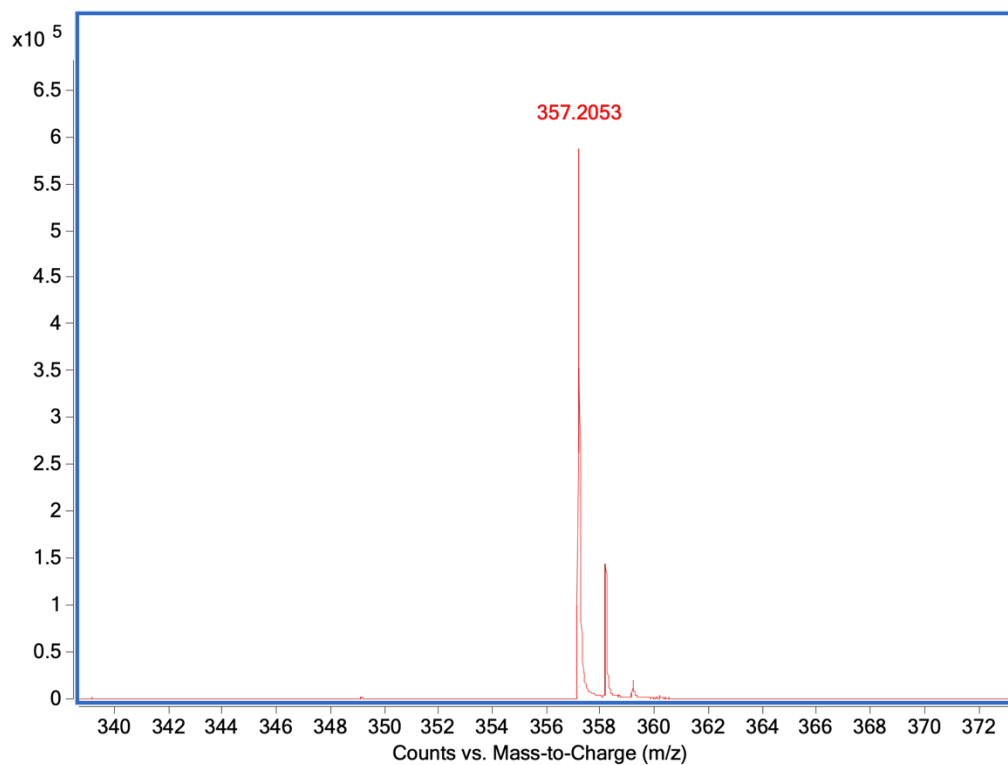


Figure S7: HR-LC-MS of **16a** ($[M-H]^-$; $C_{22}H_{30}O_4$).

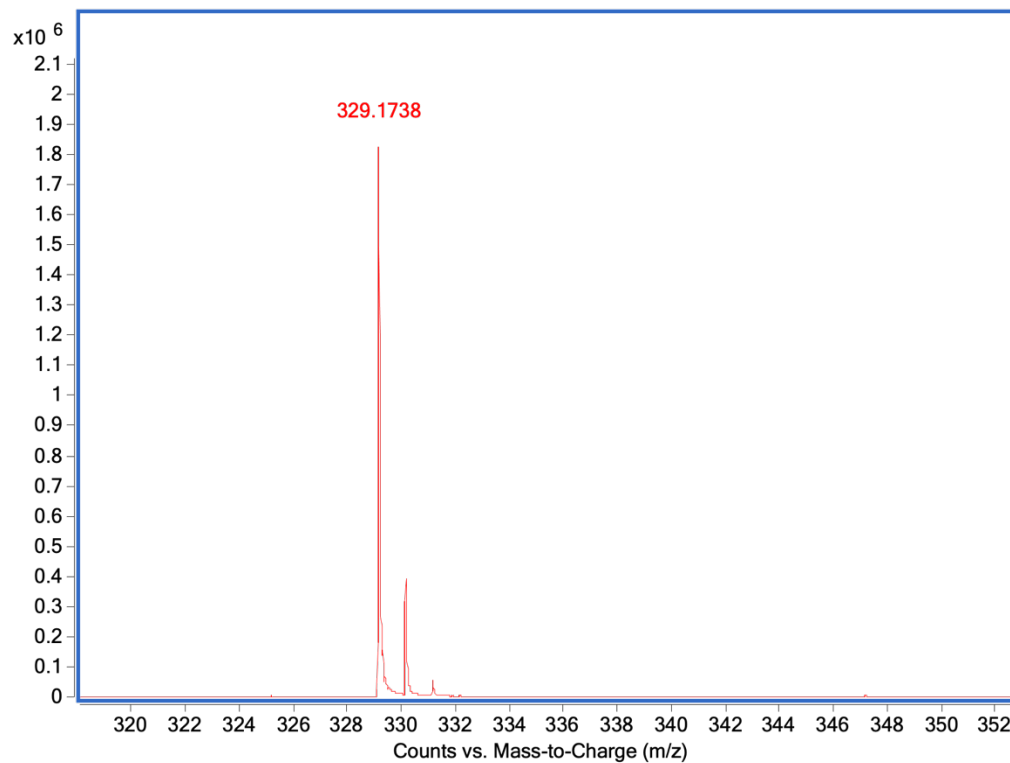


Figure S8: HR-LC-MS of **16b** ($[M-H]^-$; $C_{20}H_{26}O_4$).

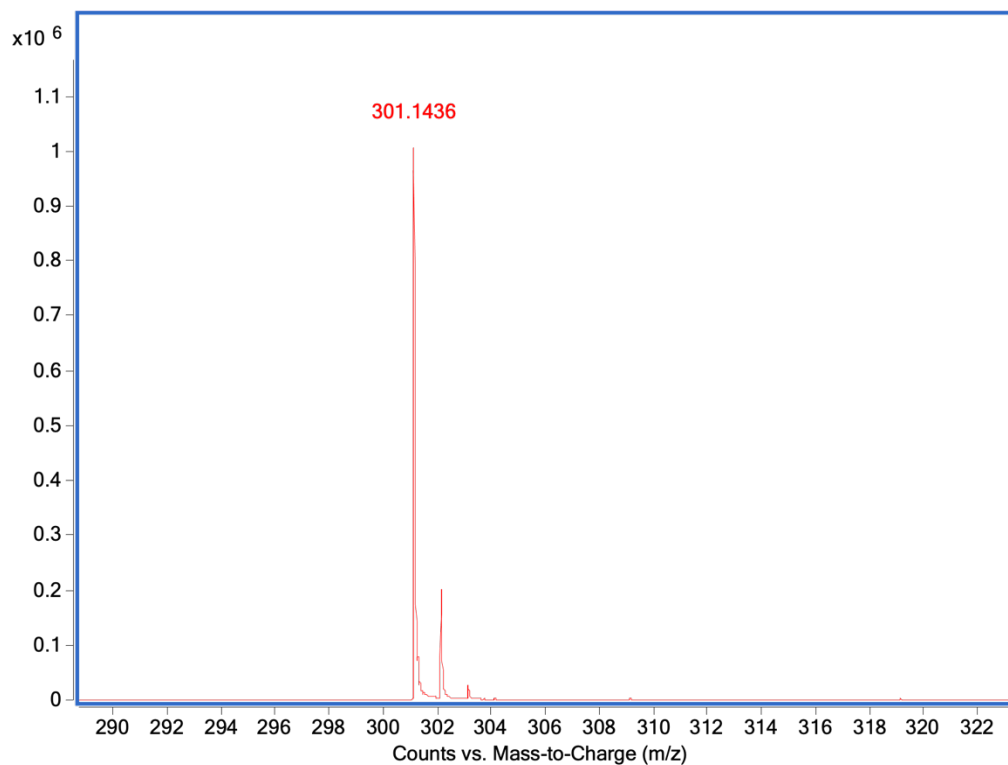


Figure S9: HR-LC-MS of **16c** ($[M-H]^-$; $C_{18}H_{22}O_4$).

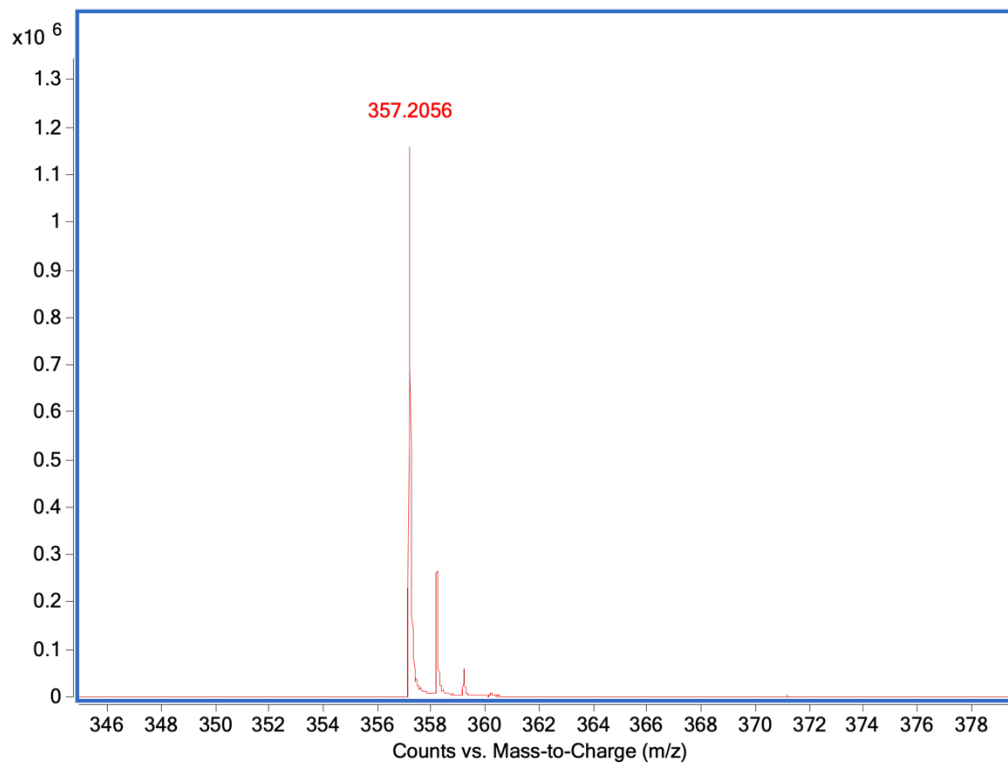


Figure S10: HR-LC-MS of **17a** ($[M-H]^-$; $C_{22}H_{30}O_4$).

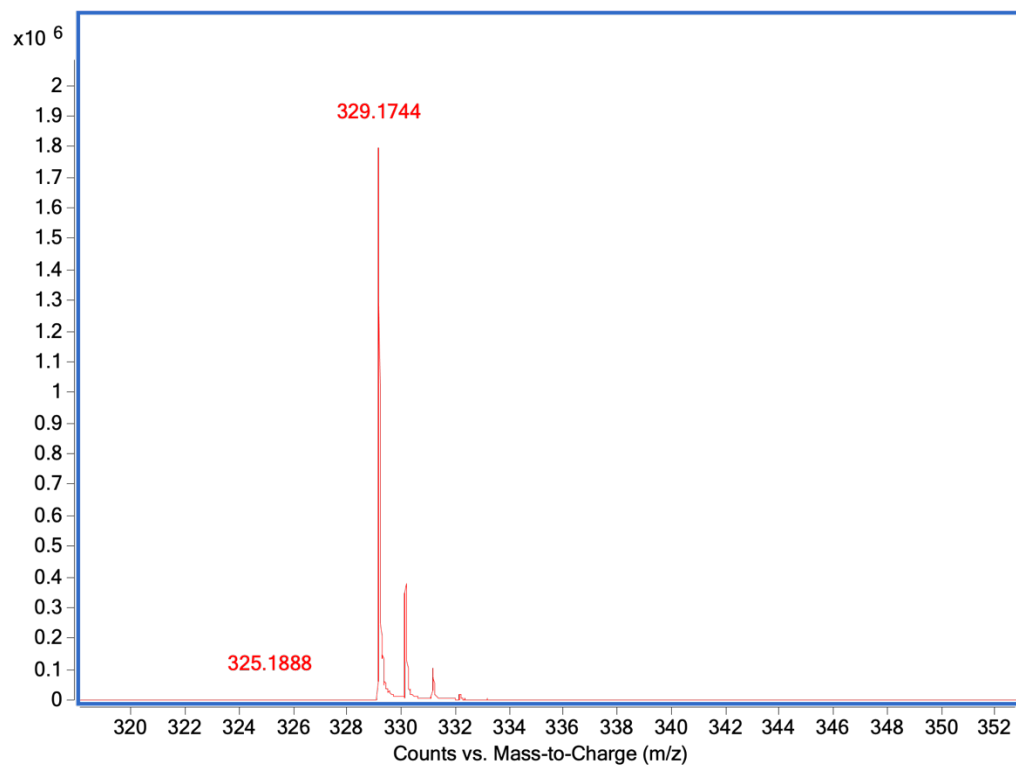


Figure S11: HR-LC-MS of **17b** ($[M-H]^-$; $C_{20}H_{26}O_4$).

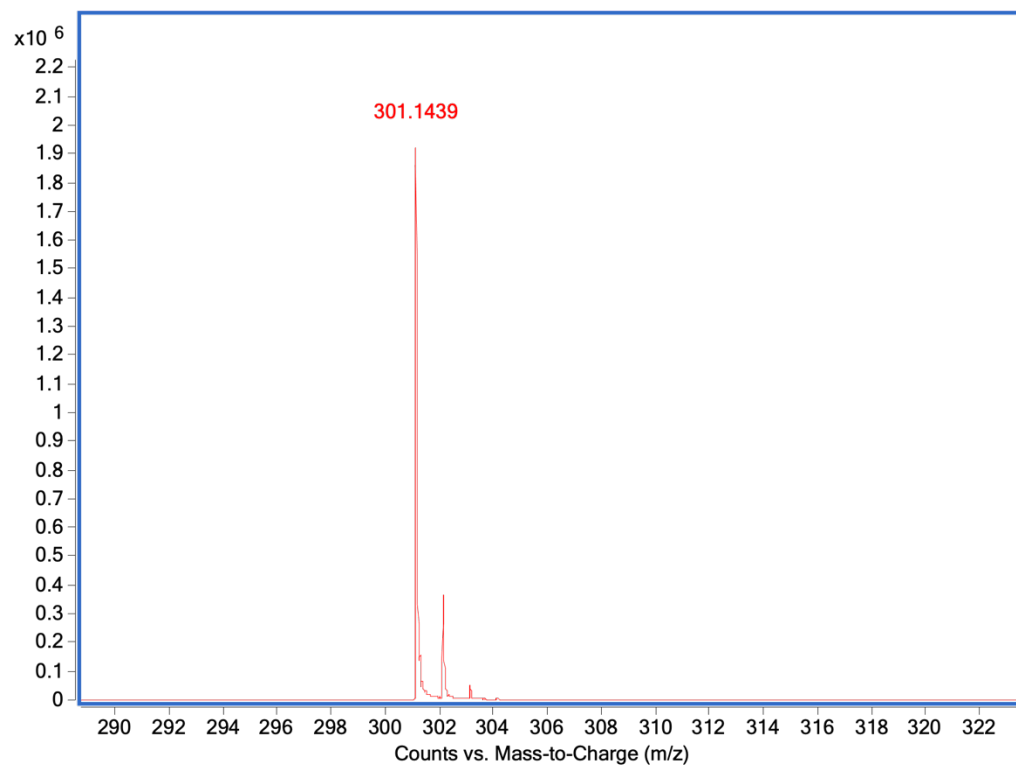


Figure S12: HR-LC-MS of **17c** ($[M-H]^-$; $C_{18}H_{22}O_4$).

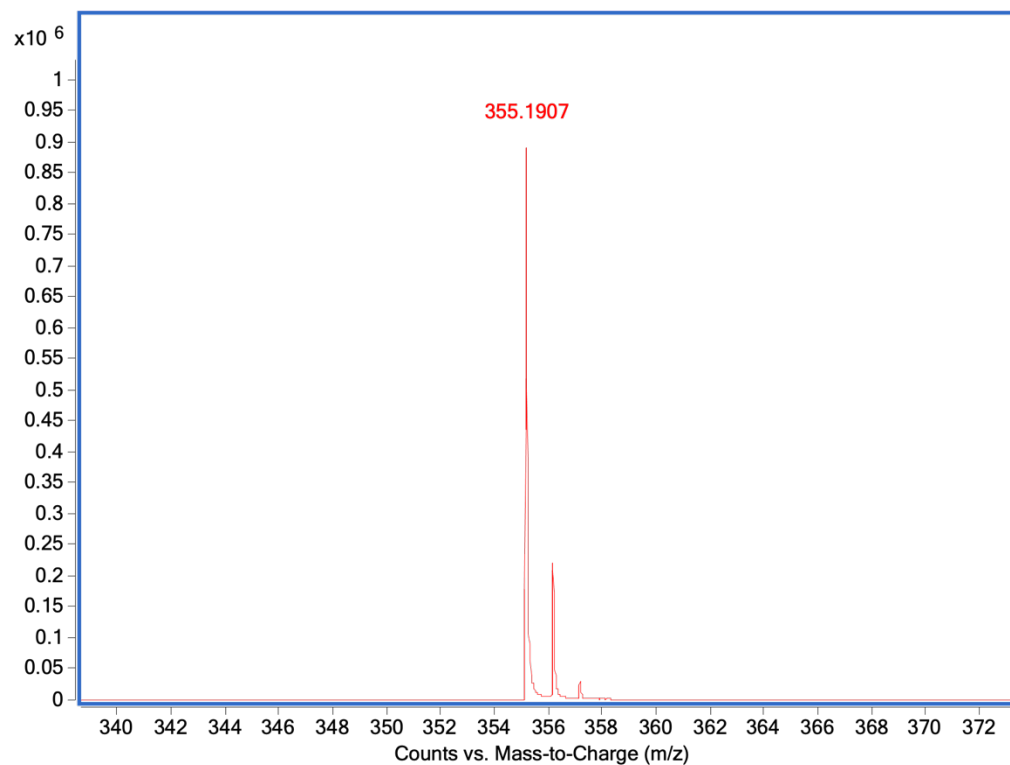


Figure S13: HR-LC-MS of **18a** ($[M-H]^-$; $C_{22}H_{28}O_4$).

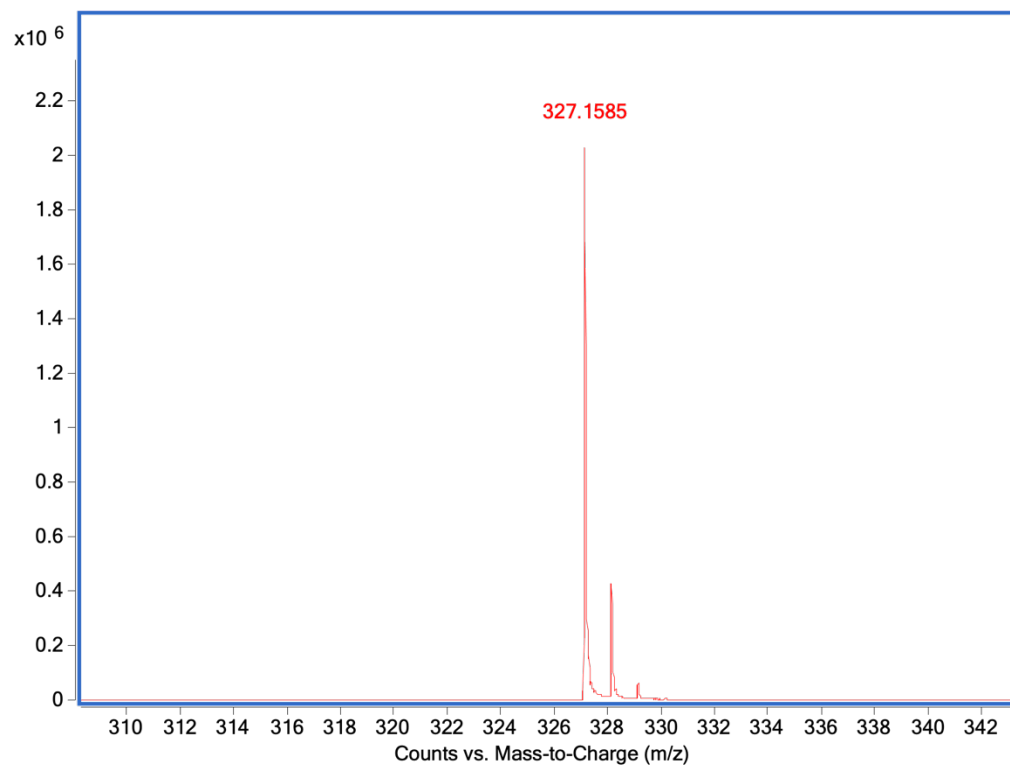


Figure S14: HR-LC-MS of **18b** ($[M-H]^-$; $C_{20}H_{24}O_4$).

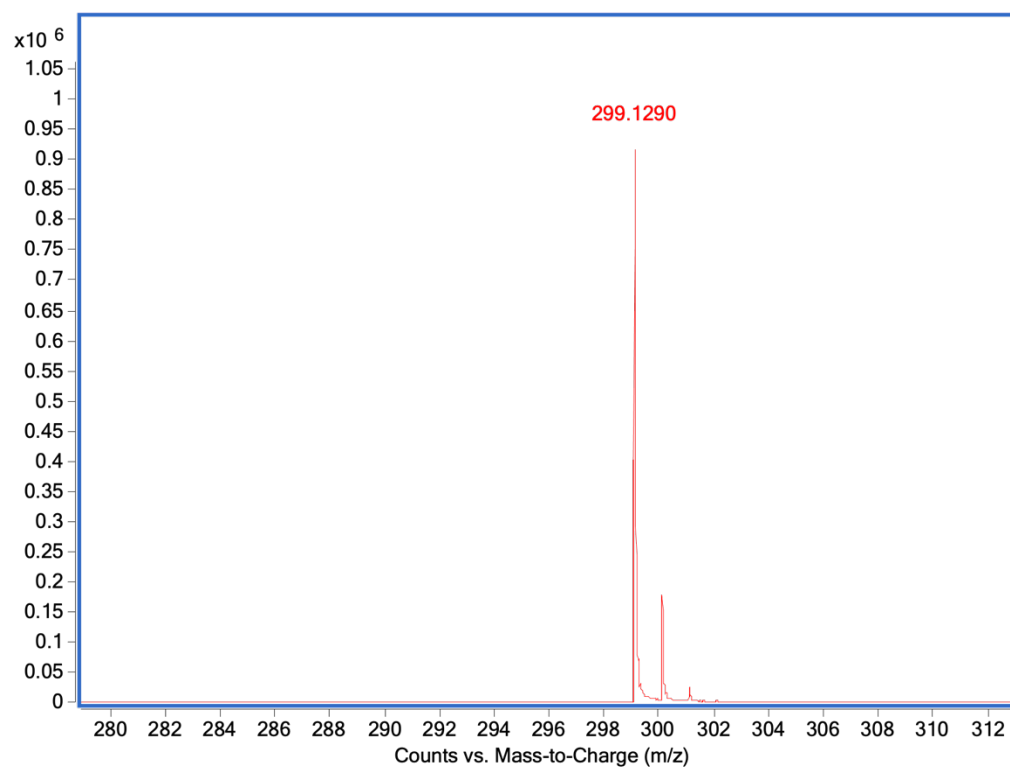


Figure S15: HR-LC-MS of **18c** ($[M-H]^-$; $C_{18}H_{20}O_4$).

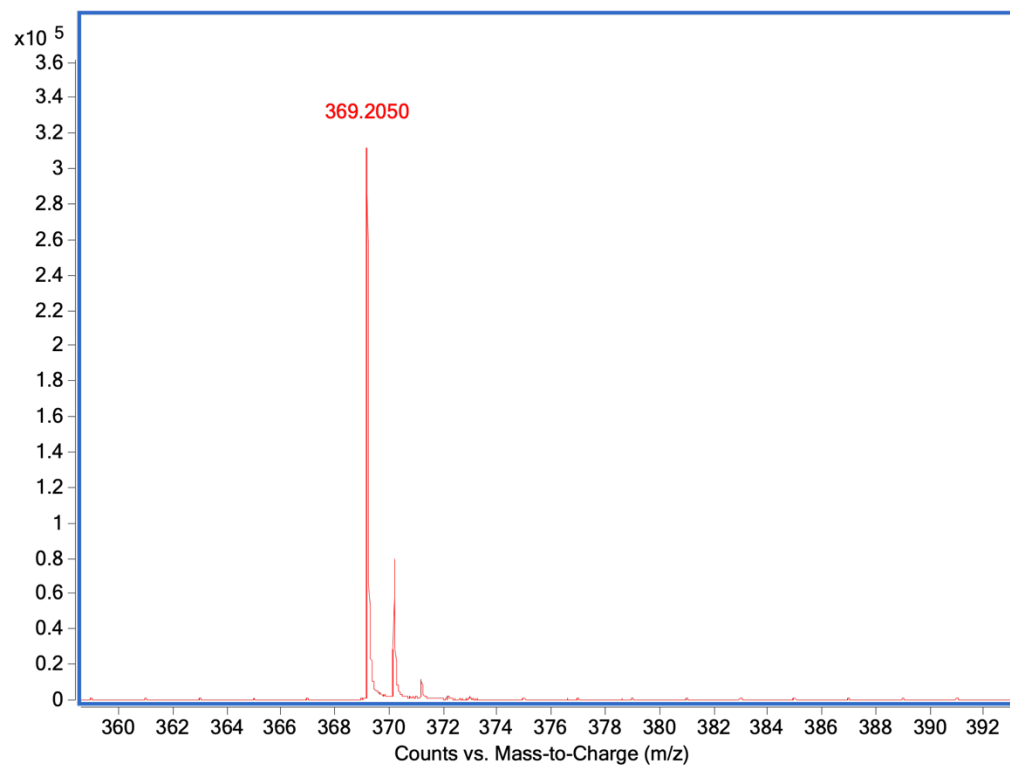


Figure S16: HR-LC-MS of **20** ($[M-H]^-$; $C_{23}H_{30}O_4$).

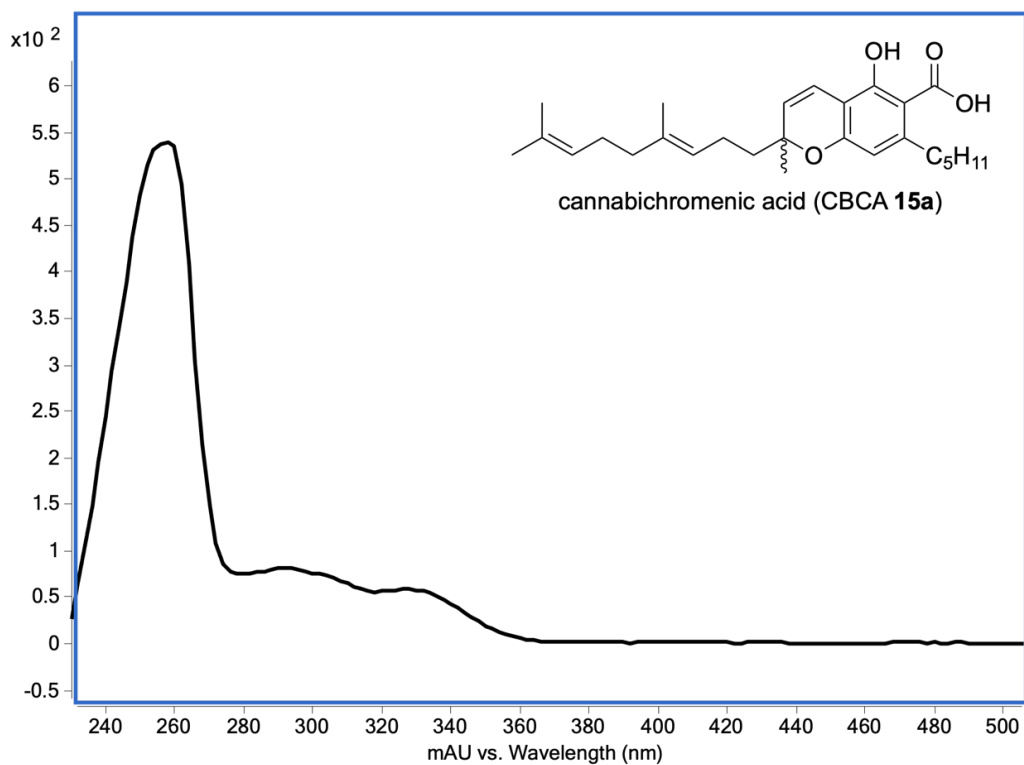


Figure S17: UV/Vis spectra of **15a**.

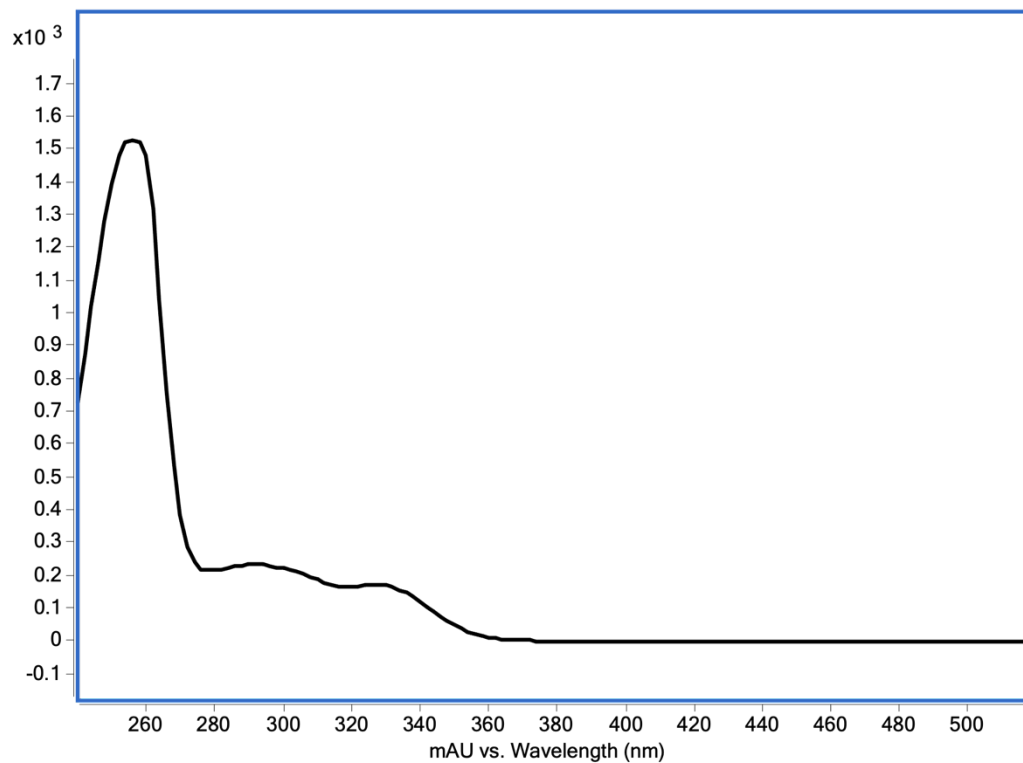


Figure S18: UV/Vis spectra of **15b**.

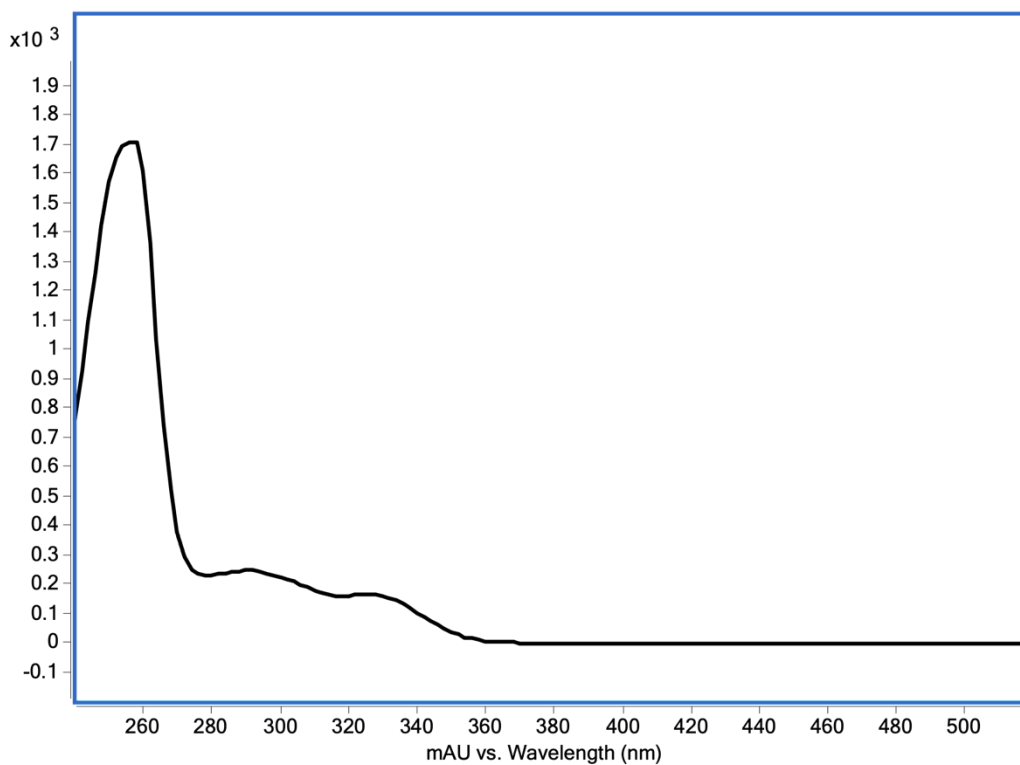


Figure S19: UV/Vis spectra of **15c**.

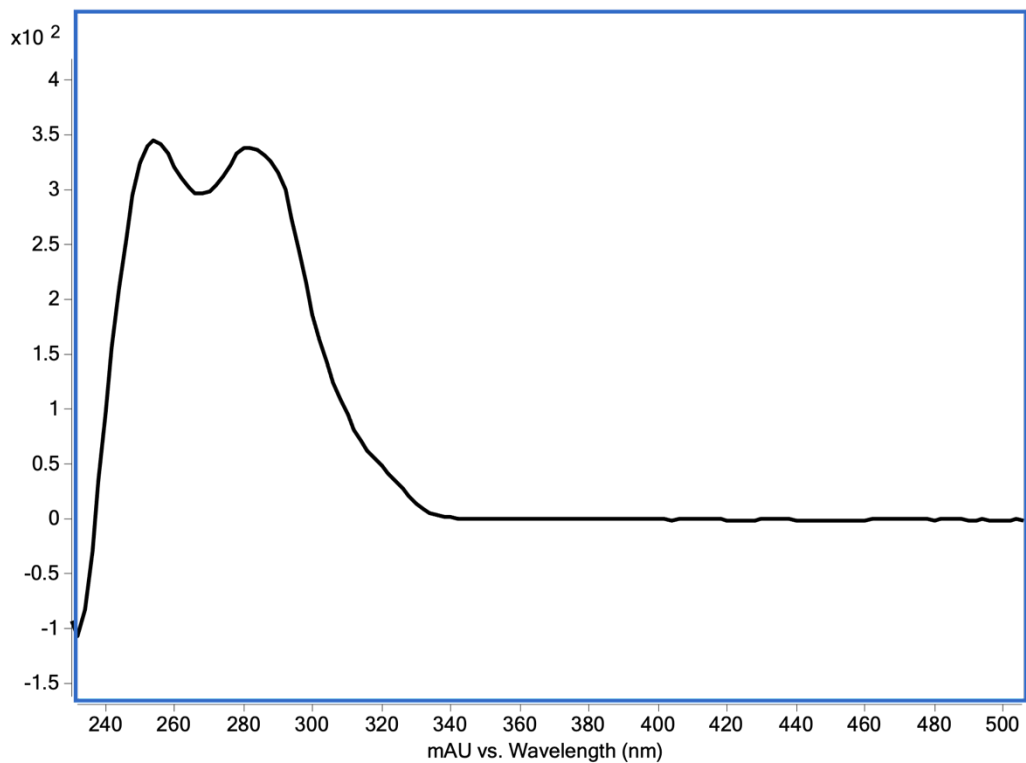


Figure S20: UV/Vis spectra of **16a**.

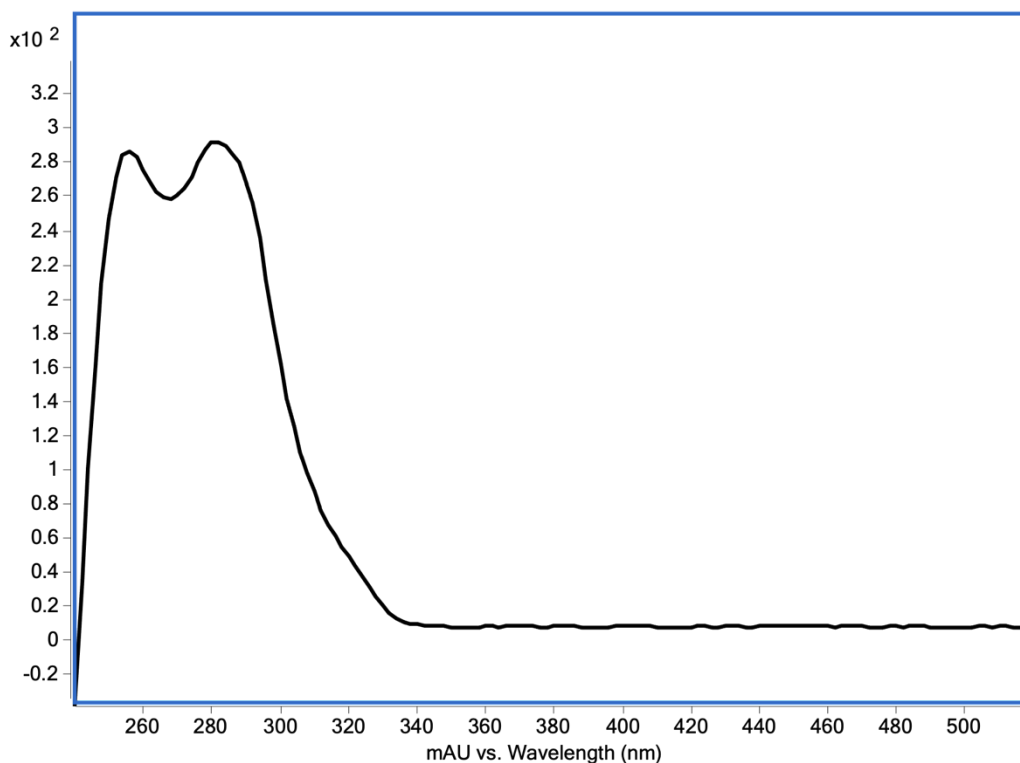


Figure S21: UV/Vis spectra of **16b**.

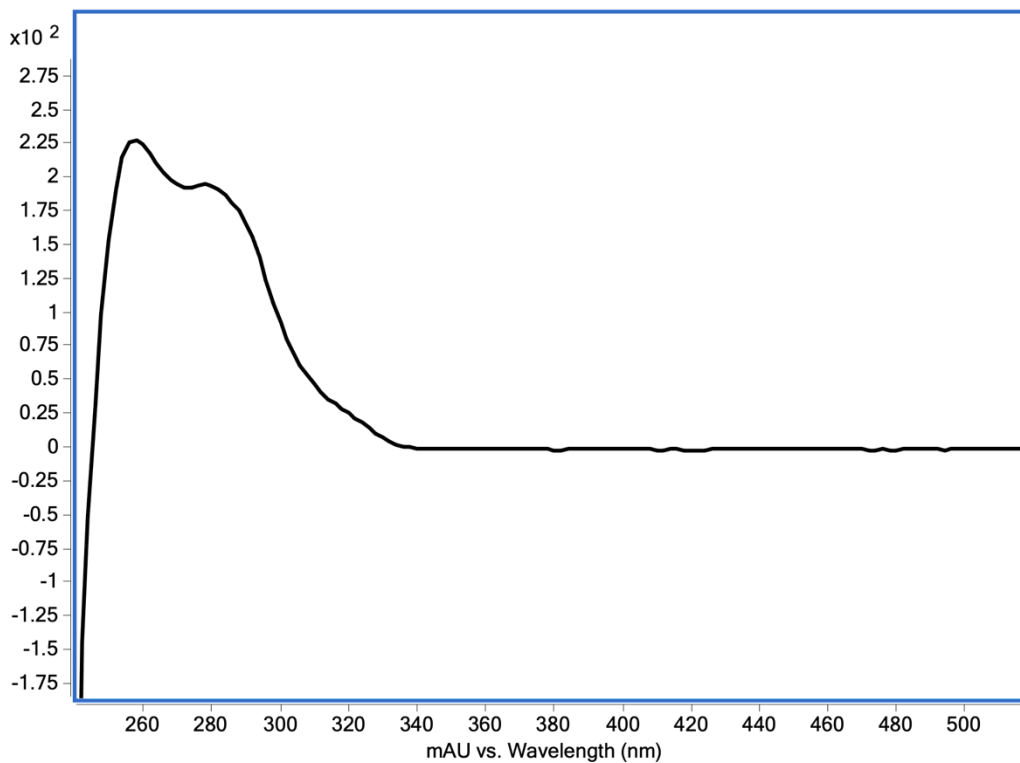


Figure S22: UV/Vis spectra of **16c**.

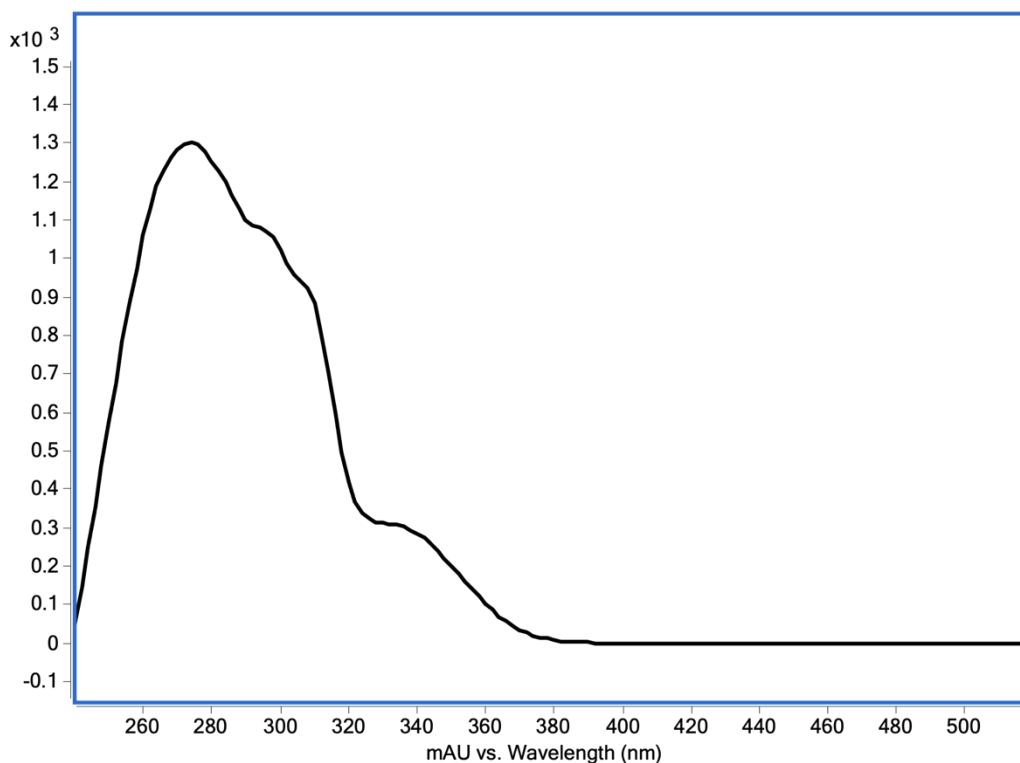


Figure S23: UV/Vis spectra of **17a**.

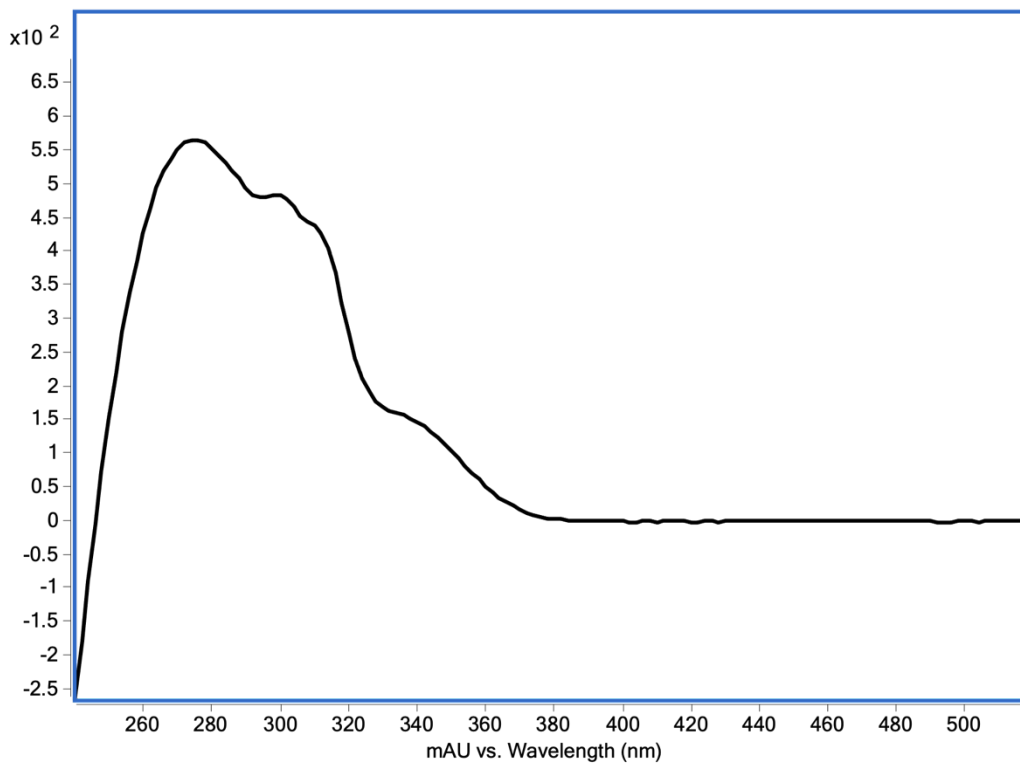


Figure S24: UV/Vis spectra of **17b**.

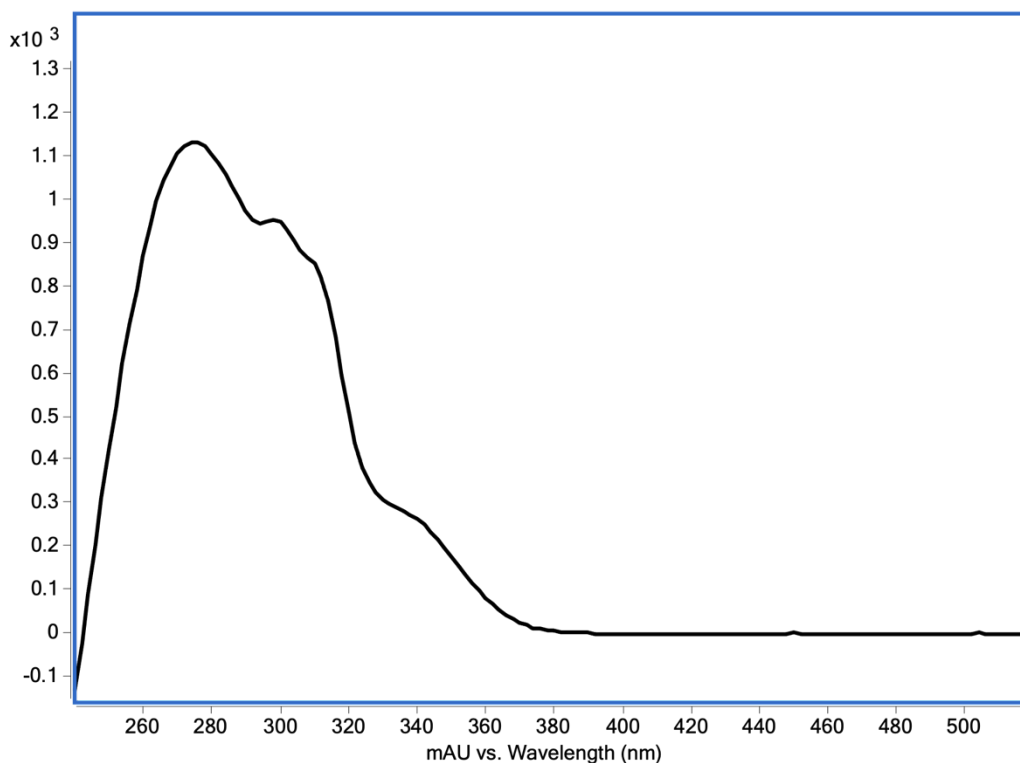


Figure S25: UV/Vis spectra of **17c**.

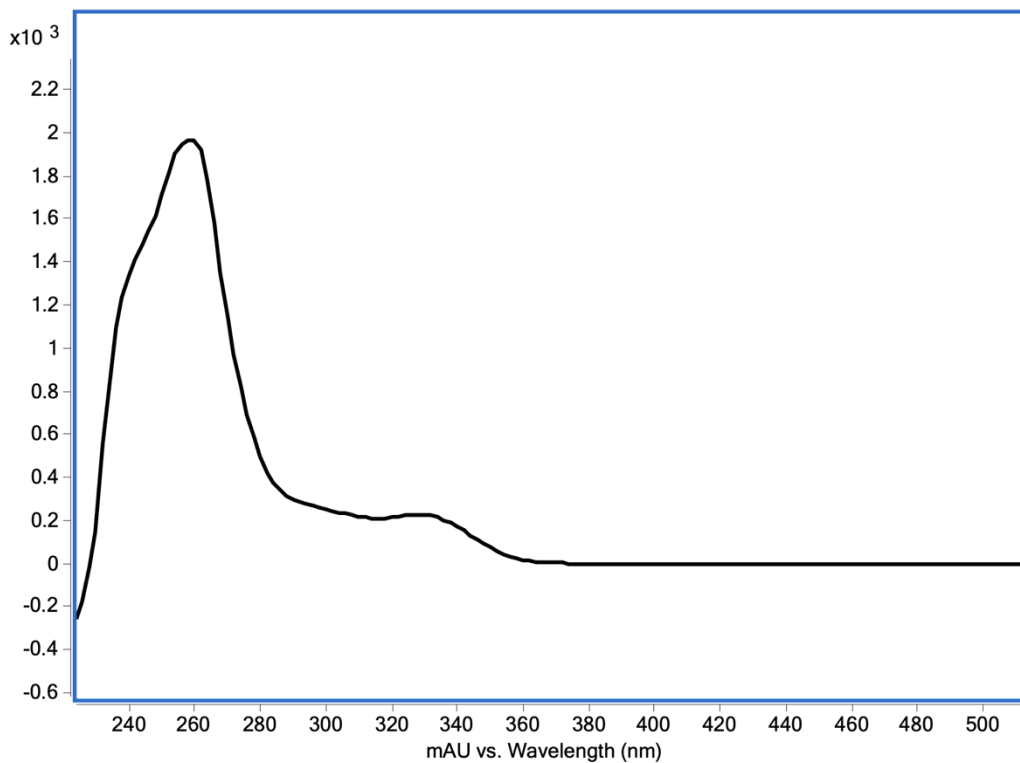


Figure S26: UV/Vis spectra of **18a**.

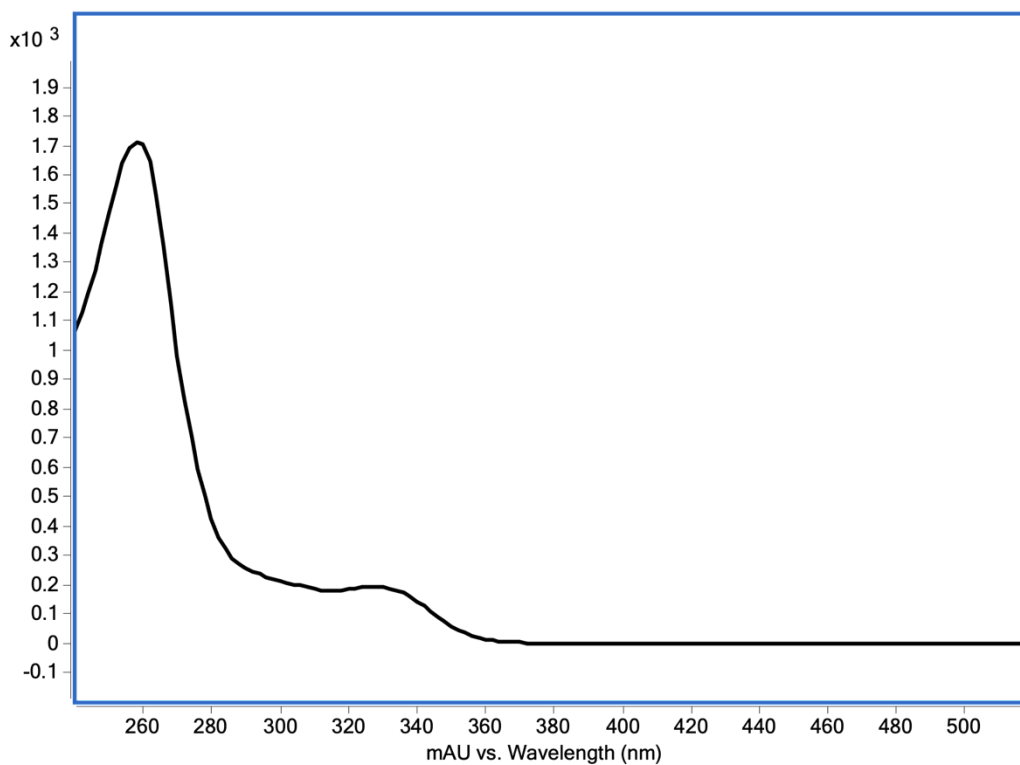


Figure S27: UV/Vis spectra of **18b**.

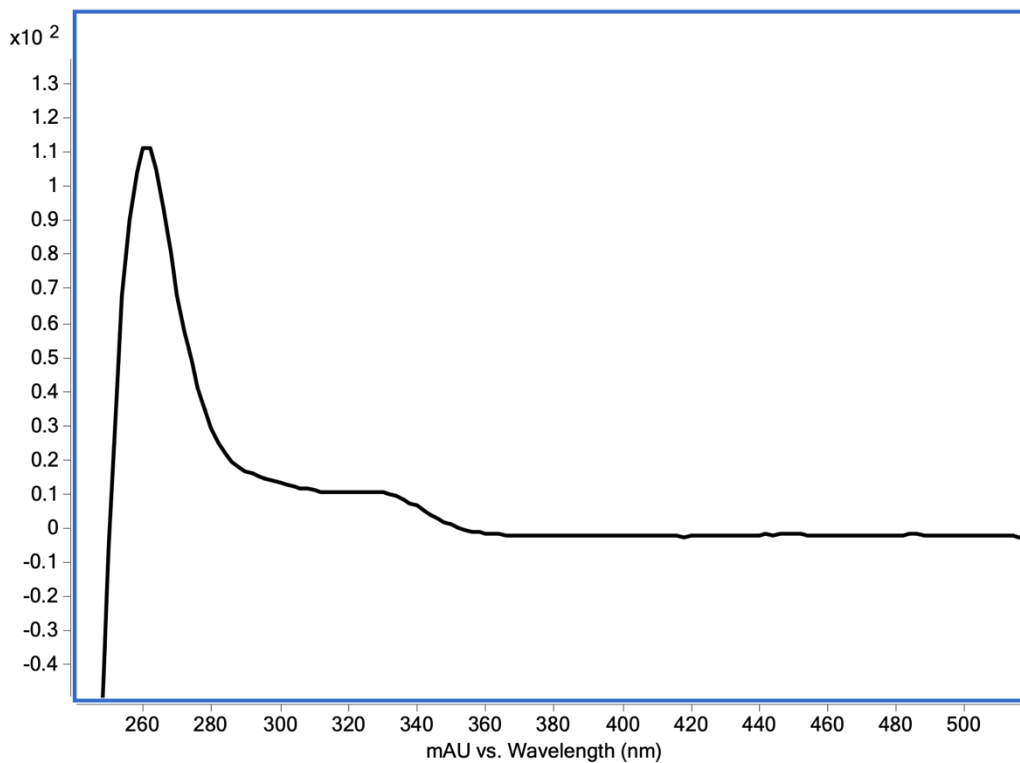


Figure S28: UV/Vis spectra of **18c**.

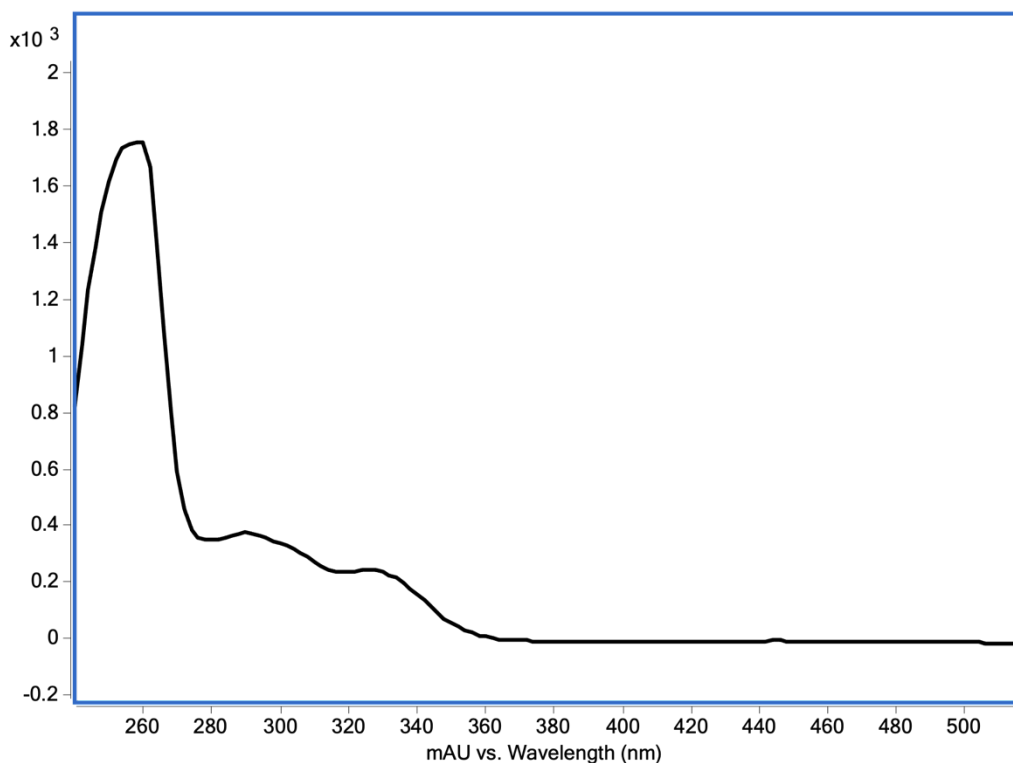


Figure S29: UV/Vis spectra of **20**.

References:

1. Mantovani, S. M.; Moore, B. S. *J. Am. Chem. Soc.* **2013**, *135*, 18032–18035.
2. Purdy, T. N.; Kim, M. C.; Cullum, R.; Fenical, W.; Moore, B. S. *J. Am. Chem. Soc.* **2021**, *143*, 3682–3686.
3. Edelheit, O.; Hanukoglu, A.; Hanukoglu, I. *BMC Biotechnol.* **2009**, *9*, 1–8.
4. Fellermeier, M.; Eisenreich, W.; Bacher, A.; Zenk, M. H. *Eur. J Biochem.* **2001**, *268*, 1596–1604.